Human Induced Pluripotent Stem Cell–based Modeling of Hepatogenesis

D i s s e r t a t i o n

zur Erlangung des akademischen Grades

d o c t o r   r e r u m   n a t u r a l i u m

(Dr. rer. nat.)

im Fach Biologie

eingreicht an der

Lebenswissenschaftliche Fakultät

der Humboldt-Universität zu Berlin

von

Peggy Matz

Gutachter/innen: 1. Prof. Dr. Hans-Dieter Volk
2. Prof. Dr. James Adjaye
3. Prof. Dr. Ann Ehrenhofer-Murray

Disputation am: 30. Mai 2016

"Zum Erfolg gibt es keinen Lift.
Man muss die Treppe benutzen!"
Emil Oesch

Acknowledgements

Contents

List of Figures

List of Tables

Abbreviations

6-well	one well of a 6-well cell culture plate, $\sim$9 cm² growth area
A1AT	antitrypsin
AA	amino acids
AACE	very low-density lipoprotein
ABCB4	ATP-binding cassette, sub-family b (MDR/TAP), member 4
ABCC2	ATP-binding cassette, sub-family c (CFTR/MRP), member 2
AFP	alpha-fetoprotein
ALB	albumin
ALCAM	activated leukocyte cell adhesion molecule
AP	alkaline phosphatase
BC	bile canaliculi
BMP	bone/body morphogenetic protein
BSA	bovine serum albumin
BSEP/ABCB11	bile salt export pump
C_T	threshold cycle
CA	cholic acid
CBF1	C promoter-binding factor 1
CC	cellular compartment
CCP	clathrin coated pits
CD31/PECAM-1	cluster of differentiation 31/platelet endothelial cell adhesion molecule 1
CDCA	chenodeoxycholic acid
CDFDA	5 (and 6)-Carboxy-2,7-dichlorofluorescein diacetate
cDNA	complementary deoxyribonucleic acid
CDX2	caudal type homeobox 2
CER1	cerberus 1, DAN family BMP antagonist
CFTR/MRP	ATP-binding cassette sub-family C
CK18	cytokeratin 18
CK19	cytokeratin 19
CM	conditioned medium
c-MET	met proto-oncogene
cRNA	complementary ribonucleic acid
CSL	CBF1/Suppressor of Hairless/LAG-1
CXCR4	chemokine (C-X-C motif) receptor 4
d	day
DAPI	4',6-diamidino-2-phenylindole
DCA	deoxycholic acid
DE	definitive endoderm

Dexa	dexamethasone
DLK1	delta-like 1 homolog (*Drosophila*)
DLL	delta-like
DMSO	dimethyl sulfoxide
DNA	deoxyribonucleic acid
DNMT3β	DNA (cytosine-5-)-methyltransferase 3 beta
dNTP	deoxyribonucleotide triphosphate
DPPA4	developmental pluripotency-associated 4
E10	day 10 after fertilization
EB	embryoid body
EBNA1	EpsteinBarr nuclear antigen 1
E-CAD/CDH-1	e-cadherin/cadherin 1
ECM	extra cellular matrix
EDTA	ethylenediaminetetraacetic acid
E-iPSC	episomal-derived iPSC
EMT	epithelial-to-mesenchymal transition
EOMES	eomesodermin
EP(s)	endodermal progenitor(s)
epi	episomal reprogramed
ERK	extracellular signal-regulated protein kinases
ESC(s)	embryonic stem cell(s)
FACS	fluorescence-activated cell sorting
FAH	fumarylacetoacetate hydrolase
FBS	fetal bovine serum
FGF2	fibroblast growth factor 2 (basic fibroblast growth factor)
FGFR	fibroblast growth factor receptor
fMSC(s)	human fetal femur mesenchymal stem cell(s)
FOXA2	forkhead box A2
FOXH1	homolog of Xenopus forkhead activin signal transducer-1
FRS2α	FGFR substrate 2α
GATA6	GATA-binding factor 6
GCA	glycocholic acid
GCDCA	Glycochenodeoxycholic acid
GDF	growth differentiation factor
GFP	green fluorescent protein
GO	gene ontology
GRB	growth factor receptor-bound 2
GSK	glycogen synthase kinase
h	hour
HE	hepatic endoderm
hESC(s)	human embryonic stem cell(s)
HEX	haematopoietically expressed homeobox
HFF1	human fetal foreskin fibroblast(s)
HGF	hepatocyte growth factor

HLC(s)	hepatocyte-like cell(s)
HLX	H2.0-like homeobox gene
HNF	hepatocyte nuclear factor
HNF3β	hepatocyte nuclear factor 3 beta
HNF4α	hepatocyte nuclear factor 4 alpha
HUVEC	human umbilical vein endothelial cells
ICG	indocyanine green
ICM	inner cell mass
IL	Interleukine
iPSC(s)	induced pluripotent stem cell(s)
IRES2	internal ribosome entry site 2
JAG	jagged
JAK	janus kinase
KLF4	kruppel-like factor 4
KRT17	keratin 17
LARGE	lost acquired retained gene expression
LATS1	large tumour suppressor homologue 1
LDL	low-density lipoprotein
LDLR	low density lipoprotein receptor
LEFTY	left-right determination factor
LGR5	leucine-rich repeat containing G protein-coupled receptor 5
LIN28	lin-28 homolog A (*C. elegans*)
MACS	magnetic activated cell sorting
MAML	mastermind-like protein
MAPK	mitogen-activated protein kinase
MEF	mouse embryonic fibroblast
MEF(s)	mouse embryonic fibroblast(s)
MEF-CM	mouse embryonic fibroblast-conditioned medium
MEK	mitogen-activated protein kinase kinase
MET	mesenchymal-to-epithelial transition
min	minute
miRNA	microRNA
MIXL1	mix paired-like homeobox
mRNA	messenger ribonucleic acid
MRP4/ABCC4	ATP-binding cassette sub-family C member 4
MST1	STE20-like protein kinase 1
MT1E	metallothionein 1E
MYC	myelocytomatosis viral oncogene homolog (*avian*)
NaB	sodium butyrate
NANOG	nanog homeobox
NES	nestin
NICD	notch intracellular domain
NTCP	Sodium-taurocholate cotransporting polypeptide
NTCP/SLC10A1	solute carrier family 10 member 1

OATP/SLCO1A2	solute carrier organic anion transporter family, member 1A2
OLT	orthotopic liver transplantation
oriP	origin of plasmid replication
OSKM	OCT4, SOX2, KLF4 and c-MYC
OSKML	OCT4, SOX2, KLF4, c-MYC and LIN28
OSM	oncostatin m
OSMR	OSM receptor
p_{adj}	false discovery rate-adjusted diff p-value
p_{det}	'detection p-value
PAS	periodic acid-schiff
PAX6	paired box 6
PBS	phosphate buffered saline
PBST	0.05 % tween 20 in phosphate buffered saline
PCR	polymerase chain reaction
PDK	phosphoinositide-dependent protein kinase
PFA	paraformaldehyde
PHH	primary human hepatocytes
PODXL	podocalyxin-like
POU5F1/OCT4	POU class 5 homeobox 1
PPARα	peroxisome proliferator-activated receptor-a
PROM1/CD133	prominin 1
PROX1	prospero-related homeobox 1
PS	penicillin/streptomycin
PSC(s)	pluripotent stem cell(s)
Px	passage x of an *in vitro* cell culture
qRT-PCR	quantitative real-time polymerase chain reaction
RAF	MAPKKK
RAS	small GTP-binding proteins
RHOA	Ras homolog gene family, member A
RNA	ribonucleic acid
ROCK	rho associated coiled-coil kinase
ROS	reactive oxygen species
R-Smad	regulated Smad protein
RSPO1	R-Spondin 1
RT	room temperature
RTK	receptor tyrosine kinase
s	second
SAV	salvador
SD	standard deviation
SDS	sodium dodecyl sulfate
shRNA	short hairpin ribonucleic acid
siRNA	small interfering ribonucleic acid
α-SMA	smooth muscle actin
SOS	son of sevenless

SOX2   SRY (sex determining region Y)-box 2
SOX17   SRY (sex determining region Y)-box 17
SSEA   stage-specific embryonic antigen
STAT   signal transducer and activator of transcription
STM   septum transversum mesenchyme
SV40LT   simian virus 40 large T antigen
T   brachyury homolog (*Mus musculus*)
TβRII   TGFβ receptor
TAZ   transcriptional co-activator with PDZ-binding motif
TBX3   t-box 3
TC   transient cells
TCA   taurocholic acid
TCDCA   taurochenodeoxycholic acid
TDO2   tryptophan 2,3-dioxygenase
TE   trophoectoderm
TEADs   TEA domain family members
TF(s)   transcription factor(s)
TGF   transforming growth factor
TGFβ transforming growth factor β
TGFP   turbo green fluorescent protein
TRA   tumor rejection antigen
TRN   transcriptional regulatory network
β-TUJ1 class III β-tubulin
UM   unconditioned medium
v   viral reprogrammed
VEGF   vascular endothelial growth factor
VEGFR   vascular endothelial growth factor receptor
VIM   Vimentin
V-iPSC   viral-derived iPSC
VLDL   very low-density lipoprotein
WNT3A   wingless-type MMTV integration site family member 3A
YAP   yes-associated protein
ZO-1   tight junction protein 1

Semantics

bp	base pairs
°C	degrees Celsius
d	day
h	hour
min	minute
s	second
g	gram
mg	milligram
μg	microgram
ng	nanogram
kV	kilovolt
l	liter
ml	milliliter
μl	microliter
mol	mole
pmol	picomole
M	molar concentration, 1 mol per liter
mM	millimolar
μM	micromolar
nM	nanomolar
mm	millimeter
nm	nanometer
μm	micrometer
R.L.U.	relative light per unit
rpm	revolutions per minute
RT	room temperature
%	percentage
U	enzyme unit

Abstract

This project generated and characterized integration-free, episomal-derived induced pluripotent stem cell (E-iPSCs) lines from human somatic cell lines of different origins. Two different somatic cell lines were used, the human fetal fibroblast cell line HFF1 and human umbilical vein endothelial cell line HUVEC. Both were reprogrammed into integration-free iPSCs and were comparable amongst themselves and to human embryonic stem cells, the gold standard of pluripotent stem cells. Furthermore, the iPSCs with different genetic background were differentiated to hepatocyte-like cells (HLCs). With the use of iPSC-derived hepatocytes different stages during hepatogenesis and the potential of maturation could be analyzed as well as compared to fetal liver and primary human hepatocytes (PHH). This study could uncover gene regulatory networks which presence bipotential progenitor populations in HLCs. Additionally, comparable transcriptome profile analyses revealed that the iPSC-derived HLCs are immature and more similar to fetal liver. However, the HLCs hold typical functionality characteristics of hepatocyte, e.g. glycogen storage, uptake and release of ICG and CDFDA, bile acid and urea secretion. Furthermore, typical structures of hepatocytes such as bile canaliculi with microvilli, lipid storage and tight junctions are visible. In order to analyze the maturation potential of HLCs a long-term culture experiment was performed using HUVEC-iPSC-derived HLCs which implies the possibility for long-term culture of HLCs while increasing maturation. Additionally, HFF1-derived iPSCs were differentiated to endodermal progenitors (EPs) to analyze the endodermal development before biliary tree and hepatoblast which can give rise to hepatocytes, cholangiocytes and pancreatic cells. The multipotent EPs hold a great potential to analyze the endodermal development of intestine, lung, liver, bile duct and gallbladder, as well as pancreas.

Zusammenfassung (German)

In dieser Studie wurden nicht-integrative Vektorkonstrukte zur Reprogrammierung von zwei menschlichen Zelllinien (HFF1, HUVEC) verwendet, um integrations-freie, episomal generierte iPSC Zelllinien (E-iPSCs) zu generieren. Darber hinaus wurden diese iPSCs zu sogenannten Leberzell-hnlichen Zellen (HLCs) differenziert. Hierzu konnten die verschiedenen Stufen der Hepatogenese und die potentielle Reifung zu Leberzellen untersucht sowie mit ftalen und ausgereiften menschlichen Leberzellen verglichen werden. Diese Studie konnte Gen-regulierende Netzwerke aufdecken, welche eine pi-potentiale Vorluferpopulation in den HLCs prsentieren. Zustzlich deckte das Transkriptions-Profil auf, dass die iPSC-generierten HLCs unreif und hnlicher den ftalen Leberzellen sind. Dennoch weisen die HLCs typische funktionelle Charakteristika von Leberzellen auf, z.B. Glykogen-Einlagerung, Aufnahme und Abgabe von Substanzen wie ICG und CDFDA, Sekretierung von Gallensure und Harnstoff. Zustzlich konnten typische Leber-Strukturen wie Gallenkanlchen mit Mikrovilli, Fettspeicherung und sogenannte tight junctions, Verbindungsgnge zwischen den Zellen nachgewiesen werden. Um die potentielle Reifung dieser HLCs voranzutreiben, wurde eine Langzeit-Kultivierung von HUVEC-iPSC-generierten HLCs durchgefhrt. Dies sollte zugleich zeigen, ob die HLCs lnger kultiviert und gleichzeitig reifen knnen. Ein zweiter Teil dieser Studie befasst sich mit der Generierung von endodermalen Vorluferzellen (EPs). Es wurden HFF1-iPSCs zu EPs differenziert um die endodermale Entwicklung vor der Entstehung der Gallenwege und des Hepatoblasten zu untersuchen. Die EPs zeigen Merkmale dafr, dass sie sowohl in Hepatozyten, Cholangozyten und auch Pankreaszellen differenziert werden knnen. Mit Hilfe dieser multipotenten EPs knnte es mglich sein die endodermale Entwicklung des Darmes, der Lunge, Leber, Gallengnge und Gallenblase sowie der Bauchspeicheldrse nher zu untersuchen.

1 Introduction

The liver is the largest gland in the human body and plays the most important role in regulation of metabolic pathways and detoxification. The liver regulates for example the glucose levels through carbohydrate storage (Glycogen) and release. Lipids and proteins are consistently rebuilt and degraded. Also, the production of bile and the metabolism of dietary compounds take place in the liver. Substances which are foreign to the body (e.g. drugs or toxicants) are inactivated and the blood homeostasis is controled by the production of blood components (e.g. Albumin and clotting factors) (reviewed by Duncan [2000]; Malarkey et al. [2005]).

In the postprandial state, glucose is taken up by the liver, is metabolized into glycogen and stored. Glucose can also be metabolized into fatty acids or amino acids. Free fatty acids are esterified with glycerol-3-phosphate to generate triacylglycerol (TAG) in hepatocytes. This TAG is secreted into the circulation as very low-density lipoprotein (VLDL) particles or can be stored in lipid droplets in hepatocytes. Amino acids (AA) are used to synthesize e.g. proteins and glucose. In order to provide energy for the body glucose and TAG are released from the liver into the circulation and metabolized by muscle, adipose tissue, and other extrahepatic tissues. Liver-generated glucose provides essential metabolic energy for extrahepatic tissues during fasting and activities (Rui [2014]).

The liver is able to catabolize AA as alternative energy source for the body. AA are oxidized by amino acid catabolizing enzymes (AACE) when other energy substrates are low, especially circulating glucose and fatty acids. In this state the proteins in the skeletal muscles is broken down, dissociated into AA, circulated in the blood and are taken up by the liver where the oxidation of AA is taken place. Additionally, fatty acids can be modulate to hepatic AA. Peroxisome proliferator-activated receptor-a (PPARa) stimulates fatty acid β-oxidation. The liver is the main organ involved in the metabolism of AA. This metabolism redounds to the generation of metabolic energy and supplies substrates for gluconeogenesis to maintain blood glucose concentration. The main source of glucose for the brain and other tissues is provided by gluconeogenic AA (Harper [1984], Kaloyianni and Freedland [1990], Young and Marchini [1990]).

Another metabolic process which executes in the liver is the urea cycle, also known as the ornithine cycle. The urea cycle enzymes convert the cytotoxic ammonia to the much less toxic urea. This process has a net energy cost. Urea is eliminated via the kidney by fluids in particular urine. The urea cycle activity regulates the nitrogen concentration in the body. The synthesis of urea plays a key role in protein catabolism. Taken together, the urea cycle is essential for life (Cushny [1917], Saheki et al. [1980], Hansen et al. [1986], Meijer et al. [1990], Dimski [1994], Young et al. [2000]).

The liver is a complex organ consisting of hepatocytes, which represent most of the liver cell mass (Figure 1.1). Hepatocytes are arranged in so called hepatic plates separated by sinusoid spaces. These hepatic plates are arranged star-like around a central vein. The bile canaliculi on the surface of adjoining hepatocytes drain bile into the bile ducts, which run parallel to portal veins and hepatic arteries to form the portal triad (Shiojiri [1984]; Duncan [2000]; Lemaigre [2003]; Malarkey et al. [2005]; Godoy et al. [2013]).
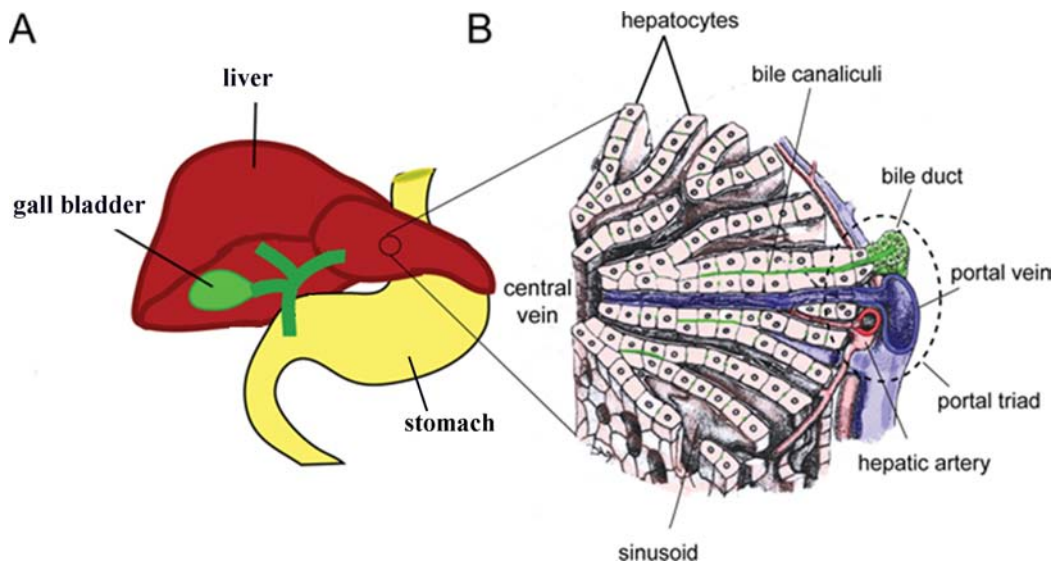
Figure 1.1: **Cellular structure of the liver.**
A) The adult human liver (red), with the gall bladder and extra hepatic ducts (green), in relation to the stomach and intestine (yellow). **B)** The cellular structure of the liver showing the hepatocytes (pink) arranged in hepatic plates separated by sinusoid spaces radiating around a central vein. Bile canaliculi on the surface of adjoining hepatocytes drain bile into the bile ducts (green), which run parallel to portal veins (blue) and hepatic arteries (red) to form the portal triad. Adapted from: http://www.stembook.org/node/512; retrieved 09.06.2014.

The catabolism of cholesterol in the liver yields bile salts. The hepatocytes generate the primary bile in their canaliculi which transport the bile to the cholangiocytes driven by an osmotic gradient. The cholangiocytes form the bile duct and metabolize the canalicular bile by secretory and reabsorptive processes. The bile salt export pump (BSEP, ABCB11) protein is located in hepatocytes and the ATP-binding cassette, sub-family C (CFTR/MRP), member 4 (MRP4/ABCC4) are in charge of the bile salt circulation from hepatocytes to the bile (Figure 1.2). Triggered by ingestion, the bile duct opens and the bile circulates into the duodenum, where lipolysis with the help of the bile takes place. The vast bulk of bile is recycled from the small intestine, where they assist with the absorption of dietary fat and fat-soluble vitamins. Additionally, the bile is important to eliminate cholesterol and various toxins. With the blood flow, the bile

returns into the liver by the solute carrier family 10 (sodium/bile acid cotransporter), member 1 (NTCP, SLC10A1) and solute carrier organic anion transporter family, member 1A2 (OATP, SLCO1A2) where the circular flow starts again (Childs et al. [1995], Bull et al. [1998], Childs et al. [1998], Kullak-Ublick and Meier [2000], Esteller [2008], Ogimura et al. [2011], Garzel et al. [2014]).
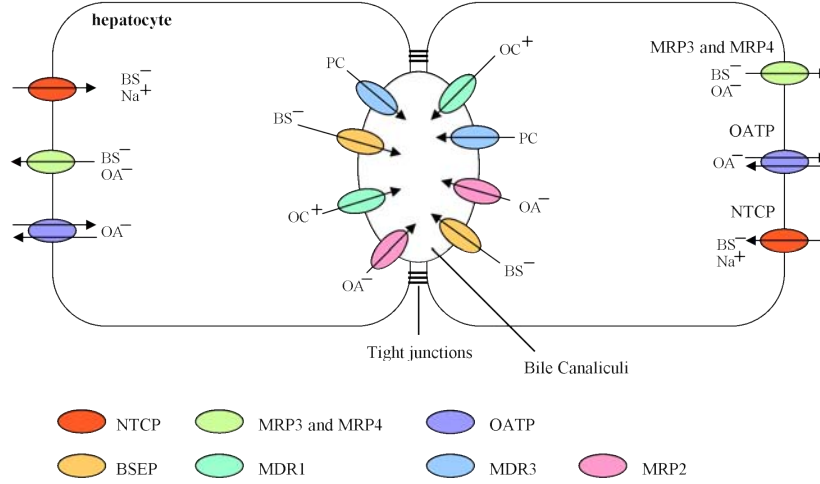
Figure 1.2: **Scheme of bile salt.**
The catabolism of cholesterol in the liver yields bile salts (BS). The bile salt export pump (BSEP) protein is located in hepatocytes and mediates the transport of BS from hepatocytes into the bile canaliculi. Simultaneously, organic anion (OA) and organic cation (OC) were released to the bile canaliculi. The ATP-binding cassette, sub-family C (CFTR/MRP), member 2 (MRP2) mediates the OA release and ATP-binding cassette, sub-family B (MDR/TAP), member 1 (MDR1, ABCB1) mediates the OC release. MDR3 is responsible for the transport of phosphatylcholine (PC) from hepatocytes into the bile canaliculi. The uptake of BS into the liver sinusoid is dependent on an OA mechanism and is mediated by the ATP-binding cassette, sub-family C (CFTR/MRP), member 4 (MRP4/ABCC4) and MRP3. The solute carrier organic anion transporter family, member 1A2 (OATP, SLCO1A2) is in charge of the sinusoidal uptake and release OA. The bile returns into the liver by sodium dependent mechanism mediated by solute carrier family 10 (sodium/bile acid cotransporter), member 1 (NTCP, SLC10A1).

Hepatocyte transplantation was pioneered 1967 when the first enzymatic isolation of hepatocytes was performed successfully (Howard et al. [1967]). Two years later a combined technique of mechanical and enzymatic isolation carried out by Berry and Friend [1969] and was further developed by Seglen [1976]. From this followed that the first attempts of hepatocyte transplantation were done at the same year. It took untill 1992 when hepatocytes were successfully transplanted in a human body. To date there is no other effective method for end stage liver patients and many genetic liver disorders as orthotopic liver transplantation (OLT) (Matas et al. [1976]; Hess et al. [1976]; Searle and Flaks [1976]; Mito et al. [1992]; Fox and Chowdhury

[2004]; Mazaris et al. [2005]; Mir et al. [2006]; Ishikawa et al. [2010]; Asgari et al. [2013]; Utsumi et al. [2014]; Girometti et al. [2014]). However, this method includes the risk of surgery and carries two major problems: first, the lack of a compatible donor and, second, the risk of organ rejection (Lorenzini et al. [2008]). Additionally, the number of people who need a liver transplantation increaes, but the number of organ donors decreases since years. 1,305 new patients came on to the existing waiting list for liver transplantation in Germany in 2013. Only 970 liver transplantations took place, including 83 after living donation (Eurotransplant International Foundation Annual Report 2013, https://www.organspende-info.de/sites/all/files/files/ Jahresbericht_Eurotransplant_2013.pdf, retrieved 25.11.2014; Deutsche Stiftung Organtransplantation Jahresbericht 2013, http://www.dso.de/uploads/tx_dsodl/JB_ 2013_Web_05.pdf, retrieved 25.11.2014). One million patients die each year from acute and chronic liver diseases worldwide. The orthotopic liver transplantation (OLT) is still the only effective cure for end-stage liver patients and many genetic disorders. OLT is the transplantation of a healthy liver from a deceased person or the transplatation of a part of a healthy liver from a healthy person into a liverish patient. This treatment includes the risk of donor incompatibility, transplantation surgery and organ rejection (Fox and Chowdhury [2004]; Mazaris et al. [2005]; Mir et al. [2006]; Ishikawa et al. [2010]; Lorenzini et al. [2008]; Gonzalez and Keeffe [2011]; Asgari et al. [2013]; Girometti et al. [2014]; Utsumi et al. [2014]). In order to close the gap between needed and available livers for transplantation alternative strategies are required. Therefore, one of the future goals of regenerative medicine is to derive a whole liver from patient specific cells. With the entering of induced pluripotent stem cells and differentiation of patient specific cells great hopes emerged to tackle this challenge. Immunoreaction could be avoided and thus the risk of rejection will drop dramatically. Soon this vision could become reality: obtain some skin cells and make a whole liver from them. This idea is not new, but until now it has not been carried out successfully. Before generating a whole liver *in vitro* the liver as a whole including its development (hepatogenesis) needs to be understood.

1.1 Hepatogenesis

Hepatogenesis is best understood in mice and rats. The endodermal specification in the mouse embryo starts at the six somite-stage from day seven to nine after fertilization. At day 10 after fertilization (E10) the liver bud is formed by hepatoblasts, which further differentiate into hepatocytes (Figure 1.3). The maturation of the liver continues postnatally (Houssaint [1980]; Medlock and Haar [1983]; Cascio and Zaret [1991]; Watt et al. [2001]; Tremblay and Zaret [2005]; Zhao and Duncan [2005]; Watt et al. [2007]). Hepatocytes constitute the liver's biggest cell mass accounting for more than 75 % (Figure 1.1). The liver is able to regenerate itself *in vivo*. If two thirds are removed, the cells start to proliferate immediately and the lost cell mass will be replaced. *In vitro* the cells lose this ability and several experiments were conducted to activate the ability for regeneration *in vitro*. Although, rodent hepatocytes can be expanded. It is not possi-

ble to culture human hepatocytes *in vitro* highlighting the liver as a complex structure (Richman et al. [1976]; Shimaoka et al. [1987]; Mitaka et al. [1991]; Block et al. [1996]; Mitaka [1998]; Runge et al. [2000]; Mizuguchi et al. [2001]; Uyama et al. [2002]; Zhao and Duncan [2005]; Shan et al. [2013]). During development (hepatogenesis) many pathways and cytokines are involved to generate this complex organ. Before generating a whole liver *in vitro* the liver as a whole including the hepatogenesis needs to be understood.
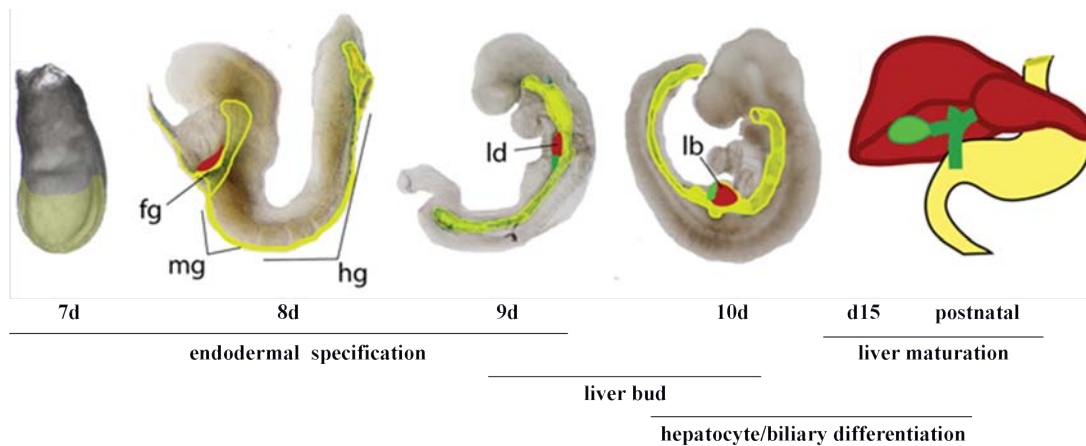
Figure 1.3: **Time line of mouse liver development.**
Schematic of liver development in mouse. The endodermal specification in the mouse embryo starts at the six somite-stage from E7 to E9. The endoderm is patterned along the anterior-posterior (A - P) axis into foregut (fg), midgut (mg) and hindgut (hg) progenitor domains at E8. The liver diverticulum (ld) forms by E9. At E10 the liver bud (lb) is formed. Around E15 hepatoblasts are differentiating into hepatocyte and biliary cells. The maturation of the liver continue untill after birth. Adapted from: http://www.stembook.org/node/512; retrieved 09.06.2014.

1.1.1 Embryogenesis - essential signaling pathways

Hippo pathway

One of the main pathways involved in early developmental processes is the Hippo pathway. The Hippo pathway is responsible for early embryonic development, embryonic and adult stem cells, cell proliferation, differentiation, apoptosis, organ size, specific functions in adult organs, tissue regeneration and tumorgenesis (Pan [2007]; Camargo et al. [2007]; Dong et al. [2007]; Zhao et al. [2007]; Zhao et al. [2011a]; Tremblay and Camargo [2012]; Cockburn et al. [2013]; Harvey et al. [2013]; Li et al. [2013]; Lin et al. [2013]; Yimlamai et al. [2014]).

The Hippo pathway operates as follows. The STE20-like protein kinase 1 (MST1) and MST2 (known as Hippo in *Drosophila melanogaster*), their co-factor Salvador (SAV) as well as the Large tumour suppressor homologue 1 (LATS1) and LATS2 (known as Warts in *D. melanogaster*) are the core components of the mammalian Hippo pathway (Figure 1.4A). SAV activates MST and MST phosphorylates LATS. The activity of the Hippo

pathway is mediated by the phosphorylation of LATS proteins. The LATS proteins phosphorylate the yes-associated protein (YAP) and the transcriptional co-activator with PDZ-binding motif (TAZ) on multiple sites. YAP and TAZ form a complex. This phosphorylated YAP/TAZ complexes persist in the cytoplasm, accumulate and were degraded by proteasomes. Dephosphorylation of YAP and TAZ inactivates the Hippo pathway. The YAP/TAZ complex translocates into the nucleus, accumulates there and regulates gene transcription combined with DNA-binding transcription factors as the TEA domain family members (TEADs) (Figure 1.4A; Zhao et al. [2007]; Halder et al. [2012]).

The Hippo signaling pathway influences fate and size of liver cells and it is essential for the maintenance of the differentiated hepatocyte state. *In vivo* experiments in mice show that inactivation of the Hippo signaling pathway adult hepatocytes dedifferentiate and acquire progenitor characteristics. For example, the lack of NF2 results in over expression of YAP in liver, which induces an overgrown liver. Over expression of the oncoprotein Yes-associated protein 1 (YAP1) in mice leads to increased liver size of more than 4-fold (Camargo et al. [2007]; Yimlamai et al. [2014]). The removal of MST1 and MST2 function in mice leads to overgrown of organs such as liver and heart, as well as the hyperproliferation of intestinal epithelium resulting from YAP hyperactivation. Another experimental animal is *Drosophila melanogaster*. The overgrown of adult structures in flies come from mutations in most components of the Hippo pathway (Halder and Johnson [2011]; Halder et al. [2012]).

The core components of the Hippo pathway are regulated by several inputs such as cell-cell adhesions and apicobasal polarity complexes. For example, angiomotin family proteins are localized to junction proteins (e.g. adherens and tight junctions). Angiomotin family proteins can bind to MST, LATS or YAP and activate the phosphorylation of the YAP/TAZ complex. Another example is neurofibromin 2 (NF2), which is associated with the E-cadherin complex. E-cadherin is an important adhesion molecule. NF2 can bind to SAV, the MTS or LATS proteins to activate the Hippo pathway and phosphorylate the YAP/TAZ complex (Zhao et al. [2007]; Paramasivam et al. [2011]; Halder et al. [2012]; Cockburn et al. [2013]; Hirate et al. [2013]; Nakagawa et al. [2014]).

The YAP/TAZ complex acts as a transcriptional regulator and controls the activity of TGF-β-SMAD signaling. The transforming growth factor (TGF)-β family phosphorylate receptor-dependent SMAD2/3 which binds SMAD4. This complex translocates into the nucleus and interacts with TAZ, which is responsible for the SMAD complex to stay in the nucleus where it couples to the SMAD complex to the transcription structure (Varelas et al. [2008]). As a result of the active Hippo pathway the YAP/TAZ complex is phosphorylated and cannot shuttle into the nucleus. This leads to a suppression of SMAD nuclear accumulation and cytoplasmatic stay of the YAP/TAZ complex (Varelas et al. [2010]). In the cytoplasm the YAP/TAZ complex can also interact with the Crumbs complex which contributes to the stabilization and maturation of junctional structures (Varelas et al. [2010]). In mature hepatocytes the activity of YAP is more cytoplasmic than nuclear because they show high Hippo pathway activity (Yimlamai et al. [2014]).

Additionally, YAP plays an essential role in mammalian liver by cell fate decision and affects the Notch signaling pathway (Yimlamai et al. [2014]). The Notch signaling pathway plays an important role in ductal specification during development and is transiently activated during liver regeneration (Khler et al. [2004]; Zong et al. [2009]; Hofmann et al. [2010]).
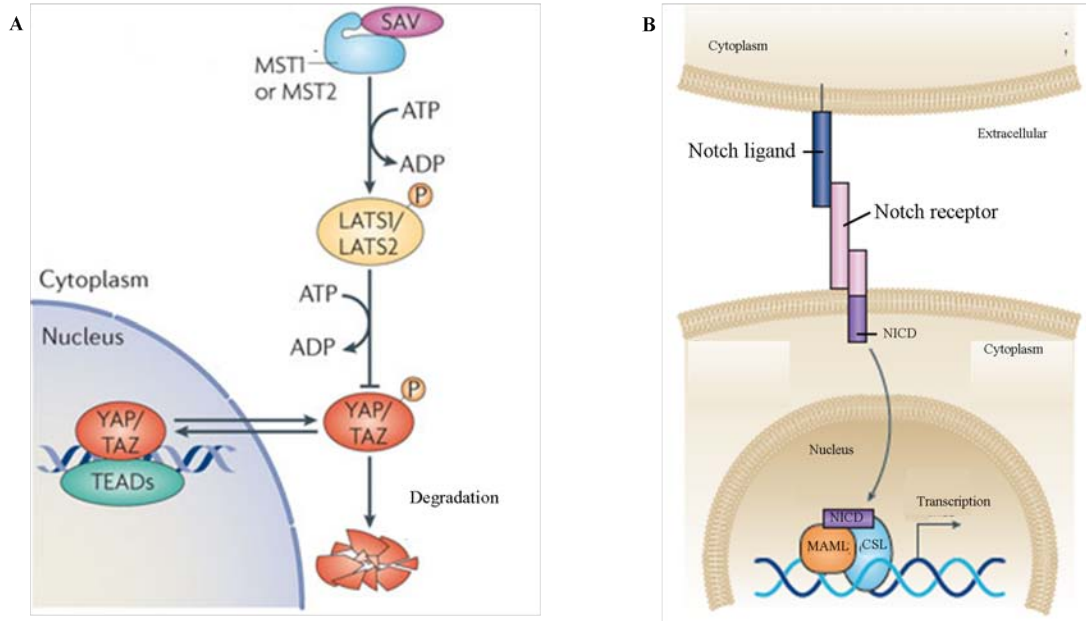
Figure 1.4: **Scheme of the Hippo and Notch pathway.**
A) The STE20-like protein kinase 1 (MST1) or MST2 together with their co-factor Salvador (SAV) promote the phosphorylation of Large tumour suppressor homologue 1 (LATS1) and LATS2. MST kinase phosphorylates LATS proteins. LATS proteins phosphorylate the yes-associated protein (YAP) and the transcriptional co-activator with PDZ-binding motif (TAZ) on multiple sites. If the YAP and TAZ are phosphorylated they stay in the cytoplasm, accumulate and were degraded by proteasome. YAP and TAZ are dephosphorylated, if the Hippo pathway is inactivated. They translocate into the nucleus, accumulate there and regulate gene transcription combined with DNA-binding transcription factors as the TEA domain family members (TEADs). Adapted from: Halder et al. [2012]. **B)** The canonical Notch signaling is characterized by the extracellular interaction of a Notch transmembrane receptor (in mammalian Notch 1 - 4) with a canonical Notch transmembrane ligand (in mammalian Jagged (JAG) 1 - 2, Delta-like (DLL) 1 - 4). The contact between receptor and ligand initiates the proteolytic cleavage of the receptor and the subsequent release of the Notch intracellular domain (NICD) of the receptor. The NICD then translocates to the nucleus, where it interacts with a CBF1/Suppressor of Hairless/LAG-1 (CSL) family DNA-binding protein (C promoter-binding factor (CBF1)) and Mastermind-like protein (MAML). The interaction initiates the transcription of Notch target genes. Adapted from: Andersson and Lendahl [2014].

Notch pathway

Notch signaling is an evolutionary conserved mechanism that plays amongst others an important role in cell fate decisions in the early liver development. Multiple Notch ligands, receptors and Hes/Hey family members are expressed in embryonic liver (Artavanis-Tsakonas et al. [1999]; Louis et al. [1999]; Crosnier et al. [2000]; Jones et al. [2000]; Nijjar et al. [2001]; Loomes et al. [2002]; McCright et al. [2002]; Flynn et al. [2004]; Kodama et al. [2004]; Sumazaki et al. [2004]; Tanimizu and Miyajima [2004]; Zong et al. [2009]; Andersson and Lendahl [2014]). The Notch pathway can be divided into canonical Notch signaling and non-canonical Notch signaling. The canonical Notch signaling is characterized by the extracellular interaction of a Notch transmembrane receptor (in mammalian Notch1 - 4) with a canonical Notch transmembrane ligand (in mammalian Jagged (JAG) 1 - 2, Delta-like (DLL) 1 - 4) (Figure 1.4B). The ligand is on the cell surface of a neighboring cell. The interaction between receptor and ligand initiates the proteolytic cleavage of the receptor and the subsequent release of the Notch intracellular domain (NICD) of the receptor. Then the NICD translocates into the nucleus. In the nucleus the NCID interacts with a CBF1/Suppressor of Hairless/LAG-1 (CSL) family DNA-binding protein, C promoter-binding factor (CBF1) and Mastermind-like protein (MAML). The interaction initiates the transcription of Notch target genes. The non-canonical Notch signaling can be initiated by a non-canonical ligand. In some forms of non-canonical signaling there is no involvement of CSL (reviewed by D'Souza et al. [2010]; Heitzler [2010]; Andersson et al. [2011]; Andersson and Lendahl [2014]).

During liver and biliary development Notch coordinates biliary fate and duct morphogenesis in a temporal- and dose-dependent way, which is a late event in liver development (Figure 1.5). In addition, the Notch pathway regulates embryonic biliary fate and second biliary layer formation as well as hepatobiliary remodeling after injury. Upregulation of Notch signaling pathway components in undamaged adult liver result in several liver diseases (Nijjar et al. [2001]; Nijjar et al. [2002]; Flynn et al. [2004]; Zong et al. [2009]). Loss of Notch signaling induces developmental block of the bile duct. Already reduced activity influences developmental processes negatively. In heterozygous mice a defect of Notch2 and Jag1 is monitored as well as in patient with Alagille syndrome. After injury the liver rejuvenate and the Notch signaling reprograms hepatocytes into endothelial biliary cells. In the liver Notch signaling is also involved in lipid content regulation. The inhibition of Notch signaling results in reduced hepatic glucose production and triggers increased fatty liver (McCright et al. [2002]; Zong et al. [2009]; Yanger et al. [2013]; Pajvani et al. [2013]; Andersson and Lendahl [2014]). Increased Notch signaling causes carcinoma in liver. The over expression of Notch1 ICD in mice results in several carcinoma. This is also observed in human cholangiocarcinoma cells, the excessive availability of NOTCH1, NOTCH3 and JAG1 could be monitored. The Notch signaling pathway is a functional important effector downstream of the Hippo transducer YAP (Villanueva et al. [2012]; Zender et al. [2013]; Yimlamai et al. [2014]).
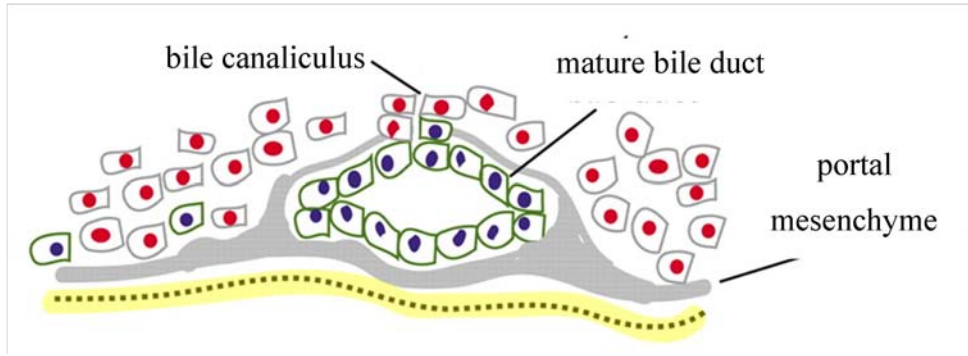
Figure 1.5: **Scheme of bile duct formation by Notch signaling.**
Endothelial-derived Jag1 positive cells activates Notch signaling and Hes1 expression in the neighboring hepatoblasts in early liver development (E12.5 - 14.5). Afterwards formation of the first ductal plate layer starts at E14.6 - 16.5. Tubulogenesis between E16.5 and E17.5 occurs at discrete sites of active Notch signaling in neighboring hepatocytes and give rise to a primitive ductal structure. Cells comprising the second (outer) layer of this asymmetric tubule undergo biliary differentiation between E17.5 and P2 (not shown here). Consecutively growth of the portal mesenchyme and loss of unincorporated biliary epithelial cells leads to the formation of a mature portal tract by P15. Biliary epithelial cells in both layers of the ductal plate express Jag1, the endothelium cells (yellow) and biliary epithelial cells (green cells with blue nuclei). Hepatocytes are the grey cells with red nuclei. Adapted from: Zong et al. [2009].

TGFβ superfamily

The TGFβ superfamily is a huge protein group including the transforming growth factor βs (TGFβs), the bone morphogenetic proteins (BMPs), Nodal, growth differentiation factors (GDFs) and Activins. Members of the TGFβ superfamily are involved in embryonic development, maintenance and differentiation of embryonic stem cells, somatic stem cells and cancer stem cells as well as in development and maintenance of various organs (Massagu et al. [1987]; Massagu [1992]; Wilson and Hemmati-Brivanlou [1995]; Brandenberger et al. [2004]; Qi et al. [2004]; Clotman and Lemaigre [2006]; Xu et al. [2008]; Watabe and Miyazono [2009]; Wu and Hill [2009]). In general, TGFβ superfamily members bind specific type I and II transmembrane serine threonine kinase receptors. This leads to their activation and phosphorylation of intracellular receptor regulated Smad proteins (R-Smad). The TGFβs, Nodal and Activins activate Smad2/3 by binding the type I receptors ALK4/5/7. In contrast, BMPs and GDFs transduce their signal through ALK2/3/6 and activating Smad1/5/8 (reviewed by Miyazono et al. [2005]; Schmierer and Hill [2007]; Ross and Hill [2008]; Wrighton and Feng [2008]; Umulis et al. [2009]; Heldin and Moustakas [2012]; Massagu [2012]).

The TGFβ pathway is eponymous for this cytokine superfamiliy and is representative of Activin and Nodal pathways (Figure 1.6). TGFβ binds to the TGFβ receptor II (TβRII) which recruits the type I receptor TGFβ receptor I (TβRI/ALK5). Transphosphorylation of TβRI activates this process and initiates downstream signaling. The type I receptor phosphorylates Smad2/3 and they form a heterotrimeric complex with the co-

Smad, Smad4. This Smad complexs consists of two receptor-regulated Smad proteins (R-Smad) and one co-Smad. In this case, two Smad2 or two Smad3 or one Smad2 and one Smad3 with Smad4 (co-Smad) form a complex. This trimer (e.g. Smad2/Smad3/Smad4) shuttles into the nucleus and regulates the transcription of various genes in collaboration with other transcription factors, co-activators and co-repressors. When inhibitors of Smad-activated proteins are active the inhibition results from a negative feedback by a diversity of mechanisms. Here Smad7 works as the inhibitor (reviewed by Kretzschmar and Massagu [1998]; Miyazono et al. [2005]; Derynck and Zhang [2003]; Schmierer and Hill [2007]; Kang et al. [2009]; Vogt et al. [2011]).
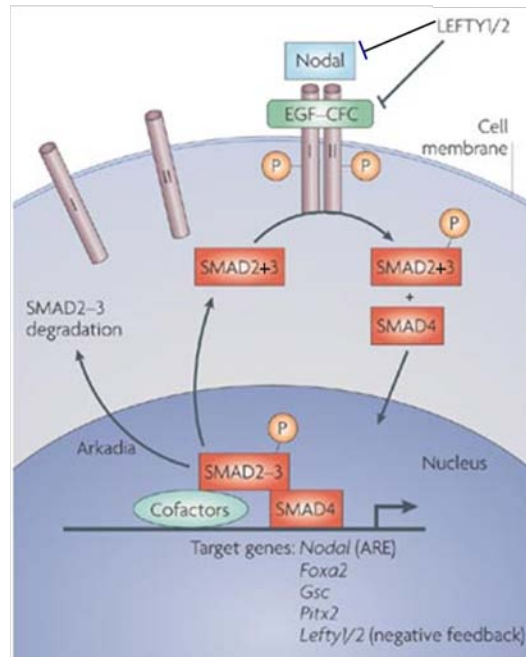
Figure 1.6: **Scheme of Nodal-Smad signaling.**
Nodal binds to its receptors EGF-CFC. These receptors phospharylate Smad2 and Smad3. Smad2/3 builds a trimer complex with Smad4 and then shuttles into the nucleus where the complex binds to the DNA. Together with co-factors this complex regulates the expression of various genes. Amongst others the expression of *Lefty1* and *Lefty2* obtain activation. This induction activates a negative-feedback circuit to the Nodal-Smad signaling pathway. Adapted from: Arnold and Robertson [2009].

In terms of signal transduction, the bone morphogenetic protein (BMP) pathway is similar to the TGFβ pathway, but receptor binding is more diverse. The BMP ligands BMP2 and BMP4 bind to type I receptor Alk3 and Alk6 which recruits the type II receptor BMPRII/ActRII and ActRIIB. In contrast, BMP6 and BMP7 bind to type II receptor ActRII/ActRIIB and recruit type I receptor Alk2, Alk3 and Alk6. In either case, the type I receptor phosphorylates receptor regulated Smad proteins (R-Smad; Smad1/5/8) and they form a heterotrimeric complex with the co-Smad, Smad4. This Smad complex consists of two R-Smad and one co-Smad and shifts as a trimer into the nucleus. There the complex binds to specific DNA sequences and regulates the tran-

scription of various genes in collaboration with other transcription factors, co-activators and co-repressors. The Smad-activated proteins are active as the inhibitors. The inhibition results from a negative feedback by a diversity of mechanisms. Here Smad6 act as a inhibitor in addition to Smad7 (reviewed by de Caestecker [2004]; Moustakas and Heldin [2009]; Heldin and Moustakas [2012]).

In undifferentiated human embryonic stem cells (hESC) TGFβ, ACTIVIN and NODAL signaling are observed by detection of phosphorylated and nuclear localized SMAD2. Upon early differentiation their activity decreased and BMP signaling increased. Depending on the concentration ACTIVIN induces definitive endoderm (DE) or mesoderm development. In mouse embryos loss of Smad2 activity results in early embryonic lethality. The development of definitive endoderm is interrupted by the loss of Smad2, Smad4 or primary targets of them: FoxH1, Foxa2 (HNF3β, Eomes) (Dufort et al. [1998]; Waldrip et al. [1998]; Tremblay et al. [2000]; Yamamoto et al. [2001]; Hoodless et al. [2001]; Vincent et al. [2003]; Chu et al. [2004]; James et al. [2005]; Tada et al. [2005]; Arnold et al. [2008]). The development and specification of DE needs high Nodal activity, which is higher than for mesoderm development. The Activin/Nodal-Smad signaling activates DE specific genes and *Eomes*. Eomes interacts with Smad2/3 and inhibits the expression of mesoderm specific genes (Hart et al. [2002]; Shen [2007]; Teo et al. [2011]).

The development of DE is dependent on the concentration of ACTIVIN and NODAL. BMP signaling induces differentiation of hESC as well as suppress E-Cadherin/CDH1 (E-CAD) and pluripotency for DE development (Xu et al. [2002]; Ying et al. [2003]; Pera et al. [2004]; Qi et al. [2004]; Teo et al. [2011]; Teo et al. [2012]; Lichtner et al. [2013]). TGFβ is a key regulator of Epithelial-to-Mesenchymal Transition (EMT). Numerous stimuli and cytokines can activate EMT, but TGFβ as SMAD-mediated and Non-SMAD-mediated signaling seems to be the main regulator of EMT. Smad-dependent signaling activates AKT and glycogen synthase kinase 3 beta (GSK3β) which leads to β-catenin nuclear translocation, E-CAD and ZO-1 inhibition and EMT. Smad-independent signaling activates e.g. RHOA, PAR6 and MAPK which leads to tight junction depletion, cytoskeleton and cell-cell contact rearrangement, stress fiber formation as well as activation of mesenchymal gene-expression (Miettinen et al. [1994]; Oft et al. [1998]; Fujita et al. [2000]; Bhowmick et al. [2001]; Rajasekaran et al. [2001]; Chen et al. [2002]; Kim et al. [2002]; Grille et al. [2003]; Masszi et al. [2003]; Barrios-Rodiles et al. [2005]; Ozdamar et al. [2005]).

1.1.2 Operative signaling pathways in Hepatogenesis

The TGFβ/Nodal signaling is one of the most important signaling pathways for the entire development of an embryo. It activates Smad2/3 and induces directly the expression of the pluripotency factor *Nanog*. It is also required to increase and maintain endodermal gene expression (Yasuo and Lemaire [1999]; Engleka et al. [2001]; Chang and Hemmati-Brivanlou [2000]; Clements and Woodland [2003]; Xu et al. [2008]). At E3.5 of mouse embryo development, when the inner cell mass (ICM) and the trophoectoderm (TE) has formed, the ICM consists of a mixture cell population (Figure 1.7A).

There are cells which express *GATA6* and cells which express *Nanog*. These cells are not uniformly arranged, but they are positioned randomly and mosaic. Two lineages segregate from the ICM, the primitive endoderm (GATA6-positive cells) and the pluripotent epiblast (Nanog-positive cells) (Chazaud et al. [2006]). Mice experiments showed that GATA6-knockout embryos died between E5.5 and E6.5 dpc. Expression of *GATA6* starts around day 3.5 dpc in the ICM and mediate TGFβ/Nodal signaling during endoderm formation (Figure 1.7; Albano et al. [1993]; Hudson et al. [1997]; Morrisey et al. [1998]; Koutsourakis et al. [1999]; Rossant et al. [2003]). *Sox17a* and *HNF1β* become directly activated by GATA6. For the full induction of *Sox17a* and *HNF1β* the activaty of GATA4, 5 and 6 is required whereby activation sequence is GATA6, GATA4 and then GATA5. These is necessary for the full endodermal gene expression and gut formation *in vivo*, too (Afouda et al. [2005]).
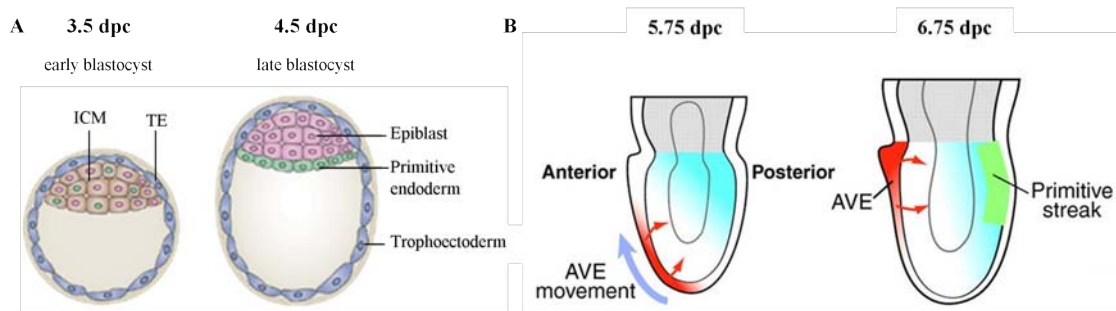
Figure 1.7: **Nodal signaling in early mouse embryo.**
A) At E3.5 of mouse embryo development the inner cell mass (ICM) and the trophoectoderm (TE) has formed. The ICM is a mixture of *GATA6* (cells with green nucleus) and *Nanog* (cells with pink nucleus) expressing cells. From the ICM two lineages segregate, the primitive endoderm (GATA6-positive cells) and the pluripotent epiblast (Nanog-positive cells). **B)** At E5.25 days post-coitum (dpc) *Nodal* is expressed in the complete epiblast and induces the formation of anterior visceral endoderm (AVE, step not shown). The Nodal signaling initiates the movement of the AVE (red area, movement shown by purple arrow) to the anterior side at E5.75 dpc. In this area the Nodal antagonists *Lefty* and *Cer1* are expressed. A high expression level of *Nodal* in the posterior area induces the development of the primitive streak (green area, shown at E6.75 dpc). Adapted from: Shen [2007] and Arnold and Robertson [2009].

Liver development requires the interaction with mesenchymal tissue in the region of the septum transversum (Figure 1.8). Liver-specific genes are not activated, if the ventral foregut endoderm from 2 - 6 somite-stage embryo is cultured without cardiac mesoderm or Fgf (Houssaint [1980]; Medlock and Haar [1983]; Deutsch et al. [2001]; Rossi et al. [2001]). Fgf signaling from the cardiogenic mesoderm induces the liver in the ventral foregut endoderm. Mouse endoderm explants which were cultured without cardiogenic mesoderm were treated only with Fgf. Other experiments could show that mouse null mutations for individual components of the Fgf signaling pathway are lethal before hepatic induction or have minimal phenotype (Yamaguchi et al. [1992]; Meyers

et al. [1998]; Weinstein et al. [1998]; Jung et al. [1999]; Miller et al. [2000]). The septum transversum mesenchyme (STM) cells derived from the lateral mesoderm plate (Figure 1.8). These cells were found in mouse explants of cardiogenic mesoderm and ventral foregut endoderm. The bone morphogenetic proteins 2 and 4 (Bmp2 and Bmp4) are strongly expressed in the STM before and during the induction of hepatic development. The development of several ventral structures in an embryo is disturbed by the deletion of Bmp4 (Jones et al. [1991];Furuta et al. [1997]; Hogan [1999]; Rossi et al. [2001]).
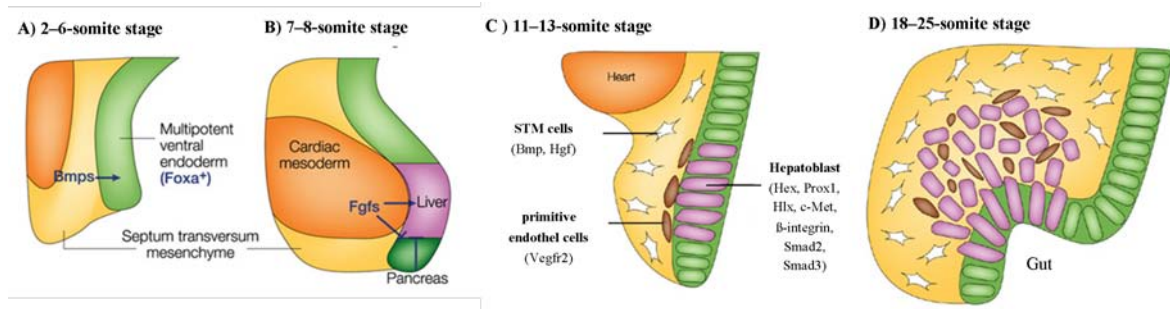
Figure 1.8: **Signal and tissue interactions which regulate liver development.**
A) At the 2 - 6 somite stage the expression of transcription factors specific for endoderm (Foxa) as well as signals which affect the endoderm (BMP signaling) initiate the liver development. The bone morphogenetic proteins (Bmp) emanate from the adjacent cells of septum transversum mesenchyme (STM). **B)** Between the somite stages seven and eight the tissue specification take place. From the cardiac mesoderm the fibroblast growth factor (Fgf) signal activates the liver gene program in proximal endoderm and blocks gene program for pancreas. **C)** The signals which specified the hepatic endoderm (HE) cells also initiate a morphological change of the cells during the 11 and 13 somite stage, the HE become pillared in shape. Signaling molecules from the STM cells and primitive endothelial cells (e.g. Bmp, Hgf and Vegfr2) and transcription factors (e.g. Hex, Prox1, Hlx and c-Met) are essential to promote the morphogenesis of the liver bud itself (see D). **D)** By formation of the rostral diverticulum of the gut the Liver-bud morphogenesis is build, the extracellular matrix around the hepatoblasts obtains remodel and the E-cadherin-based connections between the cells is build, as well as the proliferation and migration into the surrounding STM take place. The growing liver obtains invade by haematopoietic cells and the organ becomes distinct from the gut epithelium. Abbreviation: Bmp = bone morphogenetic protein; c-Met = Hgf receptor; Hgf = hepatocyte growth factor; Vegfr2 = vascular endothelial growth factor receptor 2. Adapted from: Zaret [2002].

Haematopoietic area expressed homeobox (*Hex*) and Prospero-related homeobox 1 (*Prox1*). These are two main homeodomain transcription factors which have the earliest known specific effects on hepatic endoderm (HE) and on liver-bud morphogenesis. Before induction of hepatic endoderm Hex is expressed in mouse in the anterior visceral endoderm and the anterior definitive endoderm (DE). Later on Hex is expressed in the liver, thyroid and endothelial cells in adult vertebrates. Prox1 is involved in cell - cell interactions and extra cellular matrix (ECM) remodeling and acts immediately after Hex in hepatic morphogenesis (Crompton et al. [1992]; Hromas et al. [1993]; Oliver et al. [1993]; Thomas et al. [1998]; Sosa-Pineda et al. [2000]).

β1-integrin is part of a heterodimeric receptor for laminins and collagens. The loss of β1-integrin results in failure to colonize hepatocytes in the liver of chimeric mouse (Hynes [1992]; Fssler and Meyer [1995]). The hepatoblast growth the H2.0-like homeobox gene (*Hlx*) positively regulates the synthesis of paracrine factors (Figure 1.8). In Hlx knockout mice the liver is a small bud (Hentsch et al. [1996]). The STM express the hepatocyte growth factor (Hgf) and hepatoblasts express c-Met (the Hgf receptor). Hgf and c-Met knockout mice result in apoptosis of the hepatoblasts. C-Met has a anti-apoptotic role for Hgf signaling. Smad2 and Smad3 are involved in the Tgfβ signaling. Heterozygote inactivation of both leads to fetal liver hypoplasia. In adult liver Tgfβ signaling inhibit hepatocyte proliferation. Hgf and Tgfβ both are in charge of growth signals in liver development. (Bladt et al. [1995]; Schmidt et al. [1995]; Amicone et al. [1997]; Isfort et al. [1997]; Grasl-Kraupp et al. [1998]; Weinstein et al. [2001]).

WNT/β-Catenin pathway

WNT/β-Catenin is a conserved pathway which plays an important role during vertebrate embryogenesis, tissue differentiation, organogenesis and regulates stem cell pluripotency. This cascade cross-talks with other pathways, including retinoic acid, FGF, TGF-β and BMP. WNTs are secreted glycoproteins which bind to Frizzled receptors, which then triggers displacement of the multifunctional kinase GSK-3β from a regulatory APC/AXIN/GSK-3β-complex (Figure 1.9). If the WNT signal is not operative (Off-state) CK1 and the APC/AXIN/GSK-3β-complex bind to β-Catenin and become phosphorylated. β-Catenin is also an integral E-Cadherin cell-cell adhesion adaptor protein and transcriptional co-regulator. The phosphorylation leads to its ubiquitination and proteasomal degradation by the β-TrCP/SKP pathway (Li et al. [2012]; Wehrli et al. [2000]; reviewed by MacDonald et al. [2009]; Clevers and Nusse [2012]).

Mouse studies show that the Wnt signaling is necessary for the extension of the anterior-posterior axis in the primary embryo. During the patterning of the anterior-posterior axis into forgut, midgut and hindgut the Wnt signaling is inhibited in the forgut region by e.g. SFRP, but expressed in the hindgut region. Subsequently Wnt signaling is required for hepatogenesis (Liu et al. [1999]; Yamaguchi et al. [1999]; McLin et al. [2007]).

The Leucine-rich repeat-containing G-protein-coupled receptor (LGR) 5 is a WNT target gene by binding the WNT agonist R-SPONDIN (RSPO) 1. LGR5 is part of the Frizzled/LRP receptor complex and is responsible for the activation of the WNT signaling in adult stem cells and hereby for the maintenance of the stem cells and progenitor cells as liver progenitor cells (Jaks et al. [2008]; de Lau et al. [2011]; Sato et al. [2011]; ten Berge et al. [2011]; Barker et al. [2012]; Cheng et al. [2012]; Barker et al. [2013]; Gil-Sanchis et al. [2013]; Huch et al. [2013]).
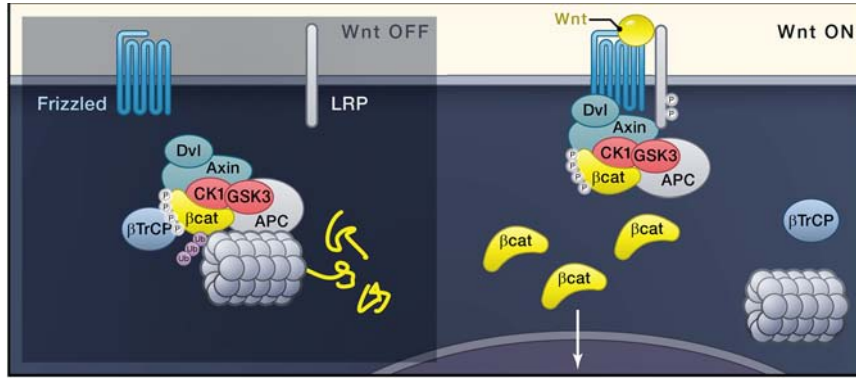
Figure 1.9: **Activation and inactivation of the Wnt/β-catenin pathway.**
If the Wnt-signal is inactive (Off-state) the destruction complex resides in the cytoplasm. There the complex binds to β-catenin through β-TrCP. This raises that β-catenin is phosphorylated and ubiquitinated. The proteasome recycles the complex by degrading β-catenin. Wnt binds to Frizzled receptors, which then triggers displacement of the multifunctional kinase GSK3β from a regulatory APC/Axin/GSK3β-complex and induces the association of the intact complex with phosphorylated LRP (low-density lipoprotein (LDL)-receptor-related protein). The complex phosphorylates β-catenin, but the ubiquitination by β-TrCP is blocked. Synthesized β-catenin accumulates and translocates into the nucleus to activate target genes. Adapted from: Clevers and Nusse [2012].

FGF pathway

The fibroblast growth factors (FGFs) play important roles during vertebrate development, liver generation and in a wide array of biological processes like cell growth, differentiation, angiogenesis and tissue repair, as well as maintenance of embryonic stem cells. In general, FGF binds to the FGF receptor (FGFR) which induces FGFR dimerization (Figure 1.10). Transphosphorylation triggers the kinase activation. Subsequently, the FGFR kinase activates its intracellular substrates by phosphorylation. The FGFR substrate 2α (FRS2α) is a major substrates of FGFR kinase, which is constitutively associated with the receptor kinase, and phospholipase Cγ1 (PLCγ1). FRS2α binds to the adaptor protein growth factor receptor-bound 2 (GRB2). GRB2 recruits the guanine nucleotide exchange factor son of sevenless (SOS) and binds it to the signaling complex. Then, SOS activates RAS GTPase, which initiates activation of the MAPK cascade. MAPK translocates from the cytoplasm to the nucleus. There it phosphorylates and, hence, activates immediate early gene transcription factors, such as FOS to induce transcription of specific genes (Kouhara et al. [1997]; Carpenter and Ji [1999]; Bttcher and Niehrs [2005]; Thisse and Thisse [2005]; Furdui et al. [2006]; Chen et al. [2008]; Turner and Grose [2010]).

During mouse embryonic development (4 - 7 somites stage) Fgf signaling from the developing heart (in addition of Bmp signaling from septum transversum mesenchyme (STM)) induces hepatic development in the ventral foregut endoderm (Figure 1.8; Burgess and Maciag [1989]; Baldin et al. [1990]; Maher [1996]; Jung et al. [1999]; Rossi et al. [2001]).
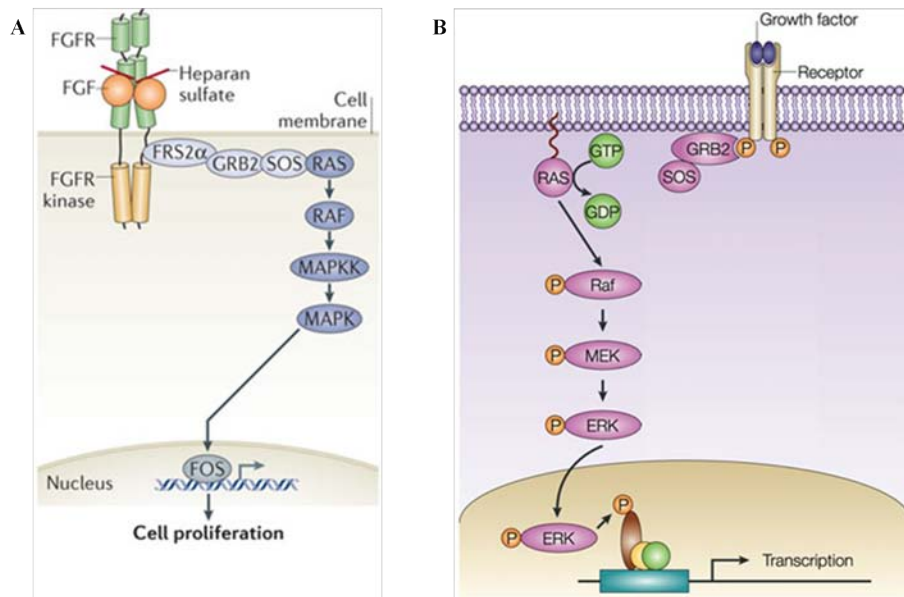
Figure 1.10: **Scheme of FGF and MAPK/ERK signaling cascade.**
A) FGF signaling: Fibroblast growth factor (FGF) binds to the FGF receptor (FGFR) which induces FGFR dimerization. Transphosphorylation triggers the kinase activation. Subsequently, the FGFR kinase phosphorylates its intracellular substrates which is activated by the phosphorylation. The FGFR substrate 2α (FRS2α) is a major substrates of FGFR kinase, which is constitutively associated with the receptor kinase, and phospholipase Cγ1 (PLCγ1). FRS2 binds the adaptor protein growth factor receptor-bound 2 (GRB2)113. GRB2 recruits the guanine nucleotide exchange factor son of seven-less (SOS) and binds it to the signaling complex. Then SOS activates RAS GTPase, which initiates activation of the MAPK cascade. MAPK translocates from the cytoplasm to the nucleus. There it phosphorylates and hence activates immediate early gene transcription factors, such as FOS to induce transcription of specific genes. **B)** MAPK/ERK signaling: Mitogen-activated protein kinase (MAPK) and the extracellular signal-regulated kinase (ERK) signaling cascade (MAPK/ERK) is activated by several receptors which are involved in growth and differentiation including receptor tyrosine kinases (RTKs). The architecture of the pathway usually includes a set of adaptors (Shc, GRB2, Crk, etc.) linking the receptor to the guanine nucleotide exchange factor son-of-sevenless (SOS) transducing the signal to the small GTP-binding proteins (RAS), which triggers the activation of MAPKKK (Raf). Raf phosphorylates the MAPKK (MEK; MAPK and ERK kinase). Then activated MEK catalyses the dual phosphorylation of the MAPK (ERK). Phosphorylated ERK translocates to the nucleus, where it phosphorylates and activates transcription factors that control the expression of genes that are required for cell growth, differentiation and survival. Adapted from: Goetz and Mohammadi [2013] and Kim and Bar-Sagi [2004].

1.2 Human Embryonic Stem Cells (hESC) and induced Pluripotent Stem Cells (iPSC)

Human embryonic stem cells (hESC) are derived from the inner cell mass (ICM) of blastocyst stage embryos and can be cultured *in vitro* (Figure 1.11). hESC have two valuable abilities which characterize these cell type. First, they have the capability to self-renew indefinitely. Second, they are pluripotent. hESC can give rise to all cell lineages of the three embryonic germ layers, which are endoderm (e.g. cells of the gastrointestinal tract), ectoderm (e.g. cells of the nervous system), mesoderm (e.g. cells of bone and muscle) and also germ cells. This pluripotent state is regulated by transcriptional and epigenetic mechanisms. Self-renewal in embryonic stem cells is maintained by a gene regulatory network orchestrated by the core transcription factors, OCT4, SOX2 and NANOG in association with the FGF2, WNT, TGFβ signaling pathway (Albano et al. [1993]; Hudson et al. [1997]; Morrisey et al. [1998]; Jung et al. [1999]; Koutsourakis et al. [1999]; Liu et al. [1999]; Yamaguchi et al. [1999]; Yasuo and Lemaire [1999]; Rossant et al. [2003]; Chazaud et al. [2006]; Greber et al. [2007]; McLin et al. [2007]; Chen and Daley [2008]; Cheng et al. [2012]).

Murine embryonic stem cell lines were isolated from pre-implantation embryos in 1981. 17 years later, in 1998, James Thomson and colleagues derived the first human embryonic stem cell lines also from pre-implantion embryos. By now, over 400 hESC lines exist, but only a few of them are well characterized. H1 for example is one of the best characterized hESCs lines. This line was derived by James Thomson and colleagues. The derivation, characterization and cultivation of such cells was a milestone in human developmental biology.

These cells paved the way for the modern drug discovery, and transplantation medicine. The tissue rejection after implantation in patients constitutes a problem. Additionally, to derive hESCs a blastocyst has to be destroyed, which raise ethical and moral concerns (Figure 1.11; Evans and Kaufman [1981]; Thomson et al. [1998]; Jensen et al. [2009]). These were solved when scientists succeeded found alternative ways to derive pluripotent cells. At first, mouse somatic cells were reprogrammed successfully in 2006 by Takahashi and Yamanaka. Shortly afterwards, two groups reprogrammed human adult fibroblasts with viral transduction mediated over-expression of four transcription factors OCT4, SOX2, KLF4 and c-MYC (Yamanaka-Cocktail) or OCT4, SOX2, NANOG and LIN28 (Thomson-Cocktail). The reprogramming of adult fibroblasts to induced pluripotent stem cells (iPSCs) marked another milestone in human developmental biology and it is used to shed light on the mechanisms of pluripotency and their maintenance. The iPSCs have the same capacities as human embryonic stem cells, including pluripotency and self-renewal. Further they share the same morphology as well as they are able to differentiate in all three germ layers *in vitro* (embryoid body formation) and *in vivo* (teratoma formation in immune deficient mice). The integration of pro-viruses into genome of viral-derived iPSCs is a risk factor for clinical applications in the future. Therefore, many non-viral reprogramming methods were developed using non-integrating adenoviruses, non-viral vectors, mRNA, miRNA or protein transfection. The major advantage of non-

viral methods is the lack of integration into the genome of tranfected cells (Takahashi and Yamanaka [2006]; Takahashi et al. [2007a]; Yu et al. [2007]; Chen and Liu [2009]; Yu et al. [2009]; Kiskinis and Eggan [2010]; Tavernier et al. [2012]). The derivation of integration-free iPSC from somatic cells and differentiating them into a donor cell type of interest are promising approaches for (i) future application in tissue replacement therapies, (ii) generation of disease models *in vitro*, (iii) toxicology and drug screening.
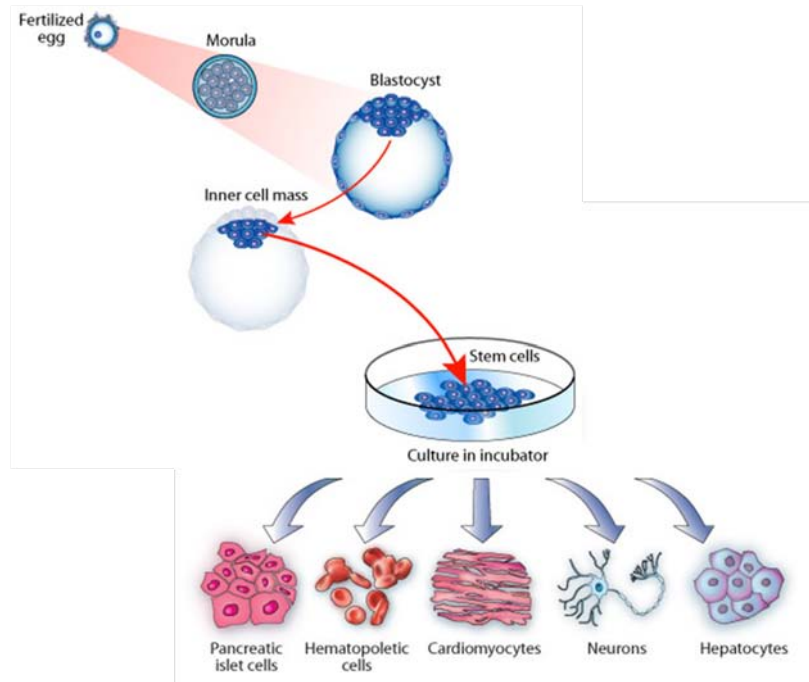
Figure 1.11: **Extraction and differentiation of ESC.**
The first step of differentiation during the development of the mammalian embryo from the inner cell mass is the formation of the blastocyst, when the morula differentiates to the trophoblast. Embryonic stem cells (ESC) are derived from the inner cell mass of the blastocyst. ESC can taken from the blastocyst, then can be cultured and differentiated *in vitro*. Adapted from: `http://www.biologyjunction.com/stemcell_article.htm`; Illustration by Cell Imaging Core of the Center for Reproductive Science, retrieved 08.06.2014.

1.3 Methods for generating iPSCs

Amongst others, iPSCs are an alternative to hESCs without raising ethical and moral concerns because they possess the same characteristics as hESCs. First Takahashi and Yamanaka [2006] derived iPSCs from mouse somatic cells with a viral approach (Yamanaka-Cocktail). One year later two groups successfully reprogrammed human adult fibroblasts with viral transduction mediated over-expression of four transcription factors using the Yamanaka-Cocktail or the Thomson-Cocktail (Takahashi et al. [2007a];

Yu et al. [2007]). The efficiency of reprogramming human fibroblasts to iPSCs by using retro-viruses is less than 1.0 % (Yamanaka 2007). The reprogramming of human fibroblasts to iPSCs by transduction of lenti-viral constructs using the Thomson-Cocktail has an efficiency of 0.02 – 0.0095 % (Yu et al. [2007]). Both methods are robust due to the fact that viral transduction is highly efficient. This is confirmed by the ability of numerous groups that have been able to reproduce these protocols (e.g. Prigione et al. [2010]; Si-Tayeb et al. [2010]; Totonchi et al. [2010] Wolfrum et al. [2010]; Jozefczuk et al. [2011]; Ohi et al. [2011]; Lichtner et al. [2013]). Derived by the fact that the efficiency is too low to generate iPSCs routinely, additional different methods were developed to reprogramm somatic cells (Hanna et al. [2007]; Nakagawa et al. [2008]; Woltjen et al. [2009]). p53 inhibition enhances the efficiency of iPSCs generation of human fibroblasts up to 100-fold. Furthermore, the transient inhibition of p53 can increase the efficiency of reprogramming human dermal fibroblasts by approximately 7-fold. To increase the efficiency of the viral reprogramming method additional factors have been used such as the viral oncogene simian virus 40 large T antigen (SVLT40). SV40LT is a 708-amino acid large oncoprotein. It is one of the two proteins expressed in infected cells by Simian virus 40 to obtain alteration of the host cells. SV40LT is able to affect a multitude of cells lines and it induces tumours in diverse animal models. The function of dedicated indicator tumour suppressors and cell cycle regulatory proteins of the host cell by binding it engineers. SV40LT inactivates the function of the tumor suppressor p53 and members of the retinoblastoma family of proteins such as pRB, p107 and p130. If the transcription of p53 is blocked the cell cycle cannot arrest and thereby the mechanism of repairing DNA damages would be inhibited (Ali and DeCaprio [2001]; Zhao et al. [2008]; Hong et al. [2009]; Kawamura et al. [2009]; Li et al. [2009]; Marin et al. [2009]; Utikal et al. [2009]; Wang and Adjaye [2011]).

To avoid mutagenesis by pro-virus integration and reactivation of oncogenic transgenes non-viral methods have been designed. The main problem of non-viral methods is the low efficiency of reprogramming. It is even lower compared to the retroviral methods. Murine somatic cells were reprogrammed into iPSCs by the transfection of two plasmids, carried the transgenes OCT4, KLF4, SOX2 and c-MYC. The reprogramming efficiency ranged between 1×10^{-6} and 2.9×10^{-5} %. Another vector-used method used a piggyback (PB) based vector system consisting of a vector and a transposon for doxycyclin inducible expression of the reprogramming factors. The reprogramming efficiency amounts to > 2 %. Also, the transfection of somatic cells with the proteins of OCT4, SOX2, KLF4 and c-MYC generated iPSCs. Using proteins is a completely vector free method to generate iPSCs. Unfortunately, the efficiency is low (around 0.001 %) and the import into the cells is problematic. In addition, there is another method which generates iPSCs that are free of vector and of transgene sequences by nucleofection of oriP/EBNA1 (Epstein-Barr nuclear antigen-1)-based episomal vectors that express reprogramming factors. The transfection of oriP/EBNA1 vectors which are derived from the Epstein-Barr virus happen without viral packaging. During culture the iPSCs which have been reprogrammed by oriP/EBNA1 vectors, the cells remove the episomal vectors with a rate of 5 % per cell division due to defective plasmid synthesis. The cis-acting oriP element on the vector and the EBNA-1 gene which encodes a replication initiation

factor the oriP/EBNA1-based vectors hold the ability of extra-chromosomal replication. The efficiency of this method to generate iPSCs increased up to 0.003 – 0.006 % and these iPSCs displayed ESCs characteristics. Analysis of whole-genome expression profiles showed that the generated iPSCs by using oriP/EBNA1 vectors are more similar to ESCs than iPSCs which were generated with other non-viral or viral methods. Moreover after 14 passages, the iPSCs had completely lost the episomal vectors (Yates et al. [1984]; Okita et al. [2008]; Chen and Liu [2009]; Kim et al. [2009a]; Woltjen et al. [2009]; Yu et al. [2009]; Yu et al. [2011]).

Not all reprogrammed cells have ESCs morphology, but are different from the parental cells. This kind of cells were described as partially reprogrammed cells. Due to impacted targeting of the reprogramming factors OCT4, SOX2 and KLF4 the state of these cells is in-between the parental cells and iPSCs. To obtain a higher efficiency of the pluripotent state and shift the partially reprogrammed cells to the iPSCs state, the cells can be treated with so-called small molecules, which are organic compounds, in order to manipulate signaling pathways (Park et al. [2008]; Takahashi et al. [2007b]; Sridharan et al. [2009]).

The inactivation of the TGFβ pathway (described in section 1.1.1) by using the small molecule inhibitors SB431542 increase the efficiency and the kinetics of iPSCs generation (Figure 1.12). An important process during the embryonic development is the induction of epithelial to mesenchymal transition (EMT) which also has effects for iPSCs generation. Amongst others TGFβ has a growth inhibitor function and is also involved to that process of EMT by e.g. decreasing expression of epithelial markers such as E-Cadherin and ZO-1 as well as increasing expression of mesenchymal markers e.g. fibronectin. Therefore, a temporal inhibition of the TGFβ pathway increases the reprogramming efficiency. Later, the TGFβ inhibition has to be removed in particular when TGFβ acquires the active role of pluripotentcy maintenance. The induction of pluripotency is favoured by the change of mesenchymal to epithelial (MET) development (Miettinen et al. [1994]; Hartsough and Mulder [1995]; Inman et al. [2002]; Barrios-Rodiles et al. [2005]; Willis and Borok [2007]; Lin et al. [2009]; Wang et al. [2010]).

It is also evident that reprogramming using epithelial cells such as keratinocytes results in an increased efficiency as compared with dermal fibroblasts or MSCs which are of mesenchymal origin. The chemical compound PD0325901 an inhibitor of the MAP/ERK kinase (MEK) pathway (described in section 1.1.2 and Figure 1.10). Extracellular signals are activate the MAP kinase pathway which activates MEK. This pathway plays a major role in the regulation of growth and differentiation of cells (Figure 1.12). The chemical compound PD0325901 inhibits this pathway through blocking the phosphorylation of ERK by MEK (Barrett et al. [2008]). The inactivation of the TGFβ and the MEK-ERK pathways in fully reprogrammed iPS or ES cells by using the small molecule SB431542 and PD0325901, respectively, results in differentiation. Therefore, extended use of these small molecules during reprogramming is not advisable.
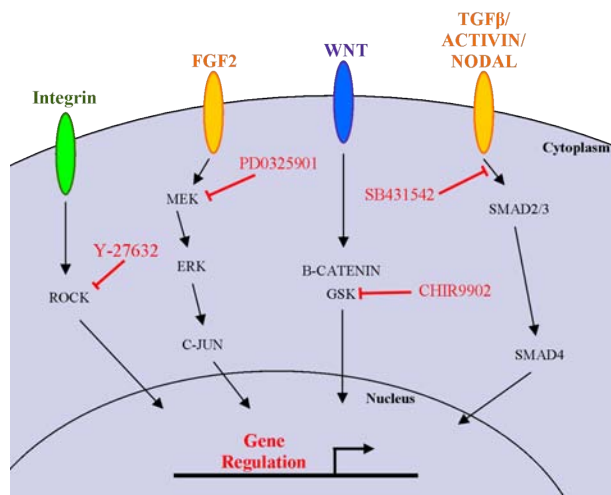
Figure 1.12: **Inhibition of pathway by the use of small molecules.**
To raise the efficiency of episomal based reprogramming of somatic cells chemical compounds so called small molecules were used. In this case four different small molecules were used to block three different signaling pathways. The small molecule SB431542 specifically inhibits the Type I receptors ALK4, ALK5 and ALK7 and thus the inactivates the TGFβ signaling pathway. Additionally, the efficiency and the kinetics of iPSCs generation increase due to the inhibition. The chemical compound PD0325901 inactivates the MAP/ERK kinase (MEK) by blocking the phosphorylation of ERK by MEK. Thereby the MAP kinase pathway which plays a major role in the regulation of growth and differentiation of cells. The small molecule CHIR9902 is blocking the glycogen synthase kinase-3 beta (GSK3β). GSK3β is a multifunctional serine/threonine (Ser/Thr) kinase which regulates several physiological processes such as apoptosis, metabolism, development, oncogenesis. Rho associated coiled-coil kinase (ROCK) is a serine/threonine (Ser/Thr) kinase like GSK and regulates several cell processes such as cytokinesis, proliferation, cell adhesion and motility. The ROCK inhibitor Y-27632 blocks this kinase.

The glycogen synthase kinase-3 beta (GSK3β) pathway (described in section 1.1.1) regulates several physiological processes such as apoptosis, metabolism, development, oncogenesis and is activated by cellular stress (ER stress, hyperosmotic stress, heat shock, oxidative stress). To raise the efficiency of episomal based reprogramming the small molecule CHIR99021 inhibits GSK3β (Figure 1.12; Chen et al. [2004]; Yu et al. [2011]; Zhou et al. [2012]).

Another small molecule is a ROCK inhibitor named Y-27632 can be used. Rho associated coiled-coil kinase (ROCK) like GSKβ regulates several cell processes such as cytokinesis, proliferation, cell adhesion and motility. The ROCK inhibitor increases the reprogramming efficiency from 1 % to 27 % (Figure 1.12; Ishizaki et al. [2000]; Watanabe et al. [2007]; Tsuchiya et al. [2011]).

All four small molecules together could be the best combination to reach a maximal effect on episomal reprogramming (Yu et al. [2011]).

In general pluripotent cells are promising candidates for the application in tissue replacement therapies and for the generation of disease models (Figure 1.13).

However, there are still unresolved problems, such as the fact that KLF4 and c-MYC are oncogenes that could be reactivated which pose risk factors for clinical applications in the future. These conditions cause a high probability of genomic instability and mutagenesis in iPSCs. Using fewer factors with OCT4, SOX2, KLF4 but without c-MYC has been suggested to enable medical applications in the future and safer reprogramming. Mouse neural stem cells which express endogenous level of c-MYC, SOX2 and KLF4 have been reprogrammed by using one factor namely OCT4 (Nakagawa et al. [2008]; Chen and Liu [2009]; Kim et al. [2009b]; Wang et al. [2010]).
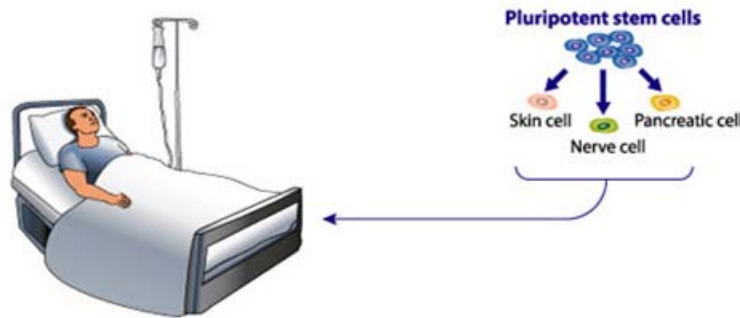
Figure 1.13: **Clinical application of iPSC.**
Induced pluripotent stem cells (iPSC) were generated as a source for any cell type of interest. After differentiation and functional analysis the cells can be transplanted in a patient. Adapted from: `http://www.biologyjunction.com/stemcell_article.htm`; Illustration by Cell Imaging Core of the Center for Reproductive Science (retrieved 08.06.2014).

1.4 Hepatocyte differentiation of hESCs and iPSCs in vitro

The transplantation of hepatocytes has been shown to be effective and minimally invasive, but there is a worldwide shortage of human liver. In addition, limited willingness of liver donation restricts the use of hepatocyte transplantation further. New methods have to be generated to tackle these problems, for example a living related liver donation and cell therapy (Figure 1.13). Since 2005 human embryonic stem cells (hESCs) were used to generate hepatocytes *in vitro*. Henceforward, this method was modified and optimized repeatedly (Lee et al. [2004]; Mazaris et al. [2005]; Schwartz et al. [2005]; Soto-Gutierrez et al. [2006]; Hay et al. [2007]; Hay et al. [2008b]; Agarwal et al. [2008]; Hay et al. [2008a]). Independent from liver diseases and shortage of liver donors iP-SCs were generated as a source for any cell type of interest. Therefore, iPSCs could be used as a source to generate hepatocytes (Takahashi and Yamanaka [2006]; Takahashi et al. [2007a]; Takahashi et al. [2007b]; Yu et al. [2007]; Yu et al. [2009]; Sullivan et al. [2010]; Jozefczuk et al. [2011]; Yu et al. [2011]; Chiang et al. [2013]; Hoyer et al. [2013]; Settmacher et al. [2013];Farzaneh et al. [2014]; Takebe et al. [2014]; Matz et al. 2016 under review).

	Stage 1 **DE**	**Stage 2** **HE**	**Stage 3** **HLC**	**Stage 4** **Maturation**
	4-6d	3-8d	5-12d	5-12d
A	Activin A + NaB	DMSO	HGF + OSM	
B	Activin A	FGF4 + HGF	OSM + Dexa	
C	Activin A	FGF4 + HGF	FGF4 + HGF + OSM + Dexa	
D	Activin A	BMP4 + FGF2	HGF	OSM
E	Activin A + Wnt3a	FGF + BMP4	HGF + Dexa + OSM	Dexa
F	Activin A	DMSO	HGF + OSM + Dexa	HGF + OSM + Dexa
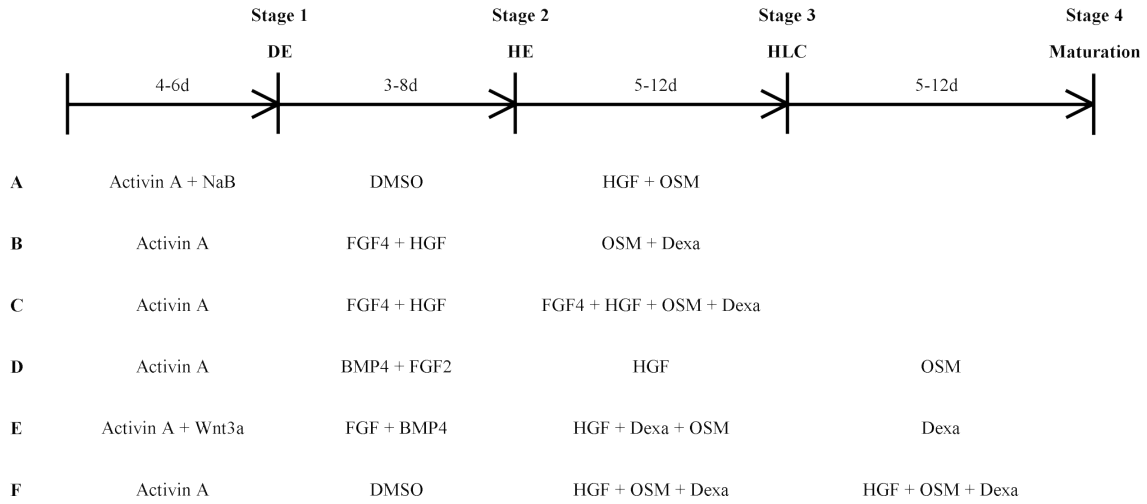
Figure 1.14: **Different protocols of HLC-derivation.**
Different protocol are shown to generate hepatocyte-like cells (HLC) from embryonic stem cells (ESC) and induced pluripotent stem cells (iPSC). Adapted from: **A)** Hay et al. [2008b]; **B)** Asgari et al. [2013]; **C)** Choi et al. [2013]; **D)** Mallanna and Duncan [2013]; **E)** Ogawa et al. [2013]; **F)** Kondo et al. [2014a].

The current hepatocyte differentiation protocols are composed of cytokine cocktails and stepwise approaches. The most hepatocyte differentiation protocols are composed of three steps. First, the generation of definitive endoderm (DE), second, the hepatic endoderm (HE) and finally the third step to generate the hepatocyte-like cells (HLCs). Many different protocols exist to generate the HLCs (Figure 1.14). It seems that each laboratory has its own specific protocol. The basal medium, the time period as well as the cytokine composition of each step vary. The most important aspect is the cytokine composition (Hay et al. [2008b]; Asgari et al. [2013]; Choi et al. [2013]; Mallanna and Duncan [2013]; Ogawa et al. [2013]; Kondo et al. [2014a]). To generate DE the concentration and composition of the cytokines has to be defined. Activin A seems to be essential to generate DE. All protocols which are listed here use Activin A to generate DE (Figure 1.14). Depending on the concentration Activin induces DE or mesoderm development. Activin and BMP4 synergistically promote the induction of DE stage (Hart et al. [2002]; Tada et al. [2005]; Sulzbacher et al. [2009]; Teo et al. [2012]). Additionally, the fibroblast growth factors (FGF) play an important role during liver generation, as well as maintain embryonic stem cells (Jung et al. [1999]; Weinstein et al. [2001]; Greber et al. [2007]). The pathways of these cytokines were described before (see on page 5). Dimethylsulfoxide (DMSO) induces differentiation of various cells typs including stem cells to endodermal cells and further to hepatic endoderm (HE), but the mechanism is still unknown (Morley and Whitfield [1993]; Hay et al. [2008b]; Pal et al. [2012]; Chetty et al. [2013]).

The hepatocyte growth factor (HGF) is essential for liver derivation. HGF binds to the cell surface receptor c-Met. This initiates the phosphorylation of a receptor-dimer and

activates amongst others the MAP/ERK signaling cascade (described in section 1.1.2).
HGF activates cell proliferation, cell survival and migration, which plays important roles
in liver development, maturation and regeneration. (Bottaro et al. [1991]; Bussolino et al.
[1992]; Ito et al. [2000]; Kamiya et al. [2001]).
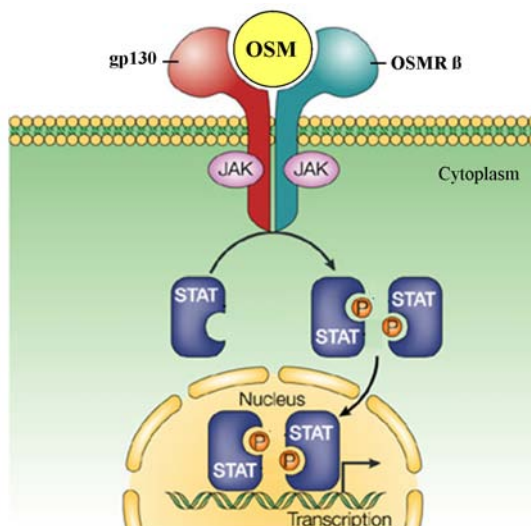
Figure 1.15: **Scheme of the Jak/Stat pathway.**
Oncostatin M (OSM) binds to the subunit glycoprotein 130 (gp130) of a cell surface receptor com-
plex and specific to the subunit OSM Receptor β chain (OSMRβ) of the OSM specific Receptor type
II (OSMR). The receptors of gp130 and OSMRβ form a heterodimer which activates the receptor-
associated Janus kinase (JAK). JAK phosphorylates the signal transducer and activator of transcrip-
tion (STAT)1 and STAT3. An STAT1/3 heterodimer translocates to the nucleus, bind to specific DNA
sequences and activates the transcription of hepatic differentiation markers. Adapted from: Shuai and
Liu [2003].

As well as HGF the cytokine Oncostatin M (OSM) induces liver differentiation. OSM
is a member of the Interleukine 6 (IL-6) family of cytokines which all use gp130 as a
co-receptor (Figure 1.15). On the one hand OSM binds this subunit glycoprotein 130
(gp130) of a cell surface receptor complex with low affinity and on the other hand binds
specific the subunit OSM Receptor β chain (OSMRβ). The receptors of gp130 and
OSMRβ form a heterodimer which can activate two major pathways, the MAPK/ERK
pathway (described in section 1.1.2 and Figure 1.8) or the JAK/STAT pathway (Fig-
ure 1.15). In adult liver OSM induces amongst others low density lipoprotein recep-
tor (LDLR) expression, shown in human hepatoma cell line (HepG2), mice and rats.
Thereby OSM regulates the cholesterol metabolism. In rat was shown that OSM mediate
proliferation as well as anti-apoptosis of hepatocytes and, thereby, induces regeneration
of hepatocytes after liver injury (Grove et al. [1991]; Gearing et al. [1992]; Faris et al.
[1996]; Mosley et al. [1996]; Hirano et al. [1997]; Liu et al. [1997a]; Liu et al. [1997b];
Stancato et al. [1997]; Lindberg et al. [1998]; Tanaka et al. [1999]; Ito et al. [2000];
Kamiya et al. [2001]; Okaya et al. [2005]; Hamada et al. [2007]; Drechsler et al. [2012]).

Dexamethasone (Dex) was used to complete the cocktail of supplements, which was used in this work to generate hepatocytes *in vitro*. Dex is a synthetic glucocorticoid which suppresses *AFP* expression and up-regulates *albumin* expression shown in rats (Blanger et al. [1981]; Nawa et al. [1986]; de Juan et al. [1992]). Dexamethasone is necessary for maturation of hepatocytes. OSM alone is not able to initiate this process (Kamiya et al. [1999]; Kojima et al. [2000]; Matsui et al. [2002]; Agarwal et al. [2008]).

In the past, pharmaceutical companies used Primary human hepatocytes (PHH) for toxicology test and drug screenings. The culturing of PHH is problematic because, firstly, they cannot be expanded *in vitro*, secondly, PHH are difficult to obtain routinely and thirdly, it is difficult to isolate them in sufficient quantities (Elaut et al. [2006a]; Elaut et al. [2006b]; Fraczek et al. [2013]). Human hepatocarcinoma-derived and transformed, permanent cell lines, including HepG2, THLE and HepaRG are used as alternatives, but these cell lines have phenotypes significantly diverged from normal primary hepatocytes (Hart et al. [2010]; Jennen et al. [2010]; Gerets et al. [2012]; Cuconati et al. [2013], Jetten et al. [2013]).

The differentiation of iPSCs to hepatocyte-like cells (HLCs) could be a potential alternative for pharmaceutical toxicology test and drug screenings. HLCs generated from human iPSC have shown great promise as an inexhaustible source of cells that mirror the genotype of the donor to satisfy this need. Multifunctional applicable HLCs generated from iPSCs can serve as cellular models for drug screenings and toxicology studies, as well as serve a source for disease modeling. Several groups have shown multifunctional applicable HLCs already. Most studies using viral approach to derive iPSCs and further to generate HLCs. However, these have drawbacks (e.g. genome integration) and most studies focus on one aspect of the multifunctional application of the HLCs. These studies are focused on the generation of HLCs from iPSCs, the maturation, modeling liver diseases or drug screening and toxicology (Greenhough et al. [2010]; Rashid et al. [2010]; Sullivan et al. [2010]; Hannan et al. [2013]; Jozefczuk et al. [2011]; Teo et al. [2011]; Yusa et al. [2011]; Asgari et al. [2013]; Choi et al. [2013]; Gieseck et al. [2014]; Subba Rao et al. [2013]; Kondo et al. [2014a]; Kondo et al. [2014b]; Nakagawa et al. [2014]; Takayama et al. [2014]; Takebe et al. [2014]).

1.5 Aim of this work

The liver is the largest gland in the human body and plays the most important role in regulation of metabolic pathways and detoxification. Hepatocytes are the main cell type supporting the detoxification function of the liver and as such they are already extensively used for toxicology screens. Original primary human hepatocytes (PHH) cannot be expanded *in vitro*, are difficult to obtain routinely and difficult to obtain in sufficient quantities. Additionally, alternative hepatocarcinoma-derived and transformed, permanent cell lines diverge significantly from normal primary hepatocytes. Due to these stated facts another alternative must be found.

Induced pluripotent stem cells (iPSCs) have the same capacities as human embryonic stem cells, including pluripotency, self-renewal, same morphology and they are able to differentiate in all lineages of the three germ layers. The common way to generate iPSCs from human somatic cells uses virus-approach. The integration of pro-viruses into genome of viral-derived iPSCs is a risk factor for clinical applications in the future (Chen and Liu [2009]). Therefore, this study demonstrates the generation and characterization of integration-free, episomal-derived induced pluripotent stem cell (E-iPSCs) lines from human somatic cell lines with different origin. The transcriptome of the E-iPSC lines were compared to that of hESCs and to that of a viral-derived iPSC line (V-iPSC). Additionally, the E-iPSCs were used to derive and characterize hepatocyte-like cells (HLCs). Analysis about the functionality and life span were done. Additionally, the transcriptome profile of these HLCs were compared to that of fetal liver and PHH to identify commonalities and differences. Furthermore, an attempt was made to untangle hepatogenesis-associated gene regulatory networks.

Due to the fact that the hepatogenesis is best understood in mice and rats so far, this work also tried to gain insights into molecular and gene regulatory networks governing the hepatogenesis in human.

This PhD thesis addresses four main goals:

- Generation of stable viral-free and integration-free human induced pluripotent stem cells (E-iPSC).

- Differentiation of E-iPSCs to hepatocyte-like cells (HLCs) to model the hepatogenesis.

- Generate HLCs with a higher functional quality and longer functional life span.

- Generation of endodermal progenitors (EP) from E-iPSCs to study the early time span of hepatogenesis.

To achieve these goals, the following investigations were carried out:

- Episomal vector-based reprogramming of two different human somatic cell lines (HFF1, HUVEC).

- Full characterization of generated E-iPSC-lines and transcriptome analysis compared to human embryonic stem cells (hESC.).

- Step-wise differentiation of E-iPSCs to HLCs and characterization of HLCs.

- Analyses of quality, functionality and life span of HLCs.

- Transcriptome profile analysis of HLCs compared to the transcriptome profile of fetal liver and primary human hepatocytes (PHH).

- Generation and characterization of endodermal progenitors (EPs).

- Transcriptome profile analysis of EPs compared to HLCs, fetal liver and PHH.

2 Preliminary Work

Episomal-based reprogramming of HFF1-cells

In a previous study (my master thesis, 2012) I generated and characterized viral-free induced pluripotent stem cells (iPSCs) (Figure 6.2). To achieve this, HFF1-cells were transfected with oriP/EBNA1-based episomal vectors which are derived from the Epstein-Barr virus without viral packaging and avoid genetic modification, because they do not integrate into the genome. The vectors express the reprogramming factors OCT4, SOX2, NANOG, KLF4, LIN28, c-MYC and SV40LT (Yu et al. [2009]; Figure 6.1). To enhance the efficiency of reprogramming the following small molecules, (i) TGFβ-pathway inhibitor (SB431542), (ii) MEK-ERK pathway inhibitor (PD0325901) and (iii) GSK3β inhibitor (CHIR99021) were supplemented one day after nucleofection for 23 days (Yu et al. [2011]). Indeed, the iPSC-line (epiHFF1-iPS-B1) shown here is integration free (Figure 2.1; Matz and Adjaye [2016]) and has the same characteristics as human embryonic stem cells (hESCs) lines (Figure 2.2 - 2.6; Matz and Adjaye [2016]; Supplementary Figure S1 and S2).
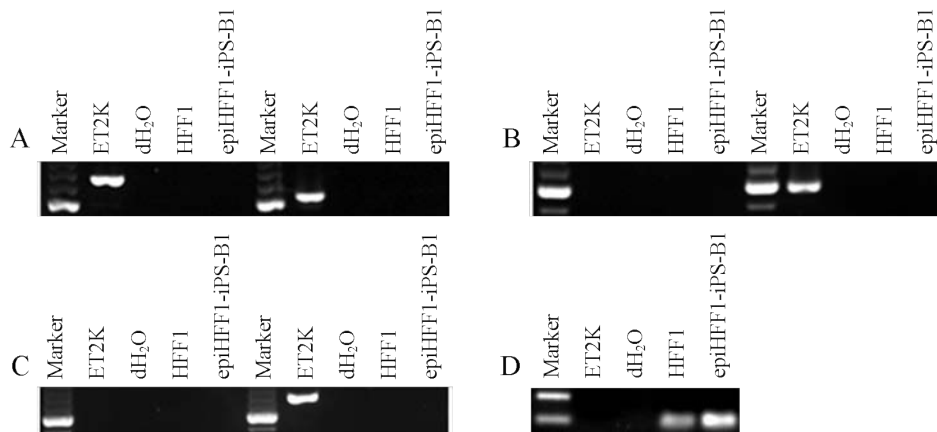
Figure 2.1: **PCR of plasmid detection in epiHFF1-iPS-B1.**
A) Detection of the plasmid gene sequences of EBNA-1 and OriP which are included in each vector. **B)** Detection of the plasmid gene sequences of LIN28 and SV40LT. **C)** Detection of the plasmid gene sequences of NANOG and OCT4. **D)** Detection of the human genome gene sequence of OCT4. 100 bp Marker was used. The vector ET2K, which is one of the three transfected vectors, was used as a positive control, ddH₂O was used as the negative control, as well as HFF1 the original cell line. Modified from Matz and Adjaye [2016].

The epiHFF1-iPS-B1 express pluripotent maker genes and amongst others the surface marker genes *AP*, *TRA-1-60*, *TRA-1-81*, *SSEA-4*, but not *SSEA-1*. *SSEA-1* is a marker of differentiation in human ESC though a marker of the undifferentiated state in mouse ESCs (Thomson et al. [1998]; Takahashi et al. [2007a]; Yu et al. [2007]) as well as *OCT4*, *NANOG*, *SOX2* (Figure 2.2 and 2.3; Matz and Adjaye [2016]). These iPSC-line can differentiate *in vitro* in all three germ layers endoderm, ectoderm and mesoderm by formation of embryoid bodies (Figure 2.4; Matz and Adjaye [2016]). The karyotype analysis confirmed that epiHFF1-iPS-B1 is a human male iPSC-line, but Chromosome 12 contains an aberration. The DNA fingerprint is identical to the fingerprint of the human fibroblast line HFF1, but different compared to the hESC lines H1 and H9 (Figure 2.5; Matz and Adjaye [2016]). The expression pattern of pluripotency genes were measured by quantitative real-time PCR (qRT-PCR) and compared to the pattern of H1 cells. The expression pattern of the iPSC-line is similar to H1 and is stable over the time (Figure 2.6).
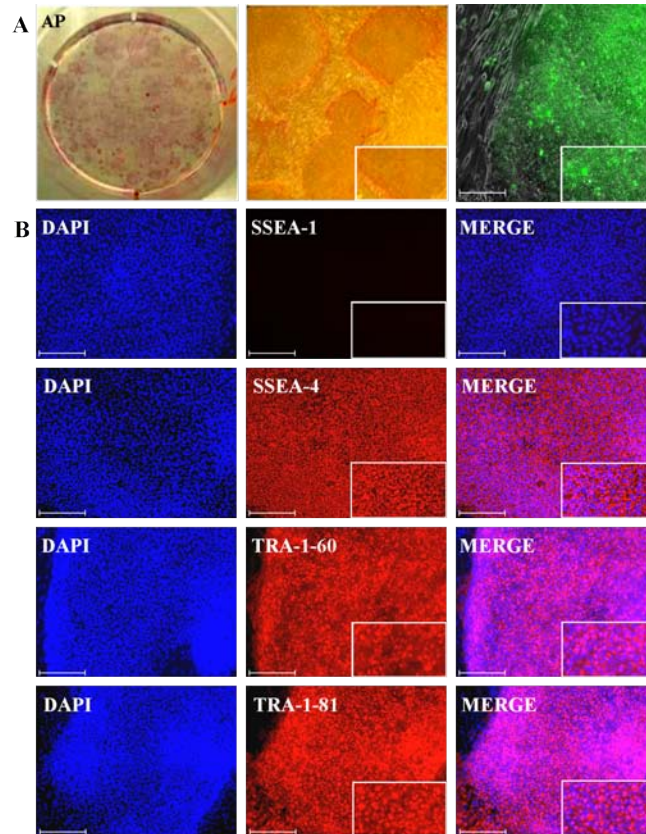
Figure 2.2: **Immunofluorescence-based detection of surface markers in epiHFF1-iPS-B1.**
A) Staining of the surface protein alkaline phosphatase (AP) overview of the well, microscopy image and live stained cells (from left to right). **B)** Immunofluorescence-based protein stainings for the surface markers SSEA-4, TRA-l-60 and TRA-1-81 were positive, SSEA-1 was negative. DAPI stained the nucleus. Scale bar: 200 μm, Alexa Flour 594 (red), Alexa Fluor 488 (green). Modified from Matz and Adjaye [2016].
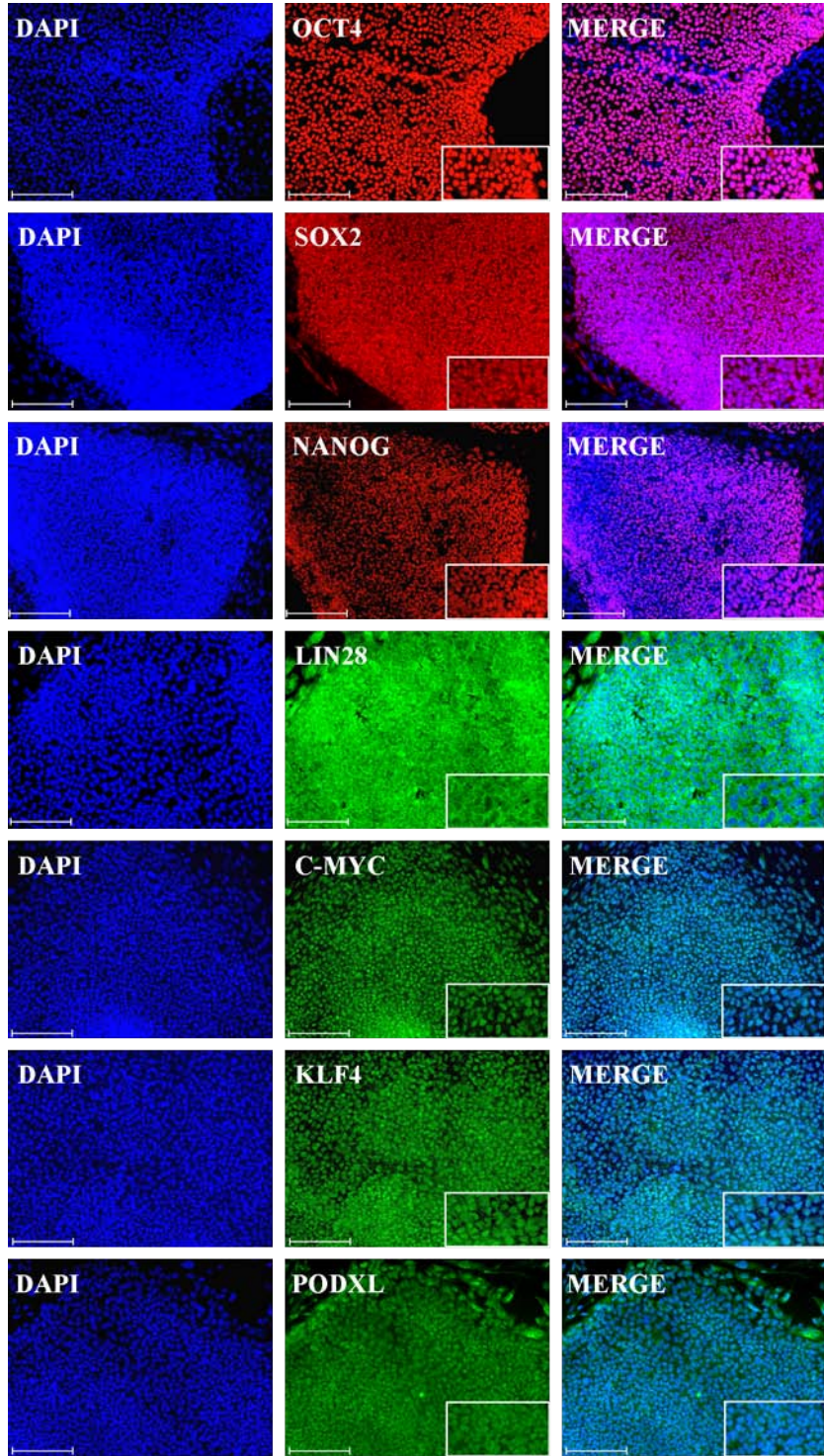
Figure 2.3: **Immunofluorescence-based detection of pluripotency markers in epiHFF1-iPS-B1.**

Immunofluorescence-based protein stainings for pluripotency markers OCT4, NANOG, SOX2, KLF4, c-MYC, LIN28 and PODXL were positive. DAPI stained the nucleus. Scale bar: 200 μm, Alexa Flour 594 (red), Alexa Fluor 488 (green). Modified from Matz and Adjaye [2016].
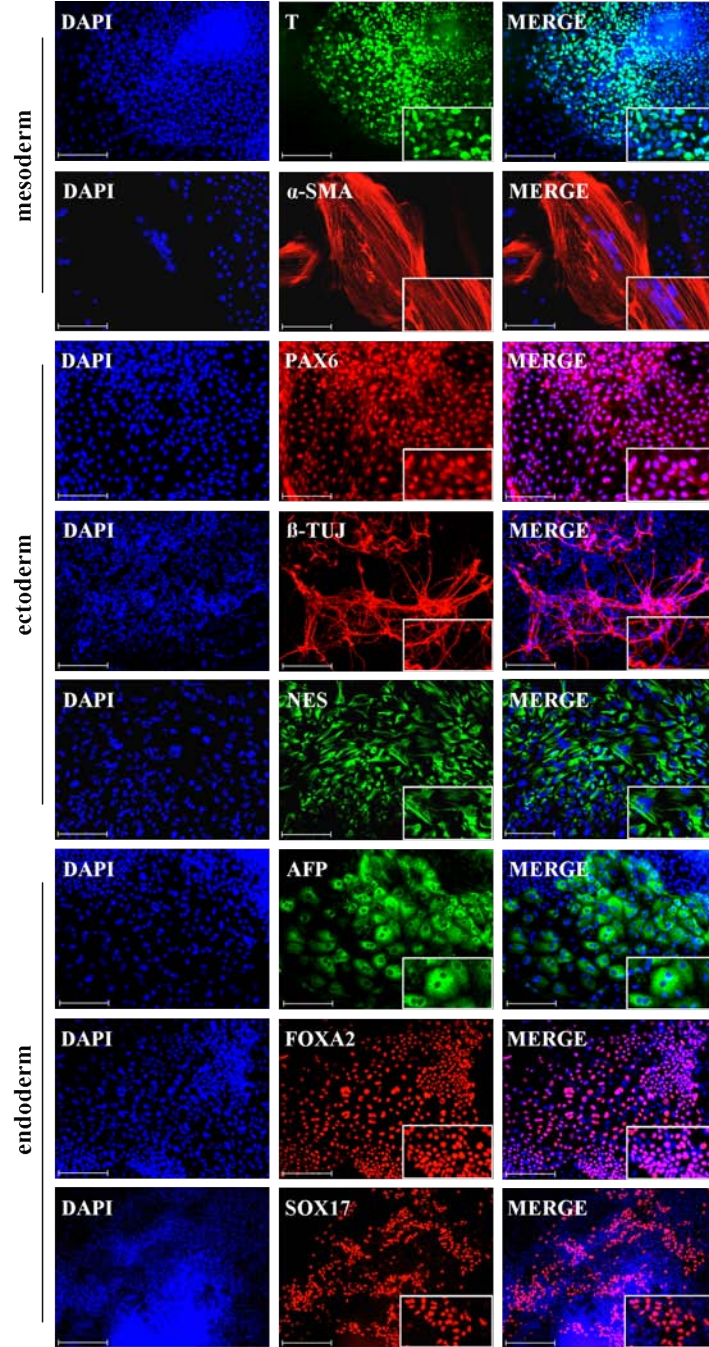
Figure 2.4: **Immunofluorescence-based detection of germ-layer specific proteins EBs derived from epiHFF1-iPS-B1.**
All three germ layers mesoderm, ectoderm and endoderm were detected *in vitro* by formation of embryoid bodies. The detection of the proteins T and α-SMA are markers of mesoderm layer, PAX6, β-TUJ1 and NES detect the ectoderm layer and AFP, FOXA2, SOX17 are markers of endoderm layer. DAPI stained the nucleus. Scale bar: 200 μm Alexa Flour 594 (red), Alexa Fluor 488 (green). Abbreviations: T = brachyury homolog (mouse); α-SMA = Smooth Muscle Actin; PAX6 = Paired Box 6; β-TUJ1 = class III β-Tubulin; NES = Nestin; AFP = α-Fetoprotein; FOXA2 = Forkhead box A2; SOX17 = SRY (sex determining region Y)-box 17. Modified from Matz and Adjaye [2016].

31
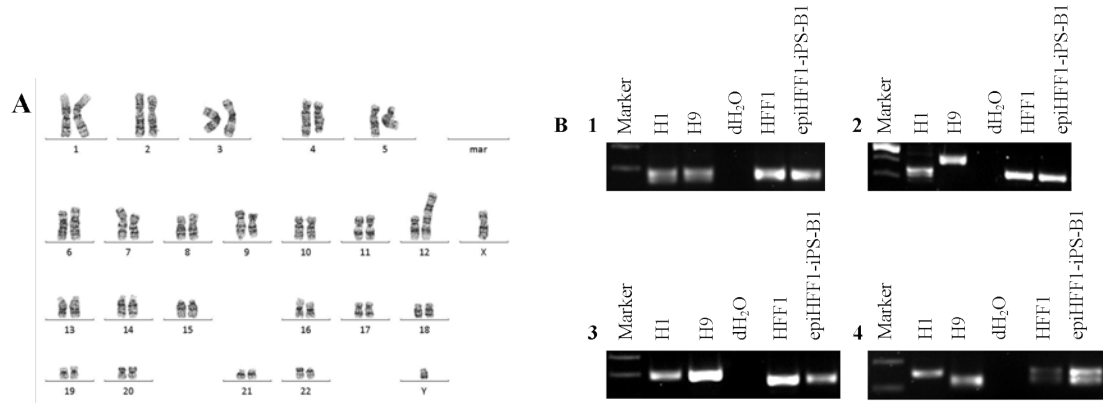
Figure 2.5: **Karyogram and DNA fingerprinting of epiHFF1-iPS-B1.**
A) Presence of a male karyogram 46,XY,add(12)(p13) from epiHFF1-iPS-B1. The Chromosome 12 containing additional material of unknown origin and different banding pattern. The additional material has the size of a long arm of chromosome 6. mar = minimal altered region. **B)** Genomic DNA from hESCs H1 and H9, HFF1 cells and the viral-free epiHFF1-iPS-B1 for PCR were used. 1: Genomic PCR with the primer of D7S796. 2: Genomic PCR with the primer of D10S1214. 3: Genomic PCR with the primer of D17S1290. 4: Genomic PCR with the primer of D21S2055. Modified from Matz and Adjaye [2016].
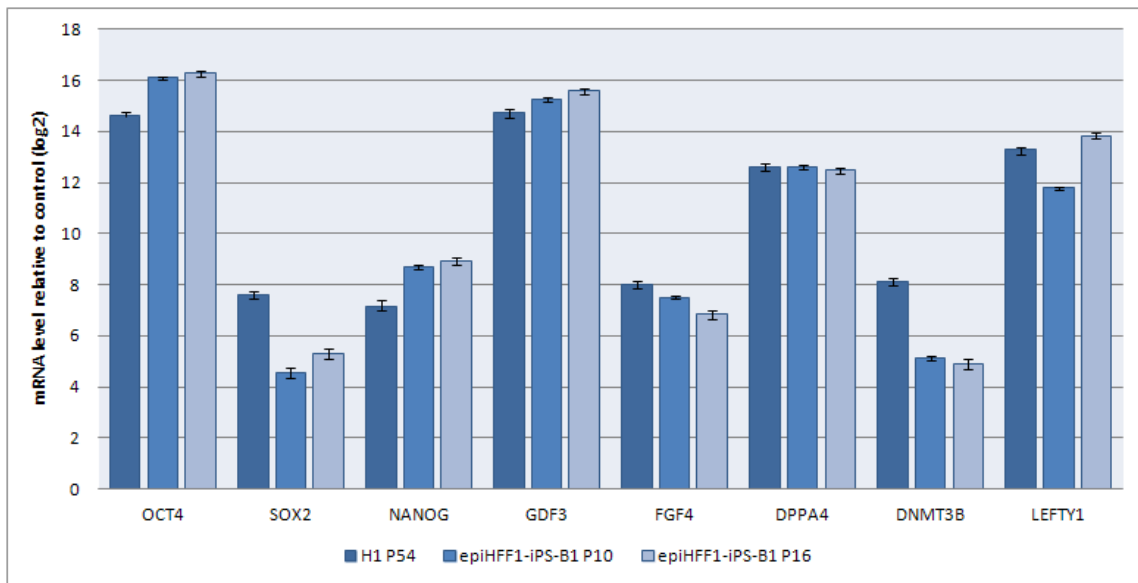
Figure 2.6: **Quantitative real-time PCR of epiHFF1-iPS-B1.**
Expression pattern of pluripotency markers relative to HFF1 from hESC-line H1 and the iPSC-line epiHFF1-iPS-B1 in passage 10 (P10) and passage 16 (P16) are shown. The standard deviation is depicted by the error bars. Abbreviations: HFF1 = human foreskin fibroblast; hESC = human embryonic stem cell; iPSC = induced pluripotent stem cell.

3 Results

3.1 Episomal-based reprogramming of somatic cells

3.1.1 Characterization of human fetal fibroblast-derived iPSC line

The viral-free, episomal-based reprogramming of the human fetal fibroblast line HFF1 and most of the characterization was done in a previous work and is described in Chapter 2. However, the *in vivo* confirmation was not done. Therefore to complete the characterization of the episomal reprogrammed induced pluripotent cell (iPSC)-line epiHFF1-iPS-B1 teratoma formation in immunodeficient mice was performed. The presence of all three germ layers in the teratoma were detected (Figure 3.1; Matz and Adjaye [2016]). Hence, the final required step for demonstrating that epiHFF1-iPS-B1 is pluripotent has been completed.
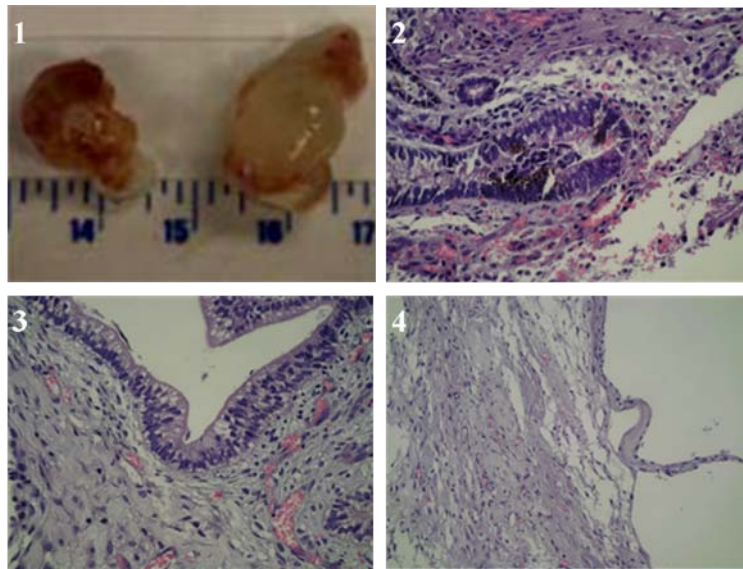
Figure 3.1: **Teratoma of epiHFF1-iPS-B1.**
In vivo teratoma formation of epiHFF1-iPS-B1 upon transplantation into NOD scid gamma mice. **1)** total tumor, histological structures corresponding to **2)** ectoderm (pigmented neuronal epithelium), **3)** endoderm (epithelium with goblet cells), **4)** mesoderm (connective tissue) lineages are depicted. Modified from Matz and Adjaye [2016].

Global gene expression analyses

Reprogramming of somatic cells to iPSCs results in major changes in transcriptional profile of the cells (Wolfrum et al. [2010]). To analyze potential changes of human fetal fibroblasts (HFF1), episomal reprogrammed iPSC-line epiHFF1-iPS-B1 from HFF1 cells (E-iPSCs) and human embryonic stem cells (hESCs) the Illumina Bead-Studio platform was used (Figure 3.2A). During the reprogramming process the transcriptome profile of the parental cells shifted towards a hESC-like stage. The parental HFF1 cells lost their expression upon reprogramming while other sets of genes were activated upon reprogramming. A third set of genes was maintained in both states (Figure 3.2A, Supplementary Table 1). To visualize the distinct and overlapping genes expression patterns in HFF1 versus E-iPSCs and hESCs a Venn diagram was generated (Figure 3.2B). We identified gene signatures representative of cellular housekeeping functions (11994 genes; e.g. *GAPDH*, *ACTB*, *PGK1*, *LDHA*), donor cell (HFF1)-specific genes (1373 genes; e.g. *APOL3*, *CUX1*, *DOK1*, *EPS8*, *FOXF2*), donor cell-memory genes (213 genes; e.g. *LAMA4*, *TERC*), self-renewal and pluripotent genes (1417 genes; e.g. *POU5F1*, *SOX2*, *NANOG*, *LIN28*, *GDF3*), iPSC (E-iPSC)-specific gene expression signature (450 genes; e.g. *DAZ4*, *FGD4*, *GJC3*, *LHX4*, *SDC3*) and hESC-specific genes (537 genes; e.g. *FGFBP1*, *FGF9*, *GSC*, *WNT3A*) (Figure 3.2B, the entire gene lists are presented in Supplementary Table 2). The intersection of hESC and E-iPSC from the Venn diagram contains genes (e.g. *CDH1*, *EOMES*, *FGF8*, *HAND1*, *JAG2*, *LEFTY1*, *LEFTY2*, *LIF*, *MIXL1*, *NODAL*, *SOX2*, *T*, *WNT10B*) which are involved in biological processes such as developmental signaling, pluripotency, self-renewal and embryogenesis (Figure 3.2C - D).
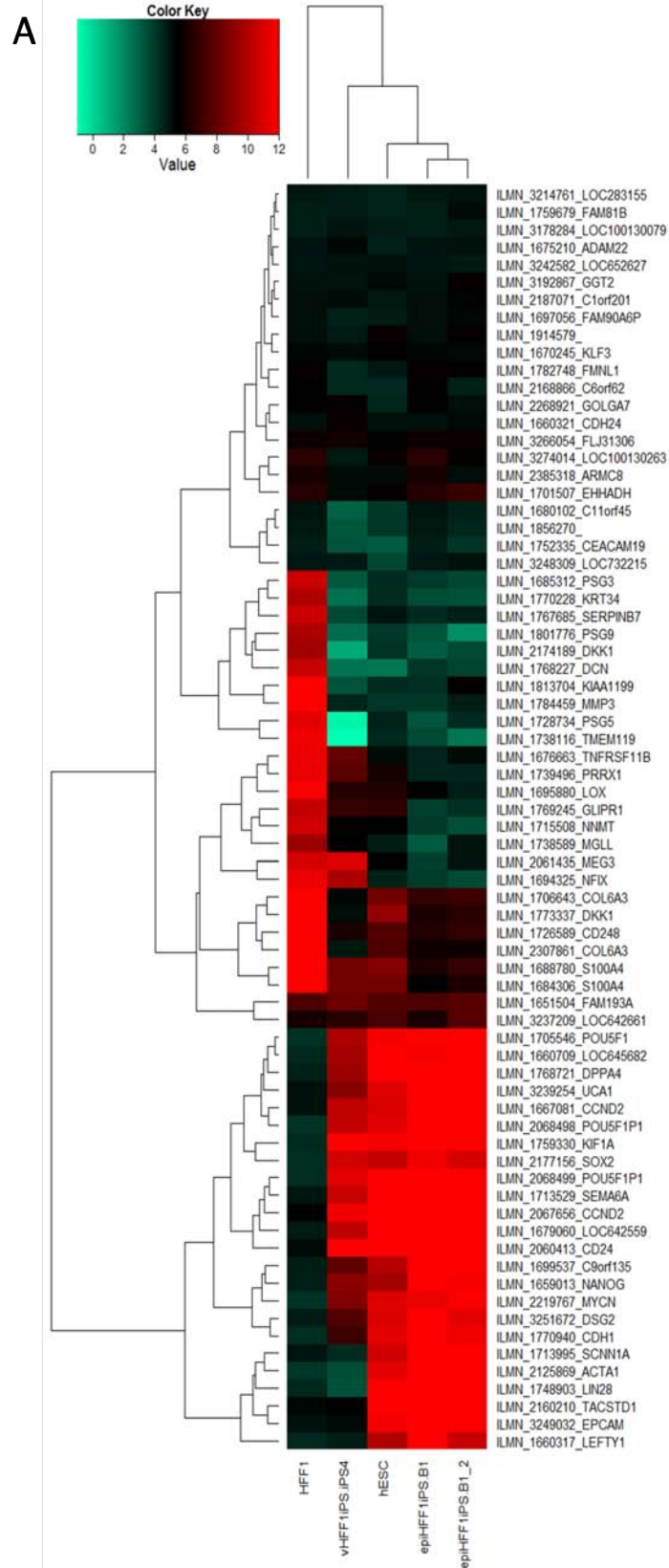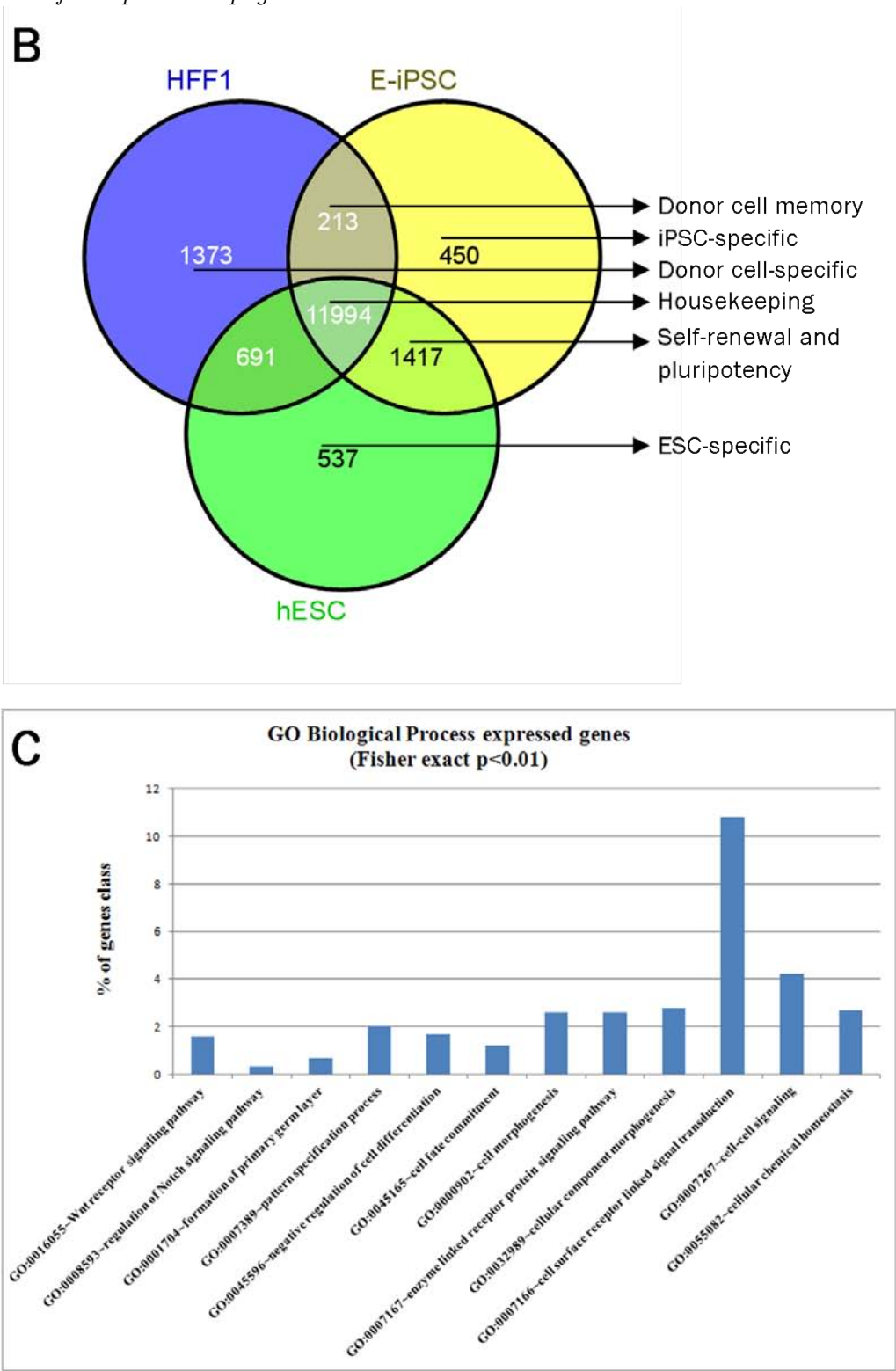
continued from previous page
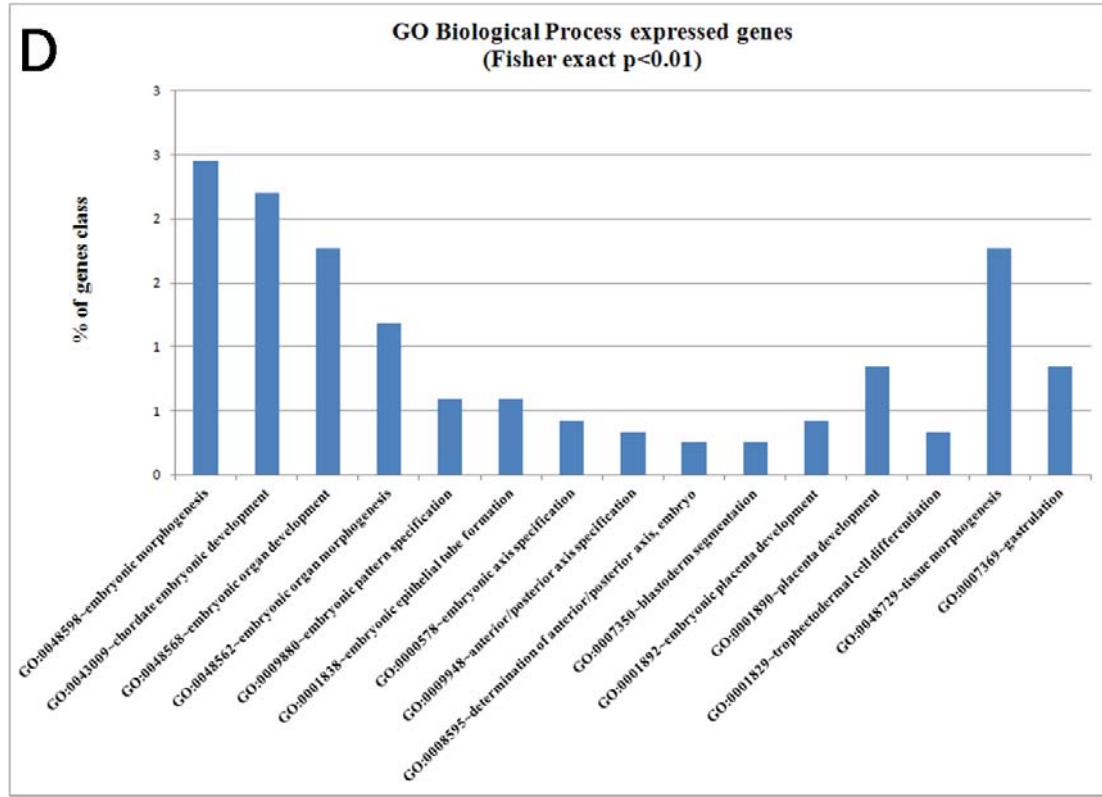
Figure 3.2: **Microarray data analyses.**
A) Heatmap visualizes expression pattern changes during cellular reprogramming. Expression pattern of hESCs, episomal reprogrammed HFF1-cell line epiHFF1-iPS-B1 (E-iPSC), retro-viral reprogrammed HFF1-cell line vHFF1-iPS-iPS4 (V-iPSC) and the somatic cell line HFF1 were compared. The top 24 genes with transcription activity either unchanged (Retained), low (Lost) or high (Acquired) expression values of iPSCs relative to the parental cell line (HFF1) were selected. **B)** Venn diagram analysis of the transcriptome profile from HFF1, E-iPSC and hESC portraying distinct and overlapping transcriptional signatures. **C)** Graph of biological processes related to embryogenesis to percentage of genes from the intersection of E-iPSC and hESC from the venn diagram (B). **D)** Graph of biological processes related to embryogenesis signaling and pluripotency to percentage of genes from the intersection of E-iPSC and hESC from the venn diagram (B). Abbreviations: hESCs = human embryonic stem cells; HFF1 = human foreskin fibroblast 1; E-iPSC = episomal reprogrammed induced pluripotent stem cell; V-iPSC = retro-viral reprogrammed induced pluripotent stem cell.

Comparison of transcriptome profile from viral and non-viral reprogrammed iPSCs

In order to assess whether the episomal or viral reprogramming method induces weaker or less alterations in gene expression we compared the gene gene expression signatures of episomal-derived iPSCs (E-iPSCs), viral-derived iPSCs (V-iPSCs) and human embryonic stem cells (hESCs) (Figure 3.3). E-iPSCs and V-iPSCs were derived from the same genetic background, the human fetal fibroblast cell line HFF1. The retro-viral reprogrammed iPSC-line vHFF1-iPS-iPS4, which was used for this study, was generated in our laboratory and is fully characterized (Prigione et al. [2010]; Wang et al. [2010]). RNA-based microarray analysis showed that the transcriptome profile of E-iPSCs is closer to that of hESCs (R^2 = 0.9363) than the transcriptome profile of V-iPSCs (R^2 = 0.8176) (Figure 3.3A). The cluster analysis reinforced this result (Figure 3.3B). Further, pluripotency gene expression levels were analyzed. The transcriptome profile of E-iPSCs is closer to that of hESCs than V-iPSCs (Figure 3.3C). The expression pattern of the viral reprogrammed cell line vHFF1-iPS-iPS4 is closer to the origin cell line HFF1. Karyotype analysis demonstrated that epiHFF1-iPS-B1 contains an aberration on chromosome 12 of unknown origin, but the karyotype of vHFF1-iPS-iPS4 has no aberration (Figure 2.5; Prigione et al. [2010]). The RNA-based microarray data of the expression level of the genes which are located on the short arm of chromosome 12 were analyzed to clarify if the aberration is a duplication of the short arm (Figure 3.3C). The genes are all most expressed in epiHFF1-iPS-B1 which could be an indication for a duplication. However, the expression pattern of epiHFF1-iPS-B1 is closer to that of hESCs than to the vHFF1-iPS-iPS4.

Further comparative analyses were performed to uncover difference and commonalities between the different iPSC-lines and hESCs. A Venn diagram was generated to visualize the distinct and overlapping genes expression patterns in V-iPSCs versus E-iPSCs and hESCs (Figure 3.4). We identified gene signatures representative of cellular housekeeping functions and pluripotency-associated genes (12,366 genes; e.g. *GAPDH*, *ACTB*, *OCT4/POU5F1*, *SOX2*, *NANOG*), V-iPSC-specific genes (960 genes; e.g. *IRAK4*, *MASP1*, *SLMF7*, *TLR4*), donor cell-memory genes (222 genes; e.g. *LAMA4*, *TERC*), E-iPSC-specific gene expression signature (441 genes; e.g. *DAZ4*, *FGD4*, *GJC3*, *HSF1*, *TDGF3*, *TCF15*) and hESC-specific genes (621 genes; e.g. *FGFBP1*, *GATA3*, *GSC*, *PEG3*, *WNT3A*) (Figure 3.4, the entire gene lists are presented in Supplementary Table 3). The intersection of hESC and E-iPSC from the Venn diagram contains genes (1,045 genes; e.g. *BMP4*, *CDH1*, *CER1*, *DNMT3B*, *EOMES*, *FGF4*, *FGF8*, *HAND1*, *JAG2*, *LEFTY1*, *MIXL1*, *NODAL*, *T*, *TDGF1*) which are involved in biological processes such as developmental signaling, pluripotency, self-renewal and gastrulation. The intersection of hESC and V-iPSC from the Venn diagram contains genes (607 genes; e.g. *FGF9*, *HAND2*, *SOX7*, *TBX1*, *WNT8A*) which are involved in developmental processes (Figure 3.4A).
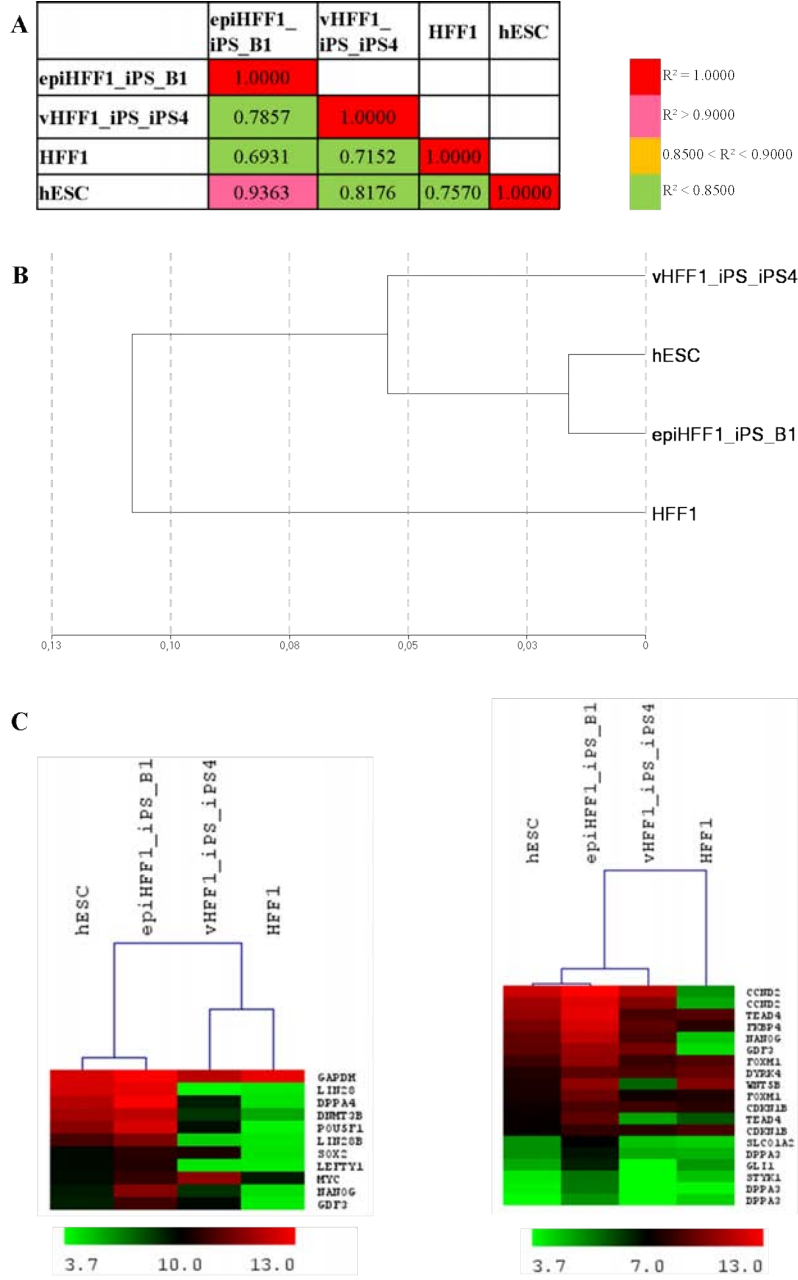
Figure 3.3: **Transcriptome profiling of non-viral, episomal reprogrammed iPSC line epiHFF1-iPS-B1.**
A) Pearson correlation co-efficient of the entire expression data (Illumina microarrays) between indicated cell types uncovered the similarity between E-iPSCs and hESCs ($R^2 = 0.9363$). In comparison the transcriptome profile of viral reprogrammed iPSCs deviated from hESCs to a greater extent ($R^2 = 0.8176$). **B)** A dendrogram analysis confirmed that the transcriptome profile of epiHFF1-iPS-B1 is similar to hESC (ES). **C)** Analysis of the transcriptome relations of pluripotency genes between hESC, epiHFF1-iPS-B1, vHFF1-iPS-iPS4 and HFF1 (left hand). Analysis of the transcriptome relations at cell cycle, pluripotency and development related gens located on the short arm of chromosome 12 between hESC, epiHFF1-iPS-B1, vHFF1-iPS-iPS4 and HFF1 (right hand). Abbreviations: hESC = human embryonic stem cell; iPSC = induced pluripotent stem cells; HFF1 = human foreskin fibroblast; epi = episomal reprogrammed; v = viral reprogrammed.

39

In order to analyze the similarity of viral- and episomal-derived iPSC as well as the resemblance to hESCs a heatmap of pluripotent-associated and transcription factor genes was created (Figure 3.4B). This heatmap underlines that E-iPSCs are more similar to hESCs than V-iPSCs. Common pluripotent-associated genes and transcription factor genes such as *NANOG*, *LIN28*, *LEFTY1*, *DNMT3B*, *POU5F1* (*OCT4*) and *KLF4* are down regulated in V-iPSCs compared to E-iPSCs and hESCs (Figure 3.4B). Hence, this underlines the similarity between E-iPSCs and hESCs as well as the difference between E-iPSCs and V-iPSCs as well as hESCs and V-iPSCs.
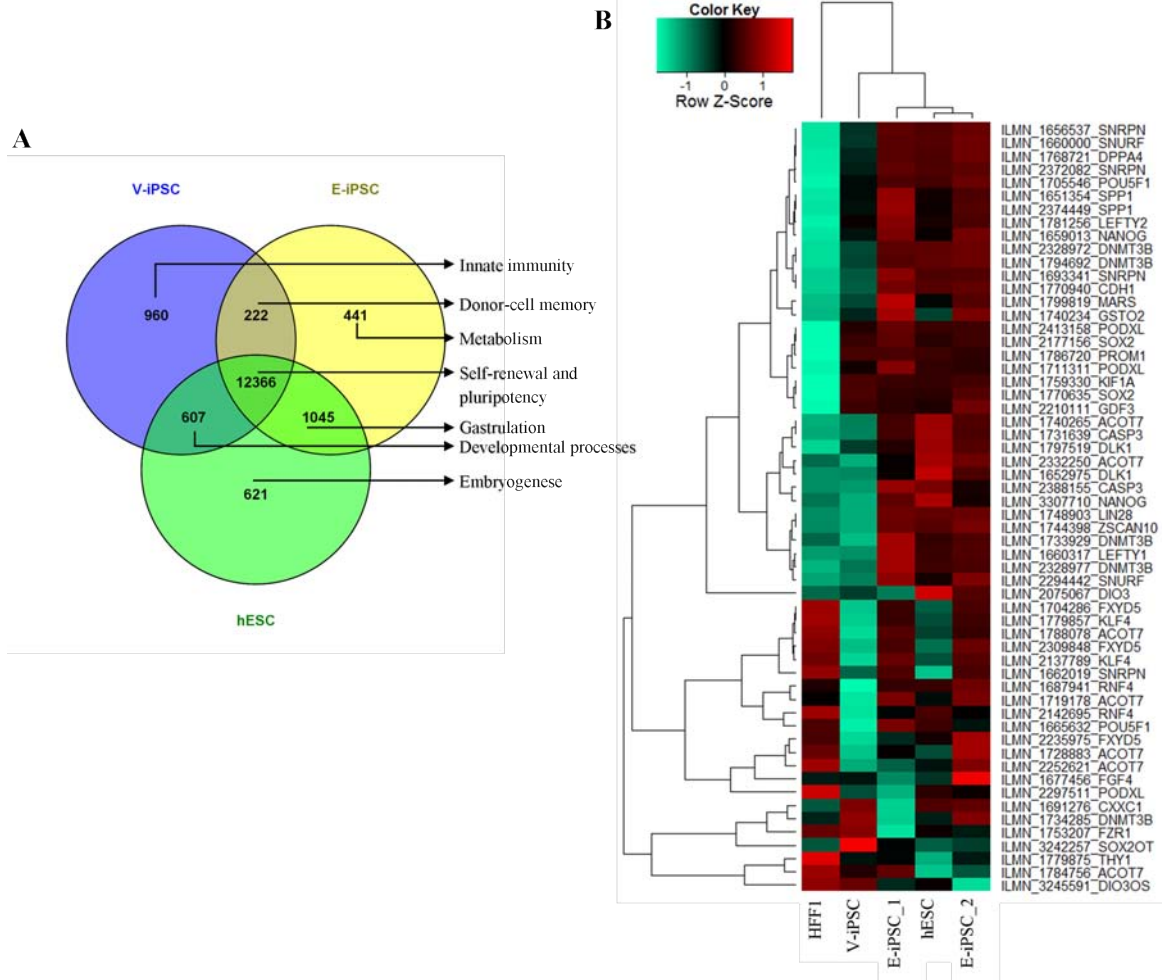
Figure 3.4: **Microarray-based gene expression profiling.**
A) Venn diagram analysis of the transcriptome profile from vHFF1-B1 (V-iPSC), epiHFF1-B1 (E-iPSC) and hESC portraying distinct and overlapping transcriptional signatures. **B)** Heatmap of pluripotent-associated and transcription factor genes. Expression pattern of hESCs, episomal reprogrammed HFF1-cell line epiHFF1-iPS-B1 (E-iPSC), retro-viral reprogrammed HFF1-cell line vHFF1-iPS-iPS4 (V-iPSC) and the somatic cell line HFF1 were compared. Abbreviations: V-iPSC = viral reprogrammed induced pluripotent stem cell; E-iPSC = episomal plasmid-based reprogrammed induced pluripotent stem cell; hESC = human embryonic stem cell; HFF1 = human fetal fibroblasts.

3.1.2 Characterization of human umbilical vein endothelial cell-derived iPSC line

Reprogramming of the human fetal fibroblast cell line (HFF1) was shown already in this study (Chapter 3.1.1). In addition, we could show that the episomal-based reprogramming method results in induced pluripotent stem cells (iPSCs) which are more similar to the characteristics of human embryonic stem cells (hESC) than the viral-based reprogrammed iPSCs (Chapter 3.1.1). In order to assess whether cells of other origin can be also reprogrammed with the episomal-based method, we used human umbilical vein endothelial cells (HUVECs). HUVECs were reprogrammed using the same protocol which was described in Chapter 2 for the reprogramming of HFF1. The nucleofection of a GFP-vector showed in HUVECs a transduction efficency of 77.0 %. The reprogramming efficiency ranged between 1.9 and 2.5 %, retrovirus reprogramming of HUVEC yield an efficiency of 2.5 - 3.0 % (Supplementary Figure S7; Panopoulos et al. [2011]). After picking of clones the master plates were stained positive for the pluripotency markers OCT4 and PODXL as well as for the surface marker TRA-1-60, TRA-1-81 and SSEA-4. The cells were negatively stained for CD31, a HUVEC marker, and SSEA-1, a marker for differentiation in human pluripotent stem cells (Figure 3.6).
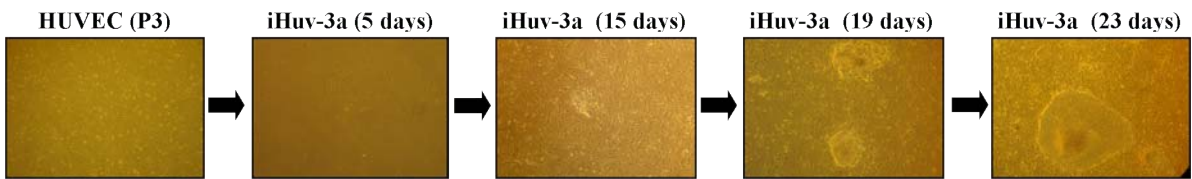
Figure 3.5: **Illustration of HUVEC reprogramming.**
Microscopy images showing morphology changes during the episomal reprogramming of HUVECs to induced pluripotent stem cells (iPSC). The first image is HUVEC passage 3 before reprogramming. The cells were episomal reprogrammed, cultured the first seven days in HUVEC-medium and were treated with small molecules one day after reprogramming. The second image represent reprogrammed HUVEC (iHuv-3a) on day 5. On day seven the cells were trypsinized and seeded on mouse embryonic fibroblasts (MEFs). Eight days later iPSC-HUVEC-colonies were visible (Image 3), additional four days later the iHUVEC-colonies seem stable and the small molecules were displaced (Image 4). Last image shows a iHUVEC-colony which was selected and transferred after taking this picture.
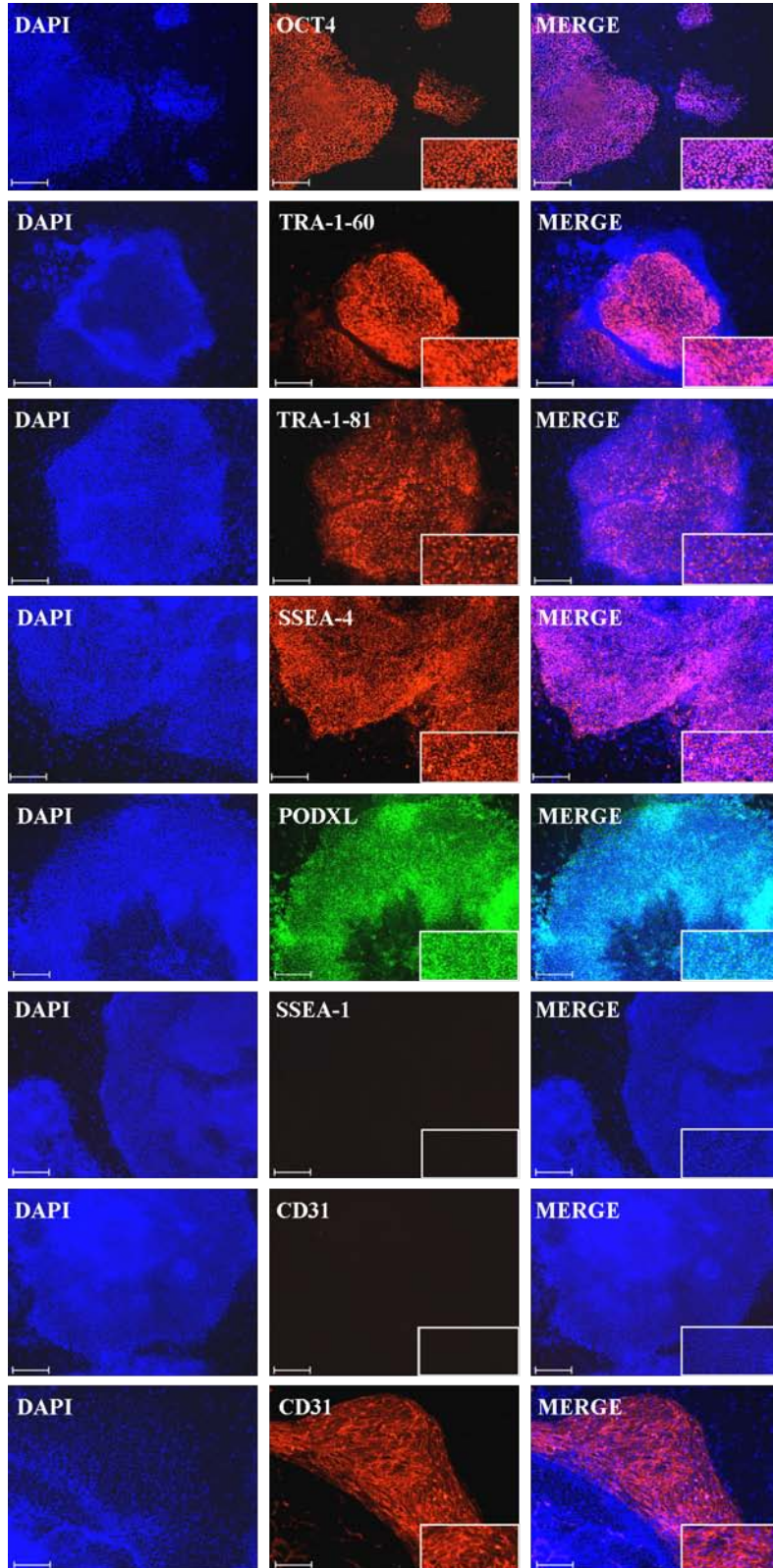
Figure 3.6: **Immunofluorescence-based characterization of HUVEC-derived iPSCs.**
Detection of the pluripotency marker OCT4, surface marker TRA-1-60, TRA-1-81, SSEA-4 and
PODXL, as well as the absence of the surface marker SSEA-1 and CD31. DAPI stained the nucleus.
Scale bar: 200 μm, Alexa Flour 488 (green), Alexa Flour 594 (red).

The iPSC-line (epiHUV-iPS-3a) which was generated and characterized in this study is genome integration free (Figure 3.7; Matz and Adjaye [2015]) and has similar characteristics as hESC lines (Figure 3.9 - 3.12; Matz and Adjaye [2015]; Supplementary Figure S1 and S2).

The epiHUV-iPS-3a expresses pluripotency associated makers, such as OCT4, SOX2, NANOG and amongst others the surface markers TRA-1-60, TRA-1-81, SSEA-4, but not SSEA-1 (Figure 3.8 and 3.9; Matz and Adjaye [2015]). SSEA-1 is a marker protein of differentiation in human embryonic stem cells (hESCs) though a marker of the undifferentiated state in mouse ESC (Thomson et al. [1998]; Takahashi et al. [2007a]; Yu et al. [2007]). The karyotype analysis demonstrated that epiHUV-iPS-3a is a karyotypic normal human female cell line. The DNA fingerprint is identical to the fingerprint of HUVECs, but differs when compared to the hESC lines H1 and H9 (Figure 3.10; Matz and Adjaye [2015]). The expression pattern of pluripotency genes was quantified by qRT-PCR and compared to the pattern of H1 cells and the iPSC line epiHFF1-iPS-B1. The expression pattern of the iPSC-line epiHUV-iPS-3a is similar to H1 and epiHFF1-iPS-B1 (Figure 3.11). These iPSC line has the capacity differentiate *in vitro* in all three germ layers endoderm, ectoderm and mesoderm by formation of embryoid bodies (Figure 3.12; Matz and Adjaye [2015]) and also *in vivo* by teratoma formation in imundificient mice (Figure 3.13; Matz and Adjaye [2015]).
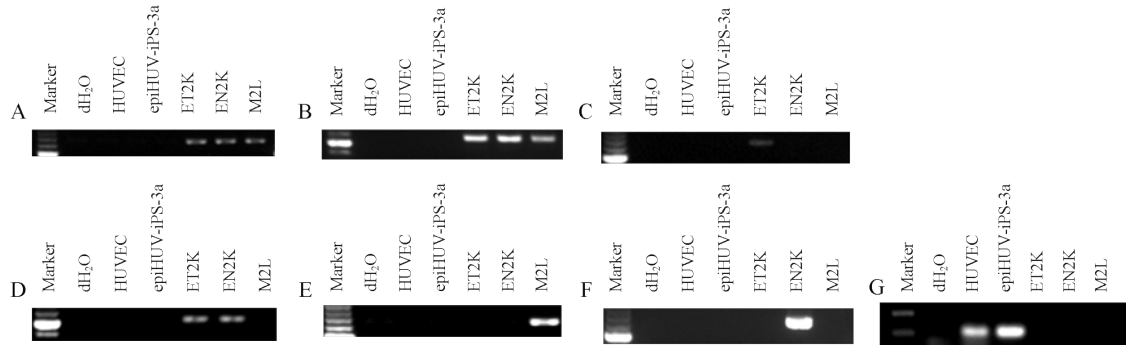
Figure 3.7: **PCR of plasmid detection in epiHUV-iPS-3a.**
A) EBNA-1 detection of the plasmid vector. **B)** OriP detection of the plasmid vector. **C)** SV40LT detection of the plasmid ET2K vector. **D)** OCT4 detection of the plasmid ET2K and EN2K vectors. **E)** LIN28 detection of the plasmid M2L vector. **F)** NANOG detection of the plasmid EN2K vector. **G)** Detection of the human OCT4 genome gene sequence. 100 bp Marker was used. The vectors ET2K, EN2K and M2L which were transfected into the HUVEC cells, were used as a positive control, the original cell line (HUVEC) and water were used as the negative controls. Modified from Matz and Adjaye [2015].
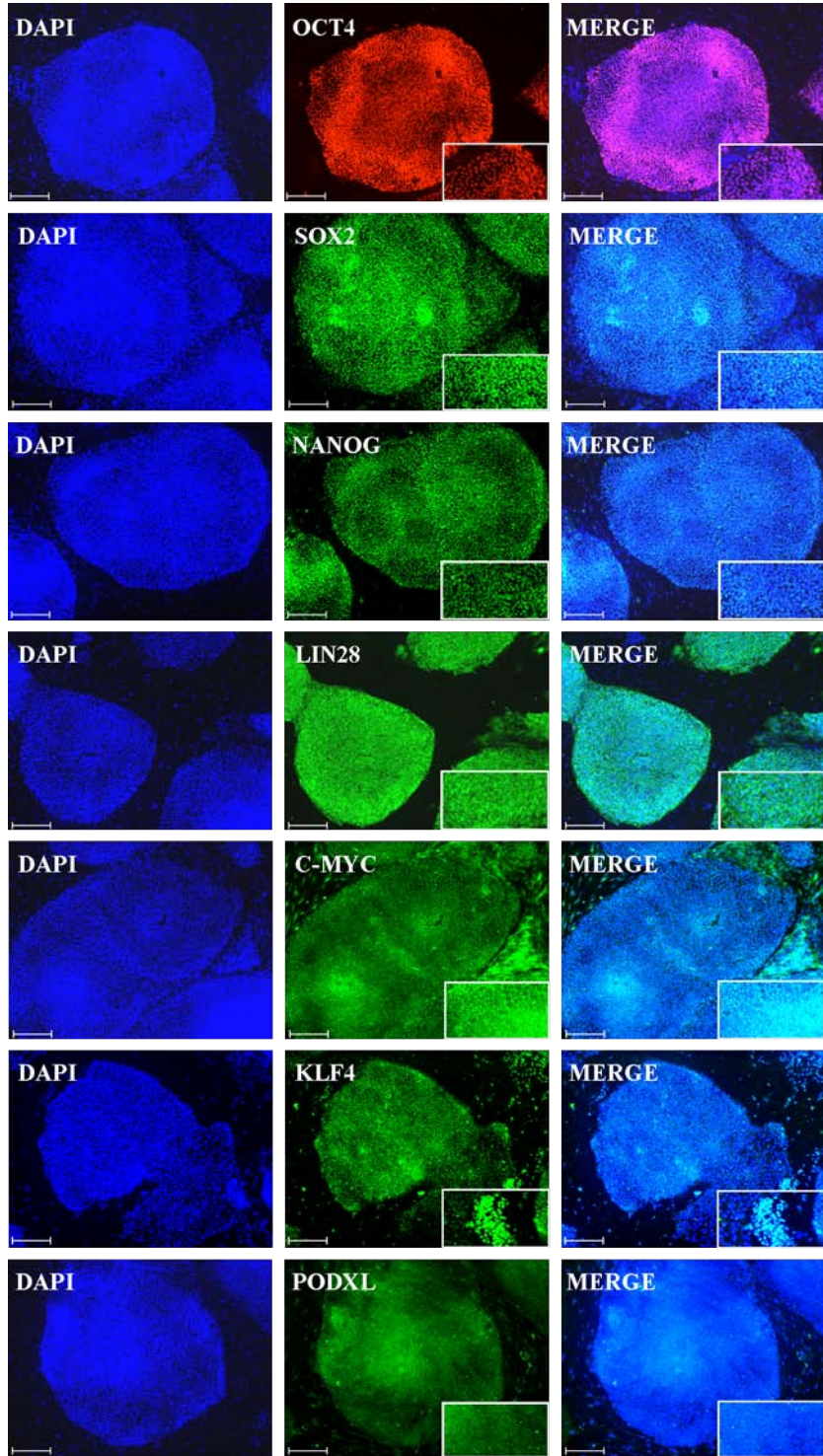
Figure 3.8: **Immunofluorescence-based detection of pluripotency markers in epiHUV-iPS-3a.**
All protein stainings for pluripotency markers OCT4, NANOG, SOX2, KLF4, c-MYC, LIN28 and PODXL were positive. DAPI stained the nucleus. Scale bar: 200 μm, Alexa Flour 594 (red), Alexa Fluor 488 (green). Modified from Matz and Adjaye [2015].
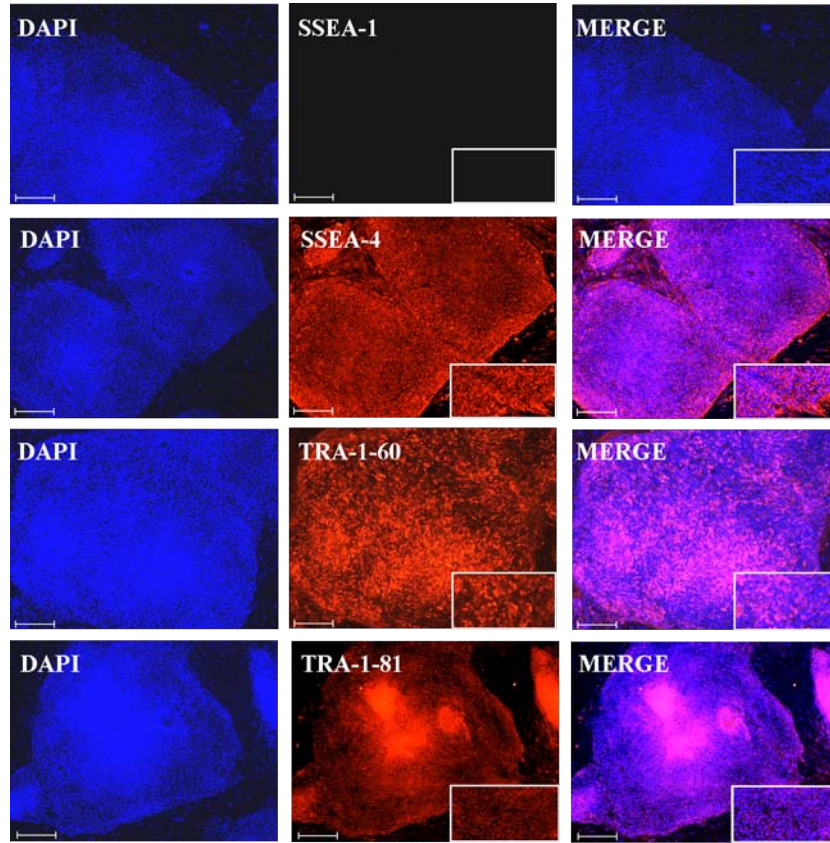
Figure 3.9: **Immunofluorescence-based detection of surface markers in epiHUV-iPS-3a.**
Protein stainings for the surface markers SSEA-4, TRA-l-60 and TRA-1-81 were positive, SSEA-1 was
negative. DAPI stained the nucleus. Scale bar: 200 μm, Alexa Flour 594 (red). Modified from Matz
and Adjaye [2015].
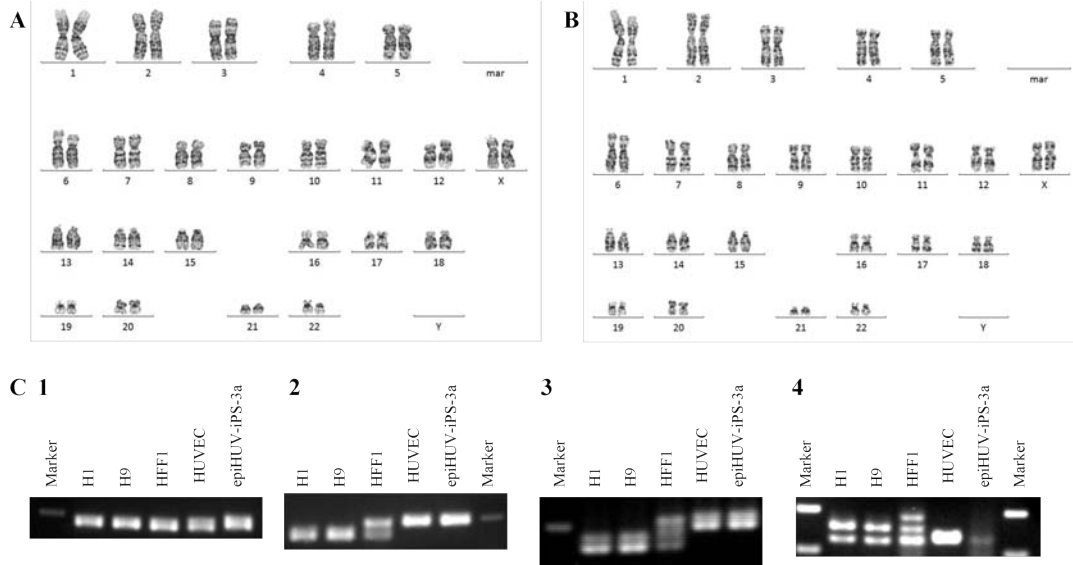
Figure 3.10: **Karyogram and DNA Fingerprint of epiHUV-iPS-3a.**
A) A normnal female karyogram 46,XX of HUVEC. **B)** A normnal female karyogram 46,XX of epiHUV-iPS-3a derived from HUVEC. mar = minimal altered region. **C)** Genomic DNA from hESCs H1 and H9, HFF1 cells, HUVEC and the viral-free epiHUV-iPS-3a for PCR were used. 1: Genomic PCR with the primer of D7S796. 2: Genomic PCR with the primer of D10S1214. 3: Genomic PCR with the primer of D17S1290. 4: Genomic PCR with the primer of D21S2055. 100 bp Marker was used. Modified from Matz and Adjaye [2015].
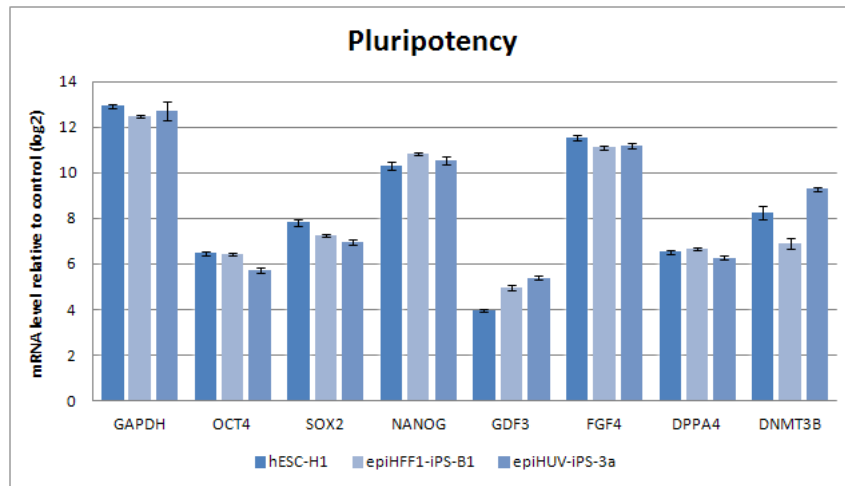
Figure 3.11: **Quantitative real-time PCR of epiHUV-iPS-3a.**
Expression pattern of pluripotency markers relative to HUVEC from hESC-line H1, the iPSC-line epiHFF1-iPS-B1 and the iPSC-line epiHUV-iPS-3a are shown. Three biological replicates in technical triplicates of each sample were analyzed against HFF1 as control. The standard deviation is depicted by the error bars.
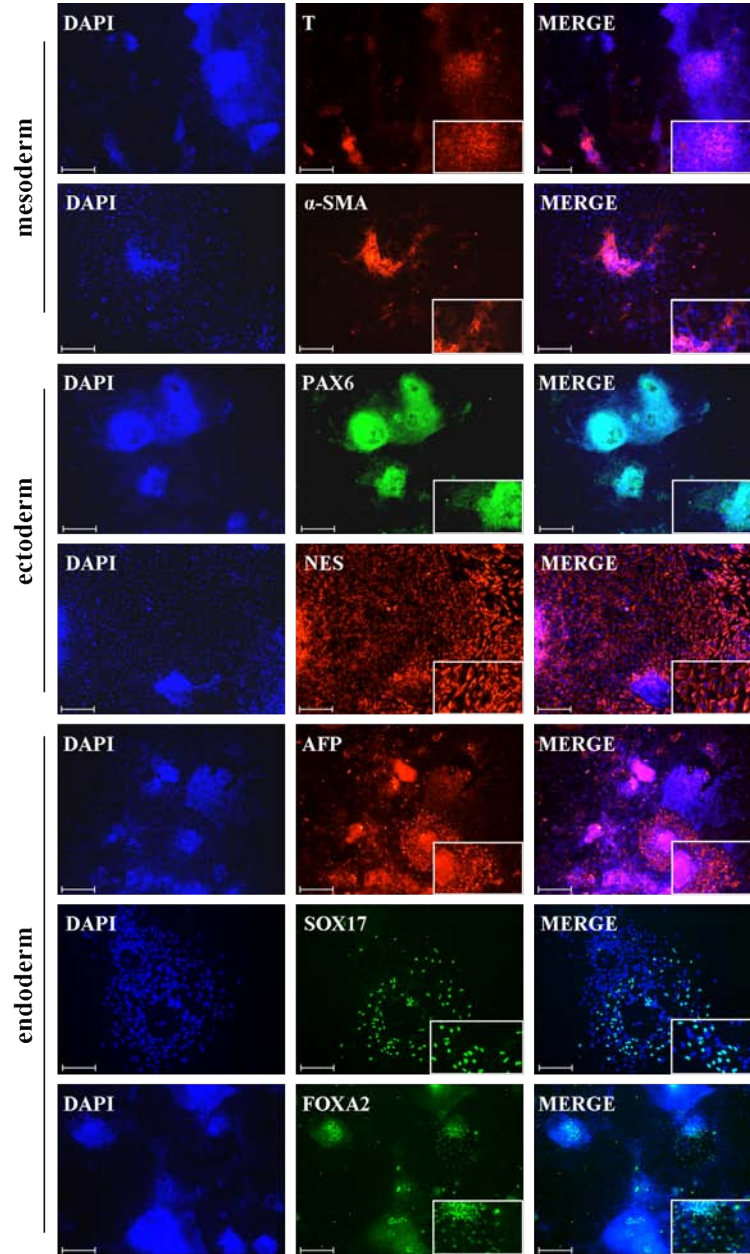
Figure 3.12: **Immunofluorescence-based detection of germ-layer specific proteins EBs derived from epiHUV-iPS-3a.**
All three germ layers mesoderm, ectoderm and endoderm were detected *in vitro* by formation of embryoid bodies. The detection of the proteins BRACHYURY and Smooth Muscle Actin (α-SMA) are markers of mesoderm layer, Paired Box 6 (PAX6) and NESTIN detect the ectoderm layer and AFP, SOX17, FOXA2 are markers of endoderm layer. DAPI stained the nucleus. Scale bar: 200 μm Alexa Flour 594 (red), Alexa Fluor 488 (green). Modified from Matz and Adjaye [2015].
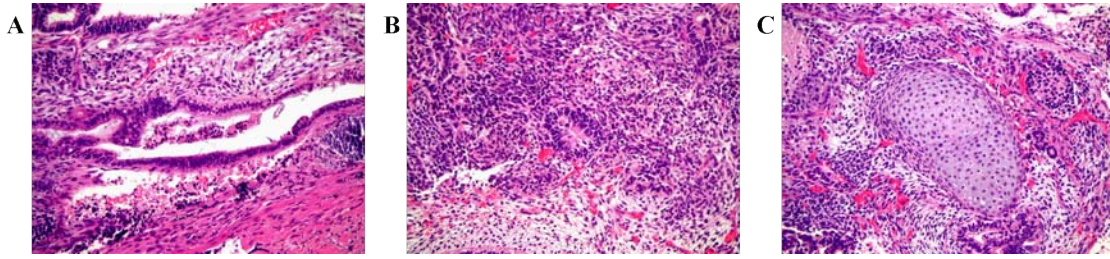
Figure 3.13: **Teratoma of epiHUV-iPS-3a.**
In vivo teratoma formation of epiHUV-iPS-3a upon injection into NOD scid gamma mice. Representative images of histological structures corresponding to **A)** endoderm, **B)** ectoderm, **C)** mesoderm lineages are depicted. Modified from Matz and Adjaye [2015].

Global gene expression analyses

The iPSCs derived from human umbilical vein endothelial cells (HUVECs) were derived and fully characterized (Chapter 3.1.2). Reprogramming of somatic cells to iPSCs results in major changes in transcriptional profile of the cells (Wolfrum et al. [2010]). To analyze these changes during the reprogramming procedure of HUVECs RNA-microarray analyses were performed by the use of the Illumina Bead-Studio platform. In addition, the transcriptome profiles of HUVECs and the episomal reprogrammed iPSC-line epiHUV-iPS-3a from HUVEC (E-iPSCs) were confirmed to that of human embryonic stem cells (hESCs) (Figure 3.14). During the reprogramming process the transcriptome profile of the cell shifted from the parental towards a hESC-like stage. The parental HUVECs lost their expression upon reprogramming while other sets of genes were activated upon reprogramming. A third set of genes was maintained in both states. This expression pattern is comparable with other iPSC lines such as the HFF1-derived iPSC lines (HFF1-iPSCs) in this study (Figure 3.14A). The transcriptome profile of the iP-SCs departed from that of the donor cells and converged to the transcriptome profile of hESCs (Figure 3.14B). To visualize the distinct and overlapping genes expression patterns in HUVECs versus E-iPSCs and hESCs a Venn diagram was generated (Figure 3.14C). We identified gene signatures representative of cellular housekeeping functions (11,000 genes; e.g. *GAPDH*, *ACTB*, *PGK1*, *LDHA*), donor cell (HUVEC)-specific genes (630 genes; e.g. *CDH5*, *FAT4*, *KLK3*, *PECAM1*), donor cell-memory genes (246 genes; e.g. *AKT3*, *ENG*, *ICAM1*, *MLC1*), self-renewal and pluripotent genes (2,027 genes; e.g. *POU5F1*, *SOX2*, *NANOG*, *LIN28*, *GDF3*), iPSC (E-iPSC)-specific gene expression signature (750 genes; e.g. *ART3*, *FGD4*, *GJC3*, *PLCE1*, *SDC3*) and hESC-specific genes (1,187 genes; e.g. *DDX20*, *FGFBP1*, *FGF9*, *MIXL1*, *WNT3A*, *TP63*) (Figure 3.14C, the entire gene lists are presented in Supplementary Table 4). The intersection of hESC and E-iPSC from the Venn diagram contains genes (e.g. *CDH1*, *CER1*, *EOMES*, *JAG2*, *KIT*, *LEFTY1*, *LEFTY2*, *NODAL*, *RSPO3*, *SOX2*, *WNT10B*) which are involved in biological processes such as developmental signaling, pluripotency, self-renewal and embryogenesis (Figure 3.14D).
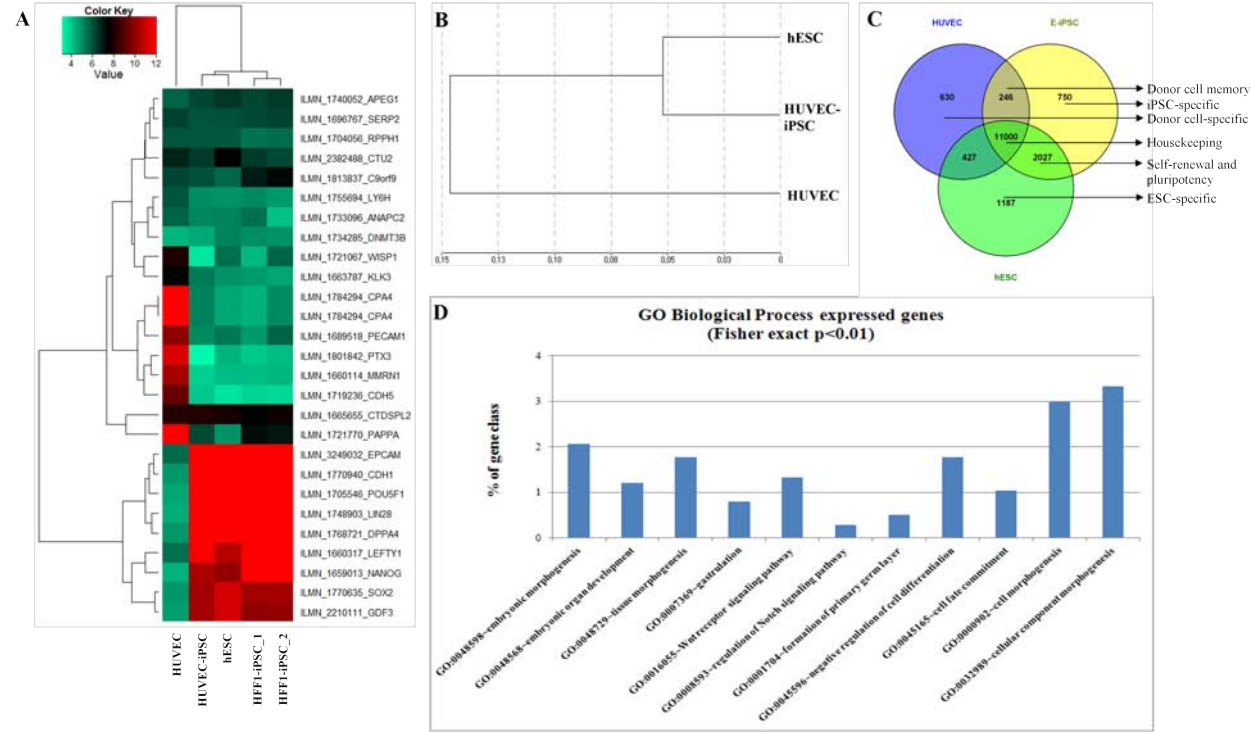
Figure 3.14: **Microarray data analyses.**
A) Heatmap visualizing principle of cellular reprogramming. Expression pattern of hESCs, episomal reprogrammed HUVEC-cell line epiHUV-iPS-3a (HUVEC-iPSC), the somatic cell line HUVEC and two HFF1-derived iPSC lines were compared. Ten genes with transcription activity either unchanged (Retained), low (Lost) or high (Acquired) expression values of iPSCs relative to the parental cell line (HUVEC) were selected. **B)** A dendogram analysis confirmed that the transcriptome profile of epiHUV-iPS-3a (HUVEC-iPSC) is similar to hESC. **C)** Venn diagram analysis of the transcriptome profile from HUVEC, HUVEC-iPSC (E-iPSC) and hESC portraying distinct and overlapping transcriptional signatures. **D)** Graph of biological processes related to embryogenesis and pluripotency to percentage of genes from the intersection of E-iPSC and hESC from the venn diagram (C). Abbreviations: hESCs = human embryonic stem cells; HUVEC = human umbilical vein endothelial cells; E-iPSC = episomal reprogrammed induced pluripotent stem cell; HUVEC-iPSC = human umbilical vein endothelial cell-derived induced pluripotent stem cell.

3.1.3 Transcriptome profile-based comparison of iPSCs

As described before during the reprogramming process the somatic cells change their transcriptome profile in several sets of genes (Wolfrum et al. [2010]). It moves from somatic cell specifics and converges into a pluripotent stem cell-like stage, which is similar to the transcriptome profile of hESCs. To show that this is also true for different somatic cell types HFF1 and HUVEC were reprogrammed and compared. Human foreskin fibroblasts were isolated from neonatal foreskin (Gorman et al. [1979]). Human umbilical vein endothelial cells (HUVECs) are cells derived from the endothelium of veins from the umbilical cord (Park et al. [2006]). In order to visualize this transformation of the two independent reprogrammed cell lines a dendogram was compiled of the transcriptome profiles from HFF1, HFF1-iPSC, HUVEC, HUVEC-iPSC, hESC (Figure 3.15A). Both iPSC lines differ from their parental cell type and from the other somatic cell type. However, the transcriptome profiles of the two iPSC lines are similar to that of hESCs. In order to deliver insight into details the pearson correlation co-efficient was evaluated (Figure 3.15B). The transcriptome profile of HUVEC-iPSC correlated most with that of hESC (R^2 = 0.8989) and then with the transcriptome profile of HFF1-iPSC (R^2 = 0.8957). Furthermore, to establish differences and commonalities between the parental cell lines and the iPSCs a Venn diagram was conducted (Figure 3.15C, Supplementary Table 5). HFF1-iPSCs share 417 genes with their parental cell line HFF1. The largest percentage of these genes is involved in basic cellular processes, e.g. in organization and assembling of chromosomes, chromatin and nucleosome, DNA packaging and metabolic processes, cell cycle and cell devision (e.g. *EPC2, FZR1, SEP15, TADA2A*). HUVEC-iPSCs share 94 genes with their parental cell line HUVEC. Most of these genes are involved in homeostasis and homeostatic processes, ion transport, response to wounding as well as defense and inflammatory response (e.g. *C11ORF9, IL1A, P2RX1*). However, HFF1-iPSCs and HUVEC-iPSCs share most of the genes (1,074 genes, e.g. *EOMES, EPCAM, DPPA4, NODAL, POU5F1, SOX2, TNNT2, VGF*), which are involved in cellular processes and homeostasis as well as embryogenesis and morphogenesis.

In order to analyze the differences and commonalities between the iPSC lines and hESC a venn diagram of the three transcriptome profiles was generated (Figure 3.15D, the entire gene lists are presented in Supplementary Table 6). The intersection of all three samples contains genes which are involved in biological processes such as developmental signaling, pluripotency, self-renewal and embryogenesis (e.g. *CDH1, CER1, EOMES, JAG2, KIT, LEFTY1, LEFTY2, NANOG, NODAL, POU5F1, RSPO3, SOX2, WNT10B*). Analyses of the intersections HEFF1-iPSC vs. hESC and HUVEC-iPSC vs. hESC as well as genes expressed only in hESC uncovered the maximum difference was arranged in the expression of genes which are involved in transcription and regulation of transcription (intersection of HEFF1-iPSC vs. hESC 894genes, e.g. *MIXL1, ZNF488, ZNF583*; intersection HUVEC-iPSC vs. hESC 520 genes, e.g. *SOX17, ZFP14, ZNF536*; section of hESC 720 genes, e.g. *CDX2, ZNF276, ZNF711*).
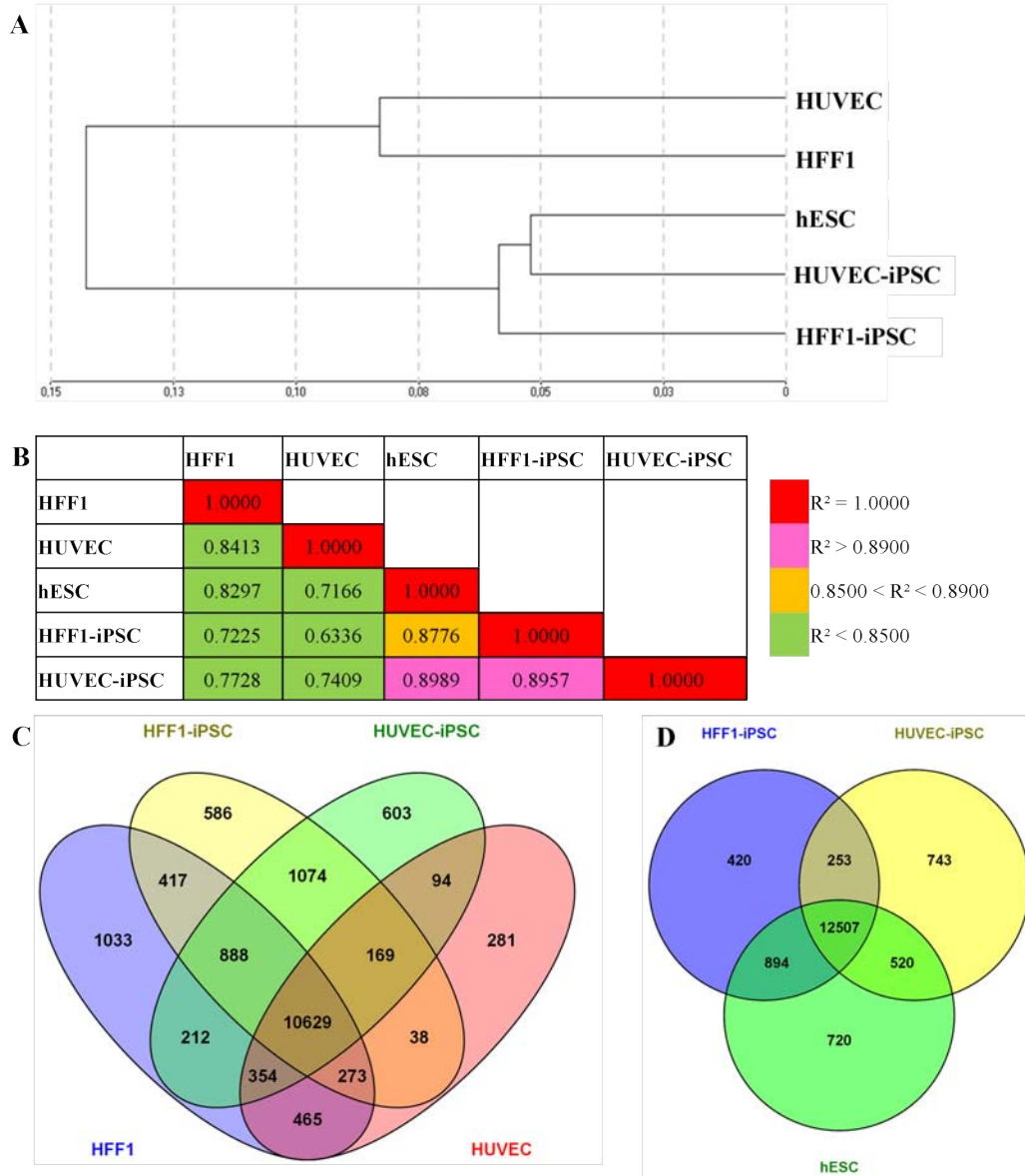
Figure 3.15: **Comparison of the transcriptome profile from episomal reprogrammed iPSC lines.**
A) A dendogram analysis confirmed that the transcriptome profile of iPSC lines is similar to hESC. **B)** Pearson correlation co-efficient of the entire expression data (Illumina microarrays) between indicated cell types uncovered the similarity between HUVEC-iPSC and hESCs ($R^2 = 0.8989$). In comparison the transcriptome profile of HFF1-iPSC deviated from hESCs to a greater extent ($R^2 = 0.8776$). **C)** Venn diagram analysis of the transcriptome profile from HFF1, HFF1-iPSC, HUVEC and HUVEC-iPSC portraying distinct and overlapping transcriptional signatures. **D)** Venn diagram analysis of the transcriptome profile from HFF1-iPSC, HUVEC-iPSC and hESC portraying distinct and overlapping transcriptional signatures. Abbreviations: hESCs = human embryonic stem cells; HFF1 = human foreskin fibroblast 1; HFF1-iPSC = episomal reprogrammed induced pluripotent stem cell derived from HFF1 cells, HUVEC = human umbilical vein endothelial cell.

3.2 Derivation and characterization of hepatocyte-like cells derived from iPSCs

3.2.1 Derivation of HLCs from HFF1-iPSC

We could show, that somatic cells can be reprogrammed with an episomal-based approach and the generated induced pluripotent stem cells (iPSCs) are similar to human embryonic stem cells (hESCs) (Chapter 3.1). In general, hESCs and iPSCs can be differentiated directly to the cell type of interest (Hay et al. [2007]; Sullivan et al. [2010]; Zhou et al. [2010]; Gherghiceanu et al. [2011]; Jozefczuk et al. [2011]; Barker et al. [2012]; Cheng et al. [2012]; Emdad et al. [2012]; Hannan et al. [2013]; Dianat et al. [2014]). In earlier studies our laboratory generated hepatocyte-like cells (HLCs) from hESC and viral reprogrammed iPSC lines (Jozefczuk et al. [2011]; Jozefczuk et al. [2012b]). In this study HLCs were derived from the episomal reprogrammed cell line epiHFF1-iPS-B1. The differentiation procedure consists of three stages (Figure 3.16). First, the undifferentiated cells were differentiated to definitive endoderm (DE), second, to the hepatic endoderm (HE) stage and third, to hepatocyte-like cells. Continuous morphological changes from the undifferentiated stage to HLCs were observed as discribed by Jozefczuk et al. [2011].
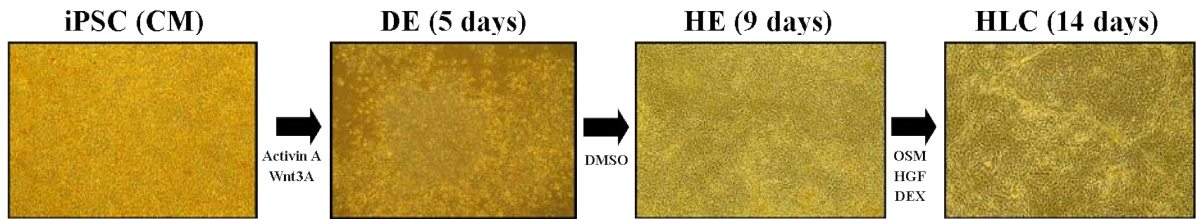
Figure 3.16: **Illustration of HLC differentiation derived from epiHFF1-iPS-B1.** Microscopy images depict morphological changes during the differentiation of epiHFF1-iPS-B1 (iPSC-line) to HLCs. The iPSC-line were cultured in CM. The generation of the first stage DE takes five days. HE is the second stage and takes four days. After 14 days the differentiation is completed and matured HLCs is the endpoint of the third stage. Abbreviations: CM = conditioned medium; iPSC = induced pluripotent stem cell; DE = definitive endoderm; HE = hepatic endoderm; HLC(s) = hepatocyte-like cell(s).

During the first differentiation step from iPSC to DE the pluripotency marker OCT4 was down regulated (Figure 3.17). Forkhead box A2 (FOXA2) was expressed, usually expressed by the DE progenitors, as well as SRY (sex determining region Y)-box 17 (SOX17), a marker of definitive endoderm. The Hepatocyte nuclear factor 4 alpha (HNF4α) is an early marker of endoderm development and is expressed during the whole HLC differentiation procedure (Greber et al. [2007]; Agarwal et al. [2008]).

Immunocytochemistry analysis of HE showed a positive staining of HNF4α, the early marker alpha-Fetoprotein (AFP) and later-stage marker Albumin (ALB) for hepatic commitment (Figure 3.18). HE cells were stained positive for Cytokeratin 18 (CK18),

which is expressed at the end of the second stage of HLC differentiation. E-Cadherin (E-CAD/CDH-1) marking the mesenchymal-to-epithelial transition (MET), established cell-cell contacts and indicates the epithelial nature of the developing liver cells (Gouon-Evans et al. [2006]; Cai et al. [2007]; Hay et al. [2008a]; Agarwal et al. [2008]; Choi and Diehl [2009]; Schietke et al. [2010]; Mah et al. [2011]; Nakagawa et al. [2014]).

At the endpoint of HLC differentiation AFP, ALB, HNF4α and E-CAD are expressed (Figure 3.19). CK18 is a marker of HE-stage and whose expression is decreased at HLC stage. The expression of alpha-1 Antitrypsin (A1AT) detect the late stage of liver differentiation and is involved in the maturation of the liver (Cai et al. [2007]; Agarwal et al. [2008]; Takayama et al. [2012]).
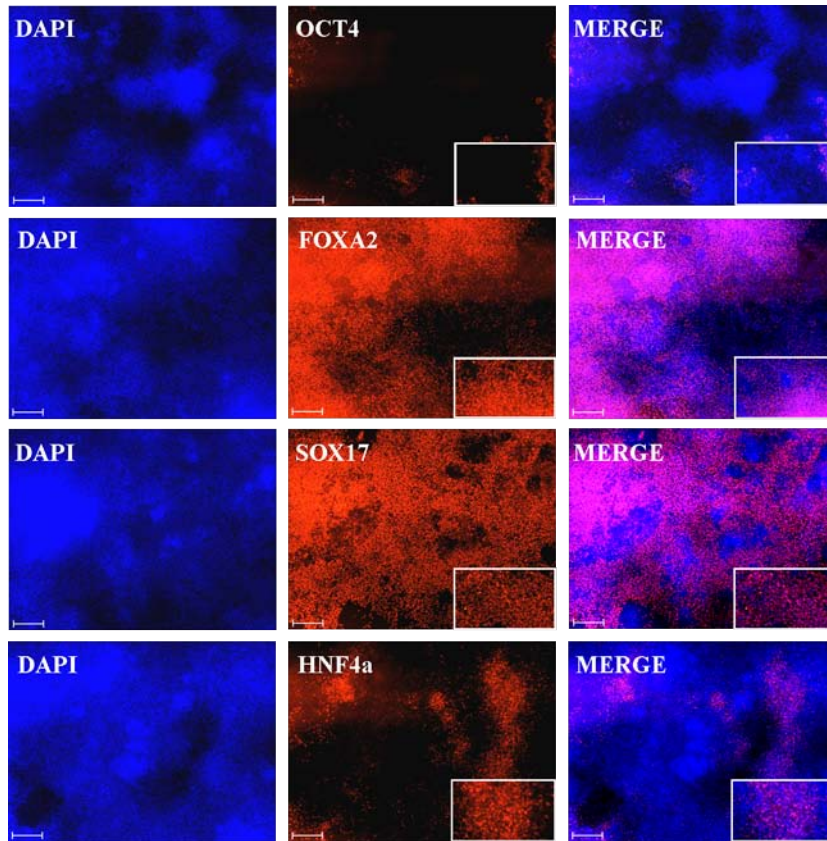
Figure 3.17: **Immunofluorescence-based detection of proteins in DE derived from epiHFF1-iPS-B1.**

Immunofluorescence for expression of a defining panel of proteins were examined. OCT4, pluripotency marker; FOXA2, SOX17 markers for DE and the transcription factor HNF4α. DAPI stained the nucleus. Scale bar: 200 μm Alexa Flour 594 (red). Abbreviations: DAPI = 4',6-diamidino-2-phenylindole; DE = definitive endoderm; FOXA2 = Forkhead box A2; HNF4α = hepatocyte nuclear factor 4 alpha; OCT4 = POU5F1, POU class 5 homeobox 1; SOX17 = SRY (sex determining region Y)-box 17.
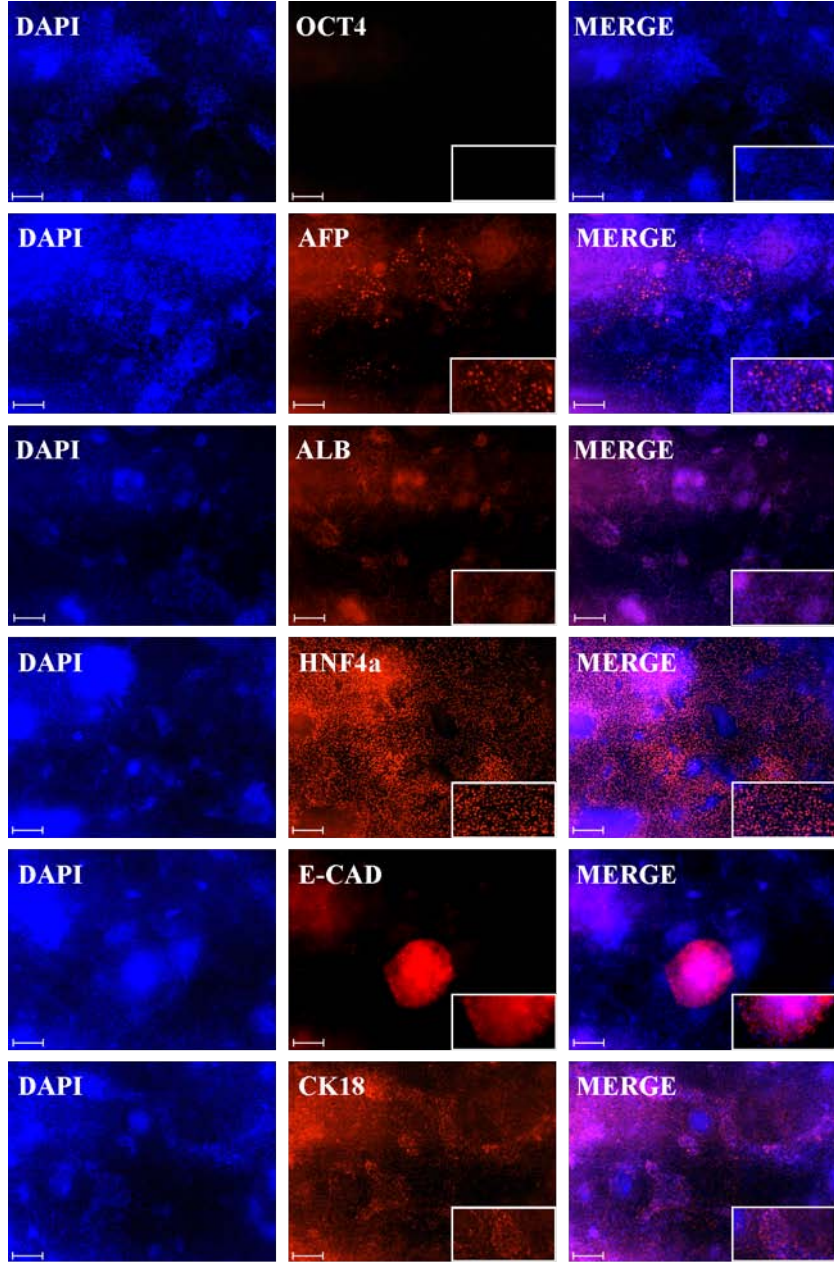
Figure 3.18: **Immunofluorescence-based detection of proteins in HE derived from epiHFF1-iPS-B1.**
The detection of the protein OCT4, pluripotency marker; AFP, ALB for early and later-stage hepatic proteins, the transcription factor HNF4α, E-CAD and CK18. DAPI stained the nucleus. Scale bar: 200 μm Alexa Flour 594 (red). Abbreviations: AFP = alpha-Fetoprotein; ALB = Albumin; CK18 = Cytokeratin 18; DAPI = 4',6-diamidino-2-phenylindole; E-CAD = E-Cadherin; HE = hepatic endoderm; HNF4α = hepatocyte nuclear factor 4 alpha; OCT4 = POU5F1, POU class 5 homeobox 1.
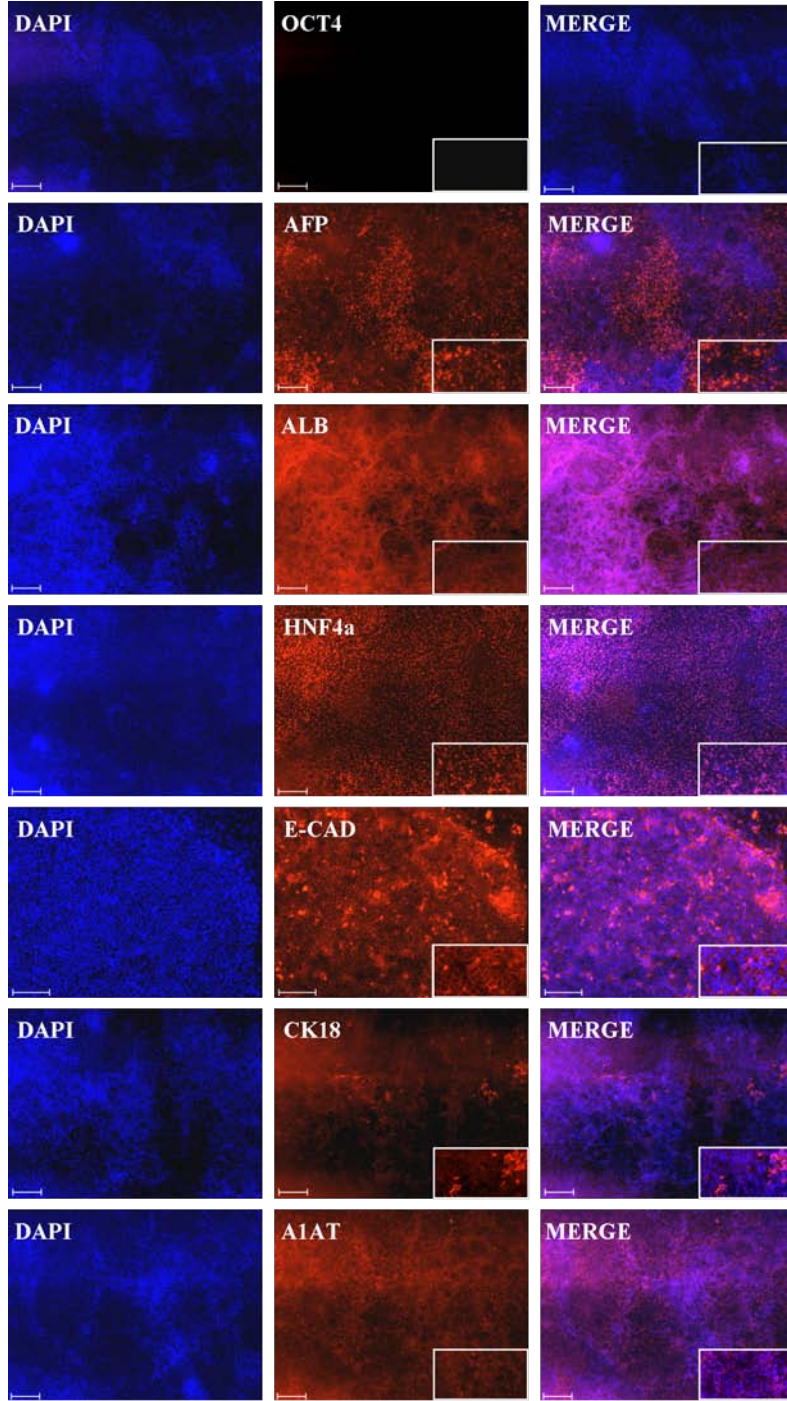
Figure 3.19: **Immunofluorescence-based detection of proteins in HLC derived from epiHFF1-iPS-B1.**
The detection of the protein OCT4, a pluripotency marker; AFP, ALB for early and later-stage hepatic proteins, the transcription factor HNF4α, E-CAD, CK18 and A1AT. DAPI stained the nucleus. Scale bar: 200 μm Alexa Flour 594 (red). Abbreviations: A1AT = Antitrypsin; AFP = alpha-Fetoprotein; ALB = Albumin; CK18 = Cytokeratin 18; DAPI = 4',6-diamidino-2-phenylindole; E-CAD = E-Cadherin; HLC = hepatocyte-like cell; HNF4α = hepatocyte nuclear factor 4 alpha; OCT4 = POU5F1, POU class 5 homeobox 1.

In order to verify the immunocytochemistry results a quantitative real time PCR (qRT-PCR) was performed. The qRT-PCR reflected the progress of expression pattern obtained by the immunocytochemistry results during the HLC differentiation of liver specific genes (Figure 3.20). The expression level of most liver markers increased from the first stage DE to the HE stage (Figure 3.20A). *SOX17*, *FOXA2* and *HNF4a* are the only genes which are highly expressed at the end of stage I, the DE stage. *SOX17* and *FOXA2* are core genes of DE and are involved in hepatic maturation. *HNF4α* is a key transcription factor and regulates different processes during the whole liver development. *AFP* is classified as an early-stage marker of hepatocytes and *ALB* as a late-stage marker, both expressions increased to the end of stage II of differentiation and increased further to the endpoint of differentiation, stage III. A1AT is a serum glycoprotein, which is synthesised and secreted by the liver. The level of gene expression changes during the differentiation is comparable to *AFP* and *ALB* (Li et al. [2000]; Watt et al. [2003]; D'Amour et al. [2005]; McLean et al. [2007]; Agarwal et al. [2008]; Hay et al. [2008a]; Takayama et al. [2011]; Takayama et al. [2012]; Teckman and Jain [2014]). T-box 3 (*TBX3*) is an important regulator of liver development and maintains the expression of hepatocyte transcription factors such as HNF4α (Figure 3.20B). The expression increased from DE to HLCs. Fumarylacetoacetate hydrolase (*FAH*) is involved in liver maturation and function. The expression increased from DE to HE and stagnated to HLCs. The Tryptophan 2,3-dioxygenase (*TDO2*) is a marker gene of mature hepatocytes and catalyses the oxidation of tryptophan to N-formyl kynurenine. *TDO2* is mostly expressed in HLCs. Prominin 1 (*PROM1/CD133*) is a proginitor and stem cell marker for embryonic and adult stem cells, but is also expressed in differentiated cells and tumors. CD133 is detectable in fetal liver. At the endpoint of HLC differentiation the expression level of *CD133* is high. Another stem cell and progenitor marker for liver cells is Leucine-rich repeat containing G protein-coupled receptor 5 (*LGR5*), which is also mostly expressed in HLCs (Yin et al. [1997]; Florek et al. [2005]; Mizrak et al. [2008]; Ldtke et al. [2009]; Schmidt et al. [2009]; Barker et al. [2012]; Cheng et al. [2012]; Huch et al. [2013]; Gil-Sanchis et al. [2013]; Prez-Carro et al. [2013]).
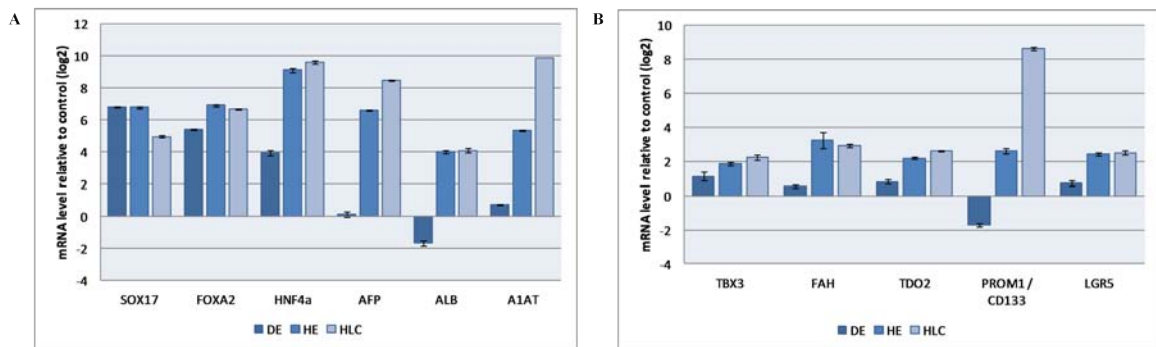
continued from previous page

Figure 3.20: **Quantitative real-time PCR profile of liver specific maker.**
A) qRT-PCR-derived expression changes of *SOX17*, *FOXA2*, *HNF4α*, *AFP*, *ALB* and *A1AT* in DE, HE and HLC. **B)** qRT-PCR-derived expression changes of (*TBX3*), *FAH*, (*TDO2*), *CD133* and *LGR5* in DE, HE and HLC. Three biological replicates in technical triplicates of each sample were analyzed. The standard deviation is depicted by the error bars. As control was used the RNA from HFF1-iPSC line (epiHFF1-iPS-B1) which was differentiated. Abbreviations: A1AT = alpha-1 Antitrypsin; AFP = alpha-Fetoprotein; ALB = Albumin; DE = definitive endoderm; FAH = Fumarylacetoacetate hydrolase; FOXA2 = Forkhead box A2; HE = hepatic endoderm; HLC = hepatocyte-like cell; HNF4α = hepatocyte nuclear factor 4 alpha; LGR5 = Leucine-rich repeat containing G protein-coupled receptor 5; qRT-PCR = quantitative real-time PCR; SOX17 = SRY (sex determining region Y)-box 17; TBX3 = T-box 3; TDO2 = Tryptophan 2,3-dioxygenase; PROM1/CD133 = Prominin 1.

Functional analysis of HFF1-iPSC-HLCs

To analyze whether or not the generated HLCs are functional several tests were conducted. First, an immunofluorescence-based detection of the protein E-Cadherin (E-CAD) was performed, which visualizes the typical polygonal morphology (Figure 3.21A). Second, the Periodic Acid-Schiff (PAS) staining was done to prove the glycogen storage, which underlines the functionality of HLCs (Figure 3.21B). Glycogen storage is one of the main characteristics of hepatocytes (Greenberg et al. [2006]; Agarwal et al. [2008]). Third, the functionality of the HLCs was confirmed by the detection of Bile salt export pump (BSEP), Sodium-taurocholate cotransporting polypeptide (NTCP) and Tight junction protein 1 (ZO-1) (Figure 3.21C). LGR5 was detected by qRT-PCR as highest expressed in HLCs and could also be detected by immunofluorescence-based protein detection in HLCs (Figure 3.21C). Fourth, the verification of the secretory function was done by using the nontoxic organic anion Indocyanine green (ICG) (Berk and Stremmel [1986]; Mller and Jansen [1998]; Ho et al. [2012]). The uptake of ICG as well as the release six hours later was documented (Figure 3.22A). The incubation with 5 (and 6)-Carboxy-2,7-dichlorofluorescein diacetate (CDFDA) is another test to show the functionality. CDFDA will passively taken up and actively deliver by the liver cells (Zamek-Gliszczynski et al. [2003]; Nezasa et al. [2006]). This process was visualized by immunofluorescence microscopy (Figure 3.22B).
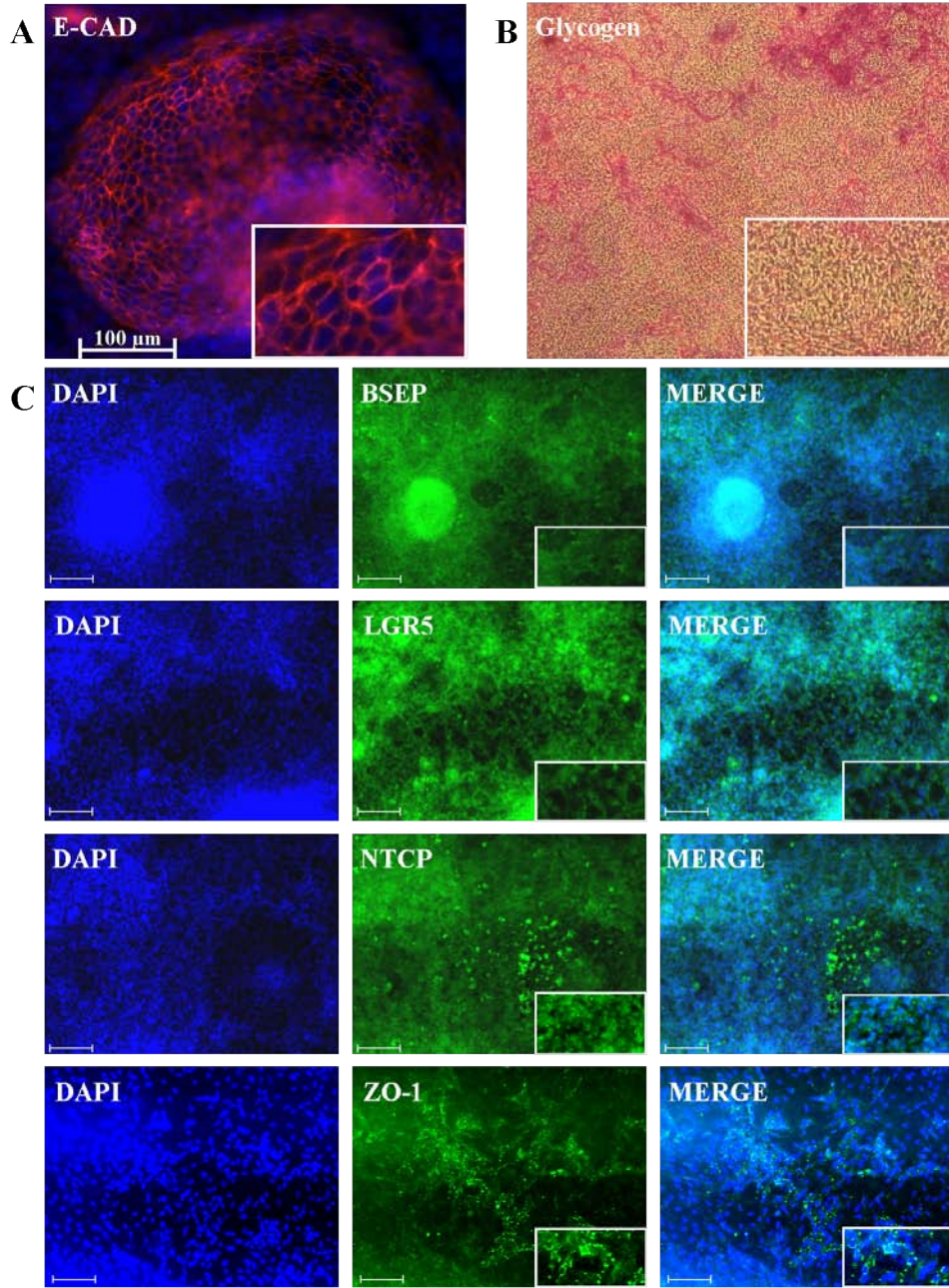
Figure 3.21: **Morphological and functional analysis of HLCs derived from epiHFF1-iPS-B1.**
A) Immunofluorescence-based detection of E-Cad and detection of the typical polygonal morphology of HLCs. **B)** Periodic acid-Schiff assay was used to demonstrate Glycogen storage as indicated by pink or dark red-purple cytoplasm. **C)** Immunofluorescence-based detection of BSEP, LGR5, NTCP and ZO-1. DAPI stained the nucleus. Scale bar: 200 μm, Alexa Flour 594 (red), Alexa Flour 488 (green). Abbreviations: BSEP = Bile salt export pump; DAPI = 4',6-diamidino-2-phenylindole; E-Cad = E-Cadherin; HLCs = hepatocyte-like cells; iPSC = induced pluripotent stem cell; LGR5 = Leucine-rich repeat containing G protein-coupled receptor 5; NTCP = Sodium-taurocholate cotransporting polypeptide; ZO-1 = Tight junction protein 1.
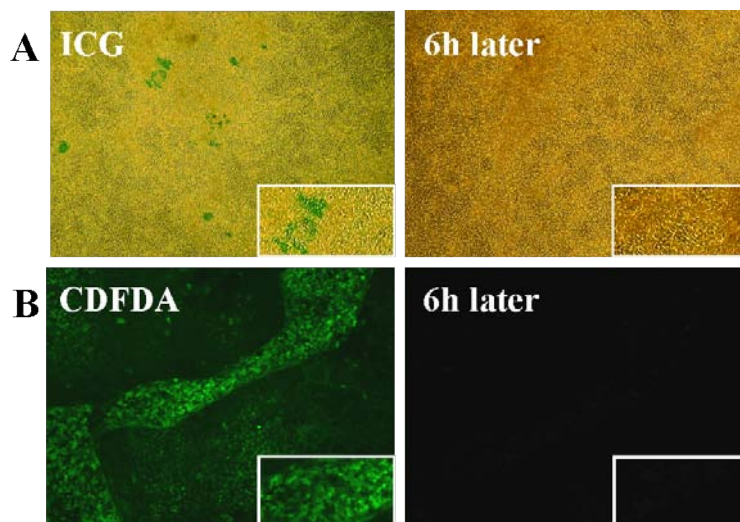
Figure 3.22: **Functional analysis of HLCs derived from epiHFF1-iPS-B1.**
A) ICG uptake and release by HLCs at the end of differentiation. Image of HLCs direct after incubation with ICG (left panel uptake) and six hours later (right panel release). **B)** Visualization of CDFDA. Immunofluorescence-based image of HLCs direct after incubation with CDFDA (left panel) and six hours later (right panel). Abbreviations: CDFDA = 5 (and 6)-Carboxy-2,7-dichlorofluorescein diacetate; ICG = Indocyanine green; HLCs = hepatocyte-like cells.

To complete the functional analysis of hepatocytes the secretion of bile acids, urea and CYP3A4 were measured (Figure 3.23). HepG2 was used as a reference. Bile acid measurement showed the excretion of primary bile acids in HLCs and in HepG2 (Figure 3.23A). The levels of urea production in HepG2 and epiHFF1-B1-HLC were quantified. The epiHFF1-B1-HLCs produced the highest amount of urea (Figure 3.23B). HLCs derived from viral-free, episomal reprogrammed iPSC-line epiHFF1-iPS-B1 (E-iPSC) also produced CYP3A4, but HepG2 cells secrete double amounts of CYP3A4 (Figure 3.23C). Quantitative RT-PCR confirmed the CYP3A4 expression as well as the expression of other members of the cytochrome P450 superfamily of enzymes (Figure 3.23D), which are involved in drug metabolism and synthesis of cholesterol, steroids and other lipids (Lamba et al. [2014]). The expression level of these enzymes were measured in all three steps of HLC differentiation generated from E-iPSCs and were compared to that of HepG2 cells as well as HLCs derived from H1 and H9, made by Justyna Jozefczuk (Jozefczuk et al. [2011]). These results were substantiated by electron microscopy evidence and shows the structural condition of the derived HLCs (Figure 3.23E). Typical structures of hepatocytes such as bile canaliculi with microvilli, lipid storage and tight junctions are visible in one image.
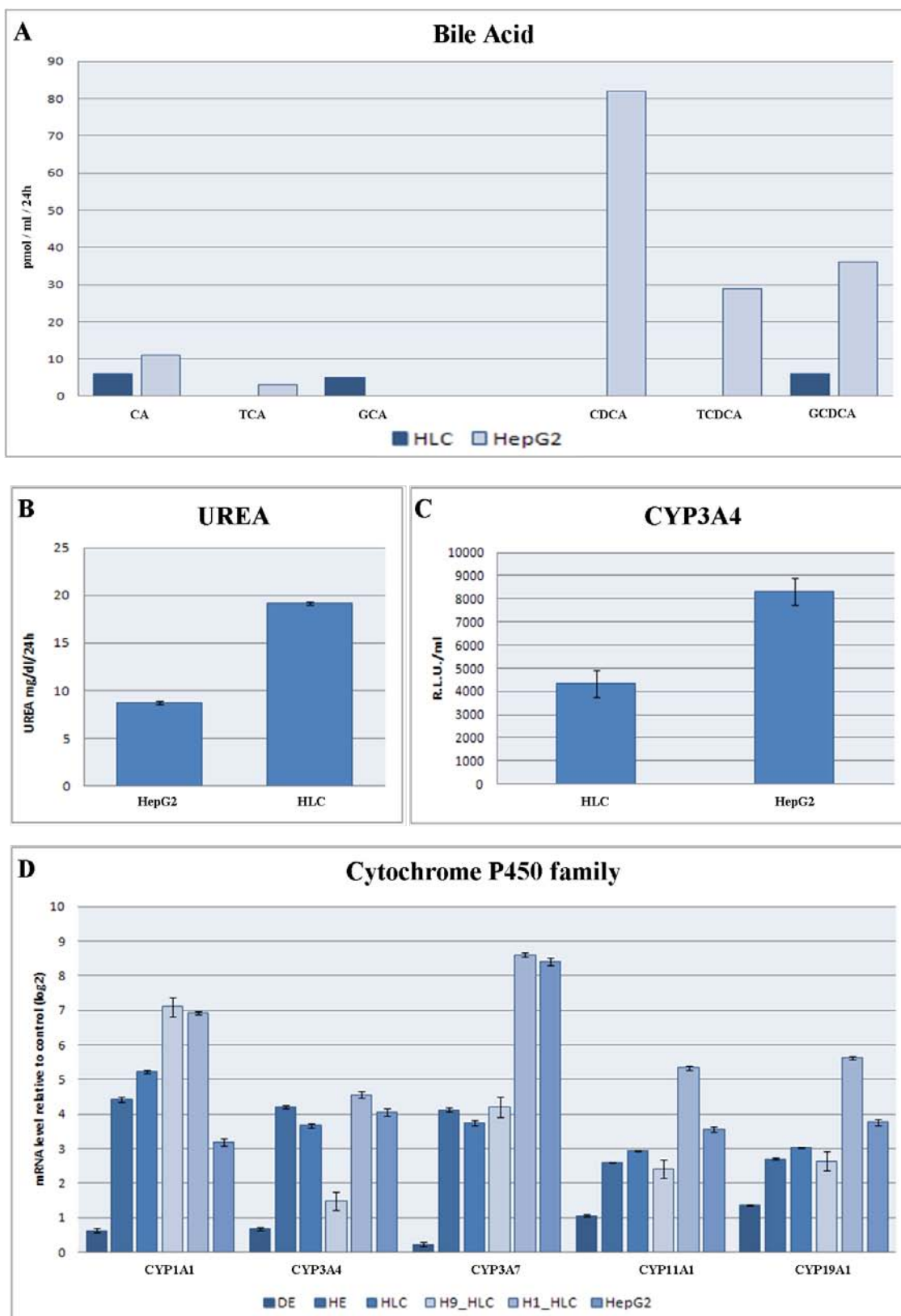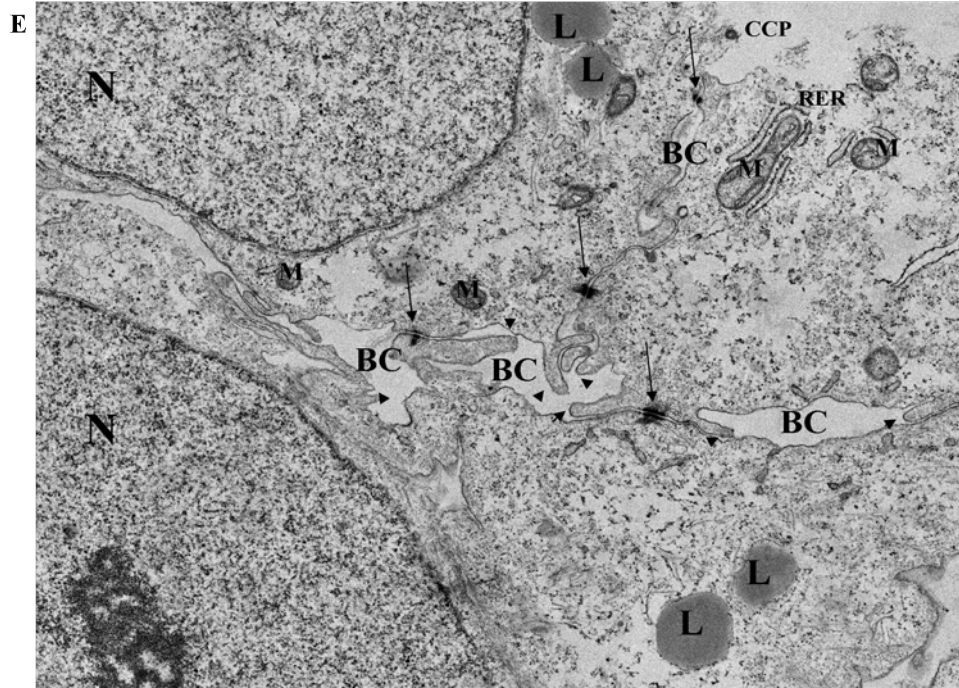
Figure 3.23: **Quantification of functionality in HLC derived from epiHFF1-iPS-B1.**
A) Analysis of bile acid production in HepG2 and epiHFF1-B1-HLC (HLC). The levels of bile acids are presented in pmol/ml/24h. **B)** Analysis of urea production in HepG2 and epiHFF1-B1-HLC (HLC). Three biological replicates in technical triplicates of each sample were analyzed. The levels of urea are measured in mg/dl/24h. **C)** Analysis of CYP3A4 production in epiHFF1-B1-HLC (HLC) and HepG2. Three biological replicates in technical triplicates of each sample were analyzed. The levels of CYP3A4 are presented as relative light units per milliliter (R.L.U./ml). **D)** Expression pattern of cytochrome P450 genes relative to iPSC-control from the three stages of HLC differentiation are shown by qRT-PCR. HepG2 was used as a positive control. The standard deviation is depicted by the error bars. Three biological replicates in technical triplicates of each sample were analyzed. **E)** The detection of hepatocyte specific structures and organelles in HLCs derived from iPSC-line epiHFF1-iPS-B1 by electron microscopy. Abbreviations: BC = bile canaliculi; CCP = clathrin coated pits; CYP3A4 = cytochrome P450, family 3, subfamily A, polypeptide 4; DE = definitive endoderm; HE = hepatic endoderm; HLC(s) = hepatocyte-like cell(s); iPSC = induced pluripotent stem cell; L = Lipid storage; M = Mitochondrion; N = Nucleus; RER = Rough ER; arrows = tight junctions; arrowheads = microvilli.

Comparative RNA-based microarray analysis of HFF1-iPSC-HLCs

Upon showing the biochemical characteristics of the iPSC-derived HLCs and the ultra-structure analysis by electron microscopy we performed comparative microarray-based gene expression profiling. Therefor RNA was isolated from E-iPSCs and from their differentiated DE, HE, HLCs. In order to assess whether the HLCs are more similar to fetal liver or adult liver RNA was isolated from fetal liver and primary human hepatocytes (PHH). The transcriptome profiles of all samples were compared. A cluster dendrogram demonstrates the high similarities of the transcriptome profiles between the biological replicates. The iPSCs, DE and HE formed a cluster which is then extended by HLCs. Furthermore, fetal liver and PHH formed a cluster (Figure 3.24A). K-means clustering identified 100 clusters (Supplementary Figure S3A and Supplementary Table 7). In these K-means cluster developmental stage-specific groups of genes were found (Supplementary Figure S3B and Supplementary Table 8), e.g. *OCT4*, *NANOG*, *SOX2* expression at the undifferentiated stage, *SOX17* marking DE stage, *HNF6* at the HE stage, *PROX1* at the HLC stage, *AFP* marking the fetal liver stage and *ALB* marking the mature liver (PHH) stage (Figure 3.24B). Transcription factor over-representation analysis using the oPOSSUM data base identified upstream regulators of genes within the six selected clusters were identified (Supplementary Figure S4, Supplementary Table 8 and 9; Kwon et al. [2012]). The iPSCs network shows the well known regulatory relations between *OCT4* (*POU5F1*), *SOX2*, *NANOG*, *KLF4*. Most significant factors from the oPOSSUM analysis were *STAT1*, *MZF1* and *KLF4* (Z-Score > 10). The DE network demonstrates *SP1*, *INSM1*, *MZF1*, *KLF4*, *REST* as most significant (Z-Score ≥ 10), in HE *LHX3*, *MIZF*, *CTCF*, in HLC *PLAG1*, *EWSR1-FLI1* and *IRF2*, in fetal liver *TAL1::GATA1*, *HNF1A*, *ZFN143*, *GATA1* as well as *HNF1B* and in PHH *HNF1A*, *CTCF*, *ZFX*, *HNF4A*, *FOXA2*, *FOXA1* and *CEBPA*. The microarray data were confirmed by qRT-PCR experiment (Figure 3.24C). *KRT17* and *CXCR4* are representatives of the definitive endoderm stage (DE), *ANXA1*, *TTR* and *TBX3* represent the hepatocyte-like cell stage (HLC), *AFP* marking the fetal liver stage and *ALB* substitutes the mature liver (PHH) stage. Furthermore, in order to visualize the development of the expression pattern during the differentiation from iPSCs to HLCs a heatmap was generated of the top 30 most abundantly expressed genes in each differentiation stage of the selected k-means clusters (Figure 3.24D and Supplementary Table 10).

Comparative transcriptome profile analysis of HLCs, fetal liver and PHH samples using a venn diagram shows the numbers of expressed genes (Figure 3.25A). The HLC-related genes *ANXA1*, *TTR* and *TBX3* as well as the fetal liver-related gene *AFP* and *ALB* represent the matured liver stage PHH and are detected in the intersection of all three samples as well as are included in the 11,506 genes (Supplementary Table 11). A closer look into the exclusively expressed genes in the HLCs (1,808 genes) uncovered tight junction specific genes such as *CLDN9*, *CLDN18*, *OCLN*, *PARD6A* and *PARD6B* (Figure 3.25B).

continued from previous page

D
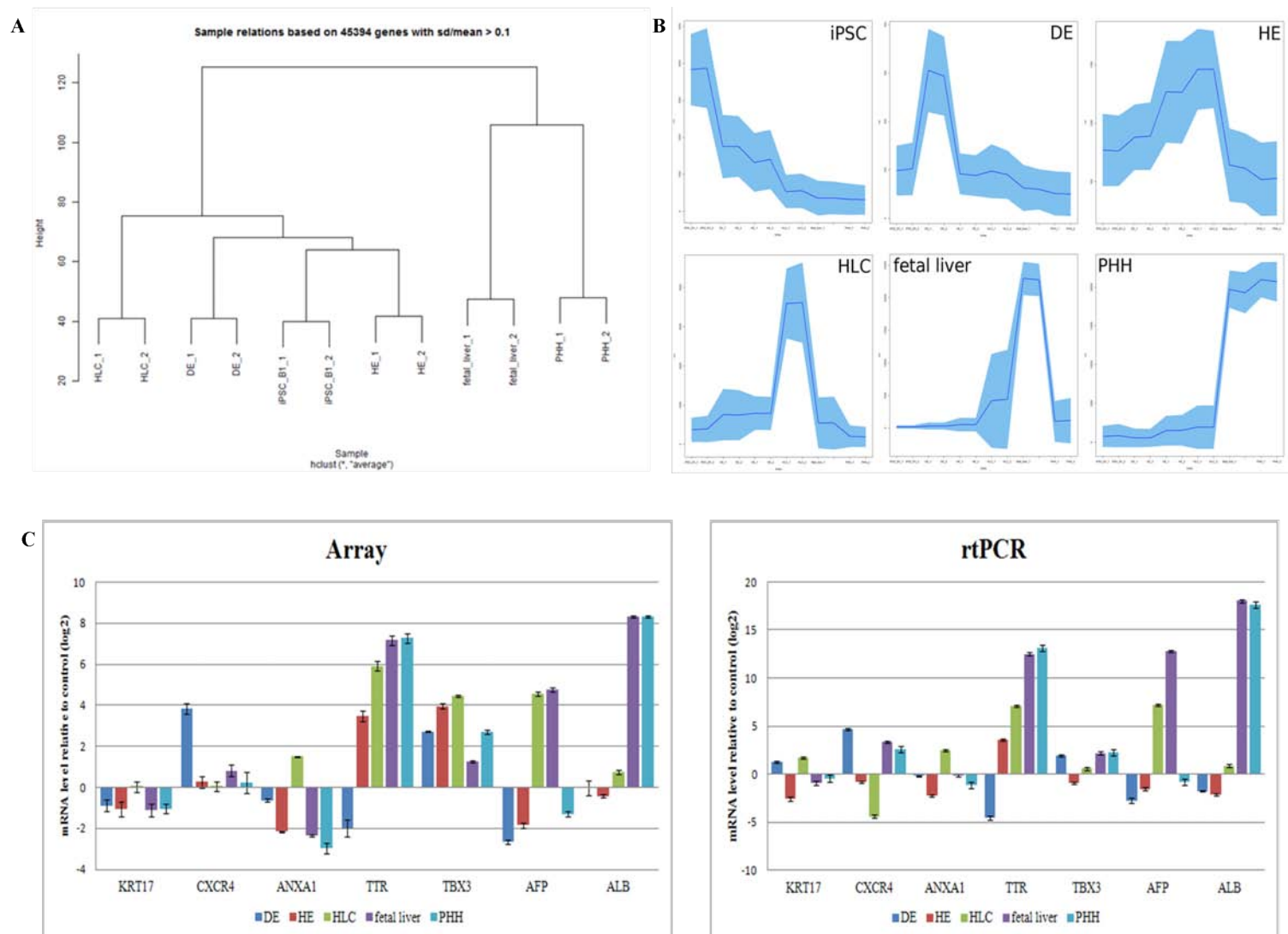
continued from previous page

Figure 3.24: **Transcription profile analyses of HLC derivation.**
A) Cluster dendrogram of E-iPSC, DE, HE, HLC, fetal liver and PHH. Fetal liver and PHH formed a cluster as well as E-iPSCs, HE and DE formed a cluster which is then extended by HLCs. **B)** K-means cluster 68 contained OCT4 marking undifferentiated stage (iPSC), cluster 81 (sub-cluster 1) contained SOX17 marking DE stage (DE), cluster 37 (sub-cluster 2) represents HE stage, cluster 51 represents HLC stage, cluster 72 contained AFP marking fetal liver stage and cluster 91 contained mature liver marker ALB (PHH). **C)** Confirmation of microarray data by qRT-PCR. On the left the array expression data and on the right the qRT-PCR expression data are depicted. The standard deviation is depicted by the error bars. **D)** The top 30 expressed genes from each K-means cluster in B were combined in a heatmap. Abbreviations: AFP = alpha-Fetoprotein; DE = definitive endoderm; HE = hepatic endoderm; HLC(s) = hepatocyte-like cell(s); iPSC = induced pluripotent stem cell; E-iPSC = endodermal reprogrammed iPSC; PHH = primary human hepatocytes; OCT4 = POU5F1, POU class 5 homeobox 1; SOX17 = SRY (sex determining region Y)-box 17.

The expression of tight junction genes is one marker for the maturation of the HLCs. In order to analyze maturation level of the iPSC-derived HLCs a Venn diagram was generated from HLC vs. fetal liver, HLC vs. PHH and fetal liver vs. PHH (Figure 3.25C, Supplementary Table 12). DAVID analysis of Hippo signaling-related genes from the intersection of HLC vs. PHH and HLC vs. fetal liver uncovered the activity of cell-cell contact related pathways, adherent and tight junction pathway. A chart of these Hippo pathway related genes underlines the predominant expression of cell-cell contact related genes in HLCs (Figure 3.25D). The Hippo pathway is responsible for maturation and stabilization of the tight junctions in hepatocytes. Furthermore, the ABC transporters are expressed, which are accountable for the uptake and efflux of e.g. bile acids and metabolites. These are over represented in HLCs, fetal liver and PHH (Figure 3.26A and 3.26B). Bile acid-related transporter genes such as *NTCP*, *MRP2*, *ASBT* and *MDR2/3* are highly expressed in HLCs compared to the DE and HE stage (Figure 3.26C). The expression of bile acid-related transporters substantiates the functionality of HLCs. In addition, the heat map in Figure 3.26D containing genes of the cytochrome p450 superfamily uncovered the commonalities between HLCs, fetal liver and PHH (Varelas et al. [2010]; Osman-Ponchet et al. [2014]; Chavan et al. [2015]).

To detect the relationship between the stages of the HLC differentiation, a Venn diagram analysis was performed, and further to analyze which genes were expressed and distinct in DE, HE, HLCs as well as in between (Figure 3.27A, Supplementary Table 13). These gene were analyzed in DAVID. It uncovered genes which are related to pathways that define the functionality of the liver such as drug metabolism, metabolism of xenobiotics and fatty acid metabolism (Supplementary Figure S5).
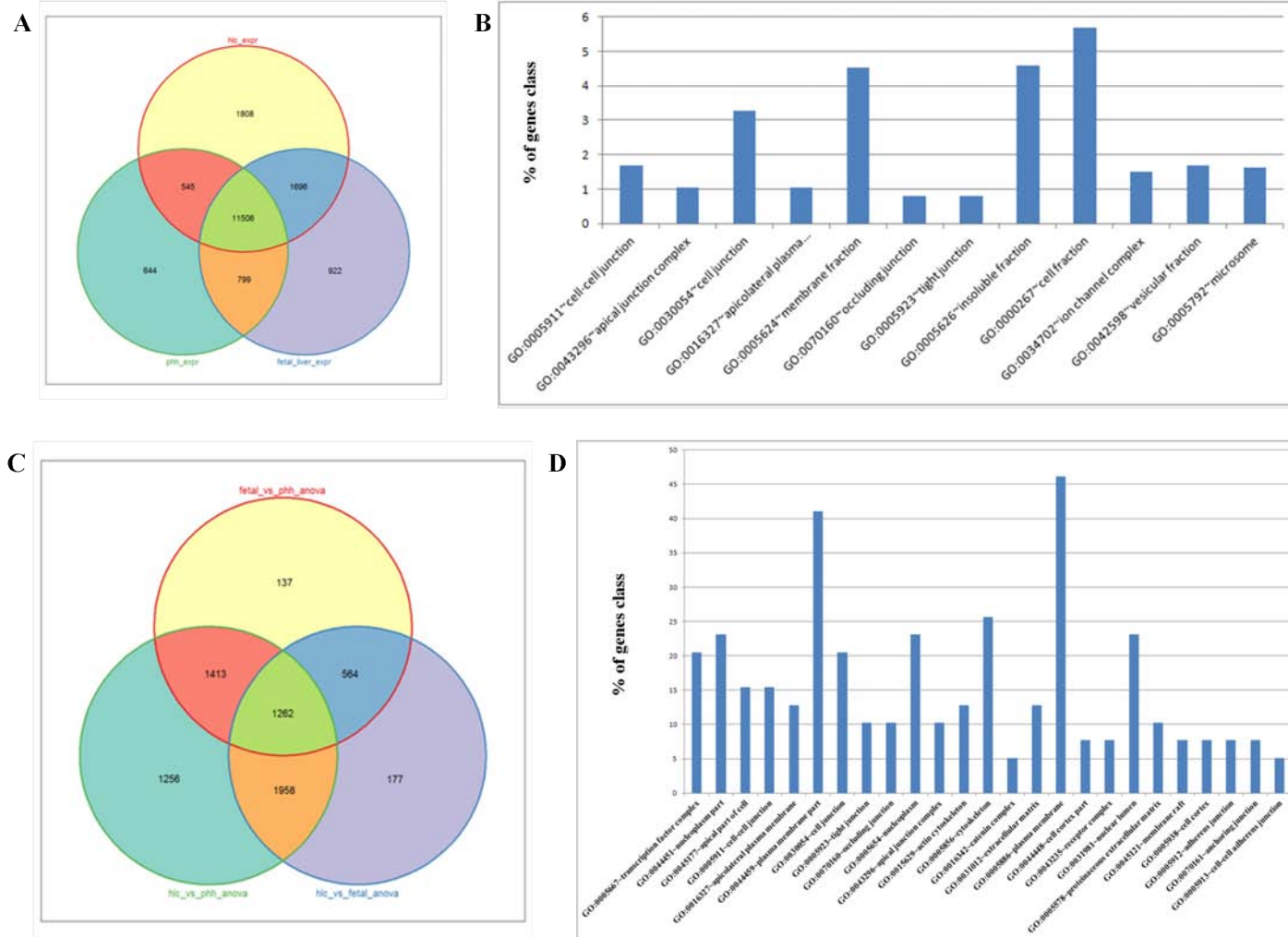
Figure 3.25: **Comparative transcription profile analyses.**
A) Venn diagram of HLC, fetal liver and PHH. **B)** David analysis: GO cellular components of HLC exclusively expressed genes (Fisher extract p < 0.01). **C)** Venn diagram of fetal liver vs. PHH anova, HLC vs. fetal liver anova and HLC vs. PHH anova. **D)** David analysis: GO cellular components of HIPPO pathway genes exclusively expressed genes (Fisher extract p < 0.01) in the intersection of HLC vs. fetal liver anova and HLC vs. PHH anova (intersection with 1,958 genes). The following samples were used for the heatmaps: E-iPSC, DE, HE, HLC, fetal liver and PHH, except for G were used E-iPSC, DE, HE and HLC. Abbreviations: DE = definitive endoderm; HE = hepatic endoderm; HLC = hepatocyte-like cells; iPSC = induced pluripotent stem cells; PHH = primary human hepatocytes.

Until now most studies on liver cell fate decision have been conducted in mice (Tanimizu et al. [2003]; Fougre-Deschatrette et al. [2006]; Vanderpool et al. [2012]). This type of analyses can be applied to human using iPSCs. Therefore, we used the transcriptome profile of all stages of HLC derivation (undifferentiated iPSC, DE, HE and HLCs) and generated a heatmap consisting of key genes which are related to hepatocytes, cholangiocytes as well as progenitor-associated gens (Figure 3.27B). Progenitor-related genes such as *HNF1A* and *HNF1B* are expressed in HE and HLCs whereas the liver progenitor specific gene *PROX1* is expressed exclusively in HLCs. *ALB*, *AFP*, *ABCB4* and *CYP3A7* as hepatocyte-specific genes are expressed in the HLC samples. Furthermore, there exists a group of hepatocyte-related genes which is expressed in HLCs and HE, e.g. *ABCC2*, *RARB* and *TTR*. Cholangiocyte-related genes such as *WNT3A*, *SOX9* and *KRT7* are expressed in both HE and HLCs, whereas *AQP1* and *DLK1* are expressed exclusively in HLCs. To analyze the relation between these genes for cell fate decision, a transcription factor network was created using the data base oPOSSUM (Figure S6). To make it more manageable transcription factors with a Z-score > 10 (green circles) and downstream regulating transcription of the progenitor genes (red circles) are shown (Figure 3.27C, Supplementary Table 9). *MYC*, *HNF1A*, *SP1*, *MZF1 5-13*, *HNF4A*, *KLF4* were the most significant upstream transcription factors (Z-score > 10, p < 1e^{-15}).

This demonstrates the associated functionalities of this core regulatory network, *HNF1A* and *HNF4A* determine the liver fate by regulating *ALB* and *AFP* while *KLF4* regulates *SOX17*. The bipotential markers *DLK1* and *NOTCH3* are both regulated by *MYC*, *KLF4*, *SP1* and *MZF1 5-13*. All cholangiocyte marker genes are regulated by *KLF4*, *SP1* and *MZF1*. *SOX9* is only regulated by these three while *ONECUT1*, *ONECUT2* and *SALL4* are regulated by these three and additionally by *MYC* and *HNF4A*. *MYC* was the most prominent transcription factor in this network (Z-score of 12.54) and regulates *PROX1* and the transcription factor *HNF1A*, which is also regulated by *HNF4A*, as well as the cholangiocyte-related gene *WNT3A* (Hay et al. [2008b]; Dianat et al. [2014]; Seth et al. [2014]; Tarlow et al. [2014]).

A HIPPO Pathway **B** ABC Transporter **C** Bile Acid Transporter **D** Cytochrome P450 Family
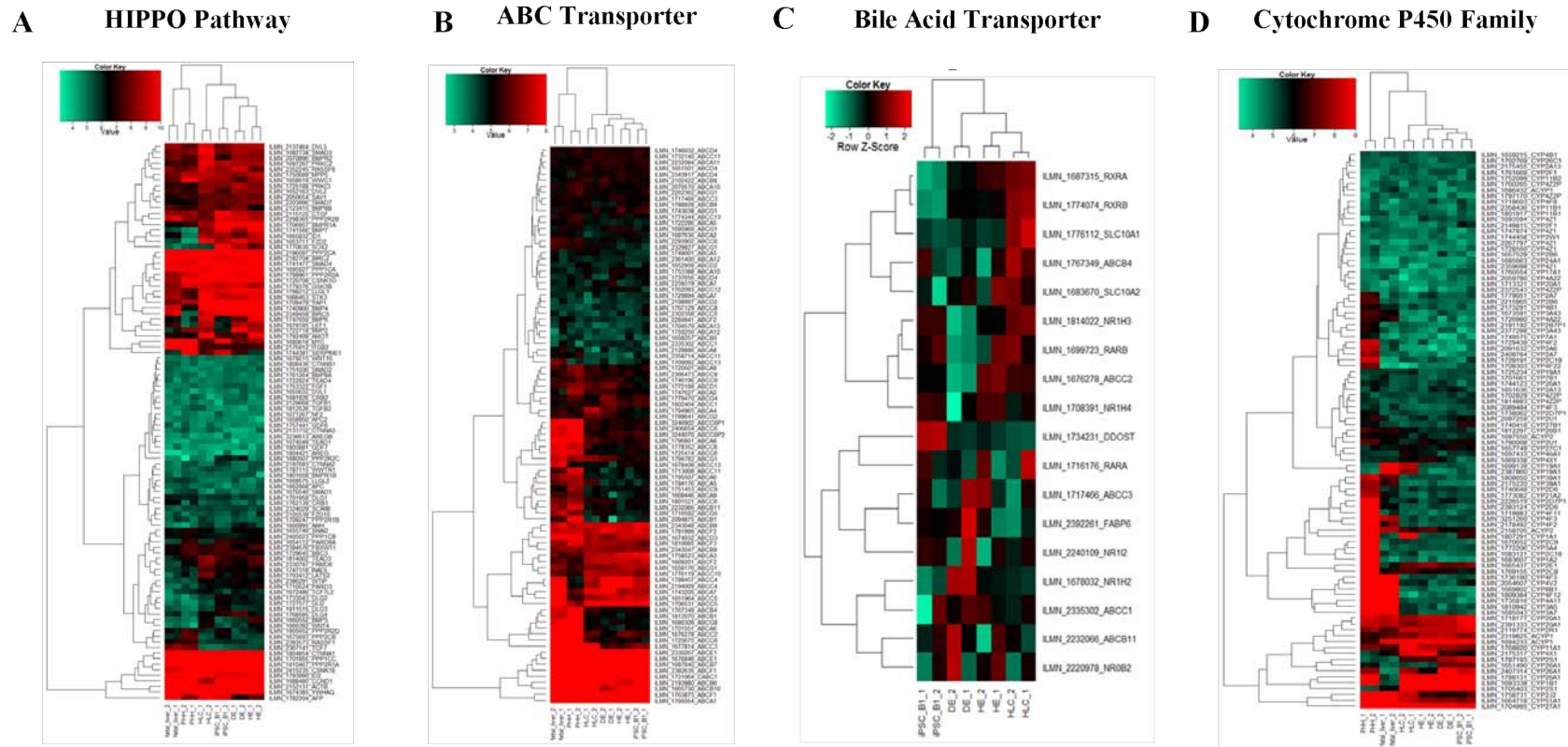
Figure 3.26: **Heatmap-based transcription profile analyses.**
A) Heatmap of HIPPO pathway-related genes and a scheme of the HIPPO signaling pathway. **B)** Heatmap of ABC transporter-related genes. **C)** Heatmap of bile acid transporter-related genes. **D)** Heatmap of cytochrome P450 superfamily-related genes. The following samples were used for the heatmaps: E-iPSC, DE, HE, HLC, fetal liver and PHH, except for G were used E-iPSC, DE, HE and HLC. Abbreviations: DE = definitive endoderm; HE = hepatic endoderm; HLC = hepatocyte-like cells; iPSC = induced pluripotent stem cells; PHH = primary human hepatocytes.

A

B

continued from previous page

Figure 3.27: **Cell fate decision during HLC derivation.**
A) Venn diagram of DE, HE and HLC. **B)** Heatmap of bipotential progenitor-associated, hepatocyte-related and cholangiocyte-associated genes. The following samples were used iPSC-B1, DE, HE and HLC. **C)** An induced network of transcription factors with a Z-score > 10 (green, size of circle corresponds to Z-score) and associated genes (red). Abbreviations: DE = definitive endoderm; HE = hepatic endoderm; HLC = hepatocyte-like cells; iPSC = induced pluripotent stem cells; PHH = primary human hepatocytes.
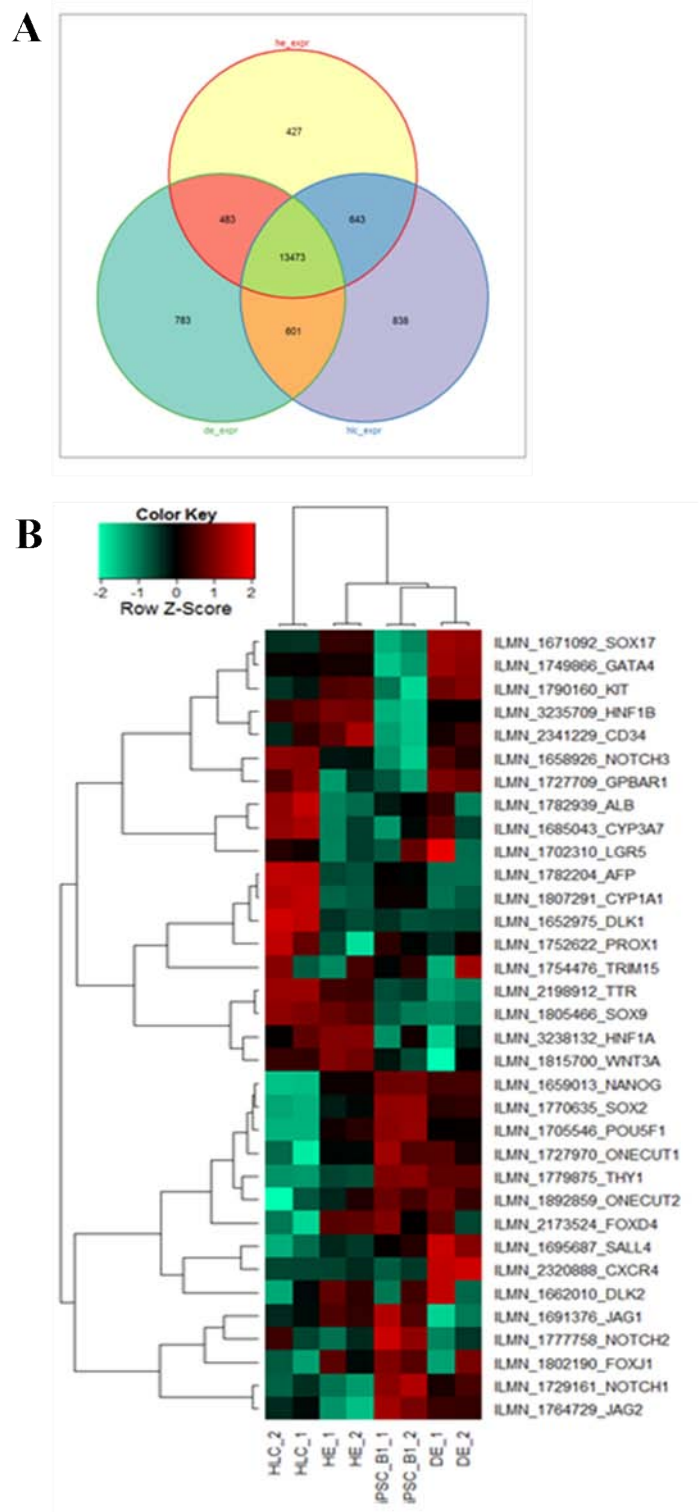
3.2.2 Generation and characterization of hepatocyte-like cells derived from HUVEC-iPSC

To generate hepatocyte-like cells (HLCs) from the episomal reprogrammed cell line epiHUV-iPS-3a the protocol from Sullivan et al. [2010] was used (as described in section 6.4). All stages of the differentiation procedure were monitored (Figure 3.28). The same differentiation protocol was used due to the fact that comparable analyses were planed.
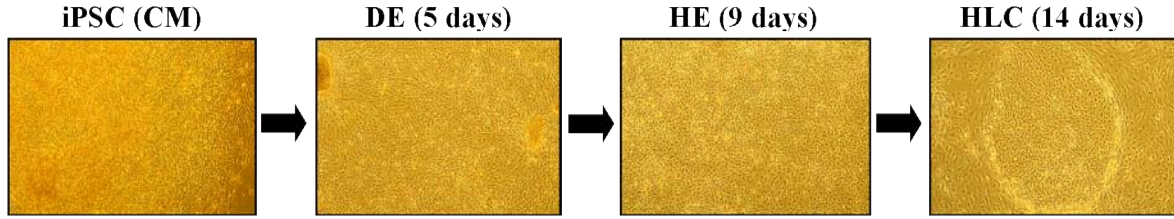
Figure 3.28: **Illustration of HLC development derived from epiHUV-iPS-3a.**
Microscopy images showing morphology changes during the differentiation of epiHUV-iPS-3a (iPSC-line) to hepatocyte-like cells (HLC). The iPSC-line were cultured in conditioned medium (CM). The generation of the first stage definitive endoderm (DE) takes five days. Hepatic endoderm (HE) is the second stage and takes four days. After 14 days the differentiation is completed and matured Hepatocyte-Like Cells (HLC) is the endpoint of the third stage.

During the first step of the protocol the iPSCs differentiated to definitive endoderm (DE) (Figure 3.29). The expression of the pluripotency associated marker OCT4 was down regulated. Forkhead box A2 (FOXA2) is expressed, which is expressed by the definitive endoderm progenitors, as well as SRY (sex determining region Y)-box 17 (SOX17), which is a marker of definitive endoderm (Greber et al. [2007]; Agarwal et al. [2008]). The hepatocyte nuclear factor 4, alpha (HNF4α) is an early marker of endoderm development and is expressed during the whole HLC differentiation (Agarwal et al. [2008]). Immunocytochemistry analysis of hepatic endoderm (HE), the second stage during HLC differentiation, showed a positive staining of HNF4α, the early marker alpha-Fetoprotein (AFP) and later-stage marker Albumin (ALB) for hepatic commitment (Figure 3.30; Gouon-Evans et al. [2006]; Hay et al. [2008a]; Agarwal et al. [2008]). Additionally, HE cells were stained positive for Cytokeratin 18 (CK18), which is expressed at the end of the second stage of HLC differentiation (Cai et al. [2007]). The hepatoblast marker CK19 was also proved by immunofluorescence-based protein detection (Cai et al. [2007]; Dianat et al. [2014]). E-Cadherin (E-CAD/CDH-1) was detected, which marks the mesenchymal-to-epithelial transition (MET), established cell-cell contacts and indicates the epithelial nature of the developed liver cells (Choi and Diehl [2009]; Schietke et al. [2010]; Mah et al. [2011]; Nakagawa et al. [2014]). Vimentin (VIM), a mesenchymal marker, identifies also the epithelial-to-mesenchymal-transition (EMT) and was expressed while the expression of E-CAD was down-regulated (Lan et al. [2013]; Mitra et al. [2014]; Nakagawa et al. [2014]). At the endpoint of HLC differenti-

ation AFP, ALB, HNF4α and E-CAD were expressed, as well as VIM in regions where E-CAD was expressed (Figure 3.31). The expression of CK18 and CK19 as markers of the HE stage were decreased. (Cai et al. [2007]; Agarwal et al. [2008]; Takayama et al. [2012]; Dianat et al. [2014]).
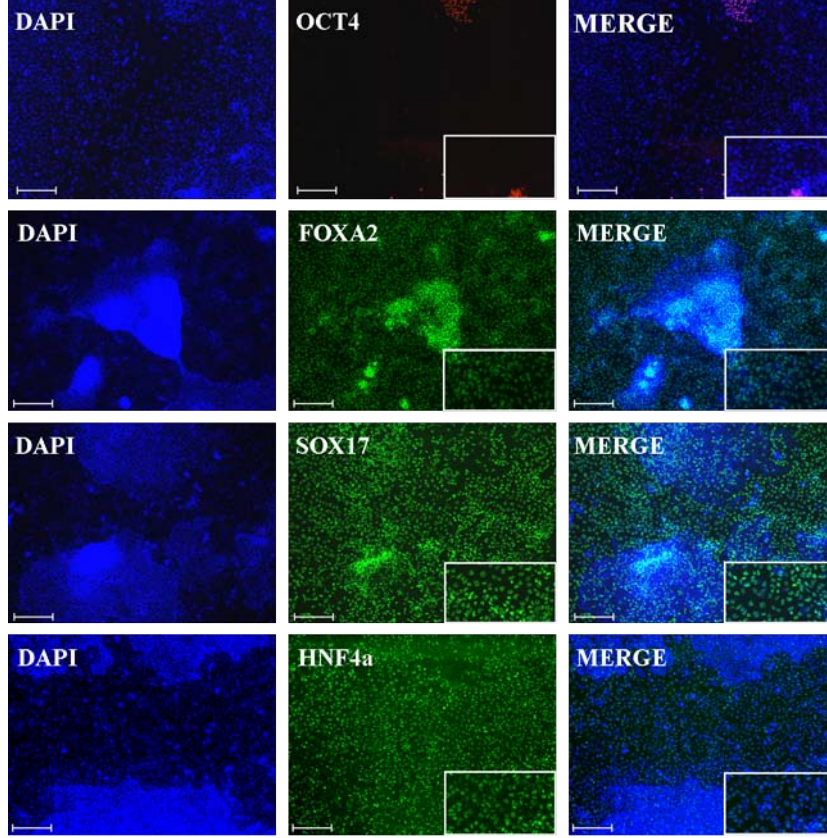
Figure 3.29: **Immunofluorescence-based detection of proteins in DE derived from epiHUV-iPS-3a.**
Immunofluorescence for expression of a defining panel of proteins were examined. OCT4, pluripotency marker; FOXA2, SOX17 markers for DE and the transcription factor HNF4α. DAPI stained the nucleus. Scale bar: 200 μm Alexa Flour 488 (green). Abbreviations: DAPI = 4',6-diamidino-2-phenylindole; DE = definitive endoderm; FOXA2 = Forkhead box A2; HNF4α = hepatocyte nuclear factor 4 alpha; OCT4 = POU5F1, POU class 5 homeobox 1; SOX17 = SRY (sex determining region Y)-box 17.
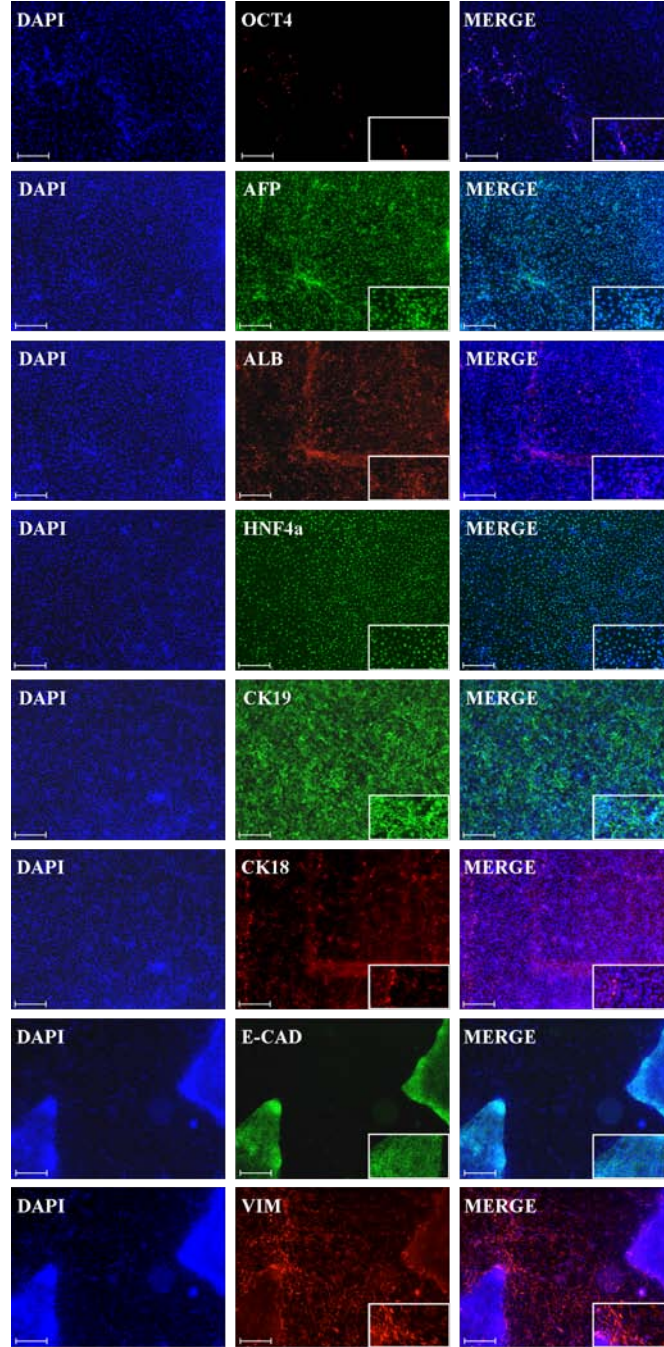
Figure 3.30: **Immunofluorescence-based detection of proteins in HE derived from epiHUV-iPS-3a.**
The detection of the protein OCT4, pluripotency marker; AFP, ALB for early and later-stage hepatic proteins, the transcription factor HNF4α, E-CAD, VIM, CK18 and CK19. DAPI stained the nucleus. Scale bar: 200 μm Alexa Flour 594 (red), Alexa Flour 488 (green). Abbreviations: AFP = alpha-Fetoprotein; ALB = Albumin; CK18 = Cytokeratin 18; DAPI = 4',6-diamidino-2-phenylindole; E-CAD = E-Cadherin; HE = hepatic endoderm; HNF4α = hepatocyte nuclear factor 4 alpha; OCT4 = POU5F1, POU class 5 homeobox 1; VIM = Vimentin.
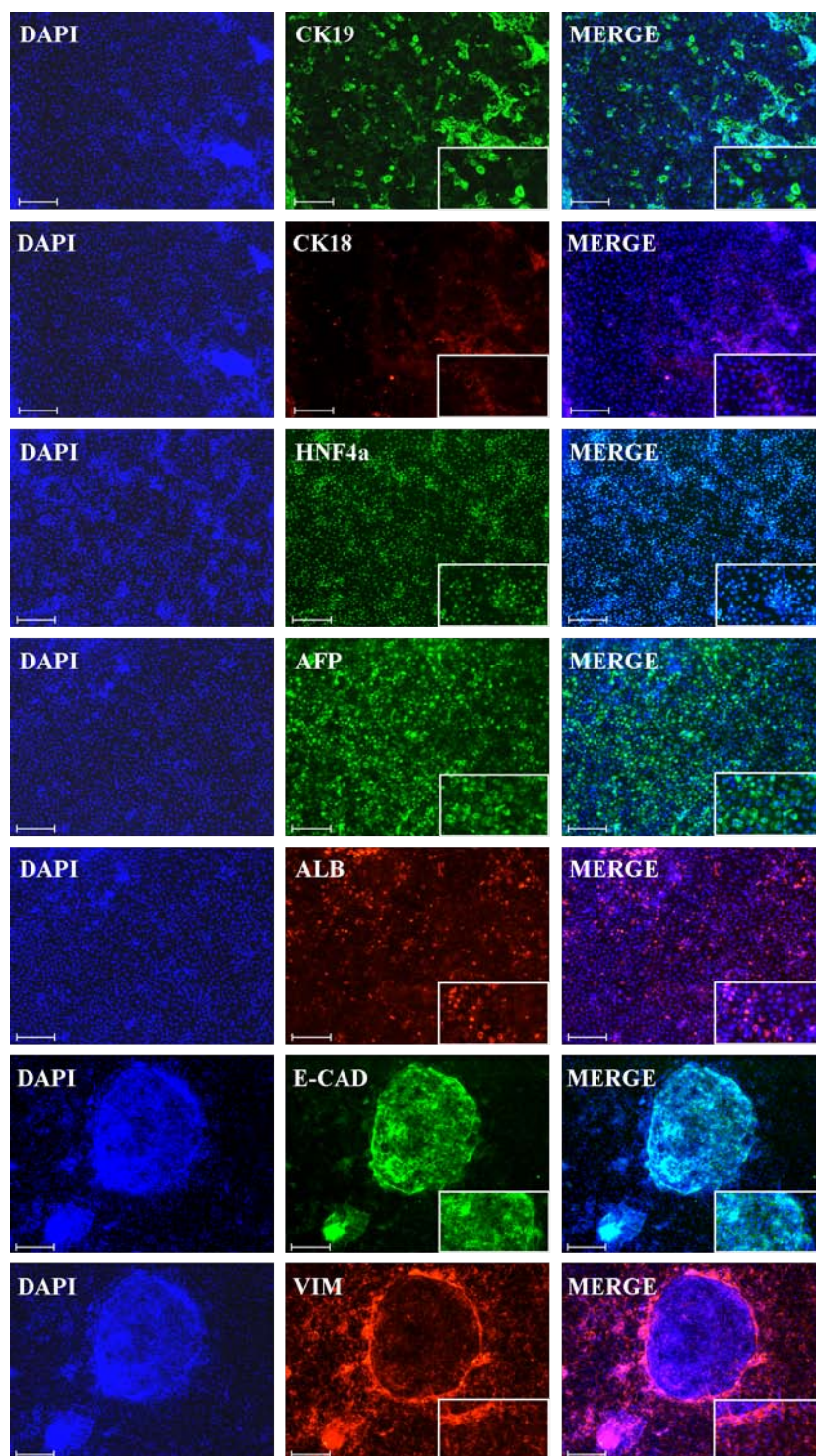
Figure 3.31: **Immunofluorescence-based detection of proteins in HLC derived from epiHUV-iPS-3a.**
The detection of the protein AFP, ALB for early and later-stage hepatic proteins, the transcription factor HNF4α, E-CAD, VIM, CK18 and CK19. DAPI stained the nucleus. Scale bar: 200 μm Alexa Flour 594 (red), Alexa Flour 488 (green). Abbreviations: AFP = alpha-Fetoprotein; ALB = Albumin; CK18 = Cytokeratin 18; DAPI = 4',6-diamidino-2-phenylindole; E-CAD = E-Cadherin; HLC = hepatocyte-like cell; HNF4α = hepatocyte nuclear factor 4 alpha; VIM = Vimentin.

To track the development of the expression pattern during the HLC differentiation of liver specific genes qRT-PCR was performed (Figure 3.32). The expression of pluripotency associated genes such as *OCT4*, *SOX2* and *NANOG* were decreased and liver stage specific genes increased (Figure 3.32A). *SOX17*, *FOXA2* and *HNF4a* are the only genes which are highly expressed at the end of stage I, definitive endoderm (Figure 3.32B). *SOX17* and *FOXA2* are core genes of DE and are involved in hepatic maturation (D'Amour et al. [2005]; McLean et al. [2007]; Takayama et al. [2011]; Takayama et al. [2012]). Keratin 17 (KRT17) is involved in the JAK/STAT pathway, induces proliferation as well as differentiation markers and is expressed in DE only (Shuai and Liu [2003]; Kim et al. [2006]; Lan et al. [2013]; Sankar et al. [2013]; Pattarachotanant et al. [2014]). *HNF4α* is a key transcription factor and regulates different processes during the liver development (Li et al. [2000]; Watt et al. [2003]; Agarwal et al. [2008]; Takayama et al. [2011]; Takayama et al. [2012]). The expression of most liver markers suddenly rose from the first stage DE to the hepatic endoderm stage. *AFP* is classified as an early-stage marker of hepatocytes and *ALB* as a late-stage marker, both expressions were increased to the end of stage II of differentiation and rose further to the endpoint of differentiation, hepatocyte-like cells (HLCs) stage III (McLean et al. [2007]; Agarwal et al. [2008]; Hay et al. [2008a]; Takayama et al. [2011]; Takayama et al. [2012]. A1AT is a serum glycoprotein which is synthesised and secreted by the liver (Teckman and Jain [2014]). The expression development during the differentiation is comparable to *AFP* and *ALB* (Figure 3.32B).

To analyze the influence of the cytokine treatment with HGF, OSM and DEX, which induce liver differentiation and maturation (1.4), and further the state of maturation of the generated HLCs two more experiments were conducted. First, HLCs were generated as described before, however, the derivation of the third stage varied. HLCs were generated a) with cytokines (HLC 5d), which is the common procedure, b) without cytokines (HLC 5d -Cytokines) as well as c) with the small molecules FH1 and FPH1 (HLC SM 5d). FPH1 induces proliferation of PHH and FH1 maturation of iPSC-derived HLCs (Shan et al. [2013]). The small molecules FH1 and FPH1 were used in a concentration of 15 μM. The RNA was isolated and qRT-PCRs were performed. The expression level of HNF4α was comparable in all three samples. The HLCs generated without cytokines showed the highest expression level of *A1AT*, *AFP* and *ALB* (Figure 3.32C). Second, HLCs were generated with cytokine treatment and were cultured further. RNA was isolated from five days HLCs (common age and endpoint of differentiation), ten days, 15 days and 18 days. The expression level of HNF4α, *A1AT* and *ALB* were increased until the differentiation endpoint. *AFP* had the expression maximum at ten days old HLC and then decreased. Immunofluorescence-based protein stainings confirmed the expression of AFP and ALB in all samples (Figure 3.32D and Supplementary Figure S8).
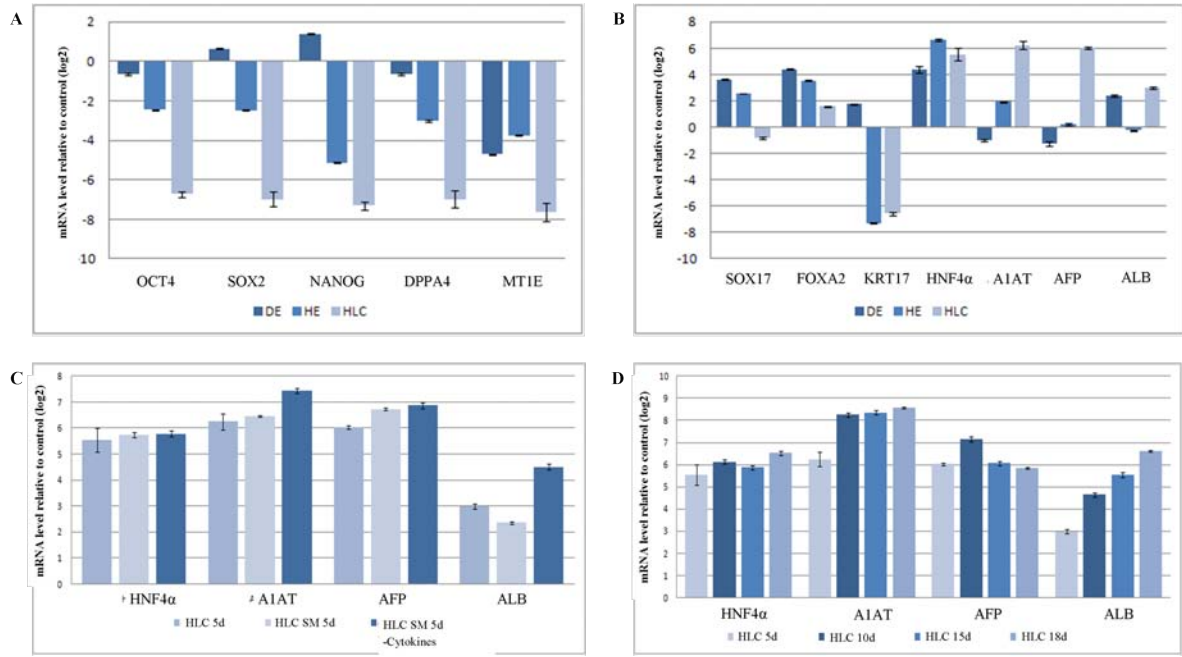
Figure 3.32: **Quantitative real-time PCR profile of liver specific maker.**
A) The expression pattern of pluripotency associated genes during the liver differentiation of epiHUV-iPS-3a were decreased. **B)** Development of the expression pattern of liver specific markers during the HLC differentiation are shown. Definitive endoderm (DE) specific marker genes *SOX17*, *FOXA2* and *KRT17* were highly expressed in DE stage and decreased during liver differentiation. *HNF4α* as a key transcription factor is highly expressed in all three stages. The liver specific genes *AFP*, *ALB* and *A1AT* were most expressed at the end stage of liver differentiation, hepatocyte-like cells (HLCs) stage III. **C)** Comparison of liver specific gene expression levels in HLCs generated under different conditions. HLCs were generated with the treatment of cytokines (epiHUV-3a HLC 5d), without cytokines and small molecules (epiHUV-3a HLC SM 5d) or without cytokines (epiHUV-3a HLC 5d -Cytokines). The expression level of HNF4α comparable in all three samples. In HLCs generated without Cytokines showed the highest expression level of *A1AT*, *AFP* and *ALB*. **D)** The expression level of HNF4α, *A1AT* and *ALB* were increased till the endpoint. *AFP* had the expression maximum at HLC ten days old and decreased then. Three biological replicates in technical triplicates of each sample were analyzed. The standard deviation is depicted by the error bars. As control was used the RNA from HUVEC-iPSC line (epiHUV-iPS-3a) which was differentiated.

Functional analysis of HUVEC-iPSC-HLCs

To analyze whether or not the derived HLCs are functional several tests were conducted. First, E-Cadherin (E-CAD, CDH-1) marks the epithelial-to-mesenchymal transition (EMT) and indicating the epithelial nature of the developed liver cells and visualized the typical cell shape of liver cells (Figure 3.33A) (Choi and Diehl [2009]; Schietke et al. [2010]; Nakagawa et al. [2014]). Second, we tested whether or not our generated HLCs store glycogen as hepatocytes do (Greenberg et al. [2006]; Agarwal et al. [2008]). To detect the glycogen in epiHUV-iPS-3a derived HLCs Periodic Acid-Schiff

(PAS) staining was performed (Figure 3.33A). Third, we tested the secretory function using the nontoxic organic anion Indocyanine green (ICG) (Figure 3.33B) and 5 (and 6)-Carboxy-2,7-dichlorofluorescein diacetate (CDFDA) (Figure 3.22C), (Berk and Stremmel [1986]; Mller and Jansen [1998]; Zamek-Gliszczynski et al. [2003]; Nezasa et al. [2006]; Ho et al. [2012]).
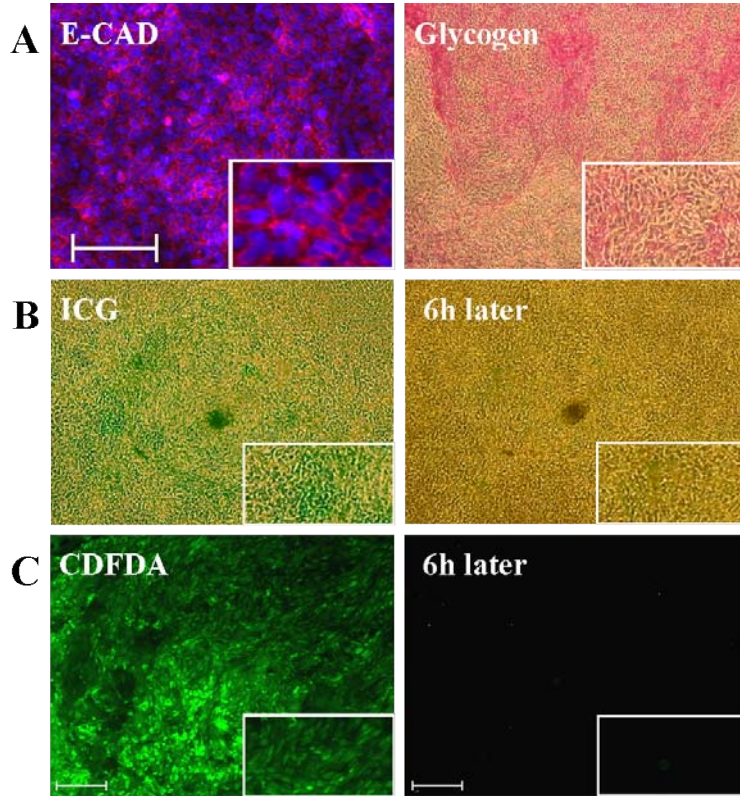
Figure 3.33: Functional analysis of HLC derived from epiHUV-iPS-3a.
Functional analysis of induced pluripotent stem cell (iPSC)-derived hepatocyte-like cells (HLC). **A)** Immunofluorescence-based detection of E-Cad is depicted on the left hand side and thereby detection of the typical polygonal morphology of HLC. DAPI stained the nucleus. Scale bar: 100 μm, Alexa Flour 594 (red). To detect Glycogen storage a periodic acid-Schiff (PAS) assay was used and is depicted on the right hand side. Glycogen storage is indicated by pink or dark red-purple cytoplasms. **B)** Indocyanine green (ICG) uptake and release. HLC at the end of differentiation was used. Image of HLC direct after incubation with ICG (left panel uptake) and six hours later (right panel release). **C)** Visualization of 5 (and 6)-Carboxy-2,7-dichlorofluorescein diacetate (CDFDA). Immunofluorescence image of HLC direct after incubation with CDFDA (left panel) and six hours later (right panel). Scale bar: 100 μm, Alexa Flour 488 (green).

Fourth, bile acid production was measured in epiHUV-3a-HLC (iHUV3a HLC), epiHUV-3a-HLC three days older (iHuv3a HLC +3d), epiHUV-3a-HLC treated with small molecules FH1 and FPH1 (iHuv3a HLC SM), epiHUV-3a-HLC without cytokines (iHuv3a HLC -Cytokines) and HepG2. The measurement shows the excretion of primary bile acids and are presented in pmol/ml/24h (Figure 3.34A). Fifth, the measurement of urea production was performed in epiHUV-3a-DE (DE), epiHUV-3a-HE (HE), epiHUV-3a-HLC five days (HLC 5d), epiHUV-3a-HLC ten days (HLC 10d), epiHUV-3a-HLC 13 days (HLC 13d), epiHUV-3a-HLC 18 days (HLC 18d) and HepG2. The levels of urea was measured in mg/dl/24h. The cells of epiHUV-3a-HLC 13 days produced most of urea (Figure 3.34B). All these results together substantiated the similarity of these iPSC-derived HLCs to hepatocytes in morphology and biochemical matter.
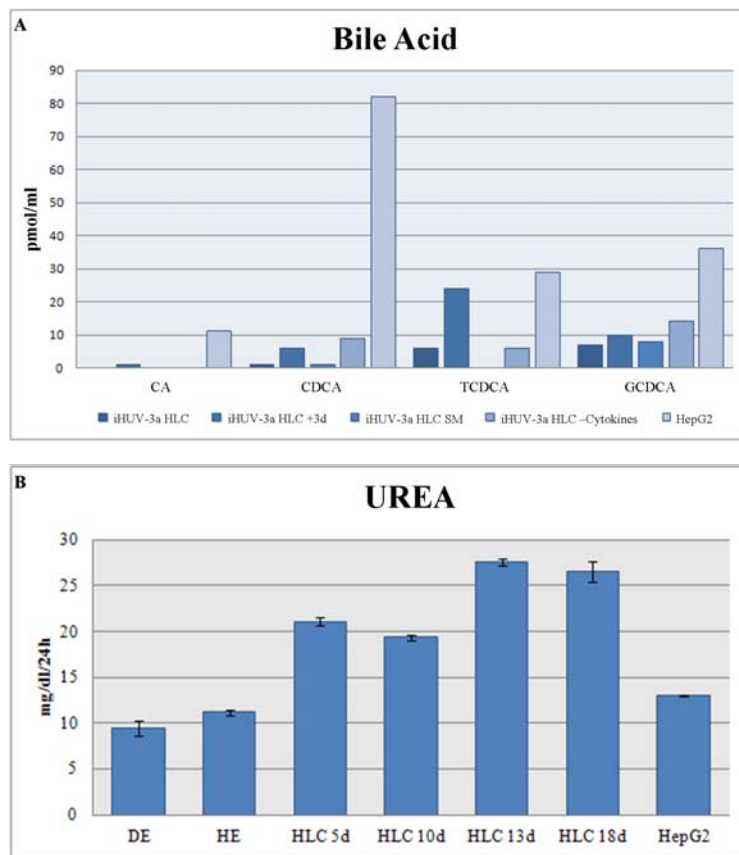
Figure 3.34: **Measurement of functionality in HLC derived from epiHUV-iPS-3a.**
A) Analysis of bile acid production in epiHUV-3a-HLC (iHUV3a HLC), epiHUV-3a-HLC three days older (iHuv3a HLC +3d), epiHUV-3a-HLC treated with small molecules (iHuv3a HLC SM), epiHUV-3a-HLC without cytokines (iHuv3a HLC -Cytokines) and HepG2. The levels of bile acids are presented in pmol/ml/24h. **B)** Analysis of urea production in epiHUV-3a-DE (DE), epiHUV-3a-HE (HE), epiHUV-3a-HLC five days old (HLC 5d), epiHUV-3a-HLC ten days old (HLC 10d), epiHUV-3a-HLC 13 days old (HLC 13d), epiHUV-3a-HLC 18 days old (HLC 18d) and HepG2. Three biological replicates in technical triplicates of each sample were analyzed. The levels of urea was measured in mg/dl/24h.

Microarray analysis of HUVEC-iPSC-derived HLCs

As described before during the reprogramming process the somatic cells change their transcriptome profile dramatically (Wolfrum et al. [2010]). It moves from characteristic of a somatic cell and converges to a pluripotent stem cell-like stage, which is similar to the transcriptome profile of hESCs. Differentiation of iPSCs to HLCs results in a directed change of the transcriptome. It should converged to the transcriptome of human primary hepatocytes (PHH). In order to visualize this transformation of the reprogrammed HUVEC line and further differentiated to HLCs a cluster dendogram was complied of the transcriptome profiles from HUVEC, HUVEC-iPSC, hESC, HUVEC-derived HLCs at different time points (HLC 14d, HLC 19d, HLC 27d), fetal liver and PHH (Figure 3.35A). The HUVEC-iPSC lines differ from their parental cell type and has a transcriptome profile similar to hESC. HLCs derived from HUVEC-iPSC cluster all together and differ from the HUVEC-iPSC line as strong as from the transcriptome profile of fetal liver and PHH. In order to show the precise distinction between the samples Pearson correlation co-efficient was evaluated (Figure 3.35B). The most similarity was located between 14 days and 19 days HLCs followed by the transcriptome profile between 19 days and 27 days HLCs. The transcriptome of 19 days HLCs holds the highest similarity to that of fetal liver and PHH in comparison to the other HLCs.
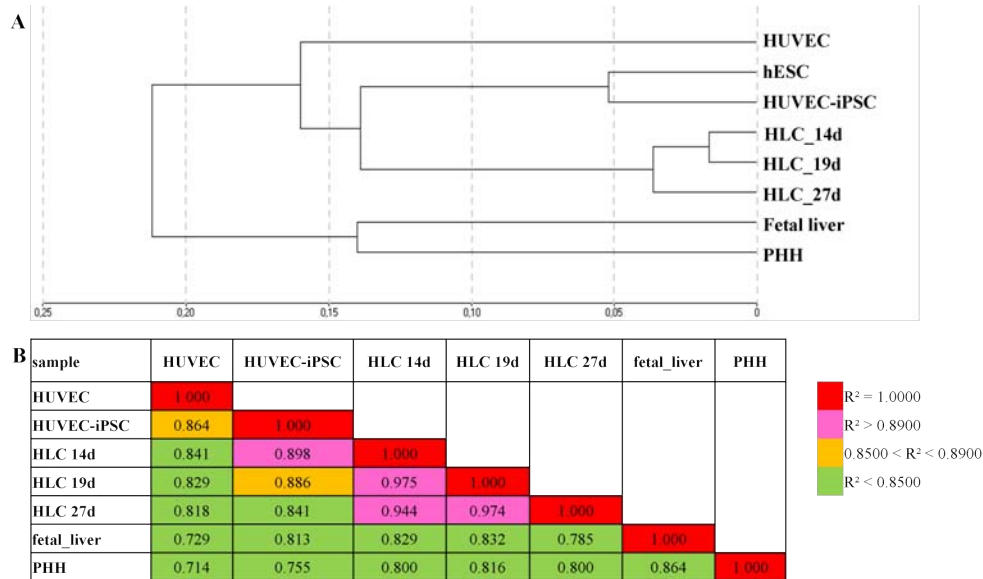
Figure 3.35: **RNA-based microarray analyses HUVEC-iPSC-derived HLCs.**
A) A dendogram analysis of the transcriptome profiles from hESC, HUVEC, HUVEC-iPSC, HLC-derived from HUVEC-iPSC at different time points (HLC 14d, HLC 19d, HLC 27d), fetal liver and PHH. **B)** Pearson correlation co-efficient of the entire expression data (Illumina microarrays) of HUVEC, HUVEC-iPSC, HLC 14d, HLC 19d, HLC 27d, fetal liver and PHH. Abbreviations: hESCs = human embryonic stem cells; HUVEC = human umbilical vein endothelial cell; HUVEC-iPSC = episomal reprogrammed induced pluripotent stem cell derived from HUVECs; HLC = hepatocyte-like cell; PHH = primary human hepatocytes.

Comparative transcriptome profile analysis of HLCs of three different time points (HLC 14d, HLC 19d, HLC 27d), fetal liver and PHH samples using Venn diagram analyses show the numbers of expressed genes (Figure 3.36). First, a Venn diagram was created using the expressed genes of 14d, 19d and 27d HLCs (Figure 3.36A, Supplementary Table 14). The HLC-related genes *ANXA1*, *TTR* and *TBX3* as well as the fetal liver-related gene *AFP* which marks the early liver development and *ALB* represent the matured liver stage are expressed in all three samples (12,380 genes). Proliferation-associated genes are exclusively expressed in 14 days old HLCs (663 genes, e.g. *BCL2*, *FGF2*, *NOG*, *TEK*). 19d HLCs express genes which are associated e.g. to cell survival and recognition (342 genes, e.g. *FGF9*, *GAP43*, *HOXB7*, *RDH12*). Defense, inflammatory, immune and wound response-associated genes are exclusively expressed in 27d HLCs (265 genes, e.g. *CXCL3*, *LYZ*, *SP100*, *TLR4*).

Second, a comparison was conducted of expressed genes in 14 days HLCs (HLC 14d) with fetal liver and PHH (Figure 3.36B, Supplementary Table 15), in 19 days HLCs (HLC 19d) with fetal liver and PHH (Figure 3.36C, Supplementary Table 16) and in 27 days HLCs (HLC 27d) with fetal liver and PHH (Figure 3.36D, Supplementary Table 17). The HLC-related genes *ANXA1*, *TTR* and *TBX3* as well as the fetal liver-related gene *AFP* and *ALB* as a matured liver stage marker are expressed in all samples. Additionally, in all samples are expressed bile acid-related transporter genes such as *SLC10A1* (*NTCP*) and *ABCC2* (*MRP2*), Hippo signaling-related genes e.g. *BBC3*, *TEAD3* and *TAZ*, cell-cell contact-related genes such as *CDH1* (*E-CAD*), *CLDN1* and *TJP1* (*ZO-1*) as well as cytochrome p450 superfamily-related genes such as *ACYP2*, and *CYP27A*.

Third, the intersections were analyzed between the HLCs vs. PHH and HLCs vs. fetal liver. Analysis of PHH vs. HLC 14d (350 genes, Figure 3.36B) by DAVID uncovered the expression of drug metabolism-related genes (e.g. *NAT2*, *TYMP*) and NOTCH signaling pathway-related genes (e.g. *JAG*, *MESP*) as well as cell-cell signaling-related genes (e.g. *FGF2*, *PANX1*, *WNT5A*). Intersection analysis of fetal liver vs. HLC 14d (1,768 genes, Figure 3.36B) by DAVID uncovered the expression of WNT signaling pathway-related genes (e.g. *FZD9*, *LEF1*, *RAC2*), embryonic development-related genes (e.g. *DLC1*, *PTK7*, *SOX8*) and cell proliferation-related genes (e.g. *LGR4*, *KIT*, *VEGFC*). Intersection analysis of PHH vs. HLC 19d (369 genes, Figure 3.36C) by DAVID uncovered the expression of drug metabolism-related genes (e.g. *TYMP*, *UMPS*) and cytochrome p450 superfamily-related genes (e.g. *CYP1A1*, *CYP2E1*) as well as regulation of cell growth-related genes (e.g. *ABTB2*, *HNF4α*, *SEMA4F*). Intersection analysis of fetal liver vs. HLC 19d (1,653 genes, Figure 3.36C) by DAVID uncovered the expression of cell adhesion molecules-related genes (e.g. *CLDN4*, *PECAM1*, *VCAM1*), developmental maturation-related genes (e.g. *GDF11*, *RUNX3*, *SOX8*) and cell cycle-related genes (e.g. *CHEK2*, *E2F2*, *TTK*). Intersection analysis of PHH vs. HLC 27d (358 genes, Figure 3.36D) by DAVID uncovered the expression of drug metabolism-related genes (e.g. *TYMP*, *UMPS*) and cytochrome p450 superfamily-related genes (e.g. *CYP1A1*, *CYP2E1*, *CYP3A4*) as well as regulation of body fluid levels-related genes (e.g. *ANXA8*, *HNF4α*, *SERPINE1*). Intersection analysis of fetal liver vs. HLC 27d (1,350 genes, Figure 3.36D) by DAVID uncovered the expression of cell adhesion molecules-related

genes (e.g. *CLDN4*, *MPZ*, *VCAM1*), gap junction-related genes (e.g. *ADCY3*, *GJA1*, *PDGFB*) and cell cycle-related genes (e.g. *CHEK2*, *MCM2*, *TTK*).

To sum up these transcriptome profile analysis of HLCs with three different time points (HLC 14d, HLC 19d, HLC 27d), fetal liver and PHH samples all three HLC samples were similar and clustered together. Each sample expressed genes comparable to fetal liver and PHH. However, the transcriptome profile of HLC 14d showed the most overlap with that of fetal liver and HLC 19d with that of PHH.
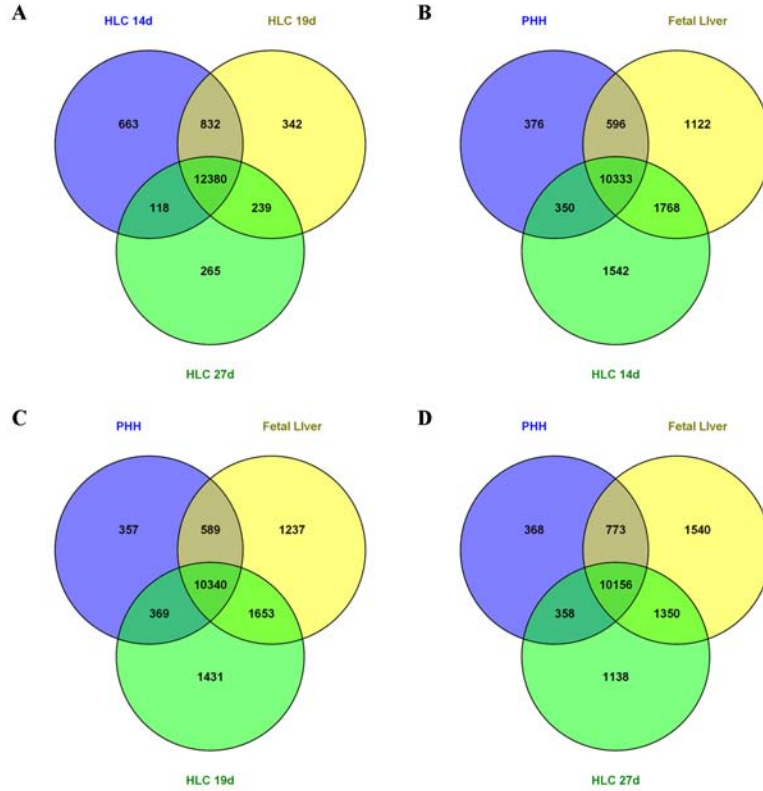
Figure 3.36: **Venn diagram analyses.**
A) Venn diagram analysis of the transcriptome profile from HUVEC-iPSC-derived HLC at different time points (HLC 14d, HLC 19d, HLC 27d) portraying distinct and overlapping transcriptional signatures. **B)** Venn diagram analysis of the transcriptome profile from PHH, fetal liver and HLC-derived from HUVEC-iPSC at day 14 (HLC 14d) portraying distinct and overlapping transcriptional signatures. **C)** Venn diagram analysis of the transcriptome profile from PHH, fetal liver and HLC-derived from HUVEC-iPSC at day 19 (HLC 19d) portraying distinct and overlapping transcriptional signatures. **D)** Venn diagram analysis of the transcriptome profile from PHH, fetal liver and HLC-derived from HUVEC-iPSC at day 27 (HLC 27d) portraying distinct and overlapping transcriptional signatures. Abbreviations: HUVEC = human umbilical vein endothelial cell; HUVEC-iPSC = episomal reprogrammed induced pluripotent stem cell derived from HUVECs; HLC = hepatocyte-like cell; PHH = primary human hepatocytes.

3.2.3 Comparison of transcriptome profiles from different HLCs

In order to visualize and analyze the distinctions and commonalities in certain areas heatmaps were generated to show the Hippo, Notch and TGFβ pathway (Figure 3.37) as well as ABC transporter-related, cytochrome P450 superfamiliy-related (Figure 3.38), liver development-related, bile acid transporter-related and tight junction-related genes (Figure 3.39).

The Hippo signaling pathway influences fate and size of liver cells and it is essential for the maintenance of the differentiated hepatocyte state. Additionally, the Hippo pathway is responsible for maturation and stabilization of the tight junctions. The expression pattern of hippo pathway-related genes in HUVEC-derived HLCs is comparable to that in HFF1-derived HLCs (Figure 3.37A). Notch signaling is an evolutionary conserved mechanism that plays amongst others an important role in cell fate decisions in the early liver development. During liver and biliary development Notch coordinates biliary fate and duct morphogenesis in a temporal- and dose-dependent way, which is a late event in liver development. HFF1-derived HLCs and HUVEC-derived HLCs show a comparable expression pattern of Notch signaling-related genes and cluster together (Figure 3.37B). In liver development the TGFβ pathway is involved in tight junction depletion, cytoskeleton and cell-cell contact rearrangement. The samples of HFF1-derived HLCs and HUVEC-derived HLCs cluster together and reveal comparable expression pattern of TGFβ pathway-related genes (Figure 3.37C).

ABC transporters are accountable for the uptake and efflux of e.g. bile acids and metabolites. The expression pattern of HUVEC-derived HLCs differs from HFF1-derived HLCs and form their own cluster. The iPSC sample expression pattern cluster together and this cluster is extended by the HFF1-derived HLCs (Figure 3.38A). The same result is shown by the heatmap of cytochrome P450 superfamily-related genes, which are involved in drug metabolism and synthesis of cholesterol, steroids and other lipids. The iPSC sample expression pattern cluster together and this cluster is extended by the HFF1-derived HLCs. The expression pattern of HUVEC-derived HLCs differs from HFF1-derived HLCs and form their own cluster (Figure 3.38B). This indicates that HUVEC-derived HLCs are more hepatocyte-like than HFF1-derived HLCs.

A short insight into the liver development was summarized in a heatmap (Figure 3.39A). The expression pattern HFF1-derived HLCs and HUVEC-derived HLCs are comparable and form a cluster. The expression of pluripotent-associated genes (*POU5F1*, *SOX2* and *NANOG*) are down-regulated and mature liver-related genes (*ALB*, *CYP1A1* and *TTR*) as well as hepatoblast-related genes (e.g. *DLK1*, *HNF1B*, *NOTCH3*) are up-regulated. The iPSC sample expression pattern of bile acid transporter genes cluster together and this cluster is extended by the HFF1-derived HLCs. The expression pattern of HUVEC-derived HLCs differs from HFF1-derived HLCs and form their own cluster (Figure 3.39B). Due to the fact that the Hippo pathway and TGFβ pathway are involved in the tight junction formation and the expression pattern of Hippo pathway- and TGFβ pathway-related genes were comparable in HFF1-derived HLCs and HUVEC-derived HLCs a heatmap of tight junction related-genes was compiled (Figure 3.39C). The HFF1-derived HLCs expression pattern is not comparable with that of HUVEC-

derived HLCs. The samples of HUVEC-derived HLCs do not cluster together. Tight junction related-genes ar most expressed in HFF1-derived HLCs.

In order to analyze the transformation of somatic fibroblast cell lines during the re-programming process and further differentiating to HLCs a cluster dendogram was complied of the transcriptome profiles from HUVEC, HUVEC-iPSC, HFF1-iPSC, HUVEC-derived HLCs at different time points (HLC 14d, HLC 19d, HLC 27d), fetal liver and PHH (Figure 3.40A). The cluster dendrogram demonstrates the high similarities of the transcriptome profiles between the biological replicates. The iPSCs formed a cluster which is then extended by HFF1-HLCs. The HUVEC-derived HLCs of different time points formed a cluster. Furthermore, fetal liver and PHH formed a cluster.

To detect the relation between HFF1-HLCs and HUVEC-HLCs a venn diagram analysis was conducted (Figure 3.40B, Supplementary Table 18). Most liver-related genes are expressed in both samples (12781 genes, intersection of HFF1-HLCs and HUVEC-HLCs venn diagram). The expression of the HLC-related genes *ANXA1*, *TTR* and *TBX3* as well as the fetal liver-related gene *AFP* and mature liver-related gene *ALB* are located in the intersection. Additionally, in both samples are expressed bile acid-related transporter genes such as *SLC10A1* (*NTCP*) and *ABCC2* (*MRP2*), Hippo signaling-related genes e.g. *BBC3*, *TEAD3* and *TAZ*, cell-cell contact-related genes such as *CDH1* (*E-CAD*), *CLDN1* and *TJP1* (*ZO-1*) as well as cytochrome p450 superfamily-related genes such as *ACYP2*, *CYP1A1* and *CYP26A1*. However, they also expressed markers which indicates that these HLCs are immature. Both expressed progenitor-related markers such as *PROM1* (*CD133*), *LEFTY2*, *DNMT3B*, *SOX2*, *NOTCH3*, *DLK1*, intestine-related gene *CDX2*, cholangiocyte-related genes e.g. *AQP1 KRT7*, *SOX9* and pancreas-related genes *MEIS2*, *ISL1* (Ahlgren et al. [1997]; Smith et al. [1997]; Swift et al. [1998], Cheng et al. [2012]; Hannan et al. [2013], Dianat et al. [2014]).

84
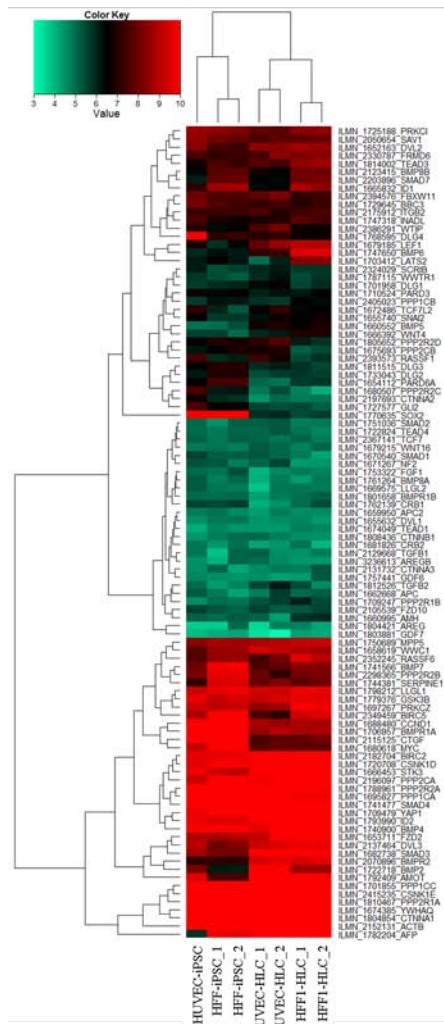
A **Hippo Pathway** **B** **Notch Pathway** **C** **TGFβ Pathway**
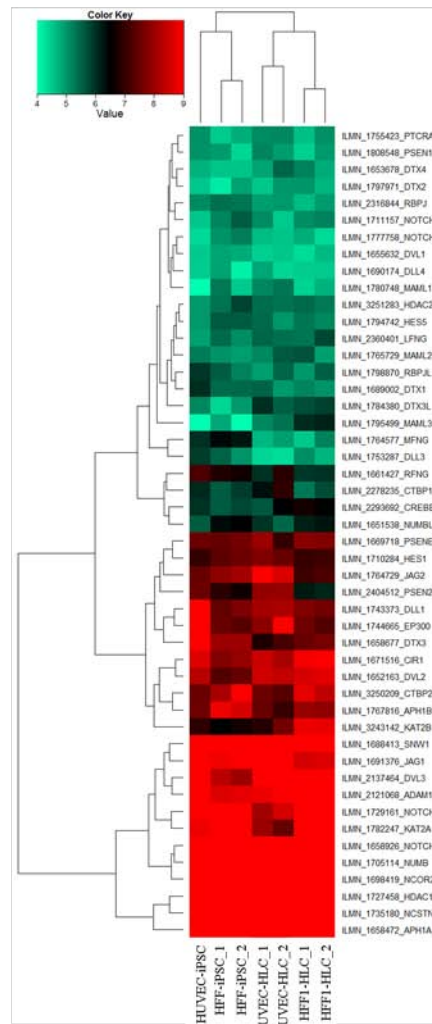
continued from previous page

Figure 3.37: **Comparative pathway analyses.**
The expression pattern of the following samples were compared: HFF1-iPSC, HFF1-HLC, HUVEC-iPSC and HUVEC-HLC. **A)** Heatmap of Hippo pathway-related genes. **B)** Heatmap of Notch pathway-related genes. **C)** Heatmap of TGFβ pathway-related genes. Abbreviations: HUVEC = human umbilical vein endothelial cell; HUVEC-iPSC = episomal reprogrammed induced pluripotent stem cell derived from HUVECs; HLC = hepatocyte-like cell.

Figure 3.38: **Comparative heatmap analyses.**
The expression pattern of the following samples were compared: HFF1-iPSC, HFF1-HLC, HUVEC-iPSC and HUVEC-HLC. **A)** Heatmap of ABC transporter-related genes. **B)** Heatmap of cytochrome P450 superfamily of enzymes-related genes. Abbreviations: HUVEC = human umbilical vein endothelial cell; HUVEC-iPSC = episomal reprogrammed induced pluripotent stem cell derived from HUVECs; HLC = hepatocyte-like cell.

Figure 3.39: **Comparative heatmap analyses of liver specificities.**
The expression pattern of the following samples were compared: HFF1-iPSC, HFF1-HLC, HUVEC-iPSC and HUVEC-HLC. **A)** Heatmap of liver development-related genes. **B)** Heatmap of bile acid transporter-related genes. **C)** Heatmap of tight junction-related genes. Abbreviations: HUVEC = human umbilical vein endothelial cell; HUVEC-iPSC = episomal reprogrammed induced pluripotent stem cell derived from HUVECs; HLC = hepatocyte-like cell.

To analyze whether or not one of the generated HLCs is more mature than the other DAVID analyses of the single sections were performed. The HUVEC-iPSC-derived HLCs exclusively expressed genes e.g. of drug metabolism, cytokine-cytokine receptor inter-action, ABC transporters, Metabolism of xenobiotics by cytochrome P450, chemokine signaling pathway and MAPK signaling pathway (1212 genes, Figure 3.40B, Supplementary Table 18). This indicates that HLCs derived from HUVEC-iPSCs are more mature and functional hepatocyte-like cells compared to HFF1-iPSC-derived HLCs. However, HUVEC-iPSC-HLC expressed progenitor-related genes such as *CXCR4*, *CER1*, *PROX1* and *PDX1* indicating that these cells are immature (Cheng et al. [2012]; Hannan et al. [2013], Seth et al. [2014]). The HFF1-iPSC-derived HLCs exclusively expressed genes related to e.g. cell adhesion molecules, cell-cell signaling and tight junction indicating that these cells are more mature on a structural level compared to HUVEC-iPSC-derived HLCs (1284 genes, Figure 3.39C and 3.40B).

In order to analyze the relation between the iPSC-derived HLC lines compared to fetal liver and PHH a venn diagram analysis of these samples was conducted (Figure 3.40C, Supplementary Table 19). The transcription profiles of the HLCs are more similar to that of fetal liver than to PHH. Both HLC lines and the fetal liver expressed genes related to cell-cycle, DNA replication and cell adhesion molecules as well as progenitor-related genes (e.g. *DLK1*, *DNMT3B*, *DPPA4*, *NOTCH3*, *PODXL*, *PROM1*).
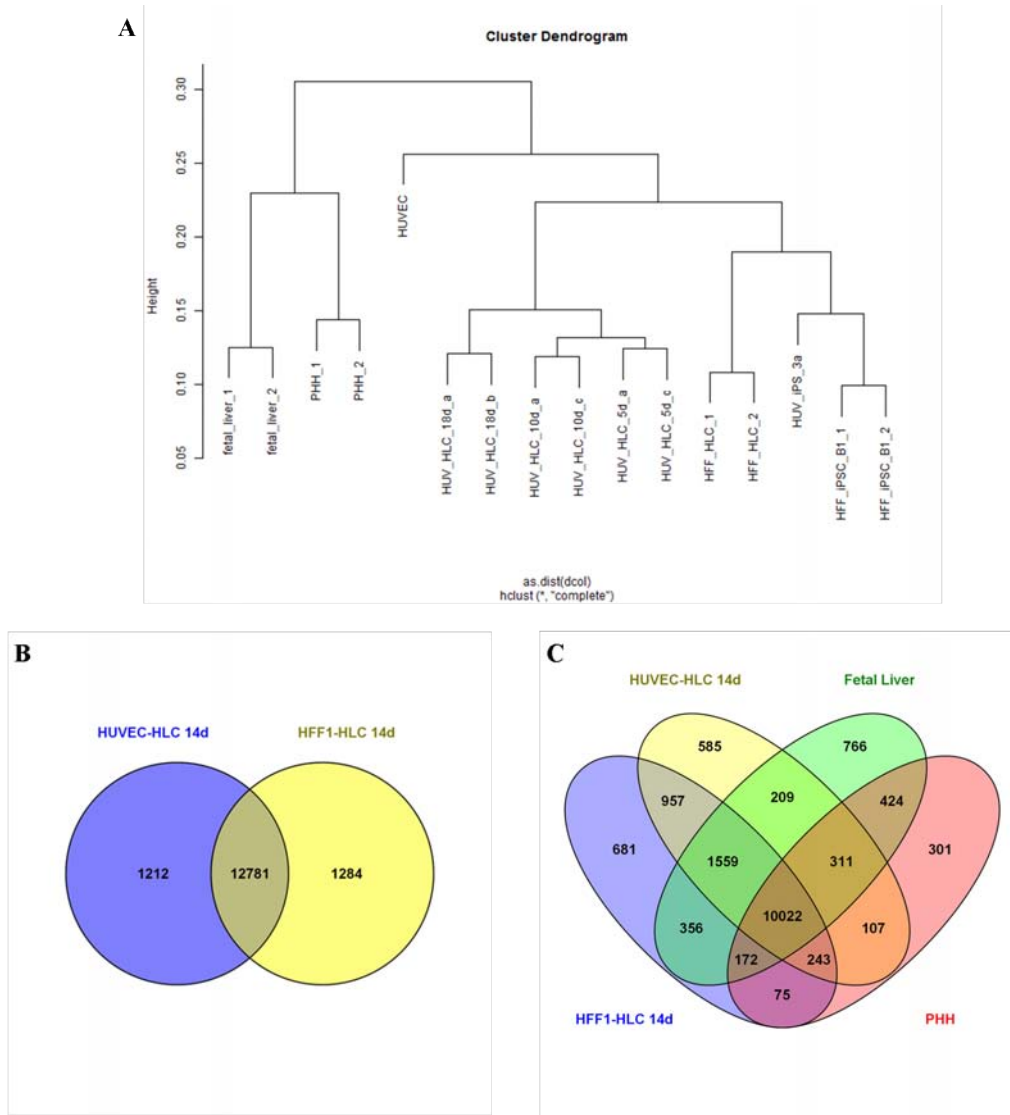
Figure 3.40: **Comparative cluster analyses.**
A) A dendrogram analysis of the transcriptome profiles from HUVEC, HUVEC-iPSC, HLC-derived from HUVEC-iPSC at different time points (HLC 14d, HLC 19d, HLC 27d), HFF1-iPSC, HLC-derived from HFF1-iPSC, fetal liver and PHH. **B)** Venn diagram analysis of the transcriptome profile from HFF1-iPSC-derived HLC (HFF1-HLC 14d) and HUVEC-iPSC-derived HLC (HUVEC-HLC 14d) portraying distinct and overlapping transcriptional signatures. **C)** Venn diagram analysis of the transcriptome profile from HFF1-iPSC-derived HLC (HFF1-HLC 14d), HUVEC-iPSC-derived HLC (HUVEC-HLC 14d), fetal liver and PHH portraying distinct and overlapping transcriptional signatures. Abbreviations: HUVEC = human umbilical vein endothelial cell; HUVEC-iPSC = episomal reprogrammed induced pluripotent stem cell derived from HUVECs; HLC = hepatocyte-like cell; PHH = primary human hepatocytes.

3.3 Derivation and characterization of endoderm progenitor cells derived from HFF1-iPSC

Human pluripotent stem cells, including human embryonic stem cells (hESCs) and induced pluripotent stem cells (iPSCs), have the capacity to self-renew and give rise to all tissue types. During the differentiation *in vitro* to mature cell types these pluripotent stem cells traverse the early embryonic development (Murry and Keller [2008]). The liver and pancreas are examples for endodermal-derived tissues. To address the early embryonic development of endodermal-derived tissues and to analyze cell fate decisions during this process we derived endodermal progenitors (EPs) from iPSCs.

Generate iPSCs is primarily to archieve immunocomparbility and also to avoid ethical and moral issues. The viral reprogramming is the most commonly used method (Prigione et al. [2010]; Wang et al. [2010]; Somers et al. [2010]; Jozefczuk et al. [2011]; Ban et al. [2011]; Cheng et al. [2012]; Sekine et al. [2012]; Takebe et al. [2014]). Here, in this project another method was used which was published by Yu et al. [2009]. The episomal-derived iPSCs, which were used for this study were derived from human fibroblasts (HFF1 cells), are viral-free and integration-free (see Chapter 2).

The endodermal progenitors (EPs) were derived from the iPSC-line epiHFF1-iPS-B1 followed the protocol by Cheng et al. [2012] with slight modifications. The differentiation procedure is split into four stages (Figure 3.41). First, the definitive endoderm (DE), which is also the first stage of HLC differentiation. Second, an intermidiate stage between definitive endoderm and endoderm progenitors, labeled as transient cells (TC). Third, the stage of pre-endoderm progenitors (pre-EP), when the maintenance medium is applied and fourth, when 3D-colonies are formed the EP stage is accomplished. The original protocol describes the second stage as a period of four weeks. In this study, the procedure was modified and reduced to three and two weeks. The procedure could be successfully shortened. Before the cells were split the first time, minor changes were observed, but no colonies were formed. After the first split the culture was homogenous. At passage 4 the first colonies were observed. The cells which were cultured two weeks as TCs (2 week cells) had formed big colonies at passage 8, as well as the three weeks TC cultured cells. The original treated cells which were four weeks at the TC stage (4 week cells) had small colonies at passage 8 in comparison to the other procedures (two and three weeks cultured TCs). During the culture the size and number of EP colonies from the 4 weeks TCs adapted to that of the other conditions (Figure 3.41).
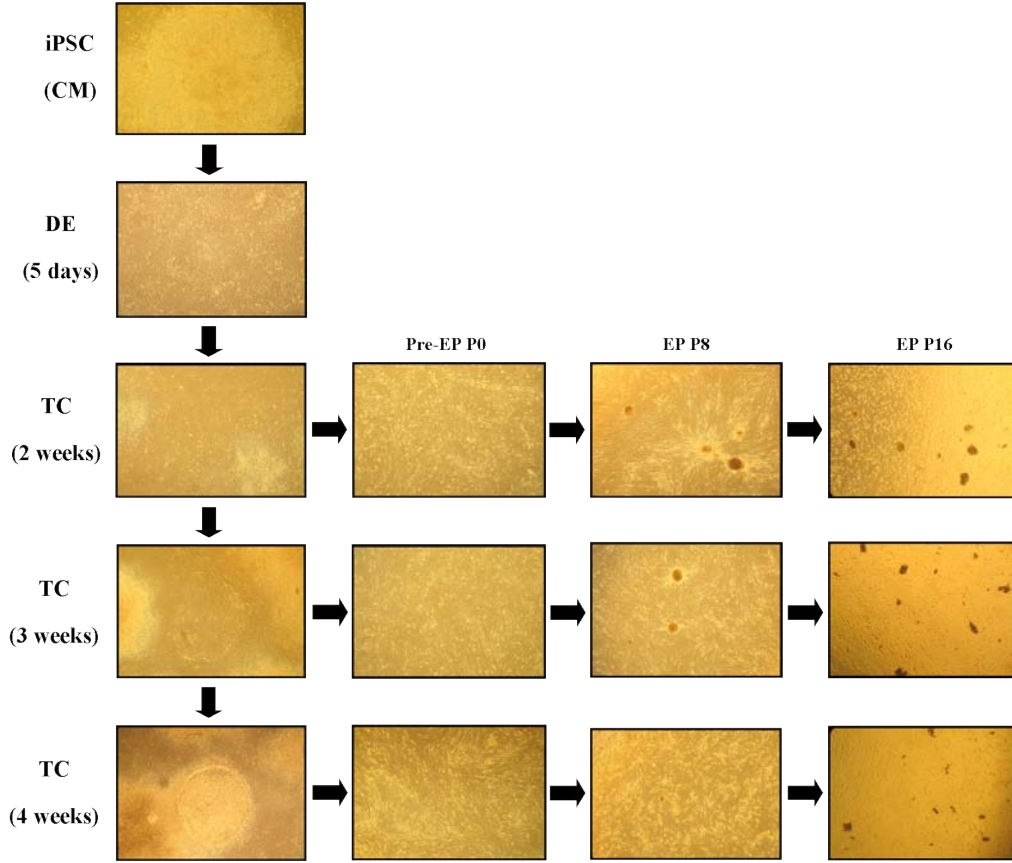
Figure 3.41: **Illustration of EP development derived from epiHFF1-iPS-B1.**
Microscopy images showing morphology changes during the differentiation of epiHFF1-iPS-B1 (iPSCs) to endodermal progenitors (EPs). The iPSC-line were cultured in conditioned medium (CM). The generation of the first stage definitive endoderm (DE) takes five days. The intermediate stage (TC) were generated in two, three and four weeks. Following the cells were split the first time to pre-EPs (P0). At passage eight (P8) the two and three week cells have big colonies, the four week cells have minor colonies in comparison. In the course of passages the cells adapt, shown in passage 16 (P16). Abbreviations: DE = definitive endoderm; EP(s) = endoderm progenitor(s); iPSC = induced pluripotent stem cell; P0 = passage zero; TC = transient cells.

After five days DE stage related maker proteins were detected (Figure 3.42). Antibody stainings showed that the expression of the pluripotency marker OCT4 was down regulated, the definitive endoderm marker chemokine (C-X-C motif) receptor 4 (CXCR4), as well as HNFα, E-Cadherin (E-CAD), the stem cell/progenitor markers leucine-rich repeat containing G protein-coupled receptor 5 (LGR5) and PROM1 (CD133) were detectable (McLean et al. [2007]; Mizrak et al. [2008]; Wang et al. [2013b]). At the end of the intermediate stage TC the expression of OCT4 was deactivated and HNF4α, E-Cadherin (E-CAD), CXCR4 and LGR5 were still detectable (Figure 3.43). At passage 4 the first EP colonies were detectable. The treatment with trypsin or accutase failed to split the colonies, therefore the colonies grew bigger. At passage 8 activated leukocyte

cell adhesion molecule (ALCAM), HNF4α, LGR5 and CXCR4 were identifiable (Figure 3.44). Due to the fact that the colonies increased in size, but not in number two needles were used to split the colonies mechanically. The colonies became smaller, more and the stainings got more pronounced intense (Figure 3.45). These progenitor cells express the self-renewal marker LGR5 and markers associated with the foregut (SOX2), midgut/hindgut (caudal type homeobox 2, CDX2), pancreas (pancreatic and duodenal homeobox 1, PDX1), liver (Albumin, ALB), definitive endoderm (chemokine (C-X-C motif) receptor 4, CXCR4) and stem cell (LGR5, CD133) (Cheng et al. [2012]; Hannan et al. [2013]).
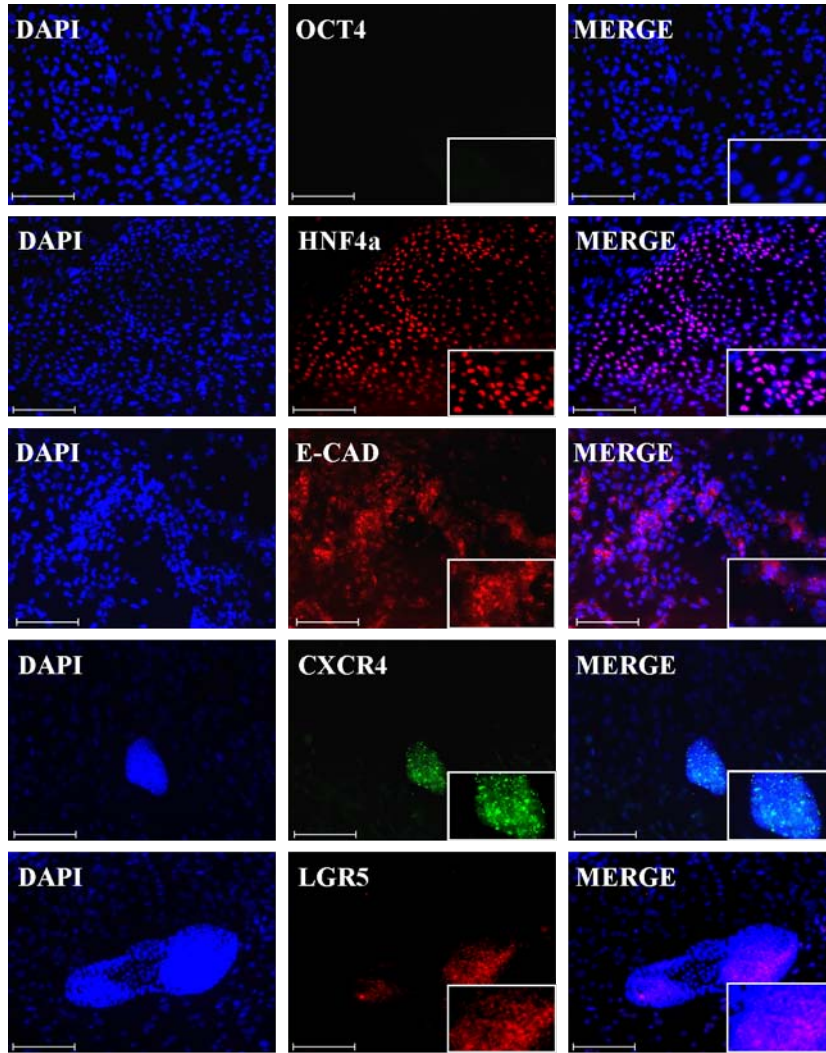
Figure 3.42: **Immunofluorescence-based detection of proteins in DE derived from epiHFF1-iPS-B1 to generate EP.**
The detection of the protein OCT4, pluripotency marker; the transcription factor HNF4α, E-CAD, CXCR4, LGR5 and CD133. DAPI stained the nucleus. Scale bar: 200 μm, Alexa Flour 594 (red), Alexa Flour 488 (green).
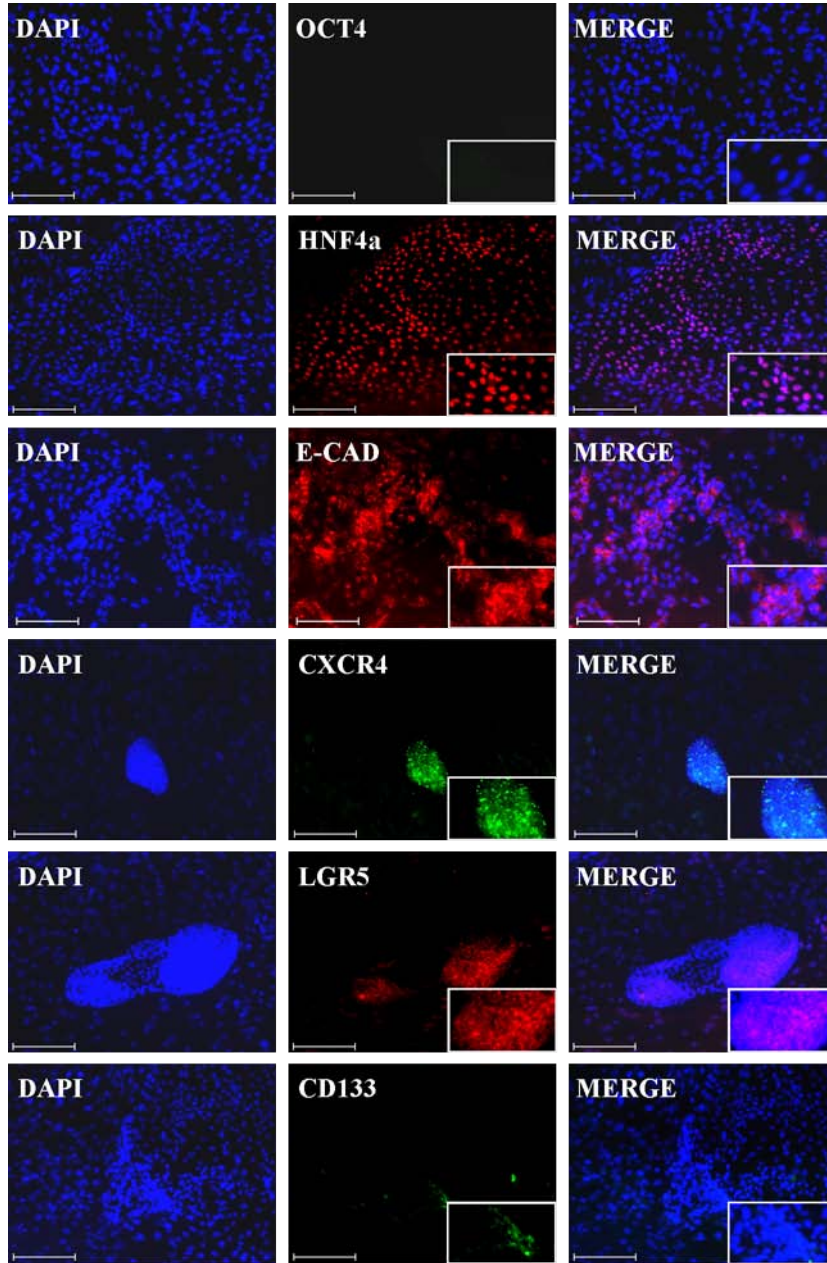
Figure 3.43: **Immunofluorescence-based detection of proteins in intermediate stage from DE to EP derived from epiHFF1-iPS-B1.**

OCT4 as a pluripotency marker was not detectable; endodermal marker such as the transcription factor HNF4α, E-CAD, CXCR4, as well as the stem cell markers LGR5 and CD133 were detectable. DAPI stained the nucleus. Scale bar: 200 μm, Alexa Flour 594 (red), Alexa Flour 488 (green).
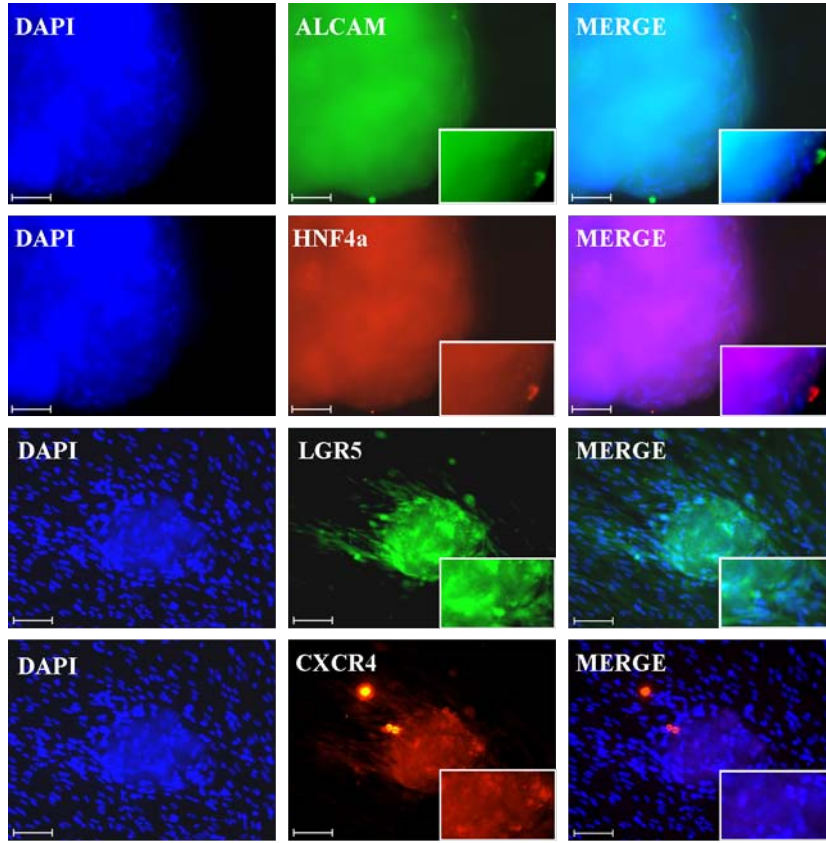
Figure 3.44: **Immunofluorescence-based detection of proteins in EP passage 8 derived from epiHFF1-iPS-B1.**
The detection of the protein ALCAM, HNF4α, LGR5 and CXCR4. DAPI stained the nucleus. Scale bar: 200 μm, Alexa Flour 594 (red), Alexa Flour 488 (green).
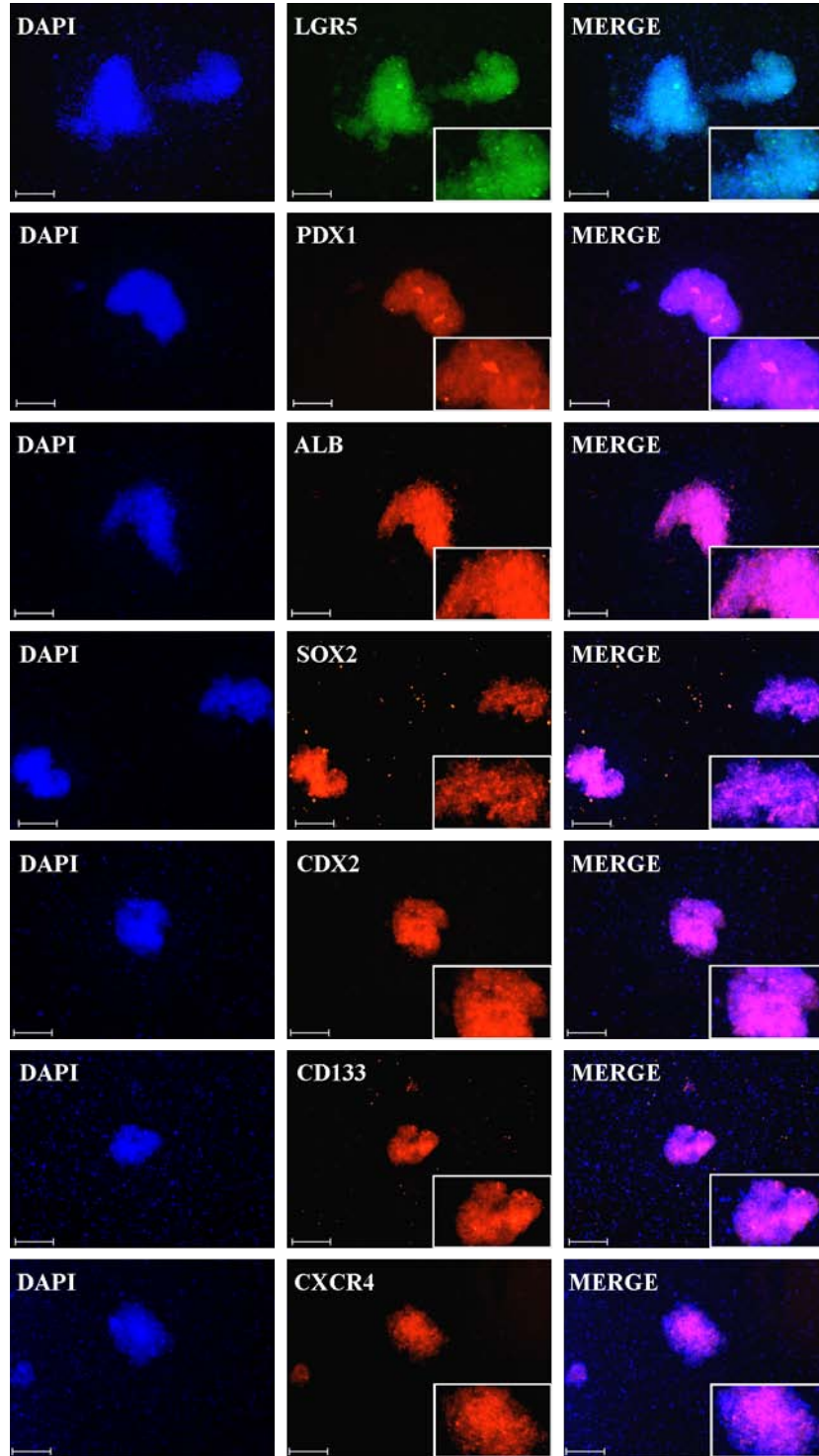
Figure 3.45: **Immunofluorescence-based detection of proteins in EP passage 16 derived from epiHFF1-iPS-B1.**
The detection of the protein LGR5 (self-renewal marker), PDX1 (pancreas marker), ALBUMIN (liver marker), SOX2 (foregut marker), CDX2 (hindgut marker), CD133 (stem cell marker) and CXCR4 (definitive endoderm marker). DAPI stained the nucleus. Scale bar: 200 μm, Alexa Flour 594 (red), Alexa Flour 488 (green).
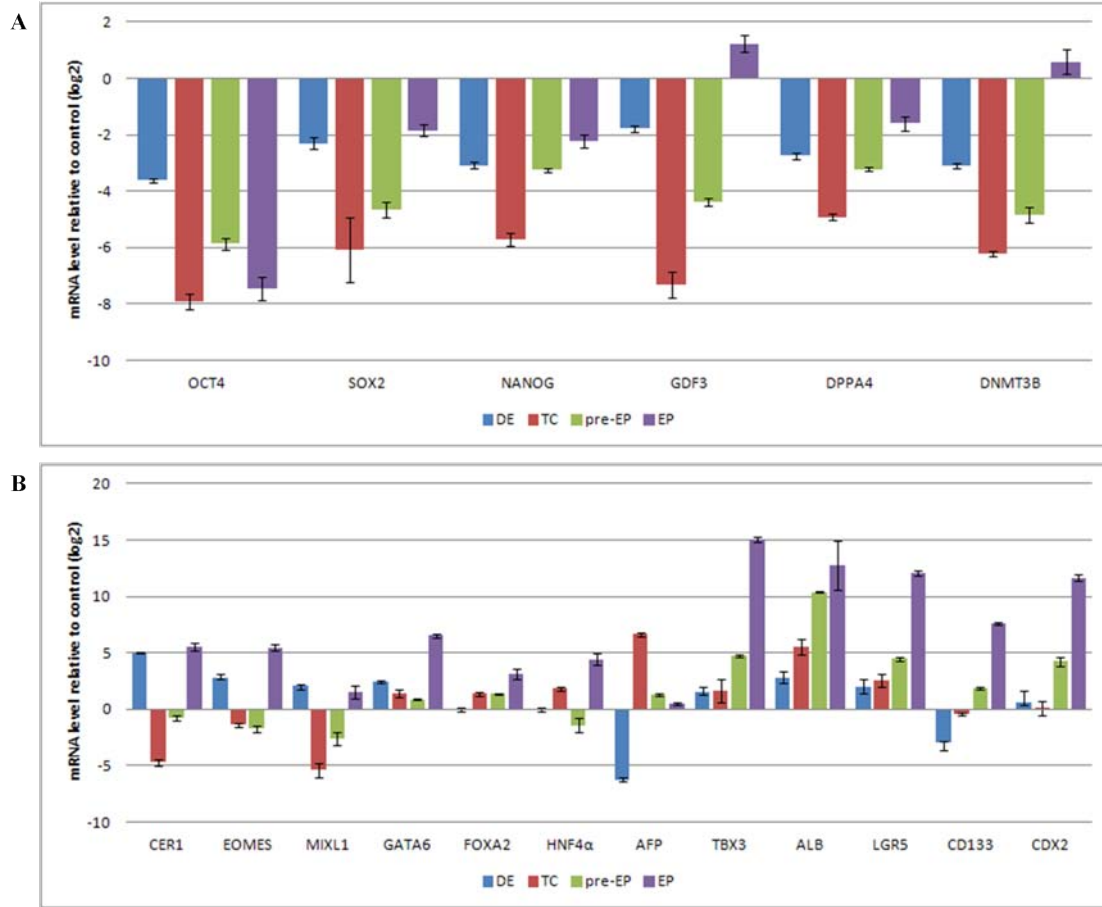
Figure 3.46: **Quantitative real-time PCR profile of EP derivation.**
A) The expression pattern of pluripotency associated genes during the endodermal progenitor (EP) derivation from epiHUV-iPS-3a were decreased. **B)** Development of the expression pattern of specific markers during the EP differentiation are shown. Definitive endoderm (DE) specific marker genes *CER1*, *EOMES*, *MIXL1* and *GATA6* were expressed in DE stage, decreased during EP differentiation and were highly expressed in EPs. *CD133* was not expressed in DE and transient cells (TC) but increased in preliminary stage of EPs (pre-EP) and was highly expressed in EPs. *HNF4α* and *FOXA2* as key transcription factors of liver development were most expressed in EPs. The liver specific genes *AFP*, *ALB* and *TBX3* were most expressed at the end stage of EP derivation. The stem cell/progenitor marker *LGR5* and intestine-specific marker *CDX2* were also most expressed in EPs. Three biological replicates in technical triplicates of each sample were analyzed against the undifferentiated state of induced pluripotent stem cells (epiHFF1-iPS-B1) as the control. The standard deviation is depicted by the error bars.

QRT-PCR analyses of all stages during EP derivation revealed the expression profile of each stage relative to the undifferentiated state of the iPSC-line which was differentiated to EPs (Figure 3.46). The expression of pluripotency-associated genes such as *OCT4*, *SOX2* and *NANOG* decreased during the differentiation to DE and transient cell (TC) stage and increased to the pre-EP and EP stage, but was still decreased compared to

the expression level of iPSCs. Immunofluorescence-based antibody staining of EPs for SOX2 uncovered the expression (Figure 3.45). However, the expression level of *GDF3* and *DNMT3B* in EPs is increased or comparable to the iPSCs (Figure 3.46A). Primitive streak-/endoderm-specific genes such as *CER1*, *EOMES*, *MIXL1*, *GATA6*, *FOXA2* and *HNF4α* are expressed most at the EP stage (Rosa [1989]; Afouda et al. [2005]; Hart et al. [2005]; Agarwal et al. [2008]; Arnold and Robertson [2009]; Takayama et al. [2011]; Teo et al. [2011]; Takayama et al. [2012]). Early and late liver specific genes such as *AFP*, *ALB* and *TBX3* are expressed most at the EP stage as well as the progenitor-related genes *CD133*, *LGR5* and the intestinal-associated gene *CDX2*(Figure 3.46B) (Renard et al. [2007]; Hay et al. [2008b]; Cheng et al. [2012]; Hannan et al. [2013]).
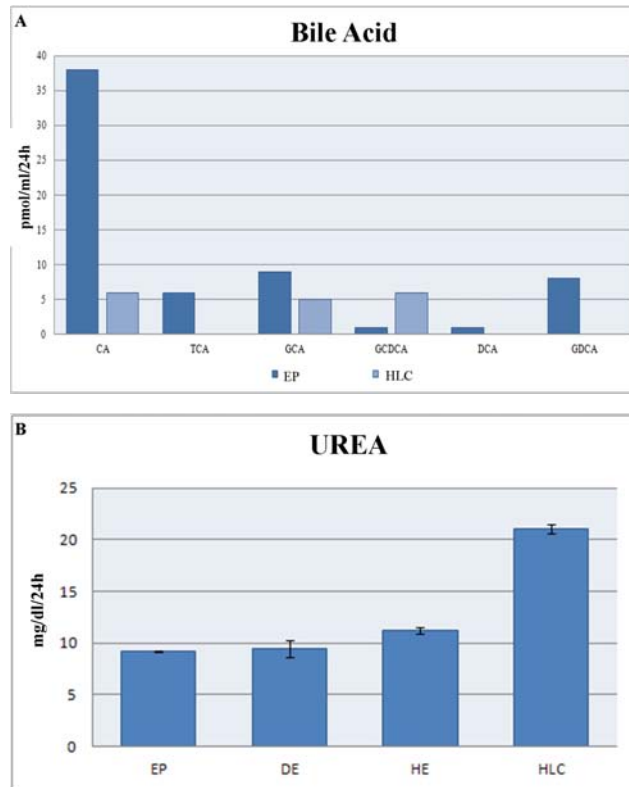
Figure 3.47: **Functional assays of EP cells-derived from epiHFF1-iPS-B1.**
A) Analysis of bile acid production in endodermal progenitors (EP) and epiHUV-3a-HLC (HLC). The levels of bile acids are presented in pmol/ml/24h. **B)** Analysis of urea production in EP, epiHFF1-B1-DE (DE), epiHFF1-B1-HE (HE), epiHFF1-B1-HLC. Three biological replicates in technical triplicates of each sample were analyzed. The levels of urea was measured in mg/dl/24h.

In order to study functional characteristics of the EPs secretion assays for bile acid and urea were done (Figure 3.47). Compared to the HLCs generated from the same iPSC-line the EPs secreted more primary bile acids (Figure 3.47A). The urea secretion was lower than the secretion level of DE cells (Figure 3.47B).

Comparative Microarray analysis of HFF1-iPSC-EP

A comparative transcriptome analysis was done by using the transcriptome profile of viral- and integration-free iPSCs as the original sample with all steps of the EP generation and the transcriptome profile of HLCs. The EPs and HLCs were generated from the same iPSC line (iPSC-B1). A cluster dendrogram was created (Figure 3.48A). The transcriptome of the EPs is distinct separated from the others. A principal component analysis of the samples was done and confirmed the result of the dendogram (Figure 3.48B). The transcriptome profile of EPs is distinct and separated from the other samples. The TC and pre-EP were clustered together.

Further analyses of the expression level of selected gene sets were done (Figure 3.49). Definitive endoderm and primitive streak related genes were expressed most in DE and pre-EP samples (Figure 3.49A-B). However, in EPs were most expressed GATA binding protein 6 (*GATA6*) and *HNF4α* of definitive endoderm-related gene set and and T-box 6 *TBX6* of primitive streak-related gene set. All are transcription factors which are important for the embryogenesis (Morrisey et al. [1998]; Yi et al. [1999]; Li et al. [2000]; Tomizawa et al. [2013]). Another gene set of transcription factors were most expressed in EPs (Figure 3.49C). These are all involved in developmental processes. Later on, Meis homeobox 2 (*MEIS2*) is involved in activating of different gene sets in the pancreas and ISL LIM homeobox 1 (*ISL1*) regulates the generation of all endocrine islet cells (Ahlgren et al. [1997]; Smith et al. [1997]; Swift et al. [1998]). T-box 3 (*TBX3*) regulates β-catenin activity in liver cell proliferation and survival (Bamshad et al. [1999]; Renard et al. [2007]). The Regulatory factor X, 6 (*RFX6*) directs β cell differentiation and keeps the matured cells in their functional activity (Aftab et al. [2008]; Piccand et al. [2014]). Forkhead box P2 (*FOXP2*) regulates lung epithelial gene transcription and is requires to generate early pulmonary endoderm cells (Shu et al. [2001]; Hannan et al. [2015]). Another set of genes includes progenitor-related genes (Figure 3.49D). Regarding to this list only two genes were most expressed in EPs, Forkhead box A1 (*FOXA1*; also known as Hepatocyte nuclear factor 3 alpha *HNF3α*) and Albumin (*ALB*). *FOXA1* is involved in maturation of liver and regulates the expression level of e.g. Transthyretin (*TTR*), which is a pre-albumin gene (Lai et al. [1990]; Domanskyi et al. [2014]; Heddad Masson et al. [2014]). *ALB* is involved in maturation of hepatocytes and maintains their functional activity (Muglia and Locker [1984]; Shiojiri et al. [1991]; Hay et al. [2008b]).
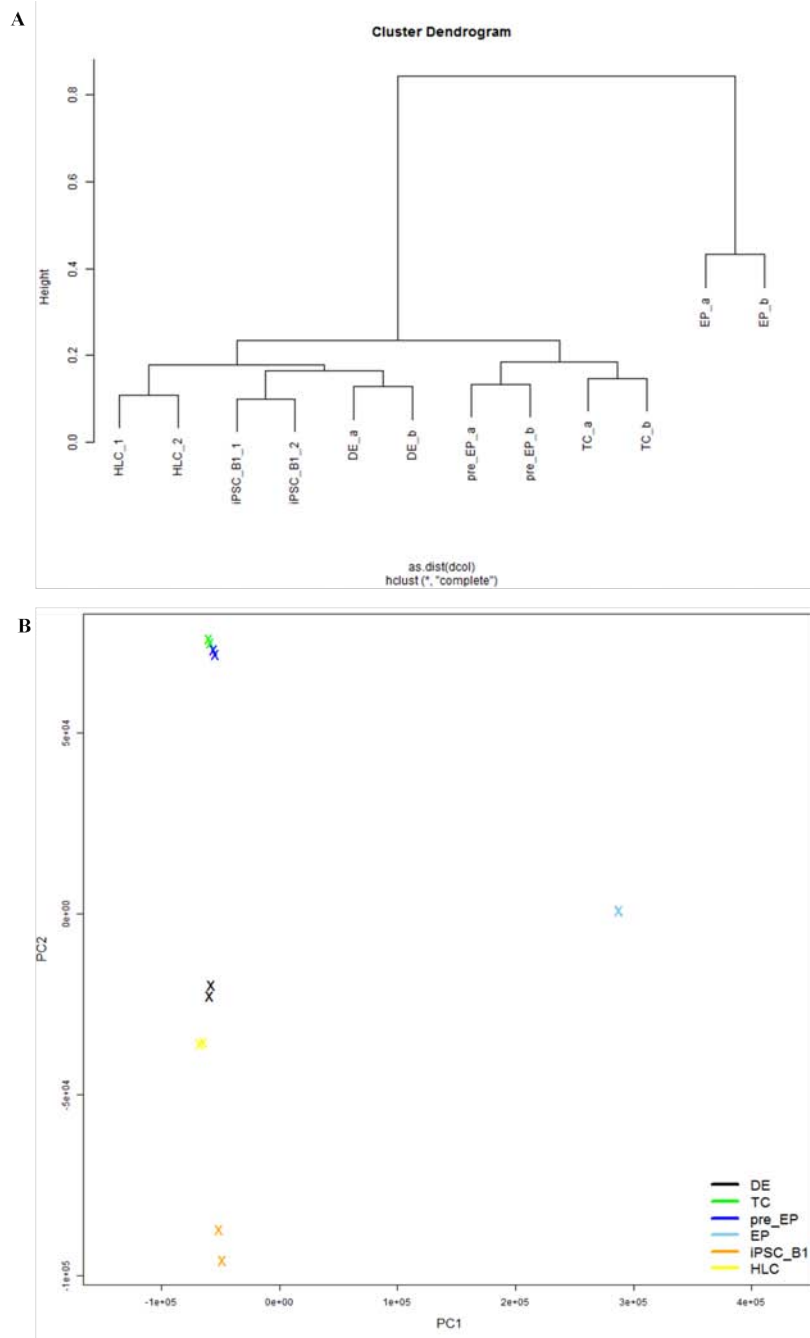
Figure 3.48: **Comparative cluster analysis of stepwise EP generation.**
A) A cluster dendrogram comparison of the the transcriptome of viral- and integration-free iPSC as the original sample with all steps of the EP generation and the transcriptome of HLC. The EP and HLC were generated from iPSC (iPSC_B1). The Transcriptome of the EP is distinct separated from the others. **B)** Principal component analysis of same samples in A. As shown in A the transcriptome of the EP is distinct and separated from the other samples. The TC and pre-EP are more similar. Abbreviations: iPSC = induced pluripotent stem cells, DE = definitive endoderm, TC = transient cells, pre-EP = pre-stage endodermal progenitor cells, EP = endodermal progenitors, HLC = hepatocyte-like cells.
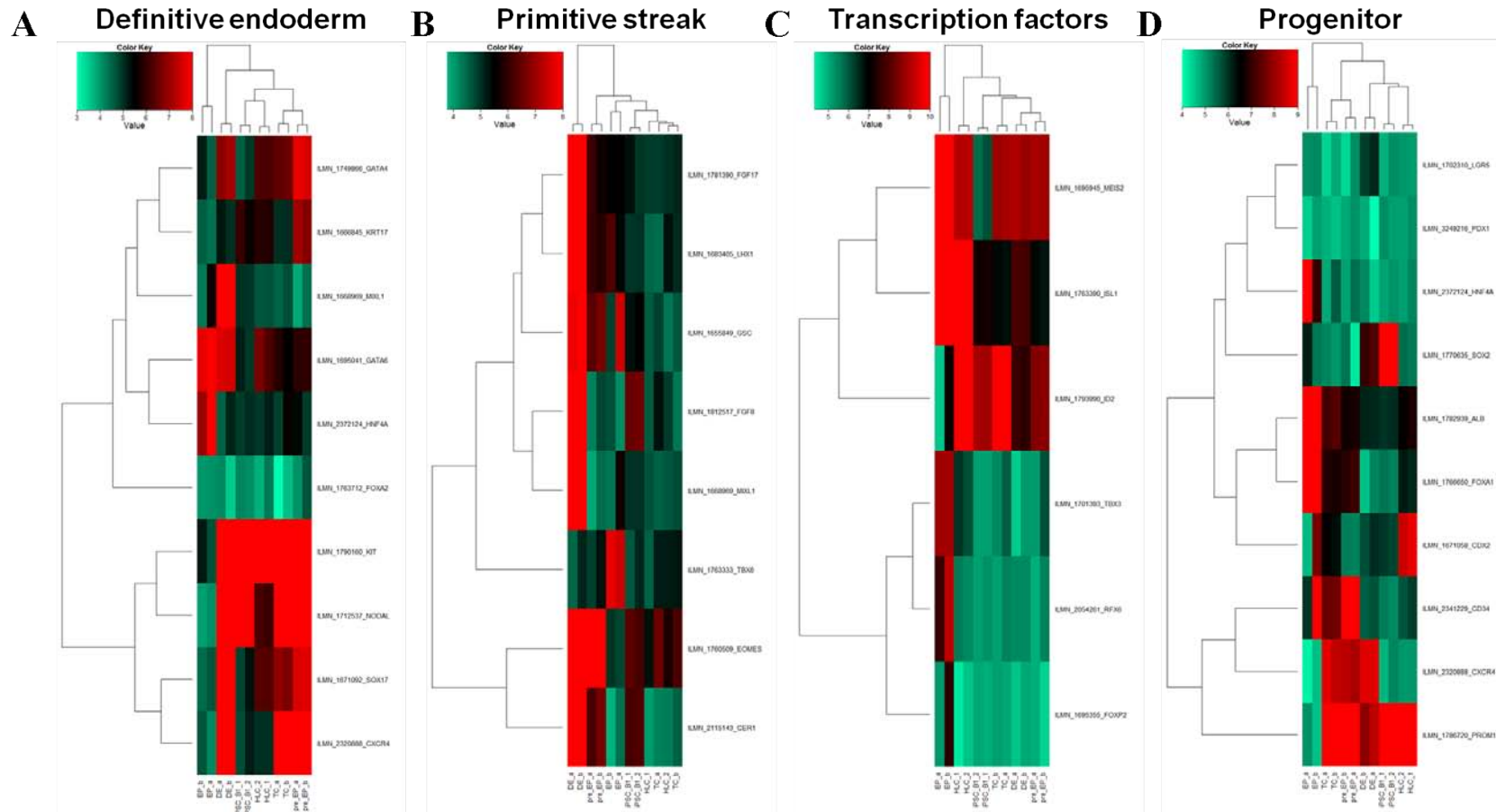
Figure 3.49: **Comparative cluster analysis of stepwise EP generation.**
A) Definitive endoderm related genes were expressed most in DE and pre-EP samples. **B)** Primitive streak related genes were expressed most in DE and pre-EP samples. **C)** Transcription factors related to early liver (TBX3), pancreas (ISL1, RFX6), lung (FOXP2) as well as ID2 and MEIS2 were overexpressed in EP. **D)** The heat map of progenitor related genes identified the EP as a panendoderm progenitor. Abbreviations: iPSC = induced pluripotent stem cells, DE = definitive endoderm, TC = transient cells, pre-EP = pre-endodermal progenitor cells, EP = endodermal progenitors, HLC = hepatocyte-like cells.

3.4 Mouse embryonic fibroblasts replaced by human fetal mesenchymal stem cells

In 1998, when Thomson et al. [1998] isolated and cultured human embryonic stem cells (hESCs) for the first time they used mouse embryonic fibroblasts (MEFs) as a supportive surface for the hESC culture. Under these conditions the hESCs were able to maintain their undifferentiated stage. By replacement of fetal calf serum with Knockout Serum Replacement (SR) and the use of the basic fibroblast growth factor (FGF2) could reduce the spontaneous differentiation level (Amit et al. [2000]). Later on a culture method was developed, which does not use MEFs (feeder-free culture system), to advance the safety profile. The feeder-free system allows to isolate pure DNA, RNA and protein from hESCs and other human cell types. However, MEFs were still used for the production of conditioned medium (CM). Xu et al. [2001] developed a feeder-free system using the medium conditions of Amit et al. [2000] to integrate the soluble factors into the medium secreted by the MEFs. To obtain MEFs a pregnant mouse has to be sacrificed and the embryos have to be harvested (see page 123). Additionally, CM complicate clinical applications of hESCs due to the potential contamination by animal pathogens. Other feeder-free media were developed and are commercial available (Liu et al. [2006]; Lu et al. [2006]; Yao et al. [2006]; Chen et al. [2011]; Beers et al. [2012]; Frank et al. [2012]; Wang et al. [2013a]). Not all media are appropriate for all cell lines. MEF conditioned medium works very well, but it is not defined, followed by mTeSR and TeSR-E8 medium (Stemcell technologies), which are defined but expensive.

To avoid overspending and killing of mice this study analyzed the use of human fetal femur mesenchymal stem cells (fMSCs) as an alternative for MEFs. Serveral studies showed the successful use of human cells as feeders to culture hESCs, e.g. human dermal fibroblasts, human amniotic epithelial cells or human adult bone marrow mesenchymal stem cells (Hovatta et al. [2003]; Cobo et al. [2008]; Lee et al. [2010]; Chen et al. [2013]; Mobarra et al. [2014]; Ghasemi-Dehkordi et al. [2015]).

First, hESCs and iPSCs were cultured on feeders (MEFs or fMSCs) with normal medium and 8 ng/ml FGF. The culture with MEFs was comparable to the culture method with fMSCs. Immunofluorescence-based antibody stainings of pluripotency associated proteins showed no significant difference between both versions (Figure 3.50; S9 - S11).
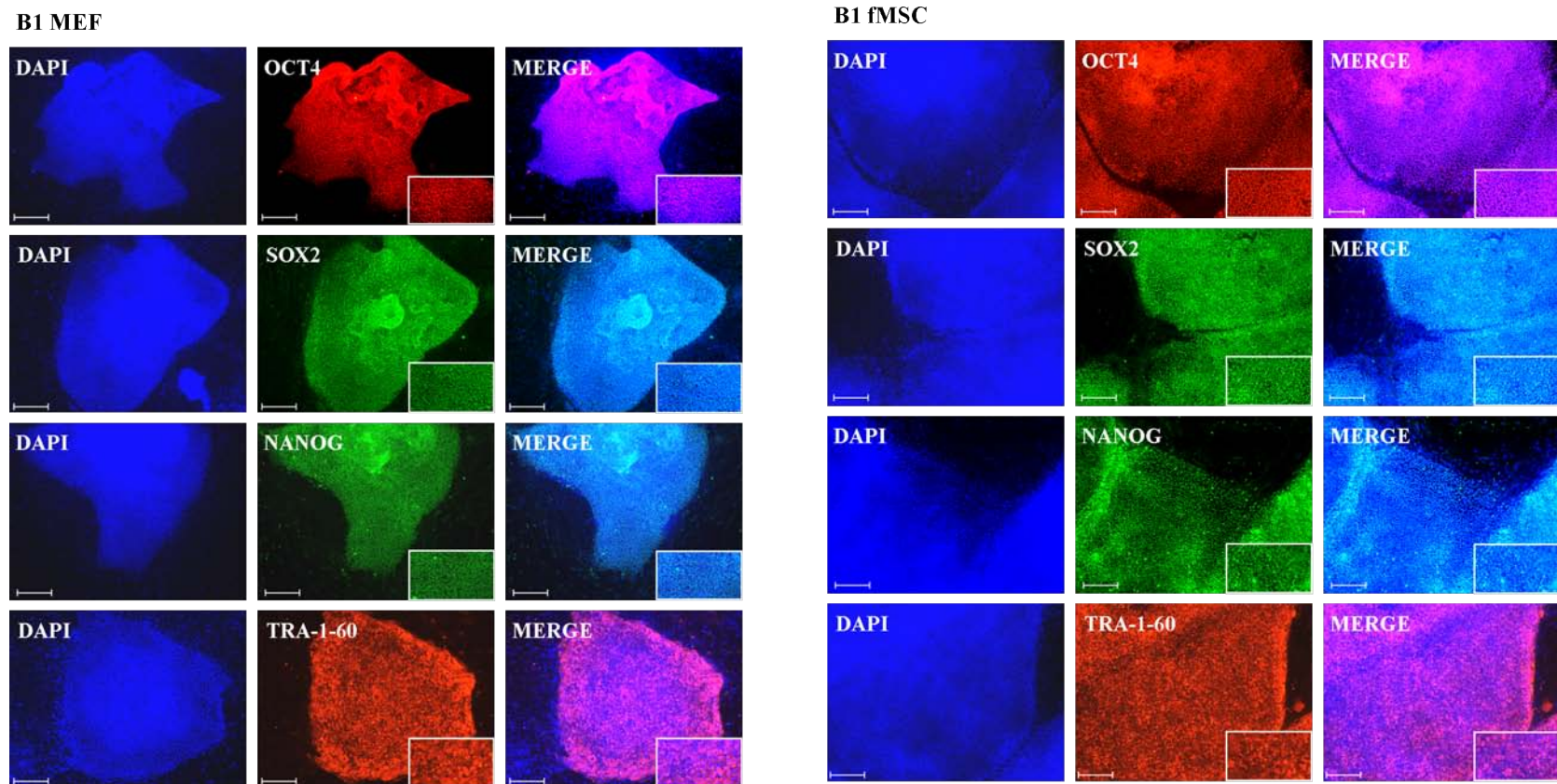
Figure 3.50: **Immunofluorescence-based detection of pluripotency markers in epiHFF1-iPS-B1.**
All protein stainings for pluripotency markers OCT4, SOX2, NANOG, and the surface marker TRA-1-60 were positive. The culture of epiHFF1-iPS-B1 on mouse embryonic fibroblasts (MEFs) is depicted on the left hand side and the culture of epiHFF1-iPS-B1 on human fetal mesenchymal stem cells (MEFs) is depicted on the right hand side. DAPI stained the nucleus. Scale bar: 200 μm, Alexa Flour 594 (red), Alexa Fluor 488 (green).

Second, conditioned medium was made from fMSCs as described for MEFs (see page 124). For both variations of CM (MEF-CM and fMSC-CM) an Activin A test was done to analyze how much and how stable Activin A was produced in each CM. The Activin A production from fMSCs were 1.7 fold higher than from MEFs and remained at a relative constant level (Figure 3.51). Before using the CM all days were mixed and the final concentration was measured. The concentration of Activin A in the CM made from fMSCs was 2.5 fold higher than in the CM made from MEFs (data not shown).

Third, hESCs and iPSCs were cultured on Matrigel with CM made from MEFs or fMSCs and with or without additional FGF (8 ng/ml). After four passages RNA was isolated and qRT-PCRs were done. Generally, no significant differences were found. In all conditions the cells kept their pluripotency. All cell lines expressed pluripotency associated genes such as *OCT4*, *SOX2*, *NANOG* and *GDF3* (Figure 3.52 and S12). Immunofluorescence-based detection of pluripotency associated proteins confirmed the qRT-PCR results (Figure 3.53, 3.54 and S13 - S16).
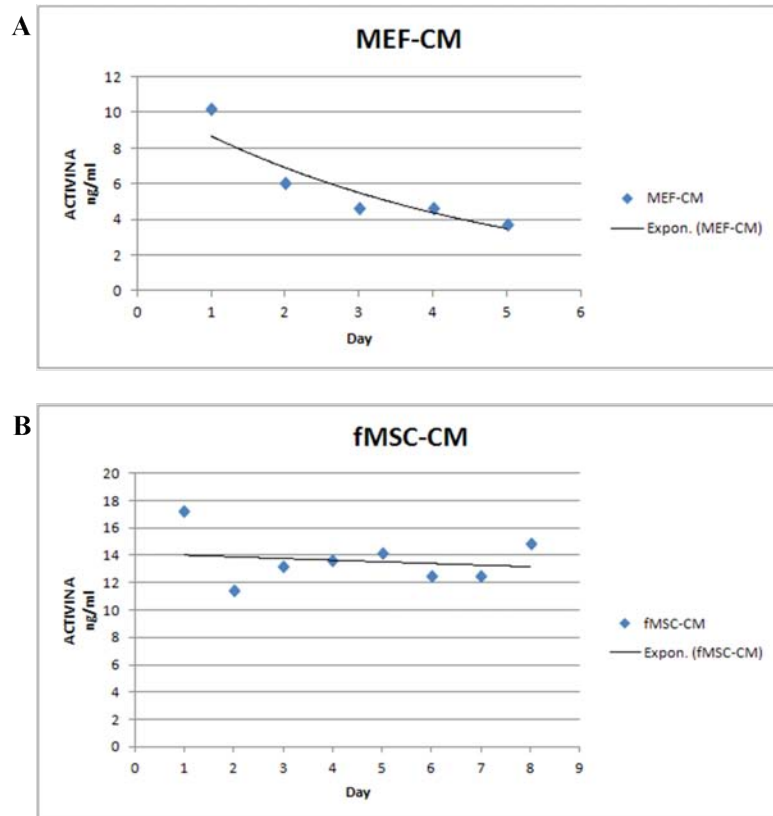
Figure 3.51: **Measurement of Activin A in CM made from MEFs and fMSCs.**
A) Analysis of Activin A production in conditioned medium (CM) made from MEFs. **B)** Analysis of Activin A production in CM made from fMSCs. Three biological replicates in technical triplicates of each sample were analyzed. The levels of Activin A are presented in ng/ml.
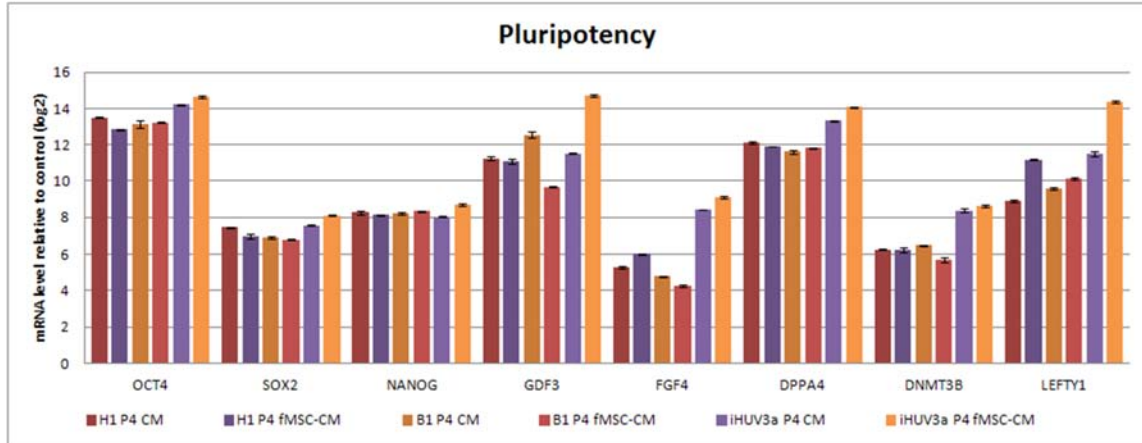
Figure 3.52: **Quantitative real-time PCR of pluripotency markers.**
Expression pattern of pluripotency markers relative to HFF1 from hESC-line H1, the iPSC-line epiHFF1-iPS-B1 and the iPSC-line epiHUV-iPS-3a are shown. The cells were cultured in conditioned medium (CM) made from mouse embryonic fibroblats (MEFs), which is the common used CM, and fetal mesenchymal stem cells (fMSCs) made CM (fMSC-CM). Three biological replicates in technical triplicates of each sample were analyzed against HFF1 as control. The standard deviation is depicted by the error bars.

B1 MEF-CM +FGF

B1 fMSC-CM +FGF
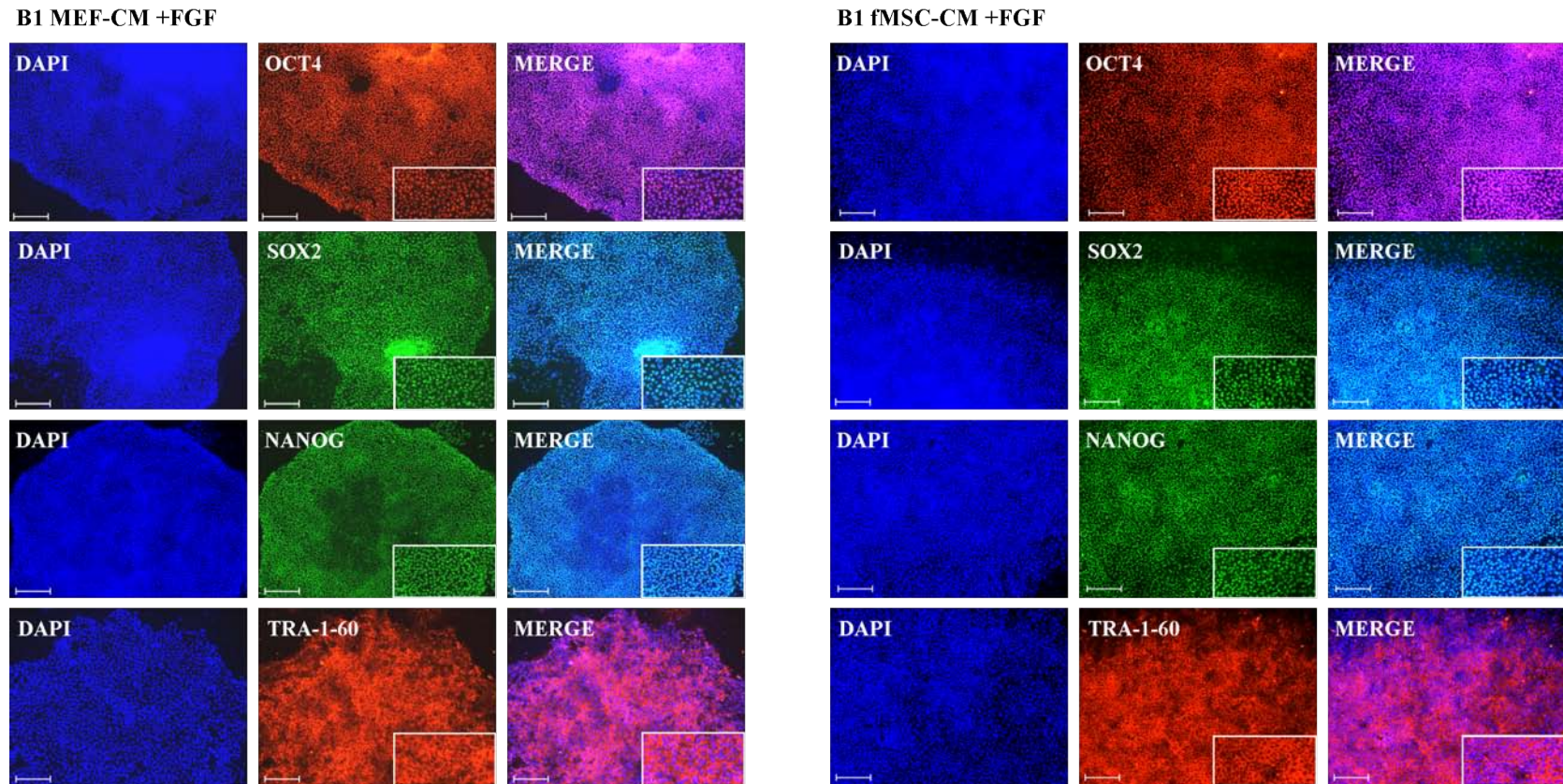
Figure 3.53: **Immunofluorescence-based detection of pluripotency markers in epiHFF1-iPS-B1.**
All protein stainings for pluripotency markers OCT4, SOX2, NANOG, and the surface marker TRA-1-60 were positive. The culture of epiHFF1-iPS-B1 on Matrigel with mouse embryonic fibroblasts (MEFs) made conditioned medium (CM) with additional FGF is depicted on the left hand side (B1 MEF-CM +FGF) and the culture of epiHFF1-iPS-B1 on Matrigel with human fetal mesenchymal stem cells (MEFs) made CM with additional FGF is depicted on the right hand side (B1 fMSC-CM +FGF). DAPI stained the nucleus. Scale bar: 200 μm, Alexa Flour 594 (red), Alexa Fluor 488 (green).

B1 MEF-CM -FGF

B1 fMSC-CM -FGF
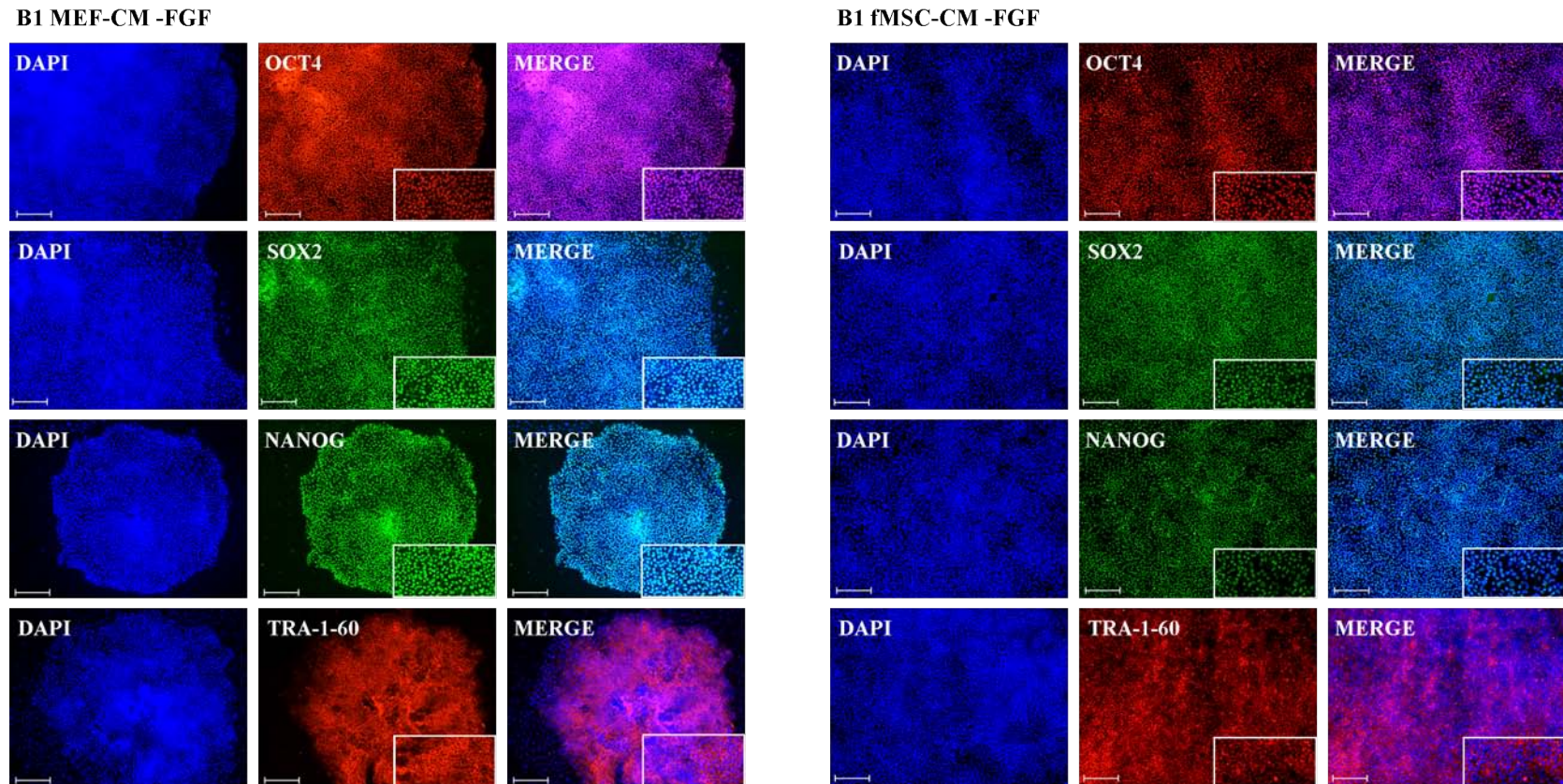
Figure 3.54: **Immunofluorescence-based detection of pluripotency markers in epiHFF1-iPS-B1.**
All protein stainings for pluripotency markers OCT4, SOX2, NANOG, and the surface marker TRA-1-60 were positive. The culture of epiHFF1-iPS-B1 on Matrigel with mouse embryonic fibroblasts (MEFs) made conditioned medium (CM) without additional FGF is depicted on the left hand side (B1 MEF-CM -FGF) and the culture of epiHFF1-iPS-B1 on Matrigel with human fetal mesenchymal stem cells (MEFs) made CM without additional FGF is depicted on the right hand side (B1 fMSC-CM -FGF). DAPI stained the nucleus. Scale bar: 200 μm, Alexa Flour 594 (red), Alexa Fluor 488 (green).

4 Discussion

4.1 Generation of iPSCs

Reprogramming of somatic cells is not a trivial task. Major roadblocks must be overcome. The cell identity that has been determined by previous cell fate decisions and subsequent epigenetic patterns that lock the cell identity in its current state have to be reset. Also pluripotency genes have to be activated and their expression maintained (Figure 4.1). Since 2006, when Takahashi and Yamanaka [2006] successfully reprogrammed somatic cells by ectopic expression of pluripotent transcription factors (TFs), several methods of reprogramming were published. The principle is the same, the methods are based on the ectopic expression of pluripotent TFs (Okita et al. [2008], Stadtfeld et al. [2008], Sridharan et al. [2009], Woltjen et al. [2009], Yu et al. [2009], Zhou et al. [2009], Plews et al. [2010], Sommer et al. [2010], Warren et al. [2010], Miyoshi et al. [2011], Nishimura et al. [2011]). The ectopically expressed TFs form complexes with co-regulatory factors, bind to specific DNA sequences across the genome and then modify transcriptional and epigenetic regulation. This results in changes of histone modifications at somatic genes, mesenchymal to epithelial transition (EMT) is initiated, as well as increased proliferation. Second, specific remodeling of chromatin causes the expression of genes in the pluripotency network to be activated and the expression of genes which promote differentiation to be suppressed. Third, the recruitment of diverse epigenetic enzymes supports the establishment of pluripotency-specific signal transduction, as well as transcriptional and epigenetic patterns. Fourth, the iPSCs are stabilized while the transgenes are silenced, the endogene core pluripotency circuit is activated, the epigenome is reset and the cytoskeleton is remodeled to an ESC-like state (Takahashi and Yamanaka [2006], Takahashi et al. [2007b], Zhao et al. [2011b], Buganim et al. [2012], Golipour et al. [2012], Hansson et al. [2012], Polo et al. [2012]).

The viral-approach is still the classic method of reprogramming human adult fibroblasts by over-expression of four transcription factors OCT4, SOX2, KLF4 and c-MYC (Yamanaka-Cocktail) or OCT4, SOX2, NANOG and LIN28 (Thomson-Cocktail) (Takahashi et al. [2007a]; Yu et al. [2007]). The efficiency amounts to 1 %. The integration of pro-viruses into genome of viral-derived iPSCs is a risk factor for clinical applications in the future. The major advantage of non-viral and non-integrating methods is the lack of integration into the genome of tranfected cells (Chen and Liu [2009]; Yu et al. [2009]). A very elegant method is the mRNA transfection. However, it is very inefficient and difficult to reproduce (Warren et al. [2010]; Tavernier et al. [2012]; Schlaeger et al. [2015]).
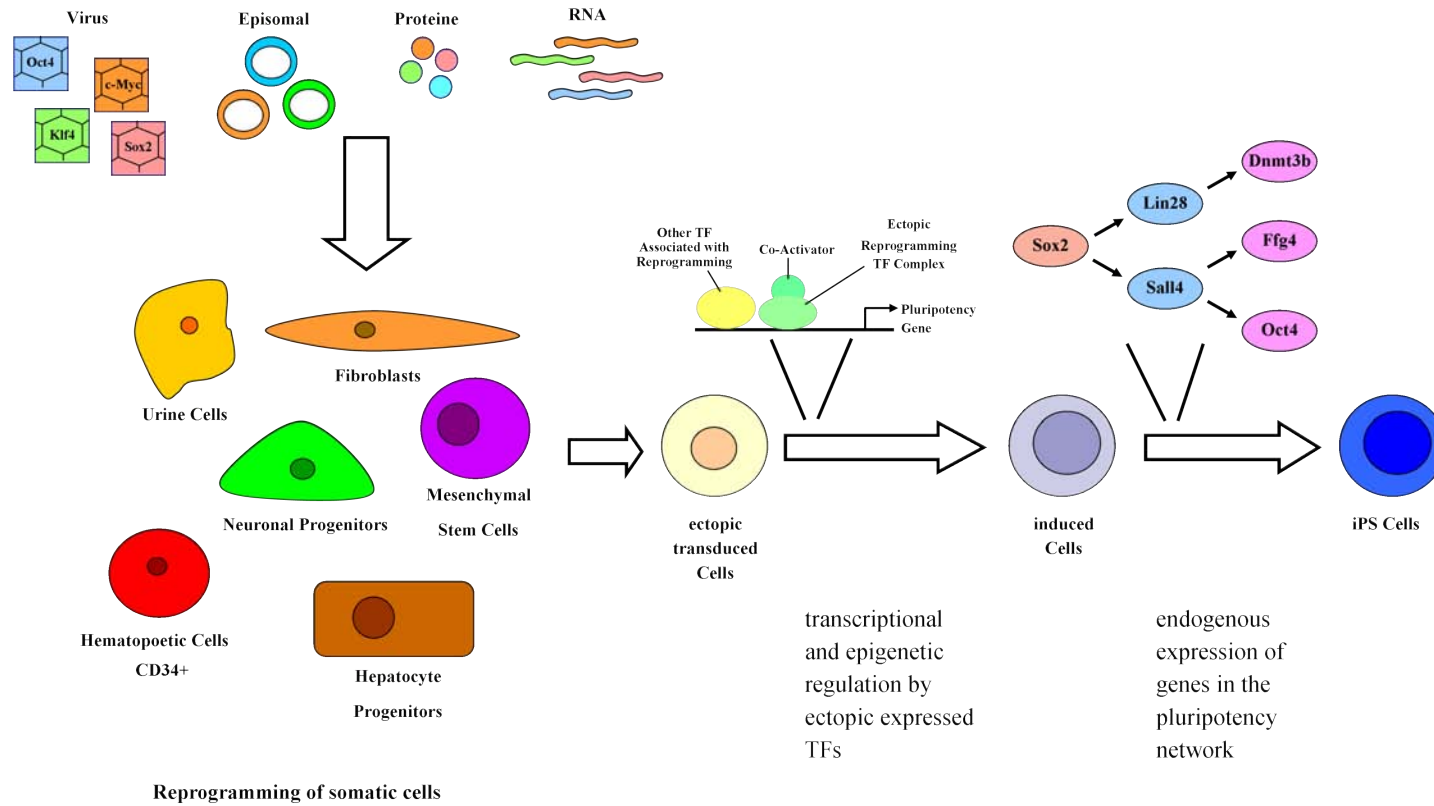
Figure 4.1: **Scheme of reprogramming process.**
The reprogramming of somatic cells can be done by different methods (vrial-, plasmid-, protein or RNA-based). The principle of the methods is the same, they based on the ectopic expression of pluripotent transcription factors (TFs). The ectopic expressed TFs form complexes with coregulatory factors and bind to specific DNA sequences across the genome and obtain transcriptional and epigenetic regulation. It is activated the endogenous expression of genes in the pluripotency network by specific remodeling of the chromatin. Additionally, the expression of genes which promote differentiation is suppressed. The iPSCs are stabilized while the transgenes are silenced, the endogene core pluripotency cycle is activated, the epigenome is reset and the cytoskeleton is remodeled to an ESC-like state (reviewed by Buganim et al. [2013] and Ma et al. [2013b]).

Hence, a non-viral, episomal-based approach described by Yu et al. [2009] was used in this study. The efficiency of this method to generate iPSCs ranges between 0.003 % and 0.006 % (Yu et al. [2009]). We improved it with human fetal fibroblasts (HFF1) cells, using the oriP/EBNA1 (Epstein-Barr nuclear antigen-1)-based episomal vectors which express reprogramming factors, with an efficiency of 0.03 %. Later on, we used human umbilical vein endothelial cells (HUVECs) with an efficiency of 2.5 %. This is an increase of more than 83 %. The retrovirus reprogramming of HUVECs results in an efficiency between 2.5 % and 3.0 % (Panopoulos et al. [2011]). The episomal-based reprogramming is able to generate an efficiency comparable to the viral-approach using HUVECs. Additionally, the efficiency of reprogramming HUVECs was much higher compared to the HFF1 reprogramming. After three weeks iPSC colonies from HUVEC reprogramming were available. Using HFF1 cells for reprogramming took four months to generate iPSCs. There are several other factors which influence the reprogramming efficiency, e.g. the age of the donor cells itself and the passage number of *in vitro* culture, the ability to undergo replication and cell cycle status, the variability in factor reactivation, and other stochastic events. (Aasen et al. [2008]; Maherali et al. [2008]; Ho et al. [2010]; Lagarkova et al. [2010]; Schlaeger et al. [2015]). One major explanation of the higher and faster reprogramming efficiency could provide the mesenchymal to epithelial transition (MET) process. The induction of pluripotency is favoured by the change of MET development. It is evident that reprogramming using epithelial cells such as keratinocytes or in this case HUVECs results in an increased efficiency as compared with dermal fibroblasts (e.g. HFF1) or MSCs which are of mesenchymal origin (Yang and Weinberg [2008]; Wang et al. [2010]). Another advantage over HFF1 cells is the expression of decay-accelerating factor (DAF) in HUVECs. DAF is a membrane protein which protects the cells from own complement-mediated injury, DNA damage and karyotype changes. It is expressed in endothelium, epithilium and hematopoetic cells. HUVECs own the highest DAF expression of all human cells that have been studied (Asch et al. [1986]; Bryant et al. [1990]; Tsuji et al. [1994]; Mason et al. [2002]; Lagarkova et al. [2010]).

The episomal-derived iPSCs (E-iPSCs) from both cell types were fully characterized and are comparable to human embryonic stem cells (hESCs). During the culture of the iPSCs all have completely lost the episomal vectors after 12 passages and no integration was detectable. The E-iPSC lines express pluripotency markers such as *OCT4*, *NANOG* and *SOX2* also the surface marker proteins SSEA-4, TRA-l-60, TRA-1-81 and TRA-2-49 but not SSEA-1. Additionally, they have the ability to differentiate to cell types of the three germ layers endoderm, ectoderm and mesoderm *in vitro* (by formation of embryoid bodies) and *in vivo* (by formation of teratoma in immunodeficient mice).

The teratoma assay is part of the "golden standard" to characterize iPSCs. Nowadays, teratoma assay should no longer used for basic characterization of iPSCs. There are too many drawbacks. The most important teratoma counter-argument is the procedure by itself. iPSC are transplanted into minimum one immunodeficient mouse to form spontaneously a teratoma which should include tissue from all three germ layers. Then, the mouse will be killed and the teratoma will be analyzed (Okita et al. [2007]). Usually,

more than one mouse will used for one iPSC line. Our laboratory made the experience that the assay do not always works and it is more or less by chance that tissues of all three germ layers are included in one teratoma. That is because during the teratoma formation the iPSCs differentiate spontaneously. It is no direct differentiation to one or the other germ layer tissue. This procedure is comparable to the embryoid body (EB) formation with the difference that EB formation happen in a dish and can be repeat as often as necessary. The EB assay is not only low priced, it is done much faster and mice are not needed. Surprisingly, it is still existing a strong market for teratoma assay. Once again, this year a protocol for teratoma assay was published (Nelakanti et al. [2015]). In this age alternatives should be used to perform the basic characterization of iPSCs. On the one hand, to show by EB assay *in vitro* the ability to differentiate in all three germ layers of a new iPSC line should be sufficient. On the other hand, direct differentiation assays for tissues of all three germ layers could be performed *in vitro* and gene expression transcriptome profile-based analysis can be conducted. Since 2011, a robust open access bioinformatic assay of pluripotency in human cells is available and called PluriTest (Mller et al. [2011]). With this tool the gene expression pattern of the new iPSC line will be compared to the expression profile of several hundreds hESC and iPSC lines from multiple laboratories all over the world. With the microarray data set the PluriTest requires as less as 10 minutes to validate the pluripotency of the cell line. We have performed the PluriTest with two iPSC lines and differentiated iPSC line to definitive endoderm (DE), which is the first step of hepatocyte differentiation (Figure 4.2). As the other performed assays this tool confirms the pluripotency of the iPSC lines and declares the DE sample as not-pluripotent as it should. To conclude, for basic characterization it is no longer necessary to perform a teratoma assay. In the future our laboratory will pass on teratoma assay to verify pluripotency.

The episomal reprogramming approach holds a high aneuploidy rate of 11.5 % and ranks on the second position when compared to other reprogramming methods. Only retroviral reprogramming approach holds a higher aneuploidy rate of 13.5 % (Schlaeger et al. [2015]). The HFF1-derived E-iPSC line we used for this study contains additional material on Chromosom 12 at the short arm 12p. This is a hot spot of gain. The hallmark pluripotency genes *NANOG* and *GDF3* are located there and are over expressed (NANOG 3.32-fold and GDF3 1.29-fold) compared to hESCs as demonstrated by quantitative real-time PCR (qRT-PCR) and transcriptome analysis (Figure 2.5; 2.6 and 3.3). This aberration does not exist in the somatic cells (HFF1). Presumably, this is a result of the selective force during the reprogramming procedure and culture adaption (Mayshar et al. [2010]; Prigione et al. [2010]). In this sector the reprogramming of HUVECs also performed better. The HUVEC-derived E-iPSC line holds a normal karyotype as the original cell line and expresses pluripotency-associated genes as hESCs shown by qRT-PCR (Figure 3.10 and 3.11).
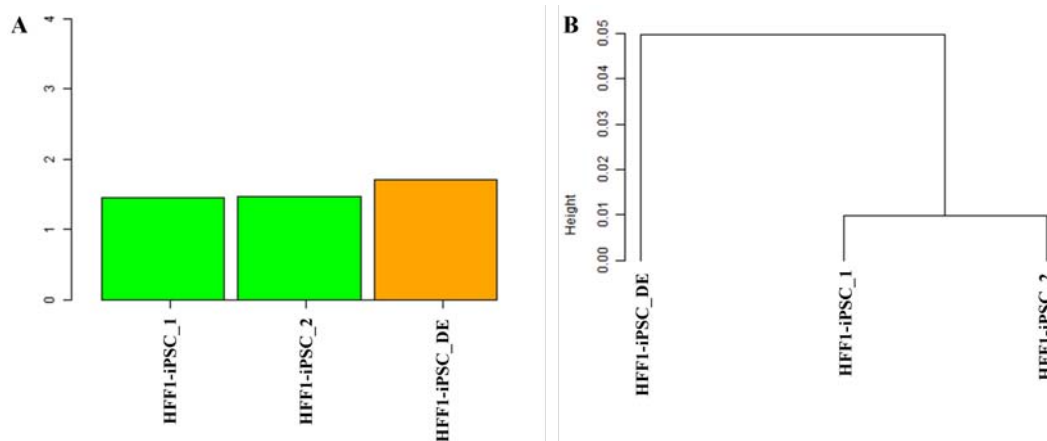
Figure 4.2: **PluriTest.**
Comparable analysis of pluripotency in new human iPSC lines and one differentiated iPSC line to definitive endoderm (DE). **A)** Novelty Score. Green colored samples are pluripotent. The orange colored sample HFF1-iPSC-DE is not-pluripotent, it is more dissimilar to the pluripotent samples in the model matrix than the other pluripotent samples. *B)* Hierarchical Clustering. The pluripotent samples HFF1-iPSC-1 and HFF1-iPSC-2 cluster together. HFF1-iPSC-DE differs from the pluripotent samples and do not cluster with them (Mller et al. [2011], http://www.scopus.com/inward/record.url?eid=2-s2.0-79953267538&partnerID=40&md5=7108a16c223225f3d2443f06cbba4ace, retrieved 08.04.2015).

In order to analyze the difference and commonalities between the iPSCs and compared to hESCs microarray-based analyses of the transcriptome profiles were performed. The transcriptome profile of the HUVEC-iPSC line is similar to that of hESCs and the HFF1-iPSC line. The transcriptome profile differences between the HUVEC-iPSC line and HFF1-iPSC line are minimal (Figure 3.15).

In general, the derivation of integration free iPSCs from somatic cells and differentiating them into a donor cell type of interest are promising approaches for (i) future application in tissue replacement therapies, (ii) generation of disease models *in vitro*, (iii) toxicology and drug screening.

However, episomal-based reprogramming will never become the "golden standard" of reprogramming. For that the reprogramming efficiency is too low and an element of risk remains that foreign particles could integrate into the host genome (Schlaeger et al. [2015]). The future belongs to methods which using human mRNA or small molecules for reprogramming somatic cells. The main advantage to other methods is that they avoid using foreign particles which could potentially integrate into the host genome and provoke gene mutation. These methods will be used for clinical approaches (Bernal [2013]; Yoshioka et al. [2013]). Reprogramming of human somatic cells with small molecules has not been developed yet, but it is merely a matter of time. Over the past years, the method using mRNA to reprogram human somatic cells has further developed. More and more companies sale mRNA-based reprogramming kits (e.g. Miltenyi Biotec, amsbio, Lonza, Stemgent, Mandal and Rossi [2013]). In the early stages it was necessary to

conduct the RNA transfection 10 times. Though, it seemed that this protocol was not reproducible. Among other laboratories ours was not able to reproduce this protocol. One explanation could be that the cytotoxicity of mRNA transfected cells is very high by trigger a strong innate immune reaction. Due to that after ten transfections almost all cells were dead. Today, the number of mRNA days has not decreased rather increased. However, the mRNA was modified so that the RNA do not trigger an immune reaction (Warren et al. [2010], Drews et al. [2012], Tavernier et al. [2012], Mandal and Rossi [2013]). Due to the fact that more and more mRNA-based iPSC lines were published and companies offer mRNA reprogramming kits it seems to be reproducable. The future step in our laboratory will be to establish a competitive mRNA-based method for reprogramming human somatic cells and further analyze the power of small molecules to reprogram human somatic cells on their own.

4.2 Generation of Hepatocyte-like cells from E-iPSCs

Hepatogenesis is best understood in mice and rats (Houssaint [1980]; Medlock and Haar [1983]; Cascio and Zaret [1991]; Watt et al. [2001]; Tremblay and Zaret [2005]; Zhao and Duncan [2005]; Watt et al. [2007]). The liver is able to regenerate itself *in vivo*. However, *in vitro* the cells lose this ability and several experiments were conducted to activate the ability for regeneration *in vitro*. It is not possible to culture human hepatocytes *in vitro* highlighting the liver as a complex structure (Mitaka [1998]; Runge et al. [2000]; Mizuguchi et al. [2001]; Zhao and Duncan [2005]; Shan et al. [2013]; Chapter 1).

One million patients die each year from acute and chronic liver diseases worldwide. The orthotopic liver transplantation (OLT) is still the only effective cure for end-stage liver patients and many genetic disorders (Girometti et al. [2014]; Chapter 1).

This gives an impression how important the research of alternatives is. The derivation of integration free iPSCs from somatic cells and differentiating them into liver cells is a promising approach for (i) future application in tissue replacement therapies, (ii) generation of disease models *in vitro*, (iii) toxicology and drug screening.

In the past, our lab differentiated hESCs and viral reprogrammed iPSC lines to hepatocyte-like cells (HLCs) (Jozefczuk et al. [2011]; Jozefczuk et al. [2012b]). In this study viral- and integration-free episomal-based iPSCs (E-iPSCs) from human neonatal foreskin fibroblast (HFF1) cells and human umbilical vein endothelial cells (HUVECs) could differentiate to HLCs (Chapter 3.2). The differentiation procedure consist of three stages (Figure 3.16 and 3.28). First, the undifferentiated cells were differentiated to the defnitive endoderm (DE), second, to the hepatic endoderm (HE) stage and third, to hepatocyte-like cells. Continued changes of the morphology from undifferentiated stage to HLCs were observed as discribed by Jozefczuk et al. [2011]. Immunofluorescence-based protein stainings and qRT-PCRs confirmed the stages of differentiation from each step. All in all both lines differentiate similar (Figure 3.17 - 3.19 and 3.29 - 3.31). Both stored glycogen and showed the uptake and release of ICG and CDFDA (Figure 3.22

and 3.33). They secrete bile acid and urea in a similar level (Figure 4.3). Both cell lines are able to differentiate into HLCs. They can be used for drug screenings and toxicology studies.
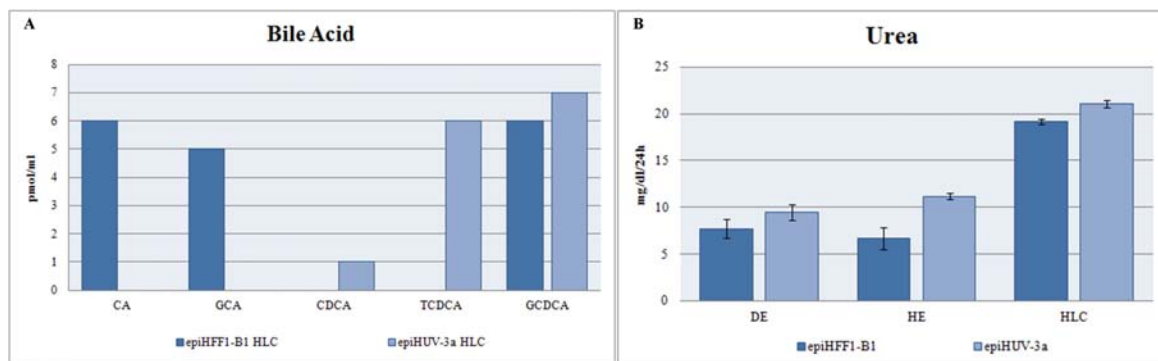
Figure 4.3: **Measurement of secretion levels in HLCs.**
A) Analysis of bile acid production in epiHUV-3a-HLC and epiHFF1-B1-HLC. The levels of bile acids are presented in pmol/ml/24h. **B)** Analysis of urea production in epiHUV-3a-HLC and epiHFF1-B1-HLC during differentiation from definitive endoderm (DE), hepatic endoderm (HE) and hepatocyte-like cells (HLCs). Three biological replicates in technical triplicates of each sample were analyzed. The levels of urea was measured in mg/dl/24h.

In order to analyze the difference and commonalities between the generated HLCs and compared to the transcriptome profile of fetal liver and PHH microarray-based anaylses were performed. The transcriptome profiles of both iPSC-derived HLC lines are comparable. Most liver-related genes are expressed in both samples. The expression of endoderm progenitor-related genes indicates that these HLCs are immature. The comparative transcriptome profile analysis to fetal liver and PHH confirmed the indication of immaturity of the HLCs (Figure 3.40).

However, the used protocol has to be optimized to generate mature HLCs. In order to achieve the maturation small molecules treatment could be used or 3D culture systems could be the right direction. There are a lot of 3D cell culture systems based on an external scaffold, which can allow the formation of 3D structures in hepatocyte cultures. Another approach is the liver bud formation without any scaffold (Godoy et al. [2013], Shan et al. [2013], Takebe et al. [2014]). The idea of liver bud formation is that mimic functional liver *in vitro* due to the fact that a liver *in vivo* do not only consists of hepatocytes. Hepatocytes are arranged in so called hepatic plates separated by sinusoid spaces. These hepatic plates are arranged star-like around a central vein. The bile canaliculi on the surface of adjoining hepatocytes drain bile into the bile ducts, which run parallel to portal veins and hepatic arteries to form the "portal triad" (Shiojiri [1984]; Duncan [2000]; Lemaigre [2003]; Malarkey et al. [2005]; Godoy et al. [2013]). The formation of a 3D liver bud depends on the interaction of signals between endodermal epithelial, mesenchymal and endothelial progenitors. For that Takebe et al. [2014] used

HUVECs as the endodermal epithelial, MSCs as mesenchymal epithelial and iPSC-derived hepatic endoderm (HE) cells. We tried to reproduce this publication but without success (data not shown). There seem to be too many stumbling blocks at the moment. In the future we want to focus on the use of small molecules. Shan et al. [2013] published a small molecule which activates the proliferation and one which induces the maturation of hepatocytes. Additionally, an experiment done by a colleague indicates that definitive endoderm (DE), the first step of HLC differentiation, can be achieved by the use of one small molecule. This year Siller et al. [2015] published the successful differentiation of iPSCs into HLCs by the use of small molecules. However, at this stage the HLCs are comparable with cytokine-derived HLCs. That means they are immature as any other generated HLC line. Using this protocol and further using the small molecules published by Shan et al. [2013] could generate more mature HLCs comparable with PHH. All together hold great promise that it will be possible to generate mature hepatocytes. Another way to generate HLCs is the direct use of fibroblasts and manipulate them by transfection with lentiviruses or synthetic modified RNA (Huang et al. [2014], Simeonov and Uppal [2014]). The direct generation of HLCs from fibroblasts is much faster, low-priced and more directed compared to the common procedure of iPSC derivation from fibroblasts and then differentiate them into HLCs. It should be possible to find the right cocktail of small molecules to derive directly HLCs from somatic cells. We want to focus on this issue in the future.

HFF1-iPSC-derived HLCs were used to analyze the human hepatogenesis in details and untangle human hepatogenesis-associated gene regulatory networks (Chapter 3.2.1). We demonstrated the potential of using E-iPSCs as *in vitro* models for studying liver cell fate decision making (Figure 3.23 - 3.27). One of the important pathway for hepatogenesis is the Hippo-signaling pathway which influences liver cell fate and size. Additionally, the Hippo pathway is responsible for maturation and stabilization of the tight junctions in hepatocytes. This pathway is over represented in HLCs, fetal liver and PHH. The existence of tight junctions in E-iPSC-derived HLCs is shown by electron microscopy. ABC transporters are also over represented in HLCs, fetal liver and PHH. These are accountable for the uptake and efflux of e.g. bile acids. A measurement assay for bile acid secretion shows that the HLCs excrete primary bile acids. Primary bile acids are involved in drug metabolism and synthesis of cholesterol, steroids and other lipids. Hepatocytes synthesize primary bile acids which then carried out by the gut microbiota convert to secondary bile acids by several reactions including dehydroxylation, dehydrogenation and epimerization (Camargo et al. [2007], Varelas et al. [2010], Hofmann and Hagey [2014], Lamba et al. [2014], Yimlamai et al. [2014]). A heatmap of bile acid related transporter genes underlines the functionality of the HLCs and shows the highest expression of NTCP, MRP2, ASBT and MDR2/3 in the HLC samples (Figure 3.25G).

The heatmap presented in Figure 3.27B implies that the HLCs also harbor cell populations with bipotential properties similar to hepatoblasts. It is shown differential expression of key cell fate regulating genes specific to the hepatic endoderm and in some cases also in the HLCs. For example, the hepatic endoderm cells (HE) express exclusively *DLK2* and a set of transcription factors specific to this stage (*Onecut1/HNF-6*). These set of transcription factors are putative candidates for directing biliary epithe-

lial cells/cholangiocytes cell fate. However, HLCs express *DLK1* and progenitor-related genes such as *PROX1* and *LGR5* which are not expressed in HEs. Though, in both stages are expressed genes such as *WNT3A*, *NOTCH3*, *HNF1A*, *HNF1B* and *SOX9*. Our overall findings based on gene expression patterns supports the perception that HE and HLCs in our hepatocyte differentiation protocol are equivalent to the DLK, HNF6 and SOX9-positive bipotential hepatoblasts present in fetal liver and are common progenitors for hepatocytes and biliary epithelial cells/cholangiocytes. The Notch signaling, hepatocyte nuclear factor-6 (HNF-6) and PROX1 are factors known to regulate lineage commitment in the bipotential hepatoblast progenitor cell population (Clotman et al. [2002], Tanimizu et al. [2003], Dudas et al. [2004], Vanderpool et al. [2012]). This implicates that it should be possible to change the fate of HE cells by manipulating the expression levels of e.g. *PROX1*, *SOX9*, and *HNF6* or even by using small molecules targeting for instance Notch signaling. Odom et al. [2006] used human hepatocytes from donors and compared these with healthy hepatocytes. They described a core transcriptional regulatory circle in human hepatocytes consisting of six transcription factors (ONECUT1/HNF-6, FOXA2, HNF1A, HNF4A, CREB1 and USF1). These transcription factors bound promoters that are central for liver development and function (Odom et al. [2006]). Our study shows the expression of the transcription factors *ONECUT1/HNF-6*, *FOXA2*, *HNF1A* and *HNF4A* in human E-iPSC-derived HLCs. Furthermore, we have demonstrated that transcription factors *HNF1A* and *HNF4A* are involved in orchestrating cell fate decision of bipotential hepatoblast cells to become either hepatocytes or biliary epithelial cells/cholangiocytes (Figure 3.27C).

The generation of a transcription factor network via the oPOSSUM data base uncovered transcription factors which are involved in cell fate decisions during hepatogenesis (Figure 3.27C, Supplementary Table S9). MYC regulates numerous biological processes such as glycolysis, cell proliferation and differentiation and is the most prominent transcription factor in our network. It also regulates the expression of bipotential hepatoblast-related genes (e.g. *DLK1*, *PROX1*), cholangicyte-related genes (e.g. *ONECUT1*, *WNT3A* and *SALL4*) as well as hepatocyte-related genes (e.g. *HNF1A*). The second prominent transcription factor is HNF4A which is a central regulator of hepatocyte differentiation and function. HNF4A regulates hepatocyte-related genes (e.g. *ALB*, *AFP*), cholangiocyte-related genes (e.g. *ONECUT1*, *SALL4*) as well as the hepatoblast-related gene *PROX1* (Watt et al. [2003], Hay et al. [2008b], Cai et al. [2013], Dianat et al. [2014], Seth et al. [2014], Qu et al. [2014]). This transcription network underlines the bipotential progenitor-related characteristics of the HE and HLC stage in our differentiation procedure. This implies that there are bipotential progenitors within HE and HLC cell populations.

In summary, K-means clustering identified 100 clusters including developmental stage-specific groups of genes, e.g. OCT4 expression at undifferentiated stage, SOX17 marking the DE stage, DLK and HNF6 the HE stage, HNF4A and Albumin is specific to HLCs, fetal liver and adult liver (PHH) stage gain an insight into hepatogenesis. Gene regulatory networks generated by oPOSSUM data base uncovered the presence of bipotential progenitor populations in both stages in HE and HLC. This analysis should lay the foundation for future efforts to generate long-term cultivable cholangiocytes and HLCs.

4.3 Generation of endodermal progenitors

The detection of progenitor cells uncovers information about the developmental process of somatic cells and organs. Especially, the liver has a unique regenerative capacities. After injury the proliferation becomes activated and the liver is able to regenerate. Remarkably, the liver is able to regenerate itself *in vivo*. If up to two thirds are removed, the cells start to proliferate immediately and the lost cell mass will be replaced. *In vitro* the cells lose this ability and serveral experiments were conducted to activate the ability for regeneration *in vitro* (Mitaka [1998]; Runge et al. [2000]; Mizuguchi et al. [2001]; Zhao and Duncan [2005]; Shan et al. [2013]; Chapter 1). This mechanism highlights the role of adult liver stem cells. In recent years, stem and progenitor cells in liver development and their cellular niche were identified. However, most studies concentrate on the biliary tree and hepatoblast which can give rise to hepatocytes, cholangiocytes and pancreatic cells (Cardinale et al. [2011], Carpino et al. [2012], Goldman et al. [2013], Nissim et al. [2014]).

Using the protocol described by Cheng et al. [2012] in this study multipotent endodermal progenitors (EPs) were derived (Chapter 3.3). Whose capability are more comprehensive than that of cells from hepatoblast or biliary tree. The protocol describes three steps to generate EPs. Pluripotent stem cells are differentiate in 5 days to definitive endoderm (DE), than to transient cells (TC) which takes 4 weeks and further to EPs within one passage. In this study the E-iPSC line epiHFF1-iPS-B1 was used. The protocol was slightly modified and separated into four steps (Figure 3.41). The first step, differentiate E-iPSC to DE was the same as described for HLC differentiation and EP derivation. The second step, differentiating DE to TC was done in 4 weeks as described by Cheng et al. [2012] and was shortened to 2 and 3 weeks, too. The first passage in EP maintenance medium is called here pre-EP stage. When organoids were formed the fourth stage, the EP, was accomplished. All versions resulted in organoids. These organoids are multipotent progenitors due to the fact that they express lineage-specific markers at the same time point detected by qRT-PCR and immunoflurorescence-based stainings (Figure 3.46 and 4.4).
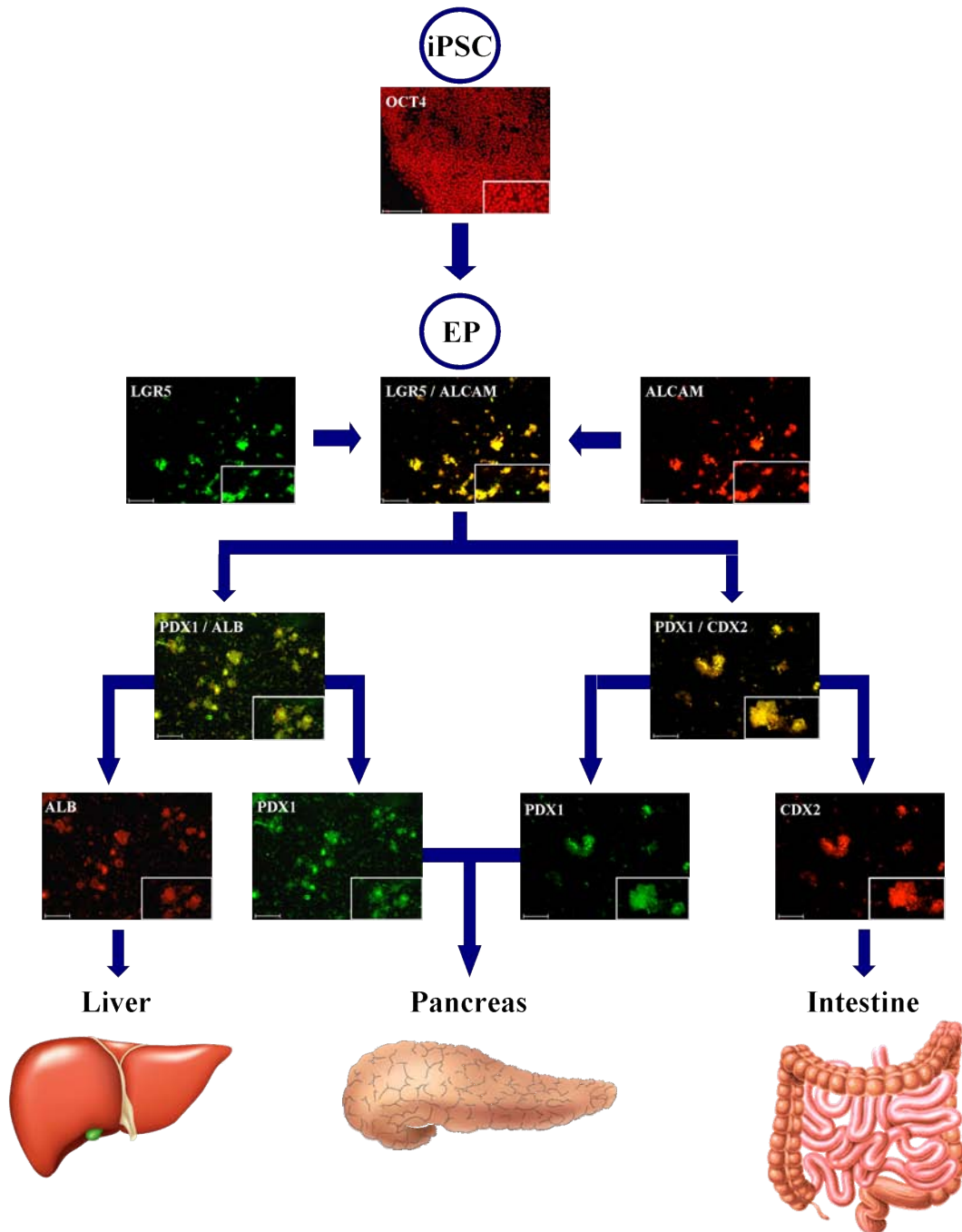
Figure 4.4:

Summary of EP generation derived from epiHFF1-iPS-B1.

A multipotent endodermal progenitor (EP) cell line was generated and characterized. The cells express at the same time LGR5 and ALCAM, liver-specific (ALB) and pancreas-specific (PDX1) marker, as well as intestine-specific marker (CDX2). DAPI stained the nucleus. Scale bar: 200 μm, Alexa Flour 594 (red), Alexa Flour 488 (green).

EPs express transcription factors related to early liver (*TBX3*), pancreas (*ISL1*, *RFX6*), lung (*FOXP2*) and specific protein marker for liver (*ALB*), pancreas (*PDX1*), intestine marker (*CDX2*), intestine- and lung (*SOX2*) as well as primitive streak-/ endoderm-specific genes such as *CER1*, *MIXL1*, *EOMES*, *FOXA2*, *HNF4α*, *GATA6*. Definitive endoderm and primitive streak related genes were expressed most in DE and pre-EP samples. Transcription factors related to early liver (*TBX3*), pancreas (*ISL1*, *RFX6*), lung (*FOXP2*) as well as *ID2* and *MEIS2* were overexpressed in EP. The heat map of progenitor related genes identified the EP as a panendoderm progenitor. A qRT-PCR uncovered primitive streak associated genes, such as *CER1*, *MIXL1* and *EOMES*, were exclusively expressed at the definitive endoderm (DE) stage. However DE specific genes, e.g. *GATA6* and *FOXA2* were also expressed in the transient cells (TC) and pre-endodermal progenitor cells (pre-EP). Lineage specific genes such as *GATA6* (DE), *TBX3* (early liver), *ALB* (mature liver), *CDX2* (pancreas) as well as *LGR5* (self-renew) are most expressed in the endoderm progenitor (EP). Immunofluorescence-based protein detection revealed that EPs express ALB as a marker for liver, PDX1 (Pancreas) and CDX2 (intestinal). Additionally, they express SOX2, which is also a marker for neuronal progenitors, and the self-renew marker LGR5 as well as the progenitor marker CD133 (Cheng et al. [2012]; Hannan et al. [2013]; Amador-Arjona et al. [2015]; Niu et al. [2015]). This indicate that these progenitors could be able to differentiate into neurons or other cell types.

The transcriptome profile analyses could not confirm all of results of immunofluorescence-based protein detection and qRT-PCR analysis due to the fact that the samples of defined EPs have not hybridized correctly. At the moment we are waiting for the results of the re-hybridized EP probes. Then the transcriptome profile of the defined EPs as well as the developmental stages of EP generation as to be analyzed in detail.

Studies are planned involving the use of the E-iPSCs derived endodermal progenitors to generate hepatocyte-like cells and pancreatic-like cells. These studies will enable uncovering the genes and associated pathways that specify a bipotential endodermal progenitor to differentiate to either liver or pancreas. In order to investigate whether or not the EPs will shift their identity when cultured in hepatocyte maintenance medium the EPs were cultured in hepatocyte maintenance medium for 4 passages. Immunofluorescence-based protein staining was done to detect LGR5, PDX1, ALB, CDX2 (Figure 4.5). The expression of CDX2 and PDX1 was decreased. However, LGR5 and ALB expression has not changed. This is a first indicator for the ability of EP differentiation. The next steps will be to culture the EPs in pancreas and hepatocyte maintenance medium in parallel. To identify and analyze the changes of the expression pattern qRT-PCR and transcriptome analysis will be performed. Furthermore, it should be thought about experiments which differentiate the EPs to lung, intestine and neuronal cells.
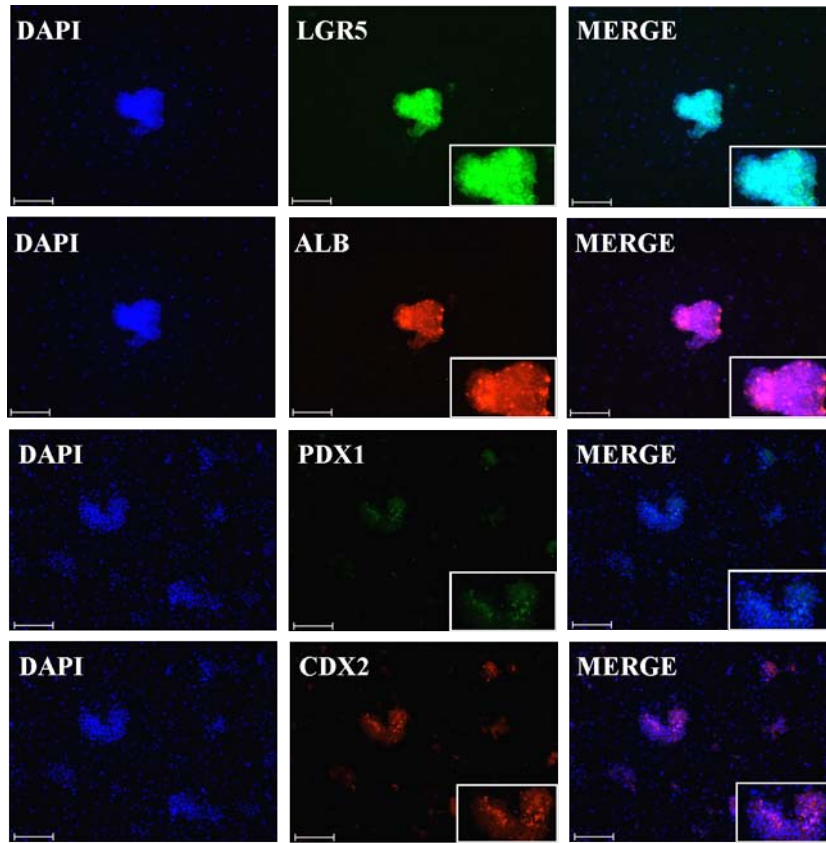
Figure 4.5: **Immunofluorescence-based detection of proteins in EP cultured in hepatocyte medium.**
Endodermal progenitor (EP) colonies were cultured in a comercial hepatocyte maintenance medium for 18 days. The detection of the protein LGR5 (self-renewal marker), PDX1 (pancreas marker), ALBUMIN (liver marker), CDX2 (hindgut marker). DAPI stained the nucleus. Scale bar: 200 μm, Alexa Flour 594 (red), Alexa Flour 488 (green).

4.4 Mouse embryonic fibroblasts replaced by human fetal mesenchymal stem cells

Today, it is still a common method to use mouse embryonic fibroblasts (MEFs) and/or MEF conditioned medium (MEF-CM) to culture human embryonic stem cells (hESCs) and induced pluriotent stem cells (iPSCs) (Jozefczuk et al. [2012a]; Kim et al. [2015]; Matz et al. [2015] under review; McKee et al. [2015]). To avoid overspending and killing of mice this study analyzed the use of human fetal femur mesenchymal stem cells (fMSCs) as an alternative for MEFs (Chapter 3.4). All cell lines (hESC and iPSC) which were cultured on fMSC or in fMSC-CM maintained their pluripotent stage comparable to these cultured with MEFs or MEF-CM. Additionally, they were all able to differentiate in cell types of all three germ layers (Figure 3.52 - 3.54 and Supplementary Figure S12 - S16).

118

The use of human fMSCs has a higher potential then only utilized for hESC and iPSC cultivation. In order to detect whether or not other cytokines are secreted by fMSCs a cytokine array was conducted by a colleague. Amongst others fMSCs secrete FGF2, FGF19, VEGF, PDGF-AA and IL-11, which are involved in proliferation processes (Wu et al. [2010]; Greber et al. [2007]; Cheng et al. [2012]; Lin et al. [2012]; Peterson et al. [2013]; Yu et al. [2013]; Chen et al. [2015]; Kiso et al. [2015]; Nguyen et al. [2015]). Fibroblast growth factor 2 (FGF2) modulates the activity of TGFβ superfamily members and is one of the most critical factors for EP cell maintenance (Greber et al. [2007]; Cheng et al. [2012]; Kiso et al. [2015]). FGF19 activates liver FGF receptor 4 (FGFR4) which is the signal for enterohepatic regulation of bile acid metabolism and the activation of liver FGFR4 is responsible for the enhanced hepatocyte proliferation (Wu et al. [2010]). The vascular endothelial growth factor (VEGF) is involved in activation of hepatocytes proliferation during liver regeneration, is important for endodermal progenitor (EP) proliferation and maintenance. Additionally, VEGF is an important target gene of the transcription factor hypoxia-inducible factor 1 (HIF1α/HIF1β) (Cheng et al. [2012]; Lin et al. [2012]; Yu et al. [2013]). Platelet-derived growth factor-AA (PDGF-AA) together with FGF2 have an synergistic effect on cell proliferation *in vitro* (Kiso et al. [2015]). Interleukin 11 (IL-11) is involved in intestinal proliferation and maintenance of intestinal homeostasis (Peterson et al. [2013]; Nguyen et al. [2015]). The secretion of FGF2, FGF19 and VEGF leads to the assumption that fMSCs could support the differentiation of iPSCs to HLCs and further give rise to HLC maturation. Additionally, the fMSCs provide the maintenance and proliferation of EPs. With a medium change fMSC secreted factors as IL-11 could differentiate the EPs into intestinal cells and maintain them.

Furthermore, it seems that the fMSCs are stay in a self-renew stage because they is an indication that they do not pass on to senescence. It is not confirmed yet, we have to perform a senescence and other test for that. The fMSCs are the perfect alternative to MEFs as well as to other human fibroblasts like HFF cells, if it is true that the fMSC are an infinite source. Once you have them you can expand them as often as you like. However, it is already published that the proliferation rate of fMSCs is enhanced and, in addition, fMSCs display significantly lower doubling times in comparison with adult-derived cells. In contrast to MEFs or other human fibroblasts such as HFF1 cells, fMSCs can be expanded for longer periods. In addition, fMSCs are fully characterized as mesenchymal stem cells and are already advocated for application in clinical approaches (Mirmalek-Sani et al. [2006]). These attributes endow fMSCs as a perfect alternative to MEFs routine and long-term propagation of pluripotent cells.

5 Conclusion

When this study started using episomal vector-based method to generate integration-free induced pluripotent stem cells (iPSCs) took the research of clinical approaches a step forward. However, it will never become the gold standard of reprogramming. First, the reprogramming efficiency is too low and second, the risk remains that foreign particles could integrate into the host genome. The future belongs to mRNA and small molecules-based techniques. For this study we decided to use an episomal-based approach because we were still in trying to overcome the roadblocks to reprogram human fibroblasts into iPSCs with mRNAs by then. We compared the episomal-derived iPSCs (E-iPSCs) with viral-derived iPSCs (V-iPSCs) from the same genetic background, both were derived from human neonatal foreskin fibroblasts (HFF1). The transcriptome profile of E-iPSCs is more similar to that of human embryonic stem cells (hESCs) than that of V-iPSCs. Furthermore, the E-iPSCs generated from human umbilical vein endothelial cells (HUVECs) was faster than that of HFF1-derived E-iPSCs. Additionally, the efficiency was higher and the transcriptome profile of HUVEC-iPSCs was more similar to that of hESCs than the transcriptome profile of HFF1-iPSCs. This discloses that not only the method of reprogramming is important furthermore the somatic cell line is crucial, too.

In the context of analyzing hepatogenesis and maturation of hepatocytes the E-iPSC differentiation to hepatocyte-like cells (HLCs) was demonstrated. E-iPSCs from both genetic background, HFF1 and HUVEC, could be differentiated to HLCs. Both showed morphology and functional characteristics of human hepatocytes. We uncovered gene regulatory networks by analyzing the transcriptome profile of HFF1-iPSC-derived definitive endoderm (DE), hepatic endoderm (HE) and HLCs. Additionally, the presence of bipotential progenitor populations were uncovered in both stages in HE and HLC. Afterwards, a transcriptome profile analysis was performed of both HLC lines, derived from HFF1-iPSCs and HUVEC-iPSCs. Supplementary, these transcriptome profiles were compared to that of fetal liver and PHH and revealed that the iPSC-derived HLCs are immature as well as more similar to fetal liver. Furthermore, to analyze the maturation potential of HLCs a long-term culture experiment was performed using HUVEC-iPSC-derived HLCs. This experiment implied the possibility for long-term culture of HLCs while increasing maturation. Therefore, one future goal will be to increase and push on the maturation while maintain the typical functional characteristics of hepatocyte, e.g. glycogen storage, uptake and release of ICG and CDFDA, bile acid and urea secretion. Then they can serve as an improved source for drug screenings and toxicology studies. In order to reach this aim co-culture with bone marrow fetal femur mesenchymal stem cells (fMSC) could help to give rise to further maturation of the HLCs. They secrete growth factors which are involved in proliferation and maintenance of hepato-

cytes. Furthermore, small molecules could support the maturation and proliferation. The fMSC and small molecules will be used in the next study.

Going a step back in the development, the endodermal progenitors (EP) generated in this study hold a great potential to analyze the endodermal development far before the biliary tree up to liver, bile duct and gallbladder, as well as pancreas, intestine and lung development. This multipotent progenitors express lineage-specific markers of all these named cell types at the same time point. Here as well could help the co-culture with fMSCs due to the fact that they express growth factors support the proliferation and maintenance of EPs. Additionally, they secrete amongst others factors which are involved e.g. in differentiation of EPs into intestinal cells and maintain them. To emphasize the capabilities: fMSCs are versatile. They support the pluripotent maintenance of hESCs and iPSC, could activate the proliferation of hepatocytes and EPs while maintanance them. In addition, fMSC secrete factors which are involved in differentiation processes. In future studies the use of fMSCs will be increase.

The overall aim is to develop liver disease models *in vitro* and derive a whole liver from patient specific cells *in vitro*. 2013, two promising methods were published which will bring the research in disease modeling *in vitro* a huge step forward. One is called transcription activator-like effector nuclease (TALEN) and the other clustered regularly interspaced short palindromic repeat (CRISPR) and CRISPR associated 9 (Cas9) endonuclease systems (CRISPR/Cas9). They can work as a tool for reporter knockin, gene knockout and gene correction. Healthy iPSC lines can be manipulated with these tools to generate specific disease models *in vitro* or the other way around the correction of mutation in patient-derived iPSCs can be conducted. The efficiency of genome modification of both methods is very high and accurate (Hockemeyer et al. [2011], Choi et al. [2013], Ma et al. [2013a], Mali et al. [2013], Osborn et al. [2013], Maetzel et al. [2014], Ye et al. [2014], Sato et al. [2015]). A future step in our laboratory will be to use the CRISPR/Cas9 method to derive a liver disease model from human iPSCs.

One million patient die each year from acute and chronic liver diseases worldwide. While the number of patient who need a liver transplantation increases the number of organ donors decreases since years. Deriving a whole liver from patient specific cells *in vitro* would mean that the gap could be finally closed between needed and available livers for transplantation. However, before generating a whole liver *in vitro* the liver as a whole including its development needs to be understood. With this study more pieces of this puzzle have been solved.

6 Material and Methods

6.1 Cell culture

The human embryonic stem cell (hESCs) lines H1 and H9 were bought from WiCell Research Institute. From ATCC the following cell lines were bought: HFF-1 (HFF-1 (ATCC; SCRC-1041)), HEK-293 (293 [HEK-293] (ATCC; CRL-1573)) as well as HepG2 (Hep G2 [HEPG2] (ATCC; HB-806)). The HUVECs were bought from Life Technologies (Gibco; C-003-5C). Human fetal femur mesenchymal stem cells (fMSCs) line H1536 was got from a collaboration partner (Kindly provided by Dr. Emmajayne Kingham and Prof. Richard Oreffo, University of Southampton, Southampton, United Kingdom). The cells were obtained after day 55 post conception according to guidelines issued by the Polkinghome Report and with ethical approval from the Southampton & South West Hampshire Local Research Ethics Committee.

6.1.1 Culture conditions

Most cell lines were cultured at 37 °C and 5 % CO_2 in an incubator (INNOVA CO-170 Incubator, New Brunswick Scientific) under humidified atmosphere. HUVECs, HUVEC-derived iPSCs and endodermal progenitors (EPs) were cultured at 37 °C, 5 % CO_2 and 5 % O_2 in an incubator (INNOVA CO-170 Incubator, New Brunswick Scientific). All treatments and maintenance procedures were carried out using a clean bench type HeraSafe (Haereus Instruments).

6.1.2 Maintenance of human pluripotent stem cells

Humen embryonic stem cell (hESC) lines as well as induced pluripotent stem cell (iPSC) lines were cultured on Matrigel-coated plates with mitotic inactivated mouse embryonic fibroblast (MEF) cells and a defined medium called unconditioned medium (UM). UM consist of KnockOut DMEM (Gibco/Life Technologies) supplemented with 20 % Knock-Out Serum Replacement (Gibco/Life Technologies), 0.1 mM non-essential amino acids (Invitrogen/Life Technologies), 0.1 mM L-glutamine (Invitrogen/Life Technologies), 0.1 mM -Mercaptoethanol (Sigma-Aldrich), 0.5 % penicillin and streptomycin and 8 ng/ml basic fibroblast growth factor (bFGF, Invitrogen/Life Technologies) as described by Wolfrum et al. [2010].

6.1.3 Maintenance of non-pluripotent cells

Human foreskin fibroblast (HFF1) cells, mouse embryonic fibroblast (MEF) cells, fetal mesenchymal stem cells (fMSCs), human hepatocellular carcinoma (HepG2) cells, human embryonic epithelial kidney (HEK-293) cells were maintained in Dulbecco's modified Eagle medium (DMEM, Gibco/Life Technologies) containing 10 % fetal bovine serum (FBS, Invitrogen/Life Technologies) and 0.5 % penicillin and streptomycin (Invitrogen/Life Technologies) as described by Wolfrum et al. [2010].

Human umbilical vein endothelial cells (HUVECs) were cultured in Medium 200 (Gibco/Life Technologies) with 2 % Low Serum Growth Supplement (LSGS; Gibco/Life Technologies).

Endodermal progenitors (EP) were cultured in Iscove's Modified Dulbecco's Medium (IMDM; Gibco/Life Technologies) with 25 % Ham's F-12 (Cellgro), 0.5 % N2-Supplement 100x (Gibco/Life Technologies), 1 % B-27 Supplement Minus Vitamin A 50x (Gibco/Life Technologies), 0.1 % Bovine Serum Albumin (BSA; Sigma-Aldrich), 50 μg/ml ascorbic phosphate magnesium (Sigma-Aldrich), 0.45 mM Monothioglycerol (Sigma-Aldrich), 50 ng/ml Recombinant Human BMP-4 (BMP-4, R&D), 10 ng/ml Recombinant Human VEGF 165 (VEGF, R&D), 10 ng/ml Recombinant Human EGF, CF (EGF, R&D), 10 ng/ml basic fibroblast growth factor (bFGF, Invitrogen/Life Technologies), 0.5 % penicillin and streptomycin.

6.1.4 Mouse Embryonic Fibroblasts Culture

To maintain the undifferentiated state of human embryonic stem cells they are grown on a layer of mitotic inactivated mouse embryonic fibroblasts (MEFs) or on a feeder-free Matrigel-coated plate with conditioned medium (CM).

Isolation of Mouse Embryonic Fibroblasts

A pregnant female mouse (CF-1, Harlan, USA) was sacrificed at 13 or 14 days post-cointum (d.p.c.) through cervical dislocation. After the uterine horns were separated out they were rinsed briefly in 70 % (v/v) ethanol and placed into a falcon with PBS (without Ca^{2+} and Mg^{2+}, Gibco/Life Technologies). Then they were put into a petri-dish where each embryo was cut from the placenta and embryonic sac. The head and red organs (liver, heart, and gut) were dissected and discarded, the carcase was washed in PBS and placed in a clean petri-dish. The tissue was minced with a sterile razor blade until it become pipettable. One ml of 0.05 % trypsine/EDTA and DNase I (USB, 100 Kunitz units per ml of trypsine) was added per embryo. Afterwards the tissue was transferred into 50ml falcon tubes and incubated for 15 min at 37 °C. Every 5 min the cells were dissociated by pipetting up and down. By adding approx 1x volume of freshly prepared MEF medium the trypsine was inactivated. Remaining pieces of tissue were trashed. The supernatant were centrifuged by low-speed, the cell pellet was resuspened in pre-warm MEF medium. Three or four embryos were plated in each T150 flask, which

were coated with 0.2 % gelatine, for two hours. Only the passage 0 (P0) fibroblasts have the ability to attach onto gelatine-coated flask. On the next day the cells were 80 - 90 % confluent. The major part of the P0 was frozen for future use. The rest of the T150 flask of P0 cells was expanded until passage three or four, inactivated and then used as feeders for culturing human embryonic stem cells or to produce conditioned medium (CM).

Freezing and Thawing Cells

MEFs or HFF1 cells were washed with PBS (amount according to the size of the culture dish). The cells were trypsinised, centrifuged at 1,000 rpm for 5 min at RT and the pellet was resuspended in freezing medium (MEF medium with 10 % DMSO). Then the cells were aliquoted into cryovials, put in a freezing container (Nalgene) and placed at -80 °C overnight. On the next day the vials were transferred to liquid nitrogen for long-term storage.
The cells were stored in liquid nitrogen. They were removed, quickly defrosted in a 37 °C water bath, the vial was sterilized by using 70 % ethanol, opened below the clean bench and the cells were transferred into 10 ml pre-warmed medium in a 15 ml centrifuge tube. After 5 min of centrifugation by 1,000 rpm at room temperature the cell pellet was resuspended in fresh pre-warmed medium.

Inactivating and Plating of MEF

T150 flasks were coated with 0.2 % gelatine and incubated at room temperature for two hours. During the incubation mitomycin C was diluted in PBS (1 mg/ml) and sterilized by filtration. Thawed or fresh made mouse embryonic fibroblasts (MEF) were washed with PBS (without Ca^{2+} and Mg^{2+}, Gibco/Life Technologies). 20 ml of MEF medium has contained 10 μg/ml of mitomycin C (Sigma-Aldrich; M4287-2MG) and were placed on the MEFs. The MEFs were incubated two hours at 37 °C. Then the medium was removed and the cells were washed twice with PBS. After the cells were trypsinised and centrifuged they were resuspended in pre-warmed medium. The cells were counted and plated in a concentration of 5.6 x 10^4 cells/cm^2 in T150 flasks. The MEFs were used for conditioned medium (CM) production for the next seven days.

Preparation of Conditioned Medium

One day after plating inactivated MEFs with a concentration of 56,000 cells/cm^2 in a T150 flask the MEF medium was exchanged with 0.5 ml/cm^2 human ES medium (unconditioned medium, UM) fresh supplemented with 4 ng/ml of FGF2. The T150 flask was incubated by 37 °C. 24 hours later arose CM was collected from the T150 flask and fresh UM containing 4 ng/ml of FGF2 was added to the feeders. This procedure was repeated the next six days. The collected CM of each day was placed at -20 °C. The CM of seven days was combined and sterilized through filtration. 50 ml aliquots were made and stored at -80 °C. To use the CM it was thaw and supplemented with 8 ng/ml of FGF2 (Peprotech) before adding to cells which are grown on Matrigel.

6.1.5 Human ESCs and iPSCs Culture

To maintain the undifferentiated state of human embryonic stem cells they are grown on a layer of mitotic inactivated mouse embryonic fibroblasts (MEFs) or on a feeder-free Matrigel-coated plate. If human ebryonic stem cells (hESCs) or human induced pluripotent stem cells (iPSCs) were cultured feeder-free on a Matrigel-coated plates the cells were fed every day with CM (supplemented freshly with FGF2 to a final concentration of 8 ng/ml) for each well of a 6-well plate. If the hESCs or iPSCs were cultured on feeders they were fed every day with unconditioned medium (UM) supplemented freshly with FGF2 to a final concentration of 8 ng/ml.

Passage of human ESCs and iPSCs

First the Matrigel-coated plates were prepared to plate cells after splitting. Matrigel were diluted in KO-DMEM to a final concentration of 5 mg/ml. Matrigel were storaged at -20 °C. One day before using Matrigel were diluted in cold KO-DMEM 1:30 and were plated. The plates were storaged over night at 4 °C. Before using the plates, they were warmed up at 37 °C. Second step the feeders were removed from liquid nitrogen, quickly defrosted in a 37 °C water bath, the vial was sterilized by using 70 % ethanol, opened below the clean bench and the cells were transferred into 10 ml pre-warmed UM in a 15 ml centrifuge tube. After 5 min of centrifugation at 1,000 rpm at room temperature the cell pellet was resuspended in fresh pre-warmed medium (supplemented with FGF2) and counted. The Matrigel solution was removed from the plates and 250,000 cells were seeded into each well of a six-well-plate and kept at 37 °C. Afterwards the hESCs or iPSCs colonies were cut manually into small pieces with a Microlance injection needle (Becton Dickinson, Madrid, Spain). The cells were gently removed with a cell scraper. The cell clumps were transferred to a 15 ml falcon tube. After centrifugation medium (supplemented with FGF2) was added to the cell pellet. The hESCs or iPSCs were seeded in an optimal split ratio of 1:3 into the wells of Matrigel-coated plate with feeders. The plates were returned to the incubator and gently shook left to right and back to front to obtain an even distribution of cells. One or two days after splitting undifferentiated cells were recognisable as small colonies. During the culturing the cells got large and compact. Due to the high density of the hESCs or iPSCs in this culture system the cells were split normally once a week.

Freezing and Thawing of hESCs

The procedure for freezing human ESCs and iPSCs is identical to that for splitting these cells. This time colonies were manually cut in bigger pieces than for seeding. The colonies will get a higher chance to survive the procedure of freezing and thawing. The cells were gently scraped with a cell scraper (Biochrom AG, Berlin), the clumps were collected, centrifuged and resuspended gently in cold hESCs freezing medium (UM with 10 % DMSO). Usually cells clumps collected from one well of a 6-well-plate were suspended in 1 ml of freezing medium and placed into one cryovial. The cells were put into a freezing container (Nalgene) and placed immediately at -80 °C overnight. The

next day vials were transfer to liquid nitrogen for long-term storage.

A cryovial containing hESCs or iPSCs was removed from the liquid nitrogen storage tank and thawed by gently swirling in a 37 °C water bath until only a small ice pellet remained. Afterwards 70 % (v/v) ethanol was used to sterilize the cryovial and the vial was allowed to air dry before opening. Cells were added dropwise, to reduce osmotic shock, into a 15 ml falcon containing 10 ml of pre-warmed UM. Cells were briefly centrifuged, resuspended in 2 ml of warm UM and added gently to a prepared plate (MEF plated on Matrigel and UM). Around 3 - 4 days before thawing the cells, 6-well plate was coated with Matrigel. One day before splitting 250,000 inactivated MEFs per well of 6-well plate were seeded. The MEF medium was aspirate, wells were washed with PBS and then pre-warmed UM supplemented with 8 ng/ml of FGF2 was pipetted on the MEF. Usually cells from one cryovial are plated into three wells of 6-well plate. However, it may take even 2 - 3 weeks before cells are ready to be expanded. These culture methods and conditions were adapted from (Xu et al. [2001]).

6.2 Episomal Reprogramming by means plasmid nucleofection
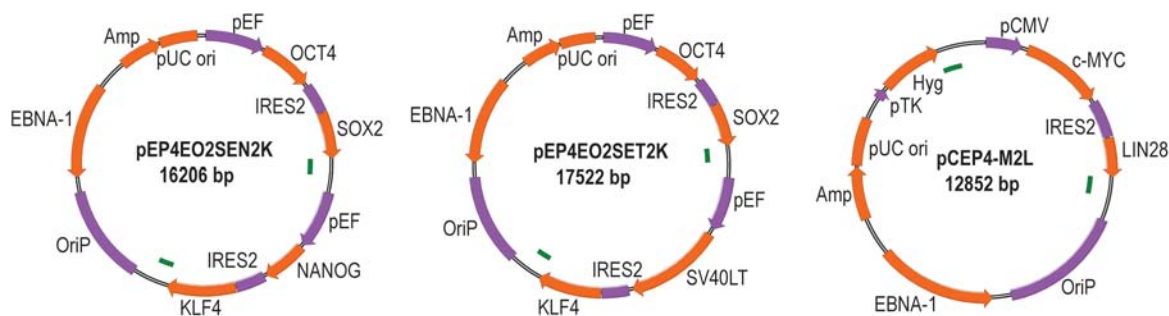
Figure 6.1: **Episomal vector combination.**
The used amount of plasmids for the nucleofection was 3.0 μg of pEP4EO2SEN2K, 3.0 μg of pEP4EO2SET2K and 2.0 μg of pCEP4-M2L respectively in combination 7F-2. Figure adapted from Yu et al. [2011].

To generate vector-free iPSCs three oriP/EBNA1 (Epstein-Barr nuclear antigen-1)-based episomal vectors published by Yu et al. [2011] were used. These vectors expresses the reprogramming factors OCT4, SOX2, NANOG, KLF4, LIN28, c-MYC and SV40LT. A nucleofection was done by using a cell-specific Amaxa Cell Line Nucleofector Kit (Lonza) and one single electroporation was sufficient. 1 x 10^6 of the cells of interest were used. The cells were centrifuged and then diluted in 100 μl Nucleofectior Solution which contained the vectors DNA. The used amount of plasmids for one nucleofection was 3.0 μg of pEP4EO2SEN2K, 3.0 μg of pEP4EO2SET2K and 2.0 μg of pCEP4-M2L as described by Yu et al. [2011]. The cells were mixed quickly and electroporated. Subsequently, 500

μl of pre-warmed medium was added to the solution and rested in a water bath at 37 °C for 10 min. The transfected cells were seeded on a Matrigel-coated 6-well-plate containing the same medium the cells were cultured before the nucleofection. One day after nucleofection the cells were treated with so called small molecules. A TGFβ inhibitor (SB431245, Sigma, in a concentration of 2 μM), a MEK inhibitor (PD0325901, Sigma, in a concentration of 1 μM) and a GSK3β inhibitor (CHIR99021, Sigma, in a concentration of 0.5 μM) were used. The nucleofected cells were treated with the small molecules for 23 days. 7 days after nucleofection the cells were trypsinized, centrifuged, diluted in conditioned medium (CM) and seeded on a Matrigel-coted and MEF-contained 6-well-plate. From this day on CM was used and was changed every other day.
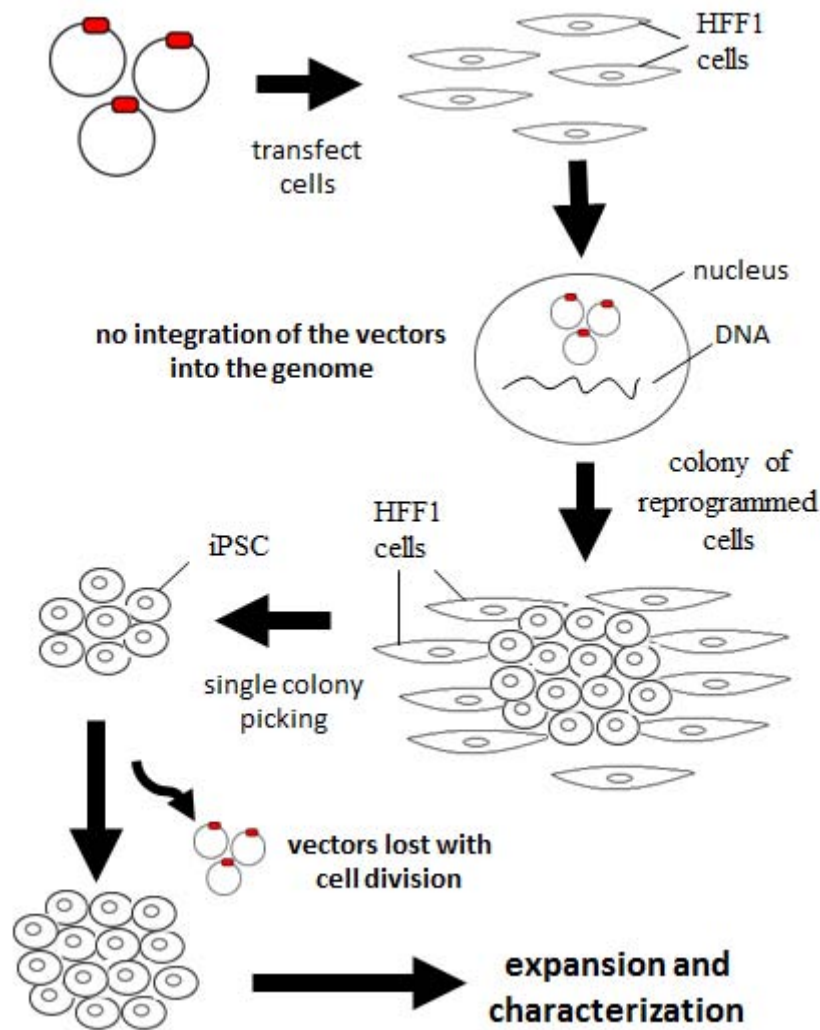
Figure 6.2: **Scheme of reprogramming HFF1 cells into iPSCs.**
Humanl foreskin fibroblast (HFF1) cells were transfected with three different vectors (Figure 6.1). The reprogrammed HFF1 cells were picked and cultured on feeders. During the course of continous culturing the iPSCs lose the vectors completely.

6.3 Characterization of Reprogrammed Cells

Generally, the cells formed colonies, were picked and cultured as single clones. During culturing the vectors were diluted out and the cells containing no ectopic material any more (Figure 6.2). In order to show convincingly that these colonies have stem cell characteristics and can be called induced pluripotent stem cells (iPSCs), a set of analysis has to be conducted. As human embryonic stem cells (hESCs) human iPSCs have the ability to self-renew and differentiate in all lineages of the three germ-layers. To demonstrate these abilities the following analyses were carried out.

6.3.1 Morphology

Two weeks after nucleofection clusters formed and the cell shape differed from the original cells. More and more these clusters grew and fromed iPSC-like colonies (Figure 6.2). Pictures as an overview of the development of the cells were taken (4,000 x 3,000 pixel; 180 dpi) through the ocular of the microscope at a 4-fold magnification with a digital camera. Pictures of stained cells were taken by using a Zeiss, LSM 510 Meta microscope with a connected camera for microscopy model AxioCam ICC3 controlled by the software Axiovision 4.6.

6.3.2 Alkaline Phosphatase Staining

hESCs and iPSCs are characterised by the expression of high levels of alkaline phosphatase. The staining procedure to visualise alkaline phosphatase was performed using the Stemgent Alkaline Phosphatase Staining Kit (00-0055, Stemgent). The cells were washed once with PBS and fixed with the Fix Solution for 2 min at RT. After the fixative was aspirated the cells were washed with PBS. The wash buffer was removed and the freshly prepared Staining Solution (mixed Staining Solution A with B at the same amount) was added to cover the cells. The cells were incubated in the dark at RT for 5 to 15 min. To stop the reaction the Staining Solution was aspirated and the cells rinsed with PBS two times. The stained cells were stored in PBS to keep them moist. Pictures were taken with a digital camera.

It is also possible to stain live cells with the Alkaline Phosphatase Live Stain from molecular probes (Life technologies). The cells were washed two times with pre-warmed DMEM/F-12 for 3 min. The 1x staining solution was made freshly from the 500x stock solution diluted in DMEM/F-12. The staining solution was added to the adherent cells and were incubated for 30 min at 37 °C. Afterwards the solution was removed and the adherent cells were washed two times with PBS for 5 min per wash. Fresh DMEM/F12 was added to the adherent cells. The fluorescence were visualized by using a Zeiss LSM 510 Meta confocal microscope with a connected camera for microscopy model AxioCam ICC3 and the software Axiovision 4.6. A standard FITC filter was used. Subsequently, DMEM/F-12 was removed and fresh pre-warmed culture medium was added to the cells.

6.3.3 Immunofluorescence-based Detection of Proteins

To detect protein expression, the cells were fixed with 4 % paraformaldehyde for 20 min and washed twice with PBS. Afterwards the cells were permeabilised with 0.1 % Triton X-100 in PBS for 10 min. Next, the cells were blocked with a solution consisting of 10 % fetal bovine serum (Invitrogen), 0.1 % Triton X-100 (Sigma) in PBS for 45 min. Subsequently, the cells were washed with PBS twice for 5 min per wash. The primary antibody was diluted in 10 % fetal bovine serum (Invitrogen), 0.1 % Triton X-100 in PBS. The cells were incubated with primary antibody solution over night at 4 °C. Next day the cells were washed three times with PBS for 5 min per wash. The secondary antibody against the species in which the first antibody was produced, was diluted in 10 % fetal bovine serum (Invitrogen), 0.1 % Triton X-100 in PBS. The cells were incubated with the secondary antibody for 1 hour at RT in the dark. Then the cells were washed three times with PBS for 5 min per wash. The nuclei of the cells were counterstained with 4,6-Diamidin-2-phenylindol (DAPI, Invitrogen) solution (200 ng/ml in PBS). 200 μl of DAPI solution was added to the cells and incubated in the dark for 20 min at RT. Finally, the cells were covered with PBS to keep them moist. The fluorophores on the secondary antibodies were visualised by using a Zeiss LSM 510 Meta confocal microscope with a connected camera for microscopy model AxioCam ICC3 and the software Axiovision 4.6.

The following primary antibodies were used in this study:

Table 6.1: List of primary antibody

Human antigene	Species	Company	Product Code
ALB (ALBUMIN)	mouse	Sigma-Aldrich	A-6684
ALCAM	mouse	Santa Cruz	sc-74558
AFP (Alpha Fetoprotein)	mouse	Sigma-Aldrich	WH0000174M1
A1AT (Alpha 1 Antitrypsin)	mouse	R&D Systems	MAB1268
BSEP	goat	Santa Cruz	sc-17292
CD133 (Prominin-1)	mouse	Millipore	MAB4399
CD31 (PECAM-1)	mouse	R&D Systems	BBA7
CDX2	mouse	Santa Cruz	sc-166830
c-MYC	rabbit	Santa Cruz	sc-764
CK18 (Cytokeratin 18)	mouse	DakoCytomation	M7010
CXCR4	mouse	Invitrogen	35-8800
E-CAD (CDH1)	mouse	Santa Cruz	sc-21791
FOXA2 (HNF3β)	goat	Santa Cruz	sc-6554
HNF4α	mouse	Santa Cruz	sc-8987
KLF4	rabbit	Santa Cruz	sc-20691
LGR5	rabbit	Abgent	ABIN389218
LIN28	rabbit	Proteintech Europe	16178-1-AP

Human antigene	Species	Company	Product Code
NANOG	goat	R&D Systems	AF1997
NES (NESTIN)	mouse	Millipore	MAB5326
NTCP	goat	santa cruz	sc-107030
OCT4	mouse	Santa Cruz	sc-5279
PAX6	rabbit	Covance	PRB-278P
PDX1	goat	Santa Cruz	sc-14664
PODXL	rabbit	Santa Cruz	sc-33138
SMA (Smooth Mucle Actin)	mouse	DakoCytomation	M0851
SOX2	goat	Santa Cruz	sc-17320
SOX17	goat	R&D Systems	AF1924
SSEA1	mouse	Millipore	SCR001
SSEA4	mouse	Millipore	SCR001
T (Brachyury)	goat	R&D Systems	AF2085
TRA-1-60	mouse	Millipore	SCR001
TRA-1-81	mouse	Millipore	SCR001
TUJ1 (class III beta TUBULIN)	mouse	Sigma-Aldrich	T8660
ZO-1	goat	Santa Cruz	sc-8146

The following secondary antibodies were used:

Table 6.2: List of secondary antibody

Human antigene	Species	Company	Product Code
anti-goat IgG, Alexa uor 488	donkey	Invitrogen	A11055
anti-goat IgG, Alexa uor 594	chicken	Invitrogen	A21468
anti-mouse IgG, Alexa uor 488	goat	Invitrogen	A11001
anti-mouse IgG, Alexa uor 594	goat	Invitrogen	A11005
anti-rabbit IgG, Alexa uor 488	donkey	Invitrogen	A21206
anti-rabbit IgG, Alexa uor 594	chicken	Invitrogen	A21442

6.3.4 Karyotyping

The Chromosomal analysis was performed after GTG-banding by Prof. Dr. G. Thiel (Praxis für Humangenetik, Friedrichstr. 147, 10117 Berlin, Germany). For each cell line 20 metaphases were counted and 10 karyograms analyzed.

6.3.5 Isolation of Genomic DNA

To isolate DNA, the cells were scraped from the well, transfered to a 15 ml tube and centrifuged. The pellet was used for the DNA isolation. The DNA isolation was done

by using the FlexiGene DNA Isolation Kit (Qiagen) according to the manufacturers guidelines. Subsequently, DNA concentration and quality was assessed by NanoDrop measurements. 1 μl was used for quality check by photometric quantification with a spectrophotometer type NanoDrop ND-1.000 and measured at a wavelength of 260 nm to determine concentration. For quality control the ratio of 260 nm and 280 nm was measured.

6.3.6 Agarose Gel Electrophoresis

For the preparation of an agarose gel (1 - 3.5 % gels were used in this study) the appropriate amount of agarose was dissolved in 100 ml 1x SB buffer. The solution was boiled using a microwave until it got clear. 0.5 μg/ml ethidium bromide was added. The solution was mixed and subsequently poured into an agarose gel tray. Finally, gel combs with the appropriated number of teeth and size of the teeth were put into the liquid gel solution. After 20 min the gel was polymerized. The gel combs were removed and the agarose gel was covered with 1x SB buffer. 6x DNA-loading buffer was added to each PCR sample and the agarose gel was loaded with the samples. The length of the amplicons was determined in relation to a DNA ladder. The gels were run at 50 V for 30 min or longer, depending on the size of the amplicon and the pore size of the agarose gel. The nucleic acids were visualised with UV light using the AlphaImager (Alpha Innotech).

6.3.7 Polymerase Chain Reaction

The PCR reactions were used to perform DNA fingerprinting of iPSCs and to detect the sequences of the episomal plasmid (Yu et al. [2011]).

Reaction mix for one DNA sample:

2.0 μl	DNA
0.2 μl	dNTP-Mix (dATP, dCTP, dGTP, dTTP each 25 mM)
1.0 μl	forward primer and reverse primer mix (100 μM)
0.25 μl	Polymerase
2.5 μl	10x reaction buffer
19.05 μl	ddH2O

Table 6.3: List of PCR primer for vector detection

Gene	Size (bp)	Symbol	Sequence 5'- 3'		Annealing Temp.
T-Oct4	657	pOCT4_F	AGTGAGAGGCAACCTGGAGA	exogen	62 °C
		pIRES_R	AGGAACTGCTTCCTTCACGA		
T-NANOG	732	pNANOG_F	CAGAAGGCCTCAGCACCTAC	exogen	62 °C
		pIRES_R	AGGAACTGCTTCCTTCACGA		
T-LIN28	447	pLIN28_F	AAGCGCAGATCAAAAGGAGA	exogen	58 °C
		pSV40pA_R	CCCCCTGAACCTGAAACATA		
T-SV40LT	491	pSV40LT_F	TGGGGAGAAGAACATGGAAG	exogen	55 °C
		pIRES_R	AGGAACTGCTTCCTTCACGA		
Oct4	113	hOCT4_F	AGTTTGTGCCAGGGTTTTTG	endogen	58 °C
		hOCT4_R	ACTTCACCTTCCCTCCAACC		
oriP	544	pEP4-SF1	TTCCACGAGGGTAGTGAACC	exogen	58 °C
		pEP4-SR1	TCGGGGGTGTTAGAGACAAC		
EBNA1	666	pEP4-SF2	ATCGTCAAAGCTGCACACAG	exogen	60 °C
		pEP4-SR2	CCCAGGAGTCCCAGTAGTCA		

The sequences were used as described from Yu et al. [2011].

Example of a PCR-program:

Step 1	94 °C	5 min.
Step 2	94 °C	15 sec.
Step 3	58 °C	30 sec.
Step 4	68 °C	1 min.
Step 5	68 °C	7 min.
Step 4	4 °C	forever

Step 2 till Step 4 were repeated 32 times before proceeding to step 5. The PCR was carried out using a Thermocycler type PTC100 (MJ Research Inc).

6.3.8 DNA Fingerprinting

The DNA fingerprinting was used to analyse the relation between the generated iPSC lines and the parental cell line. After isolation of genomic DNA from the iPSC lines (as described before) different PCRs (as described before) with the primer set D7S796, D10S1214, D17S1290 and D21S2055 were performed. The primers amplify different VNTRs (variable number of tandem repeats). The amplicons were visualised by agarose gel electrophoresis (as described before) with a concentration of 2 - 3 % agarose.

Table 6.4: List of primer sequences for DNA fingerprinting.

Gene	Primer	Sequence 5'- 3'
D7S796	forward	TTTTGGTATTGGCCATCCTA
	reverse	GAAAGGAACAGAGAGACAGGG
D10S1214	forward	ATTGCCCCAAAACTTTTTTG
	reverse	TTGAAGACCAGTCTGGGAAG
D17S1290	forward	GCAACAGAGCAAGACTGTC
	reverse	GGAAACAGTTAAATGGCCAA
D21S2055	forward	AACAGAACCAATAGGCTATCTATC
	reverse	TACAGTAAATCACTTGGTAGGAGA

6.3.9 Isolation of RNA

To isolate RNA the cells were scraped from the well, transfered to a 15 ml tube and centrifuged. The pellet was used for the RNA isolation. The RNA isolation was done by using the Direct-zol RNA Miniprep (Zymo Research, R2050) or Universal RNA Purification Kit (Roboklon, E3598-02) and according to the manufacturers guidelines. Subsequently, RNA concentration and quality was assessed by NanoDrop measurements and

gel electrophoresis. 1 μl was used for quality check by photometric quantification with a spectrophotometer type NanoDrop ND-1.000 and measured at a wavelength of 260 nm to determine concentration. For quality control the ratio of 260 nm and 280 nm was measured which should be > 2.0. 1 μl was used for the gel electrophoresis.

6.3.10 Generation of cDNA

RNA was isolated as described before. 1 μg of the RNA was mixed with Oligo dT Primer (1 μg/μl; Invitek) and filled up with ddH$_2$O to a volume of 10 μl. This solution was incubated for 10 min at 70 °C, cooled on ice and supplemented with a master mix consisting of following components:

5.0 μl	5x reaction buffer (Promega)
0.5 μl	dNTP-Mix (dATP, dCTP, dGTP, dTTP each 25 mM)
0.1 μl	MMLV (Moloney Murine Leukemia Virus) reverse transcriptase (200 U/μl, USB)
9.4 μl	ddH$_2$O

After 1 h incubation at 42 °C the reaction was stopped at 65 °C for 10 min. Afterwards the cDNA was diluted 1:5 with distilled water. The incubation was carried out using a Thermocycler PTC100 (MJ Research Inc).

6.3.11 Quantitative Real Time PCR

The qRT-PCR was performed in 384-well Optical Reaction Plates (Applied Biosystems). Reaction mix for one cDNA sample:

3 μl	SYBRGreen PCR Master Mix (Applied Biosystems)
2 μl	cDNA (1:5 dilution)
1 μl	forward primer and reverse primer mix (5 pmol/μl)
1 μl	ddH$_2$O

Table 6.5: List of rtPCR primer

Gene	Size (bp)	Symbol	Sequence 5'- 3'
GAPDH	81	forward	CTGGTAAAGTGGATATTGTTGCCAT
		reverse	TGGAATCATATTGGAACATGTAAACC
OCT4	119	forward	GTGGAGGAAGCTGACAACAA
		reverse	ATTCTCCAGGTTGCCTCTCA
SOX2	78	forward	GTATCAGGAGTTGTCAAGGCAGAG
		reverse	TCCTAGTCTTAAAGAGGCAGCAAAC
NANOG	78	forward	CCTGTGATTTGTGGGCCTG
		reverse	GACAGTCTCCGTGTGAGGCAT

Gene	Size (bp)	Symbol	Sequence 5'- 3'
LEFTY1	76	forward	AATGTGTCATTGTTTACTTGTCCTGTC
		reverse	CAGGTCTTAGGTCCAGAGTGGTG
GDF3	96	forward	TTGGCACAAGTGGATCATTGC
		reverse	TTGGCACAAGTGGATCATTGC
FGF4	109	forward	CCCTTCTTCACCGATGAGTGC
		reverse	CATTCTTGCTCAGGGCGATG
DPPA4	91	forward	TGGTGTCAGGTGGTGTGTGG
		reverse	CCAGGCTTGACCAGCATGAA
DNMT3B	93	forward	GCTCACAGGGCCCGATACTT
		reverse	GCAGTCCTGCAGCTCGAGTTTA
SOX17	86	forward	ACGTGTACTACGGCGCGATG
		reverse	CTGGTGCTGGTGCTGGTGTT
FOXA2	97	forward	TTCAGGCCCGGCTAACTCTG
		reverse	CCTTGCGTCTCTGCAACACC
HNF4	102	forward	GTGCGGAAGAACCACATGTACTC
		reverse	GAAGCATTTCTTGAGCCTGCAGTA
AFP	88	forward	AGCAGCTTGGTGGTGGATGA
		reverse	CCTGAGCTTGGCACAGATCCT
ALB	77	forward	GCGCAGATGACAGGGCGGAA
		reverse	GTGCCGTAGCATGCGGGAGG
A1AT	76	forward	GGTCACAGAGGAGGCACCC
		reverse	AGTCCCTTTCTCGTCGATGGT
TBX3	88	forward	AGTCCTCCAGTGAACAAGCAG
		reverse	TCTTTGAGGTTCGATGTCCC
FAH	79	forward	CGGGCCGGAGCCAGAAAAC
		reverse	ACCATTCCCCAGGTCTATG
TDO2	77	forward	GGTGAAAGACGGCTGTCATACAG
		reverse	TGGAACCTAGGCTCTTCCCTG
PROM1	69	forward	GACTTGCGAACTCTCTTGAATGA
		reverse	GGTAGTGTTGTACTGGGCCAAT
LGR5	118	forward	TTTGGACAAGGGAGACCTGGAGAA
		reverse	AGAGGAGAAGGACAAGAAAGCCACA
CYP1A1	195	forward	AAACAGGGCCACATAGATGC
		reverse	AGGGTCCTGGTTTGGCTAGT
CYP3A4	79	forward	GTGACTTTGCCCATTGTTTAGAAAG
		reverse	CAGGCGTGAGCCACTGTG
CYP3A7	77	forward	GATTCTGTACGTGCATTGTGCTC
		reverse	ATTTGGTCATCTCCTCTATATTACCAAGT

Gene	Size (bp)	Symbol	Sequence 5'- 3'
CYP3A11		forward	TGGTCAAACGCCTCTCCTTGCTG
		reverse	ACTGGGCCAAAATCCCGCCG
CYP19A1	100	forward	TGGCTGTGCAGGAAAGTACATC
		reverse	AACACACTGTCCTTGCAATGTCTTC
PDX1	145	forward	CTCCACCTTGGGACCTGTTTAGAGA
		reverse	CGCCCGAGTAAGAATGGCTTTATGG
CDX2	100	forward	TCCTGGTCTGGGAAGGGAAGAGAAA
		reverse	CGGAAGCCAAAGGCAGCTAAGATAG
CXCR4	79	forward	CACCGCATCTGGAGAACCA
		reverse	GCCCATTTCCTCGGTGTAGTT

6.3.12 Embryoid Body-based Differentiation

The hESC or iPSC colonies were cut manually into pieces with a Microlance injection needle (Becton Dickinson, Madrid, Spain). The cells were gently removed with a cell scraper. The cell clumps were transferred to a 15 ml falcon tube. After centrifugation DMEM medium was added to the cell pellet. The hESCs or iPSCs were seeded on ultra low attachment dishes (Corning). The cells were cultured in 10 ml of medium per cell culture dish. The cell pieces formed spheres, so called embryoid bodies (EBs), due to the fact that the cells could not attach to the surface. Those which cannot form spheres will die. The medium was changed every two days through transferring the EBs into a 15 ml tube. The EBs were settled by waiting 5 min. The medium was drawn off and fresh medium was added. The EBs were transferred back to the ultra low attachment culture dish and were put in the incubator (INNOVA CO-170 Incubator, New Brunswick Scientific) at 37 °C and 5 % CO_2 in a humidified atmosphere. The EBs were cultured seven days. Afterwards the EBs were seeded onto 12 well cell culture dishes that were coated with 0.1 % gelatin and the same medium (DMEM) was used. The EBs attached onto the gelatin surface and differentiated. Three days after seeding on gelatin some wells were fixed with paraformaldehyde to detect the early markers of the germ layers Brachyury (mesoderm) and PAX6 (neuroectoderm). To detect the other markers the EBs were fixed with paraformaldehyde 10 days after seeding on gelatin. Generally, the EBs were stained by immunofluorescence-based staining of marker proteins of the three germ layers. Stainings for SOX17, AFP and FOXA2 detecting the endoderm differentiation. Staining for Brachyury and α-SMA detect differentiation into mesoderm lineage. PAX6, β-TUJ and NESTIN were stained to detect differentiation of ectoderm germ layer. The immunofluorescence-based detection of proteins was done as described before (Chapter 6.3.3).

6.3.13 Teratoma Formation

The *in vivo* differentiation experiments (teratoma formation) were performed by EPO Berlin GmbH (Germany, http://www.epo-berlin.de, accessed 26.02.2016). Approximately 2 x 10^6 cells of the cell line were harvested by combined type IV collagenase treatment and 0.05 % Trypsin/EDTA-treatment and washed. Cells were resuspended in 50 μl PBS, then mixed with Matrigel (1:2) and immediately injected subcutaneously into NOD.Cg-rkdc^{scid} Il2rg^{tm1Wjl}/SzJ mice, commonly known as NOD scid gamma (NSG). Teratoma formation was carefully monitored and sacrificed 63d after injection. The teratomas were collected and processed by means of standard procedures for paraffin embedding, then hematoxylin and eosin staining. Histological analysis was performed by a pathologist.

6.3.14 Microarray-based gene expression profiling

Illumina bead chip hybridization

Total RNA was isolated for each sample as described in chapter 6.3.9. For global gene expression analysis on a Illumina microarray platform quality-checked total RNA was used. 500 ng RNA for each sample was used as input for the amplification and biotin labeling reactions (Illumina TotalPrep RNA Amplification Kit, Ambion, Austin, TX, USA), which precede bead chip hybridizations. The cRNA synthesis, BeadChip hybridization and scanning was performed by ATLAS Biolabs GmbH (http://www.atlasbiolabs.com, accessed 26.02.2016).

Data analysis

All gene expression data analyses were done in cooperation with the bioinformatition of our group Wasco Wruck, Institute for Stem Cell Research and Regenerative Medicine, Heinrich Heine University, 40225 Düsseldorf, Germany.

The gene expression data were background subtracted and normalized on the basis of the rank invariant algorithm of the Gene Expression Module version 1.8.0 provided with the GenomeStudio software (formerly BeadStudio, Illumina). An arbitrary cut-off value was set to eliminate negative gene expression signals, which may have resulted from background subtraction. GenomeStudio calculates a Detection p-value for every gene by comparing its signal intensity with that of negative control beads to determine the probability that this gene is expressed.

The quality of the experiments is controlled by calculation of the Pearson correlation coefficient between all experiments vs. each other. These coefficients are summarized in a table marking value ranges of the correlation coefficients in different colors to enable detection of outliers. Additionally, a dendrogram is generated via the plotSampleRelation from the Bioconductor lumi package to enable comparison of similarities between experimental samples and outlier finding by obvious misalignments in the dendrogram. For the generation of Venn Diagrams and to carry out correlation coefficient analyses, the normalized data sets were filtered for genes present in either sample or in

at least one of the samples under investigation (Detection p-value/p_{de}t < 0.01, http://bioinfogp.cnb.csic.es/tools/venny/index.html, accessed 26.02.2016). The differential gene expression was calculated using the Illumina Custom Model (Kuhn et al. [2004]). The Diff p-values (p-value, describing the probability that a genes signal intensity has changed between two samples or groups of samples) were adjusted by the Benjamini and Hochberg false discovery rate (FDR) correction algorithm (Benjamini1995). Genes had to be at least 1.5 fold up- or down-regulated between the samples of interest and the corresponding FDR-adjusted Diff p-value had to be $p_{adj} < 0.05$, to be considered differentially expressed.

Functional annotation and enrichment analyses were performed using the DAVID platform version 6.7 (http://david.abcc.ncifcrf.gov/home.jsp (accessed 26.02.2016); Dennis et al. [2003]; Huang et al. [2009]). Illumina ProbeIDs or official gene symbols were used as input against the background of Homo sapiens; analyses were executed based on DAVID default parameter settings. Expression profiles of all genes are analyzed via k-means clustering. In order to achieve a sufficient granularity k =1 00 clusters are conceived. The k-means clustering algorithm from the R/Bioconductor environment is applied for this task. An association table of Illumina probes and genes to the 100 clusters is the result of the clustering analysis. Plots of mean and standard deviation of all genes expression over all HLC differentiation phases are condensed for all clusters. Heatmaps of these clusters are generated via the heatmap2 function from R (http://www.r-project.org/ (accessed 26.02.2016); Team [2010]; G. R. Warnes and Venables [2010]).

Stage-specific clusters containing genes which are prominently expressed in dedicated stages of the differentiation. These were extracted from the k-means clustering. Four clusters were selected containing similar genes to *OCT4* (POU5F1), *SOX17*, *AFP* and *ALB*. The gene sets from these clusters were subjected to transcription factor analysis via oPOSSUM3 single site analysis using default parameters with the exception of restricting the amount of upstream/downstream sequence to 2000 / 2000 bases. To detect pathways over representation in differentiation stages stage specific genes were determined via comparisons of DE vs. iPSCs, HE vs. DE, HLCs vs. HE, Fetal liver vs. HLCs and PHH vs. fetal liver. Differentially expressed genes in these comparisons were found with the criteria a) Illumina detection p-value < 0.05 in at least one of both conditions, b) ratio < 0.75 or ratio > 1.3333 and c) limma-p-value < 0.05 and limma-q-value < 0.05. The differentially expressed genes are subjected to pathway analysis via Consensus Path DB. For cluster analysis of expression of liver-specific metabolisms cytochromes, ABC transporter genes and several other transporter genes were filtered from the microarray experiments of iPSCs, definitive endoderm (DE), hepatic endoderm (HE), hepatocyte-like cells (HLCs), fetal liver and primary human hepatocytes (PHH). Heatmaps of these clusters are generated via the heatmap2 function from R using Euclidean distance as distance measure. To detect differences and commonalities between HLCs, fetal liver and PHH genes differentially expressed in HLCs vs. iPSCs, fetal liver vs. iPSCs and PHH vs. iPSCs were compared via a Venn diagram. Differential expression was termed significant if a) limma-p-value < 0.05 and limma-q-value < 0.05, b) detection-p-value < 0.05 at least in one of both conditions and c) ratio < 0.75 or ratio

> 1.33. In order to detect differences between the three experiments in more detail an analysis of variance (ANOVA) was employed to filter genes followed by pairwise t-tests. Genes were termed significant if a) anova-p-value < 0.05 and anova-q-value < 0.05, b) t-test p-value < 0.05 and t-test q-value < 0.05 and c) detection-p-value < 0.05 at least in one of both conditions.

Opossum

The oPOSSUM database was downloaded in June 2014 and Single Site Analysis was performed on this local instance to detect over-represented conserved transcription factor binding sites in a set of progenitor associated genes (Kwon et al. [2012]). This analysis was parameterized to use the species human, 2,000 base pairs upstream and downstream each, use only JASPAR Transcription Factor Binding Site (TFBS) profile matrices which belong to the tax group vertebrates, a minimum relative TFBS position weight matrix (PWM) score of 0.85 and a minimum information content (specificity) of JASPAR TFBS profile matrices of 8. The network was drawn based on the results of the oPOSSUM analysis using only transcription factors surpassing a predefined for the Z-Score. The Z-Score shows if in the investigated up- and downstream regions of the set of genes there are more TFBS than in the background. We used a relatively restrictive threshold of 10 to focus on the core regulatory network. For all transcription factors above this threshold we extracted the conserved binding sites from the oPOSSUM analysis output and connected them with the transcription factor itself as edges in the graph. For the drawing and layout of the graph we employed the R package network (http://www.jstatsoft.org/v24/i02/paper (accessed 26.02.2016)) which was instructed to draw red circles for genes and green circles with sizes corresponding to the Z-scores for the transcription factors. For a closer look into the stages we used a threshold of 3.

Pluritest

It is a robust open access bioinformatic assay of pluripotency in human cells (Mller et al. [2011], http://www.scopus.com/inward/record.url?eid=2-s2.0-79953267538&partnerID=40&md5=7108a16c223225f3d2443f06cbba4ace, accessed 26.02.2016). With this tool the gene expression pattern of the new iPSC line will be compared to the expression profile of several hundreds hESC and iPSC lines from multiple laboratories all over the world.

Novelty Score: A score that is based on well-characterized pluripotent samples in the stem cell model matrix. Samples are color-coded green (pluripotent), orange, red (not-pluripotent) based on the probabilities given from the logistic regression model. Orange and red samples are more dissimilar to the pluripotent samples in the model matrix than the other pluripotent samples in the matrix. A low Novelty Score indicates that the test sample can be well reconstructed based on existing data from other well-characterized iPSC and ESC lines. A high Novelty Score indicates that there are patterns in the tested sample that cannot be explained by the currently existing data from well-characterized, karyotypic normal pluripotent stem cells. Partially differentiated pluripotent cells, ter-

atocarcinoma cells or karyotypically abnormal embryonic stem cells may have a high pluripotency score but cannot be reconstructed well with data from well-characterized, normal pluripotent stem cells and thus are expected have a high Novelty Score.

A plot of hierarchical clustering generated by the Lumi package after the samples were transformed with a variance stabilizing transformation (VST) and before robust spline normalization (RSN). Outlier arrays with too much technical variation might be spotted if they do not cluster with their respective technical or biological replicates from the same sample or sample type. For example, if an array hybridized with the RNA from an pluripotent cell clusters with fibroblasts on the same chip, but not with other pluripotent samples, something might be wrong with technical aspects of your experiment.

6.4 Hepatocyte-Like Cell Generation

For the differentiation of iPSCs into hepatocyte-like cells (HLCs) the three step protocol from Sullivan et al. [2010] was used. The cells have to be cultured feeder-free on Matrigel-coated plates. The first step of differentiation starts at a cell colony density of 30 - 50 %. To generate the definitive endoderm (DE) stage the cells were treated with the following medium:

Table 6.6: Medium for definitive endoderm

Amount	Component	Company	Product Code
96 %	RPMI medium	Gibco	31870-025
2 %	B27	Gibco	12587-010
1 %	Glutamin	Gibco	25030-081
1 %	Penicillin and Streptomycin	Gibco	15070-063

From day one to day three 100 ng/ml Activin A (R&D; 338-AC-010) and 50 ng/ml Wnt-3A (R&D; 5036-WN-010) were added to the medium. Day four and five 100 ng/ml Activin A only was added to the medium.

The next differentiation step is the hepatic endoderm (HE) stage which needed four days of treatment with the following medium:

Table 6.7: Medium for hepatic endoderm

Amount	Component	Company	Product Code
76.5 %	KnockOut DMEM medium	Gibco	10829-018
20 %	KnockOut Serum Replacement (SR)	Gibco	10828-028
0.5 %	Glutamin	Gibco	25030-081
1 %	Non-Essential Amino Acids	Lonza	BE13-114E
1 %	Penicillin and Streptomycin	Gibco	15070-063
0.01 %	β-Mercaptoethanol	Gibco	31350-010

Each day 1 % DMSO was added freshly to the medium.

The last step of HLC generation was modified. During the last step of differentiation we used 25 ng/ml dexamethasone instead of 10 M hydrocortisone 21-hemisuccinate. The following medium composition was used for five days:

Table 6.8: Medium for hepatocyte-like cells

Amount	Component	Company	Product Code
82 %	Leibovitz's L-15 medium	Gibco	11415-049
8 %	Fetal Bovine Serum (FBS)	Biochrom	S 0115
8 %	Tryptose Phosphate Broth solution	Sigma	8159-100ML
1 %	Glutamin	Gibco	25030-081
1 %	Penicillin and Streptomycin	Gibco	15070-063
0.01 %	Insulin Solution	Sigma	I9278-5ML

Each day 10 ng/ml HGF (Pepro Tech; 100-39), 20 ng/ml OSM (R&D; 295-OM-010) and 25 ng/ml Dexamethasone (R&D; 1126/100) were added freshly to the medium.

6.4.1 Periodic acid-Schiff (PAS) Assay

To identify glycogen storage in iPSC-derived HLCs the Periodic Acid-Schiff (PAS) Staining System (Sigma; 395B-1KT) was used. The purpose of this method is to identify carbohydrate macromolecules through chemical reaction. Periodic acid oxidizes the glucose residues and creates aldehydes, which react with Schiff reagent producing purple colour. Cells were fixed with 4 % PFA for 15 min, washed with distilled water and incubated with Periodic Acid solution for 5 min. Then washed 3 times with water and incubated for 15 min with Schiffs reagent. Afterwards the cells were washed with distilled water (5 min), stained with Hematoxylin (90 sec) and again washed with distilled water. The result was examined under an Olympus CK2 phase contrast microscope and representative morphology was recorded at a magnification of X50 using a Canon 300D digital camera.

6.4.2 Indocyanine Green (ICG) Assay

Indocyanine Green (ICG) is an indicator dye used for assessing liver and cardiac function, which after intravenous injection is bound to plasma protein (primarily albumin). This substance is rapidly taken up by the liver and then secreted unchanged into the bile. The cellular uptake and release of ICG (Cardiogreen, ICG, Sigma; I2633-25MG) was performed to prove the presence of albumin in hepatocyte-like cells derived from human iPSCs (Yamada et al. [2002]; Ho et al. [2012]). Stock solution (5 mg/ml) of reagent was prepared in DMSO (Sigma; C6164-50ML) and freshly diluted in culture media to 1 mg/ml just before application. Cells were incubated in culture media supplemented with ICG for 30 min at 37 °C. Afterwards, the cells were washed with PBS (Gibco; 10010-023) and fresh medium without substrate was added. The uptake of the dye was documented. To examine the release of ICG the cells were cultured under normal conditions for 6 h. Afterwards cellular release was analyzed. The result was examined under an Olympus CK2 phase contrast microscope and representative morphology was recorded at a magnification of X50 using a Canon 300D digital camera.

6.4.3 5 (and 6)-Carboxy-2,7-dichloroflurescein diacetate (CDFDA) Assay

5 (and 6)-Carboxy-2,7-dichloroflurescein diacetate (CDFDA) is an indicator dye (fluorescent substrate) used for assessing liver function (Zamek-Gliszczynski et al. [2003]). This substance passively diffuses into hepatocytes where it is hydrolyzed to CDF or hydrolized in the extracellular medium to CDF. CDF is taken up via an Oatp mediated process and is excreted from the liver by Mrp2 on the canicular membrane and Mrp3 on the basolateral membrane. The cellular uptake and release of CDFDA (Sigma-Aldrich; 21884-100MG) was performed to highlight canicular formation and prove the functionality of the HLCs derived from human iPSCs. CDFDA was diluted in DMSO (Sigma; C6164-50ML) and was freshly diluted in culture medium to 1 μM just for application. The Cells were incubated in culture media supplemented with CDFDA for 30 min at 37 °C. Afterwards, the cells were washed with PBS (Gibco; 10010-023) and fresh medium without substrate was added. The uptake of dye was documented by using a Zeiss LSM 510 Meta confocal microscope with a connected camera for microscopy model AxioCam ICC3 and the software Axiovision 4.6. To examine the release of CDFDA the cells were cultured under normal conditions for 6 hours. Afterwards cellular release was analysed by using a Zeiss LSM 510 Meta confocal microscope with a connected camera for microscopy model AxioCam ICC3 and the software Axiovision 4.6.
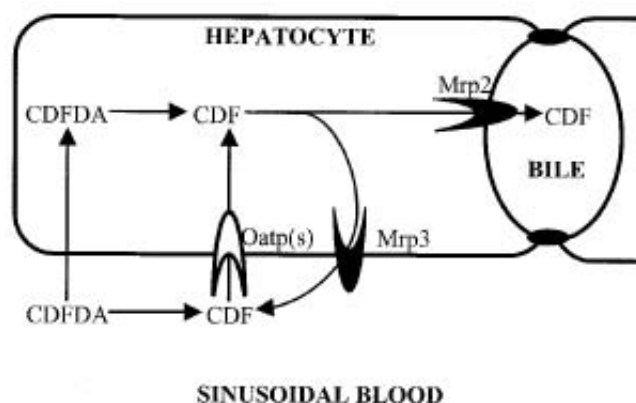
Figure 6.3: **Scheme of CDFDA uptake and release.**
CDFDA passively diffuses into hepatocytes where it is hydrolyzed to CDF or hydrolized in the extracellular medium to CDF. CDF is taken up via an Oatp mediated process and is excreted from the liver by Mrp2 on the canicular membrane and Mrp3 on the basolateral membrane. Figure adapted from Zamek-Gliszczynski et al. [2003].

6.4.4 Urea Assay

Urea is the major end product of protein catabolism in the liver. The detection of urea in the medium proves another functionality aspect of intact hepatocytes. This QuantiChrom^{TM} Urea Assay Kit (BioAssay Systems; DIUR-500) is designed to measure urea directly in biological samples without any pretreatment. The method utilizes a chromogenic reagent that forms a colored complex specifically with urea. The intensity of the color, measured at 520 nm, is directly proportional to the urea concentration in the sample. The 5 μl of water (blank), standard row (50 mg/dl; 25 mg/dl; 12.5 mg/dl; etc.) and samples were pipetted directly in wells of a 96-well-plate. Then 200 μl of working reagent were added to the wells and taped lightly to mix. After an incubation period of 10 to 20 min the optical density at 470 - 550 nm (peak absorbance at 520 nm) was measured with a plate reader. Three biological replicates in technical triplicates of each sample were analyzed. The levels of urea are presented as a percentage, considering measured levels of urea in mg/dL/24 h.

6.4.5 Bile Acid Assay

The bile acid assay was performed by Dr. Diran Herebian, Department of General Pediatrics, Neonatology and Pediatric Cardiology, Heinrich Heine University, 40225 Düsseldorf, Germany. Bile acids (cholic acid CA, chenodeoxycholic acid CDCA, deoxycholic acid DCA, ursodeoxycholic acid UDCA, lithocholic acid LCA) including their glycine- and taurine derivatives were analyzed by UPLC-MS/MS. The system consisted of an Acquity UPLC-H Class (Waters, UK) coupled to a Xevo-TQS tandem mass spectrometer (Waters, UK) which is equipped with an ESI source operating in the negative ion mode. Quantitative data were conducted in the multiple reaction monitoring (MRM)

mode. The chromatographic separation was performed on Waters UPLC BEH C18 column (100 mm, 2.1 mm ID, 1.7 m; Waters, UK) using acetonitrile and acidic water (0.1 % formic acid) as mobile phases. Analytes were separated by a gradient elution. The injection volume was 5 μl and the column was maintained at 40 °C.

6.4.6 CYP3A4 Assay

The P450-Glo^{TM} CYP3A4 Assay (Promega; V9001) provides a luminescent method to measure cytochrome CYP3A4 activity. This protein is localizes in the endoplasmic reticulum and its expression is induced by glucocorticoids and some pharmacological agents (Ek et al. [2007]). Luciferin-PFBE was freshly diluted in culture medium to a concentration of 50 μM. Cells were incubated with culture medium supplemented with Luciferin-PFBE for 4 h at 37 °C (normal culture conditions). Afterwards, 25 μl of the culture medium supplemented with Luciferin-PFBE were pipetted to 96-well opaque white luminometer plate. To initiate the luminescent reaction 25 μl of Luciferin Detection Reagent were added. This mixture was incubated for 20 min in the dark. For the read out the GloMax-Multi+ Microplate Multimode Reader with Instinct (Promega) was used. Three biological replicates in technical triplicates of each sample were analyzed. The levels of CYP3A4 are presented as relative light units per milliliter (R.L.U./ml). The error bars indicate the standard errors of the mean.

6.4.7 Electron Microscopy

EM was performed by Beatrix Fauler and Dr. Thorsten Mielke, Max Planck Institute for Molecular Genetics, Microscopy & Cryo Electron Microscopy Group, 14195 Berlin, Germany. Cells grown on Thermanox plastic coverslips (Nunc) were fixed in a modified Karnofsky solution, 2 % PFA/2.5 % GA in 50 mM Cacodylate buffer, pH 7.4 at 4 °C. Cells were washed in 50 mM Cacodylatpuffer / 50 mM NaCl and post-fixed for 90 min at RT with 0.5 % OsO4 in the same buffer. After washing steps with water, cells were incubated for 40 min with 0.1 % tannic acid in 250 mM Hepes pH 7.4 , washed with water and stained with 2 % uranyl acetate, 90 min at RT. Cells were dehydrated in a graded series of ethanol and embedded in Spurrs resin (Low Viscosity Spurr Kit, Ted Pella, CA, USA). Ultra-thin sections (70nm) were prepared with an ultramicrotome (Reichert Ultracut E, Leica) and mounted on pioloform-coated slot grids from copper. Sections were counterstained with uranyl acetate and lead citrate.
Ultrathin-sections were first examined using a Philips CM100 transmission electron microscope operated at 100 kV and finally imaged using a FEI Tecnai Spirit transmission electron microscope operated at 120 kV, which was equipped with a 2kx2k Eagle CCD camera (FEI). The MSI-Raster application within the Leginon Software package (Suloway et al. [2005]) was used to automatically image selected regions of interest at a final nominal magnification of 15,000 x applying a defocus of -4 μm. Raw micrographs were stitched using the Trakem2 plugin implemented in the Fiji software platform (Saalfeld et al. [2010]; Schindelin et al. [2012]).

6.5 Endodermal Progenitor Generation

For E-iPSC differentiation into endodermal progenitors (EPs) the three step protocol from Cheng et al. [2012] was used. The cells have to be cultured feeder-free on Matrigel-coated plates. The first step of differentiation starts at a cell colony density of 30 - 50 %. To generate the definitive endoderm (DE) stage the cells were treated with the following medium for the first day:

Table 6.9: Medium for definitive endoderm part 1

Amount	Component	Company	Product Code
89 %	RPMI medium	Gibco	31870-025
10 %	SFD-Medium	-	-
1 %	Penicillin and Streptomycin	Gibco	15070-063
40 ng/ml	Wnt3a	R&D	5036-WN-010
100 ng/ml	ACTIVIN A	R&D	338-AC-010

The next two days the cells were treated with the following medium:

Table 6.10: Medium for definitive endoderm part 2

Amount	Component	Company	Product Code
99 %	RPMI medium	Gibco	31870-025
1 %	Penicillin and Streptomycin	Gibco	15070-063
100 ng/ml	ACTIVIN A	R&D	338-AC-010
10 ng/ml	VEGF	R&D	293-VE-050
10 ng/ml	FGF	Peprotech	100-18B
0.5 ng/ml	BMP4	R&D	314-BP-050

The next two days the cells were treated with the following medium:

Table 6.11: Medium for definitive endoderm part 3

Amount	Component	Company	Product Code
99 %	SFD-Medium	-	-
1 %	Penicillin and Streptomycin	Gibco	15070-063
100 ng/ml	ACTIVIN A	R&D	338-AC-010
10 ng/ml	VEGF	R&D	293-VE-050
10 ng/ml	FGF	Peprotech	100-18B
0.5 ng/ml	BMP4	R&D	314-BP-050

The SFD-Medium was prepared with the following components:

Table 6.12: SFD-Medium

Amount	Component	Company	Product Code
74 %	IMDM medium	Gibco	21980-065
25 %	Ham's F12 medium	Cellgro	10-080-CV
1 %	Penicillin and Streptomycin	Gibco	15070-063
0.1 %	BSA	Sigma-Aldrich	A7979
0.5 x	B27 A	Gibco	12587-010
0.5 x	N2	Gibco	17502-048
50 μg/ml	L-Ascorbic Acid Phosphate	Wako	013-19641
0.45 mM	1-Thioglycerol	Sigma-Aldrich	M6145

After five days the DE stage achieved. To get the next stage of transient cells (TCs) the cells were treated in a special medium for two, three and four weeks. The original protocol from Cheng et al. [2012] described this period for 4 weeks. The medium to generate TC consists of the following components:

Table 6.13: Medium for transient cells

Amount	Component	Company	Product Code
99 %	SFD-Medium	-	-
1 %	Penicillin and Streptomycin	Gibco	15070-063
1 %	DMSO	Santa Cruz	sc-202581
100 ng/ml	HGF	Pepro Tech	100-39
50 ng/ml	BMP4	R&D	314-BP-050
20 ng/ml	TGFα	Pepro Tech	100-16A
10 ng/ml	VEGF	R&D	293-VE-050
10 ng/ml	EGF	R&D	236-EG-200
10 ng/ml	FGF	Peprotech	100-18B
0.1 μM	Dexamethasone	R&D	1126/100

After two, three or four weeks the medium was changed to the maintenance medium of EPs. After one passage culturing the TC in EP maintenance medium the pre-EPs were generated. The following components constitute the EP maintenance medium:

Table 6.14: Medium for endodermal progenitor maintenance

Amount	Component	Company	Product Code
99 %	SFD-Medium	-	-
1 %	Penicillin and Streptomycin	Gibco	15070-063
50 ng/ml	BMP4	R&D	314-BP-050
10 ng/ml	VEGF	R&D	293-VE-050
10 ng/ml	EGF	R&D	236-EG-200
10 ng/ml	FGF	Peprotech	100-18B

The EPs were generated when organoids were formed.

6.6 Activin A Assay

The TGF-β superfamily is an huge protein group including the transforming growth factor β (TGF-βs) and Activins. Members of the TGF-β superfamily are involved in embryonic development, maintenance and differentiation of embryonic stem cells, somatic stem cells and cancer stem cells as well as in development and maintenance of various organs (Massagu et al. [1987]; Massagu [1992]; Wilson and Hemmati-Brivanlou [1995]; Brandenberger et al. [2004]; Qi et al. [2004]; Clotman and Lemaigre [2006]; Xu et al. [2008]; Watabe and Miyazono [2009]; Wu and Hill [2009]). The Quantikine Human/Mouse/Rat Activin A Immunoassay (R&D; DAC00B) employs a 3-step quantitative sandwich enzyme immunoassay technique. The capture antibody is biotinylated and bound to streptavidin-coated plates. First, the plate was washed once and 100 μl Assay Diluent was pipetted into each well. Second, 100 μl standard (1,000 pg/ml; 500 pg/ml; 250 pg/ml; etc.), water (blank) and samples were pipetted to the Assay Diluent. The plate were incubated for 3 hours on a horizontal orbital microplate shaker set at 500 rpm. After washing away any unbound substances, an HRP-conjugate specific for the A subunit is added to the wells. Following a wash to remove any unbound conjugate, a substrate solution is added to the wells and color develops in proportion to the amount of Activin A bound. The color development is stopped and the intensity of the color is measured.

6.7 Cytokine Assay

The cytokine assay was done by Lucas Spitzhorn using the Proteome Profiler Array (Human XL Cytokine Array Kit; R&D Systems, Minneapolis, USA). The medium for the analysis was collected from fetal MSCs after they had reached a confluency of about 95 %. Therefore the cell culture supernatant was centrifuged at 500 x g to remove particles. The membrane was analysed by detecting the emitted chemiluminescence with the camera Fusion FX (Fusion FX; Vilber Lourmat) and the software Fusion-FX (Fusion-FX Fischer Biotec, Australia). The images were further analysed for the different pixel densitys using ImageJ (ImageJ; JAVA, National Institutes of Helath, USA).

7 Supplementary
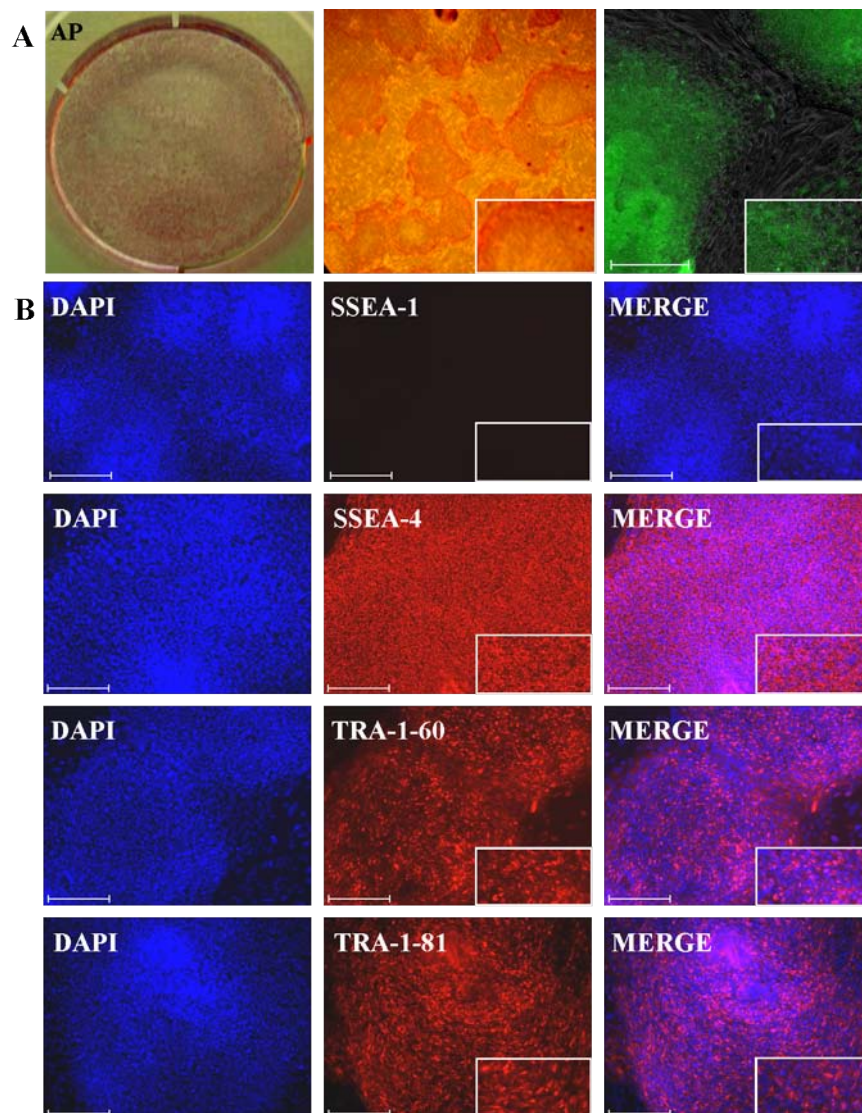
Figure S1: **Immunofluorescence-based detection of surface markers in H1.**
A) Staining of the surface protein alkaline phosphatase (AP) overwiev of the well, microscopy image and live stained cells (from left to right). **B)** All protein stainings for the surface markers SSEA-4, TRA-l-60 and TRA-1-81 were positive, SSEA-1 was negative. DAPI stained the nucleus. Scale bar: 200 μm, Alexa Flour 594 (red), Alexa Fluor 488 (green).

Figure S2: **Immunofluorescence-based detection of pluripotency markers in H1.**
All protein stainings for pluripotency markers OCT4, NANOG, SOX2, KLF4, c-MYC, LIN28 and PODXL were positive. DAPI stained the nucleus. Scale bar: 200 μm, Alexa Flour 594 (red), Alexa Fluor 488 (green).
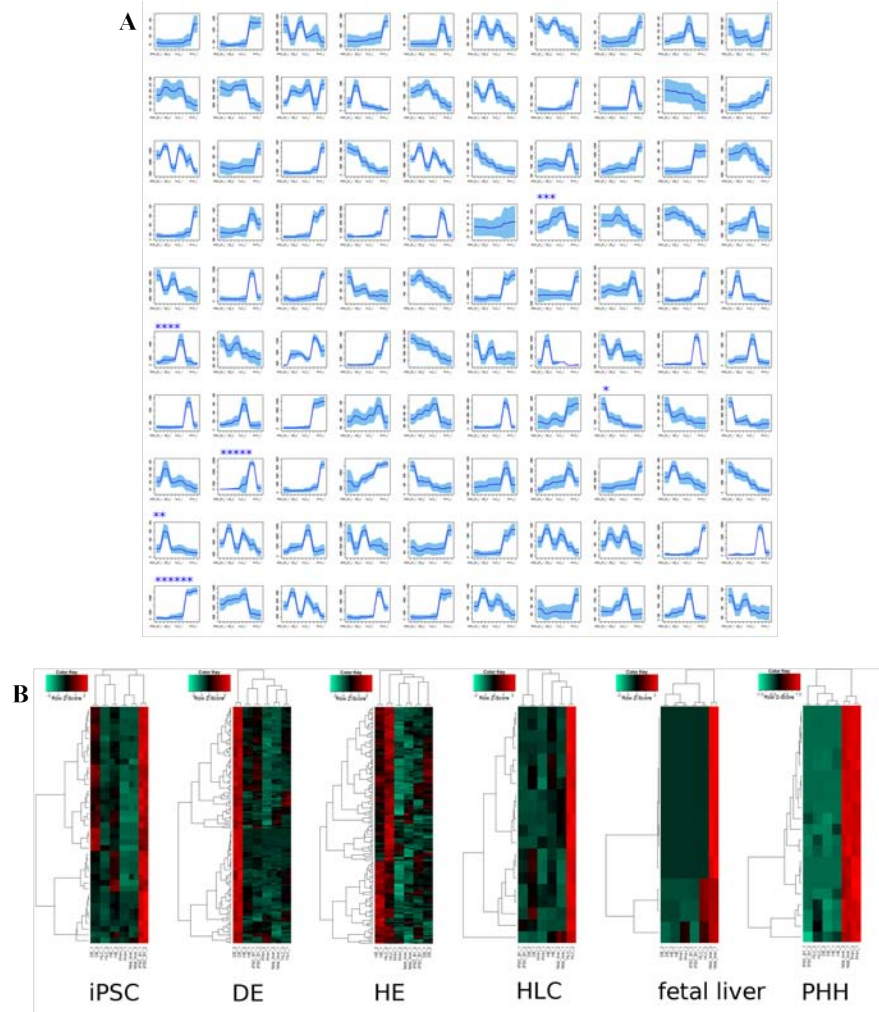
Figure S3: **Summary of k-means clustering.**
A) Listing of 100 k-means cluster of HLC differentiation compared with fetal liver and PHH generated by transcriptome profile analysis. The used k-means cluster for Figure 3.24B are marked with asterisk. One asterisk = iPSC k-means cluster, two asterisk = DE k-means cluster, three asterisk = HE k-means cluster, four asterisk = HLC k-means cluster, five asterisk = fetal liver k-means cluster and six asterisk = PHH k-means cluster. **B)** Heat map of the selected k-means cluster in A. Abbreviations: PHH = primary human hepatocytes; iPSC = induced pluripotent stem cells; DE = definitive endoderm; HE = hepatic endoderm; HLC = hepatocyte-like cells.
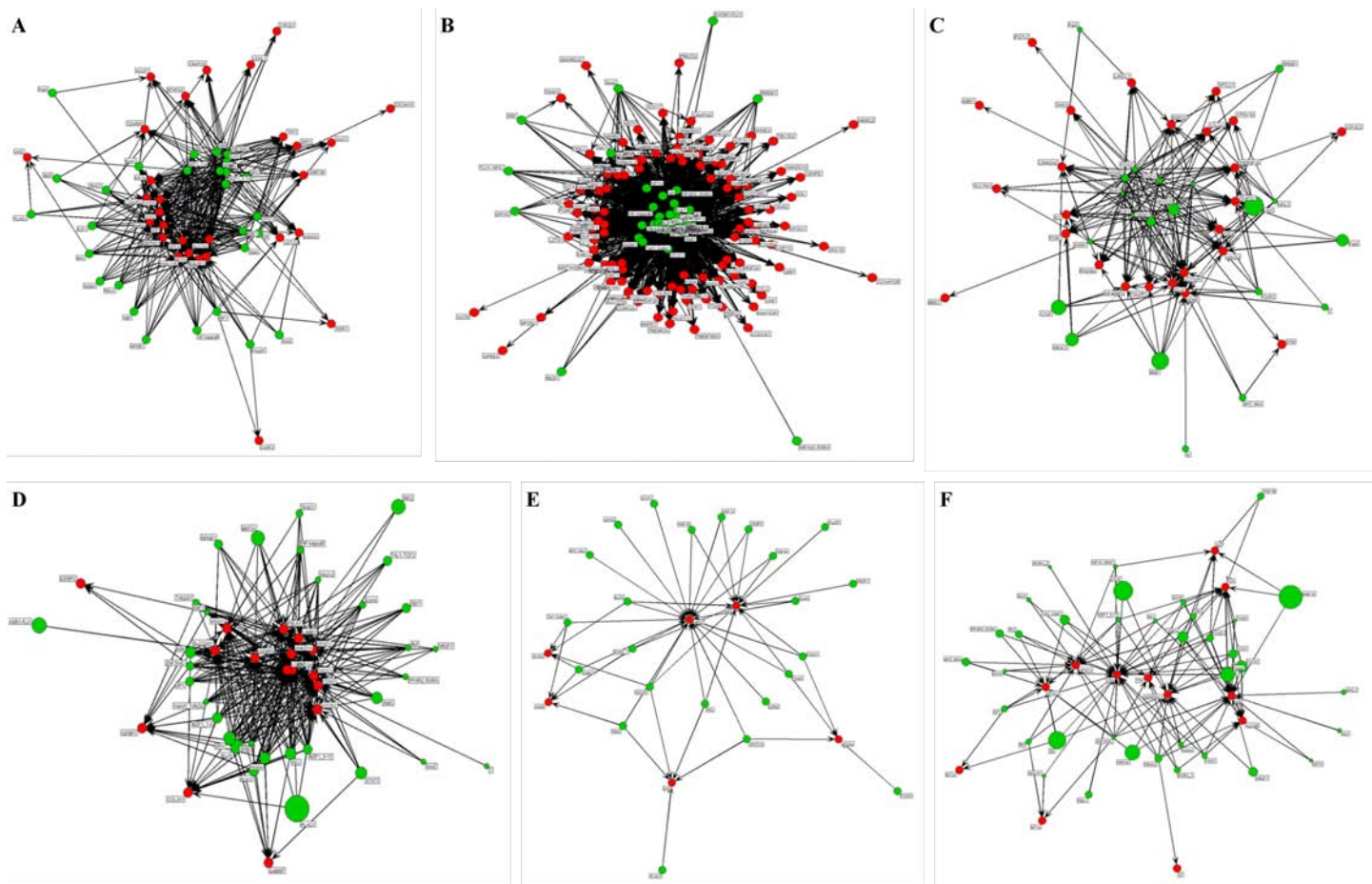
continued from previous page

Figure S4: **Summary of k-means clustering.**

Transcription factor over-representation analysis via the oPOSSUM data base (Kwon et al. [2012]).

A) The network for iPSCs shows the regulatory relations between OCT4 (POU5F1), SOX2, NANOG, KLF4. **B)** The network for DE demonstrates the regulatory relations between SP1, INSM1, MZF1, KLF4 and REST. **C)** The network for HE represents the regulatory relations between LHX3, MIZF and CTCF. **D)** The network for HLC illustrates the regulatory relations between PLAG1, EWSR1-FLI1 and IRF2. **E)** The network for fetal liver shows the regulatory relations between TAL1::GATA1, HNF1A, ZFN143, GATA1 and HNF1B. **F)** The network for PHH represents the regulatory relations between HNF1A, CTCF, ZFX, HNF4A, FOXA2, FOXA1 and CEBPA. Abbreviations: iPSC = induced pluripotent stem cells; DE = definitive endoderm; HE = hepatic endoderm; HLC = hepatocyte-like cells; PHH = primary human hepatocytes.
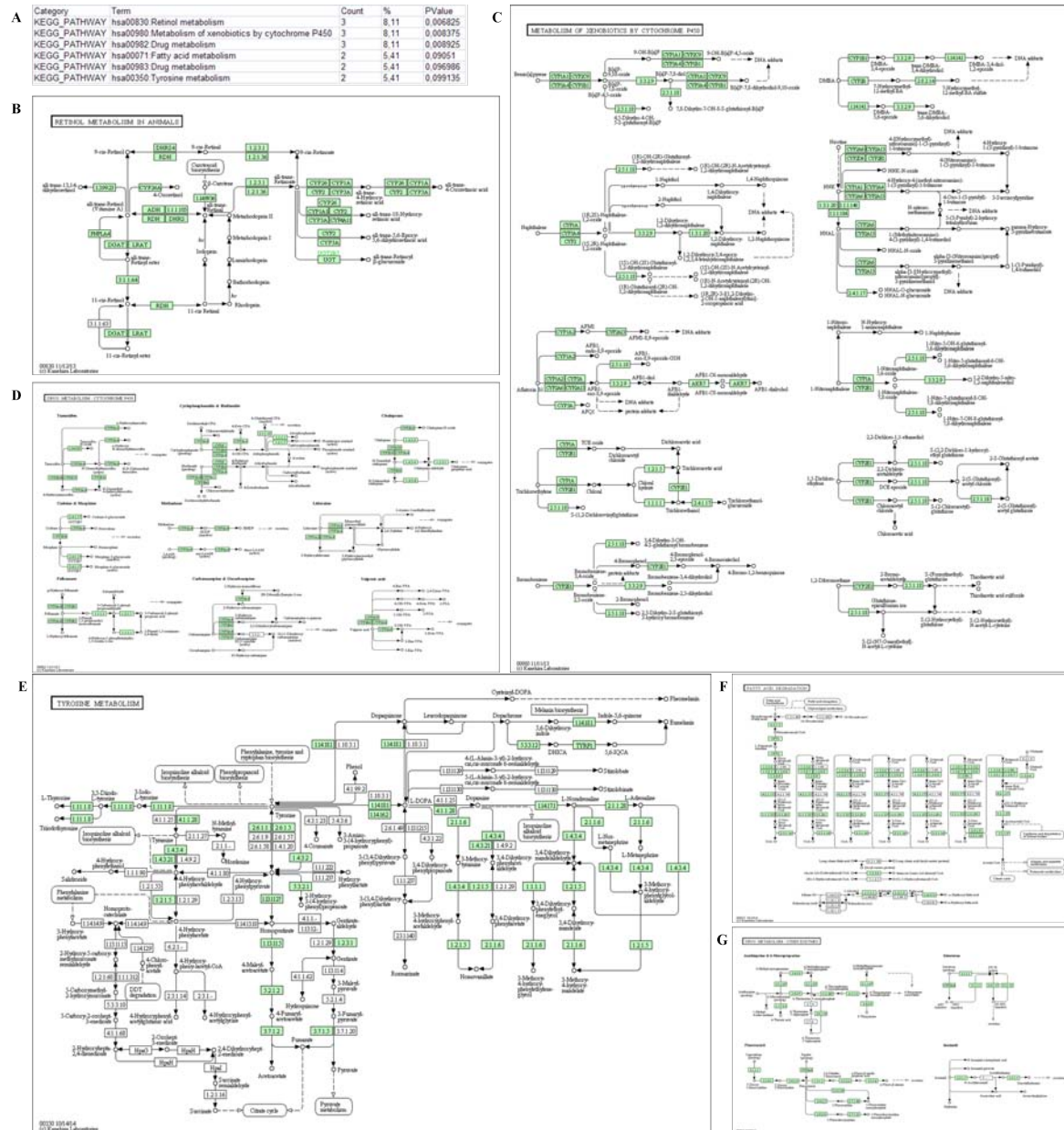
Figure S5: **Illustration of pathways.**
EpiHFF1-iPSC derived HLCs were used for transcription factor over-representation analysis via the oPOSSUM data base (Kwon et al. [2012]).

Figure S6: **Summary of k-means clustering.**
EpiHFF1-iPSC derived HLCs were used for transcription factor over-representation analysis via the oPOSSUM data base (Kwon et al. [2012]).
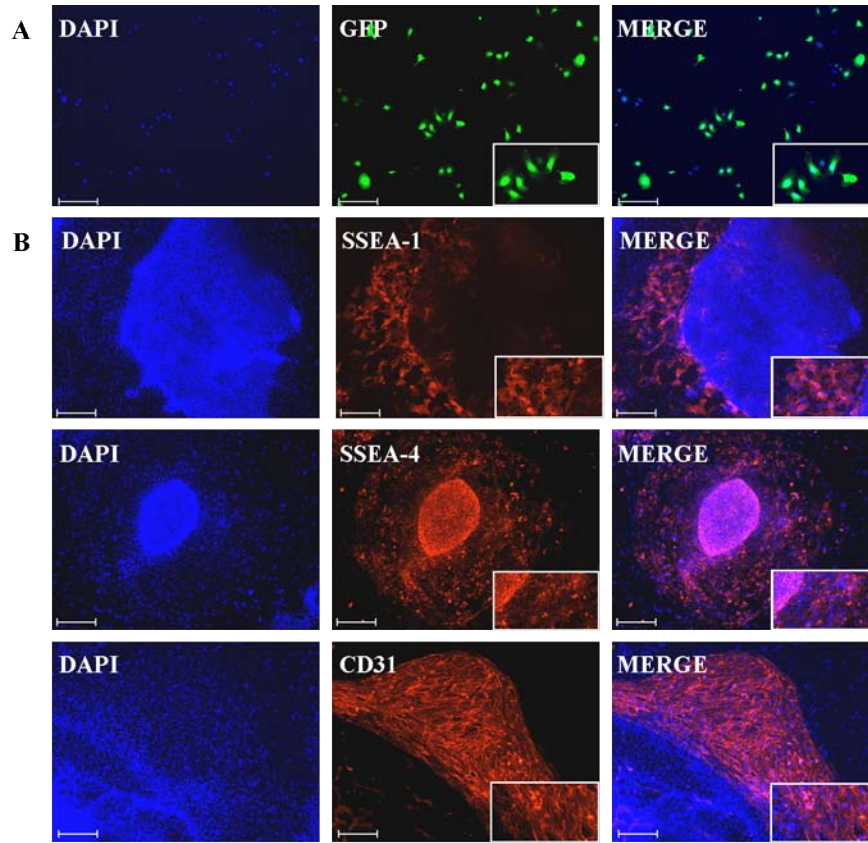
Figure S7: **Immunofluorescence-based detection of proteins in iPSC derived from HU-VEC.**
A) Destection of successful nucleofected HUVEC with GFP-Vector control. **B)** The positive detection of the surface marker in differentiated iHUVEC. SSEA-1 as a differentiation marker of human stem cells, SSEA-4 as a pluripotency marker is still detectable and CD31 as a marker of HUVEC. DAPI stained the nucleus. Scale bar: 200 μm Alexa Flour 594 (red).
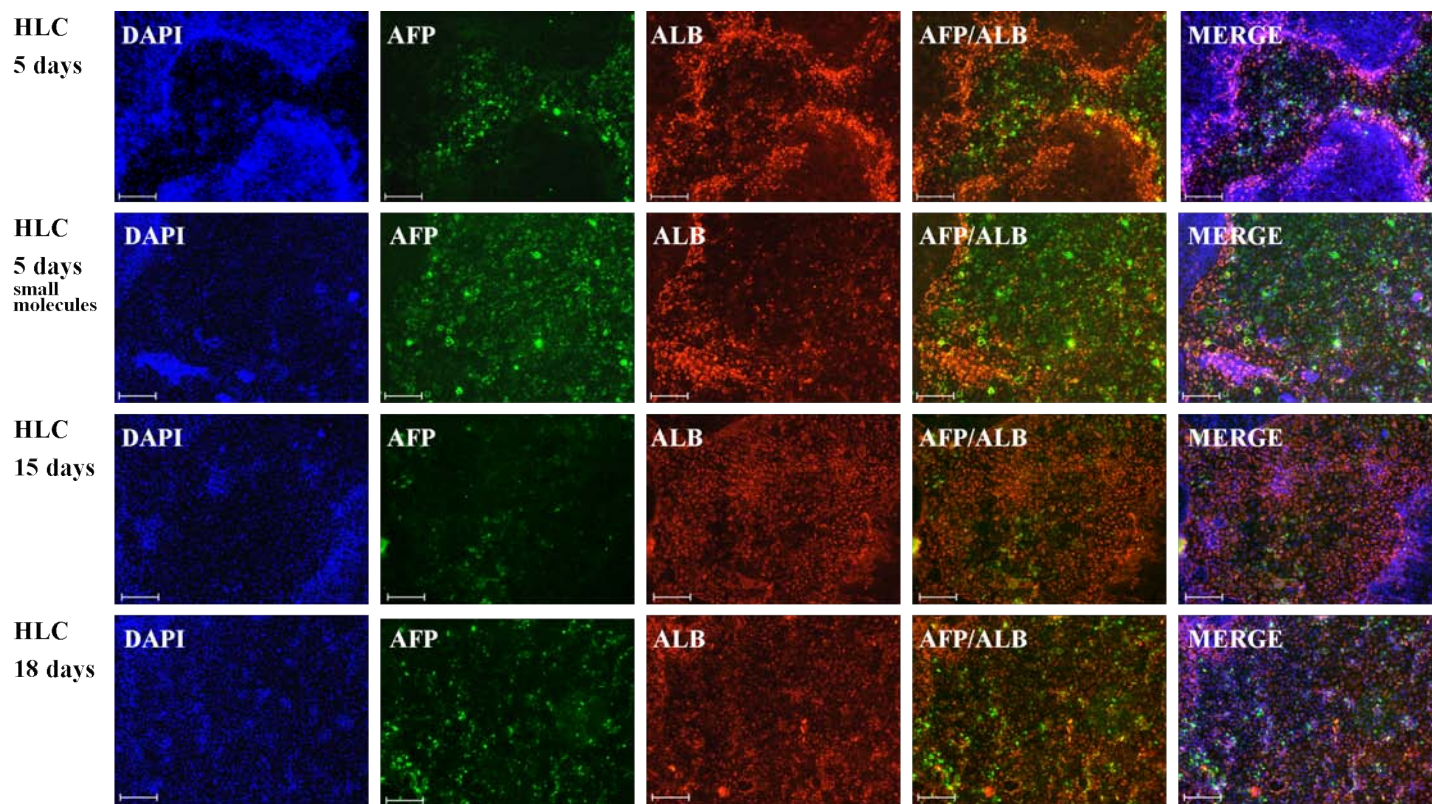
Figure S8: **Comparative immunofluorescence-based detection of liver specific markers AFP and ALB.**
Comparison of protein stainings of the liver specific marker α-Fetoprotein (AFP) and Albumin (ALB) in HLCs generated under different conditions and long-term culture. HLCs were generated with the treatment of cytokines (epiHUV-3a HLC 5d) or without cytokines and small molecules (epiHUV-3a HLC SM 5d). Additionally, HLCs which were generated with the common procedure (treatment with cytokines) were cultured longer, 15 days (epiHUV-3a HLC 15d) and 18 days (epiHUV-3a HLC 18d). In all HLCs the expression of AFP and ALB was detectable. DAPI stained the nucleus. Scale bar: 200 μm, Alexa Flour 594 (red), Alexa Fluor 488 (green).

H1 MEF

H1 fMSC
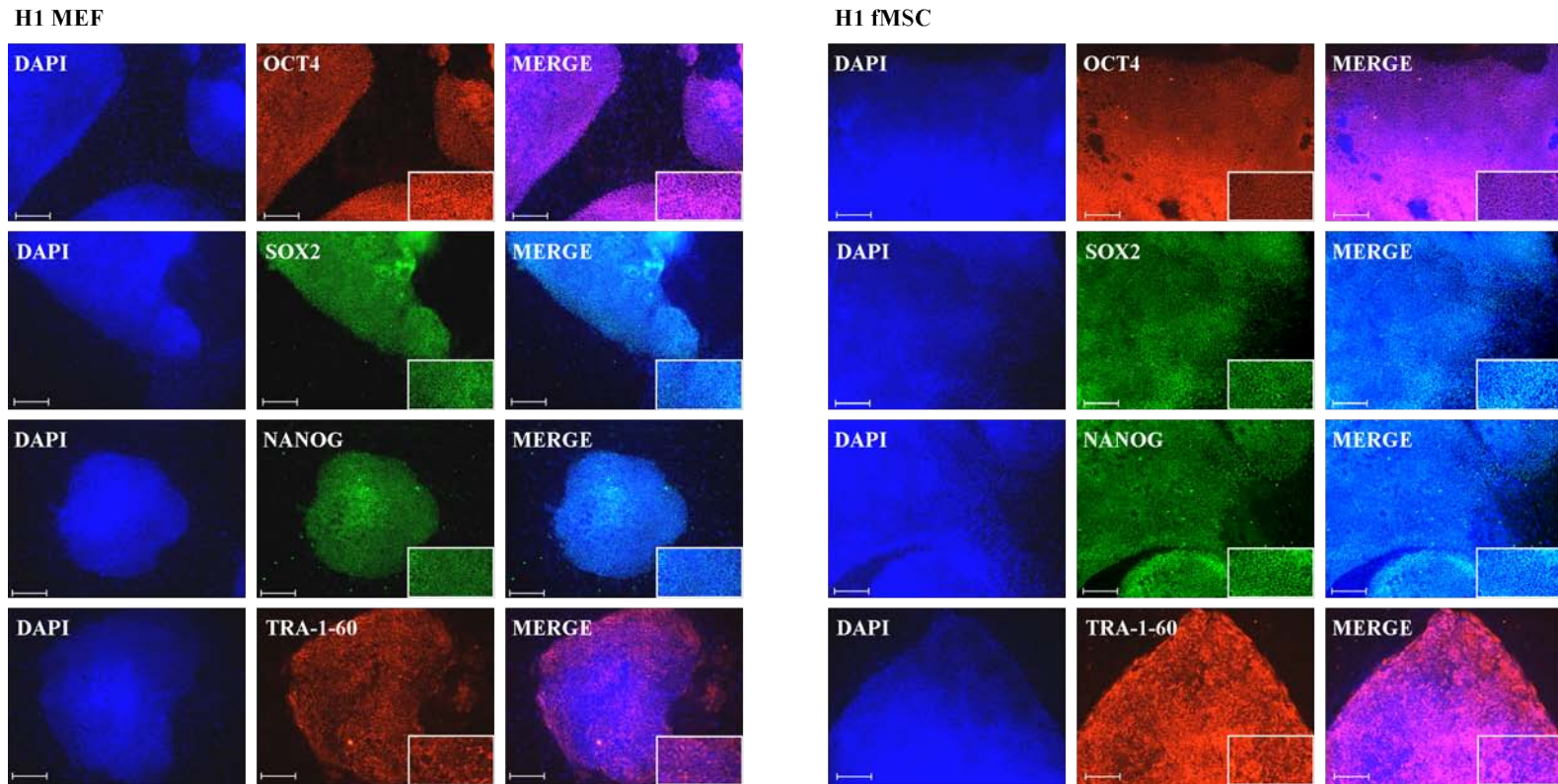
Figure S9: **Immunofluorescence-based detection of pluripotency markers in hESC-H1.**
All protein stainings for pluripotency markers OCT4, SOX2, NANOG, and the surface marker TRA-1-60 were positive. The culture of H1 on mouse embryonic fibroblasts (MEFs) is depicted on the left hand side and the culture of H1 on human fetal mesenchymal stem cells (MEFs) is depicted on the right hand side. DAPI stained the nucleus. Scale bar: 200 μm, Alexa Flour 594 (red), Alexa Fluor 488 (green).
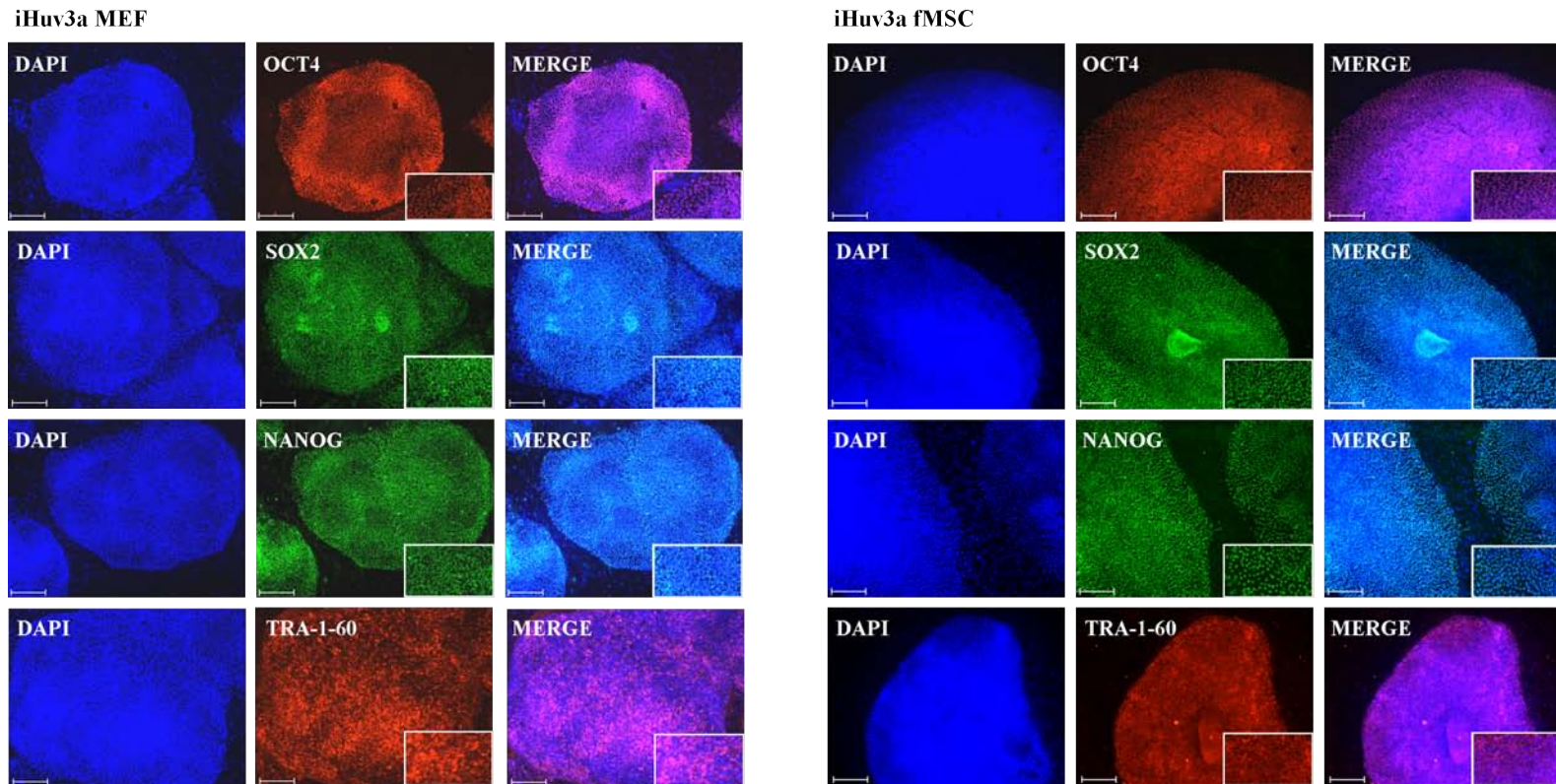
Figure S10: **Immunofluorescence-based detection of pluripotency markers in epiHUV-iPS-3a.**
All protein stainings for pluripotency markers OCT4, SOX2, NANOG, and the surface marker TRA-1-60 were positive. The culture of epiHUV-iPS-3a on mouse embryonic fibroblasts (MEFs) is depicted on the left hand side and the culture of epiHUV-iPS-3a on human fetal mesenchymal stem cells (MEFs) is depicted on the right hand side. DAPI stained the nucleus. Scale bar: 200 μm, Alexa Flour 594 (red), Alexa Fluor 488 (green).

iHuv1f MEF

iHuv1f fMSC
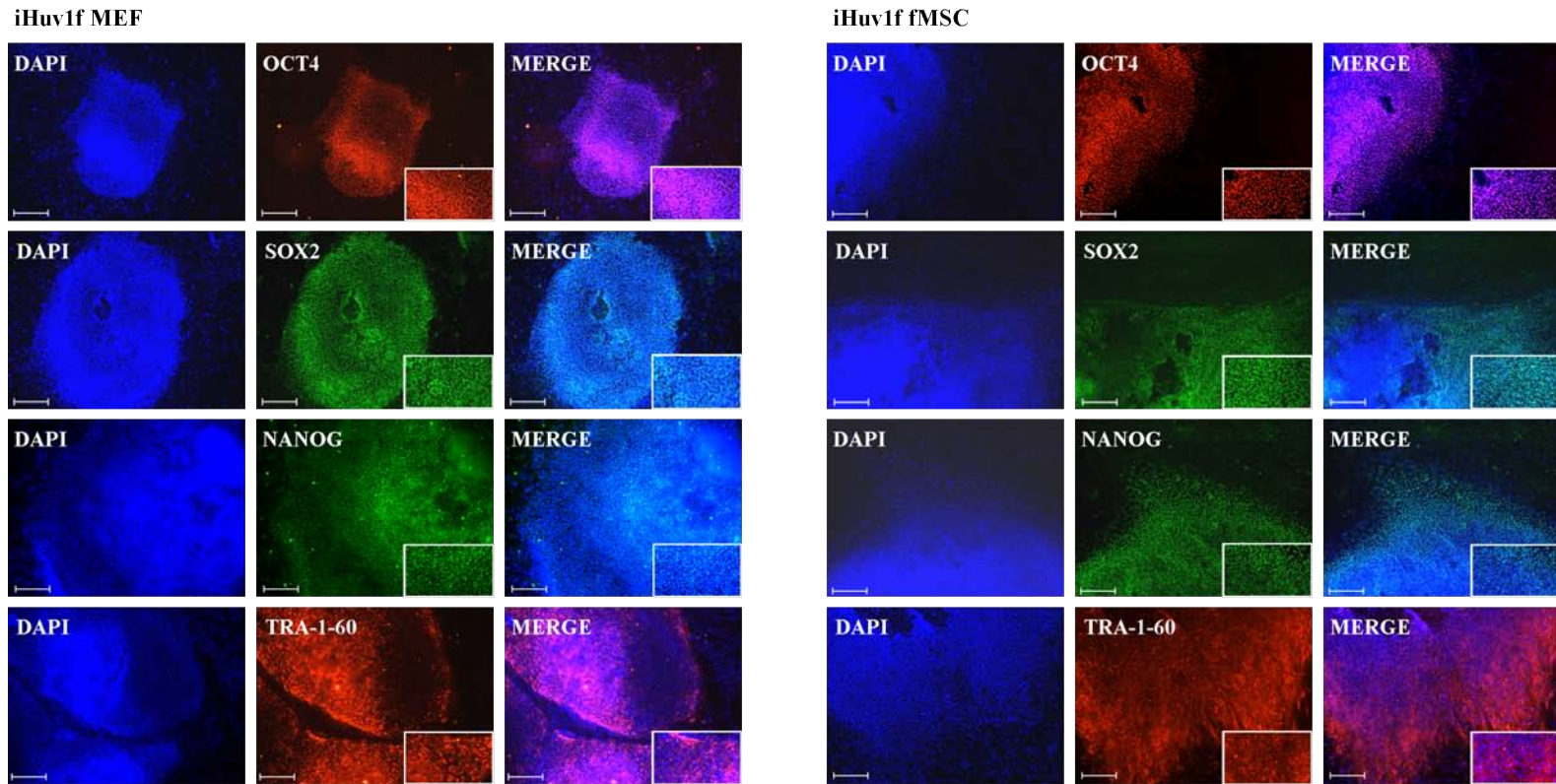
Figure S11: **Immunofluorescence-based detection of pluripotency markers in epiHUV-iPS-1f.**
All protein stainings for pluripotency markers OCT4, SOX2, NANOG, and the surface marker TRA-1-60 were positive. The culture of epiHUV-iPS-1f on mouse embryonic fibroblasts (MEFs) is depicted on the left hand side and the culture of epiHUV-iPS-1f on human fetal mesenchymal stem cells (MEFs) is depicted on the right hand side. DAPI stained the nucleus. Scale bar: 200 μm, Alexa Flour 594 (red), Alexa Fluor 488 (green).
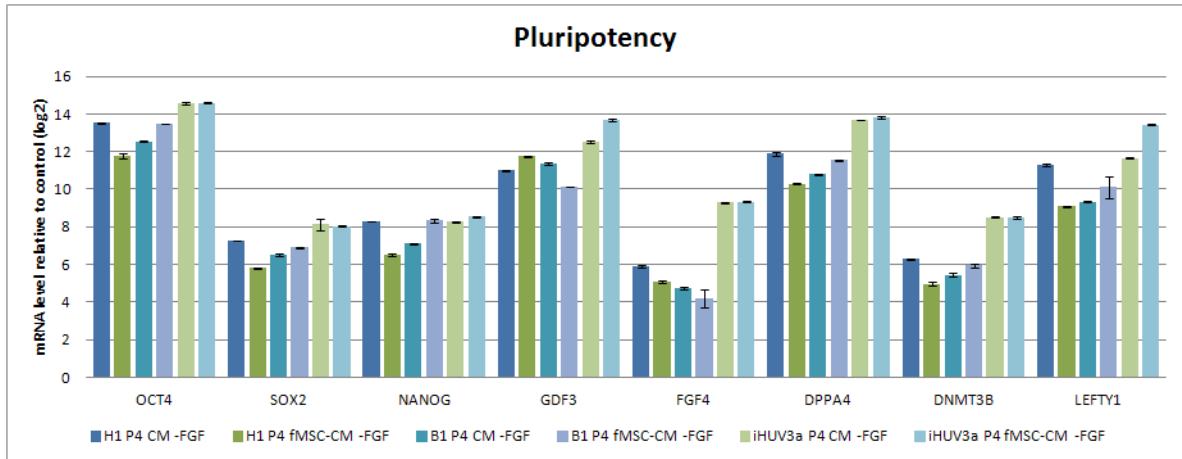
Figure S12: **Quantitative real-time PCR of pluripotency markers.**
Expression pattern of pluripotency markers relative to HFF1 from hESC-line H1, the iPSC-line epiHFF1-iPS-B1 and the iPSC-line epiHUV-iPS-3a are shown. The cells were cultured in conditioned medium (CM) made from mouse embryonic fibroblats (MEFs), which is the common used CM, and fetal mesenchymal stem cells (fMSCs) made CM (fMSC-CM). Three biological replicates in technical triplicates of each sample were analyzed. The standard deviation is depicted by the error bars.
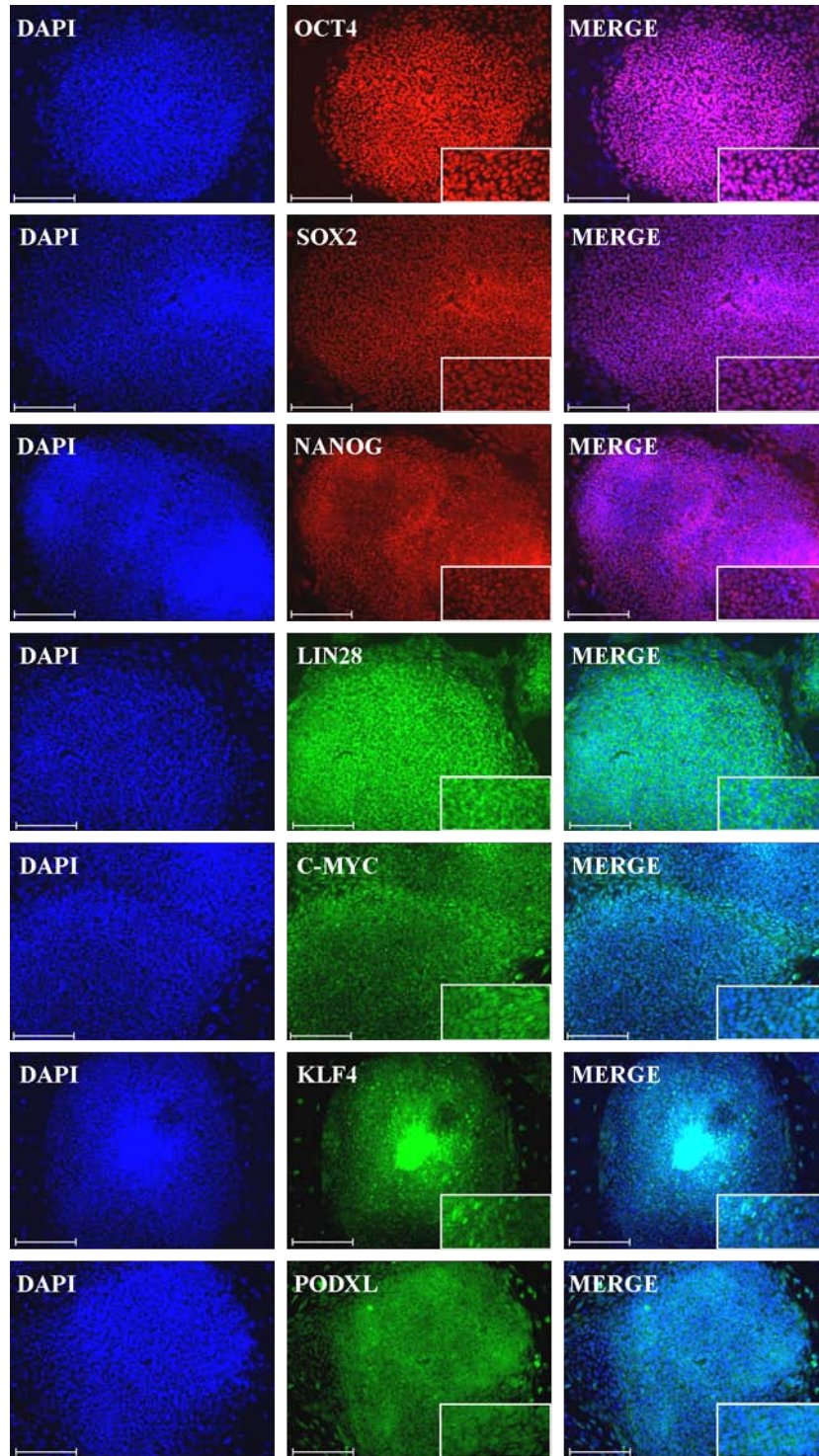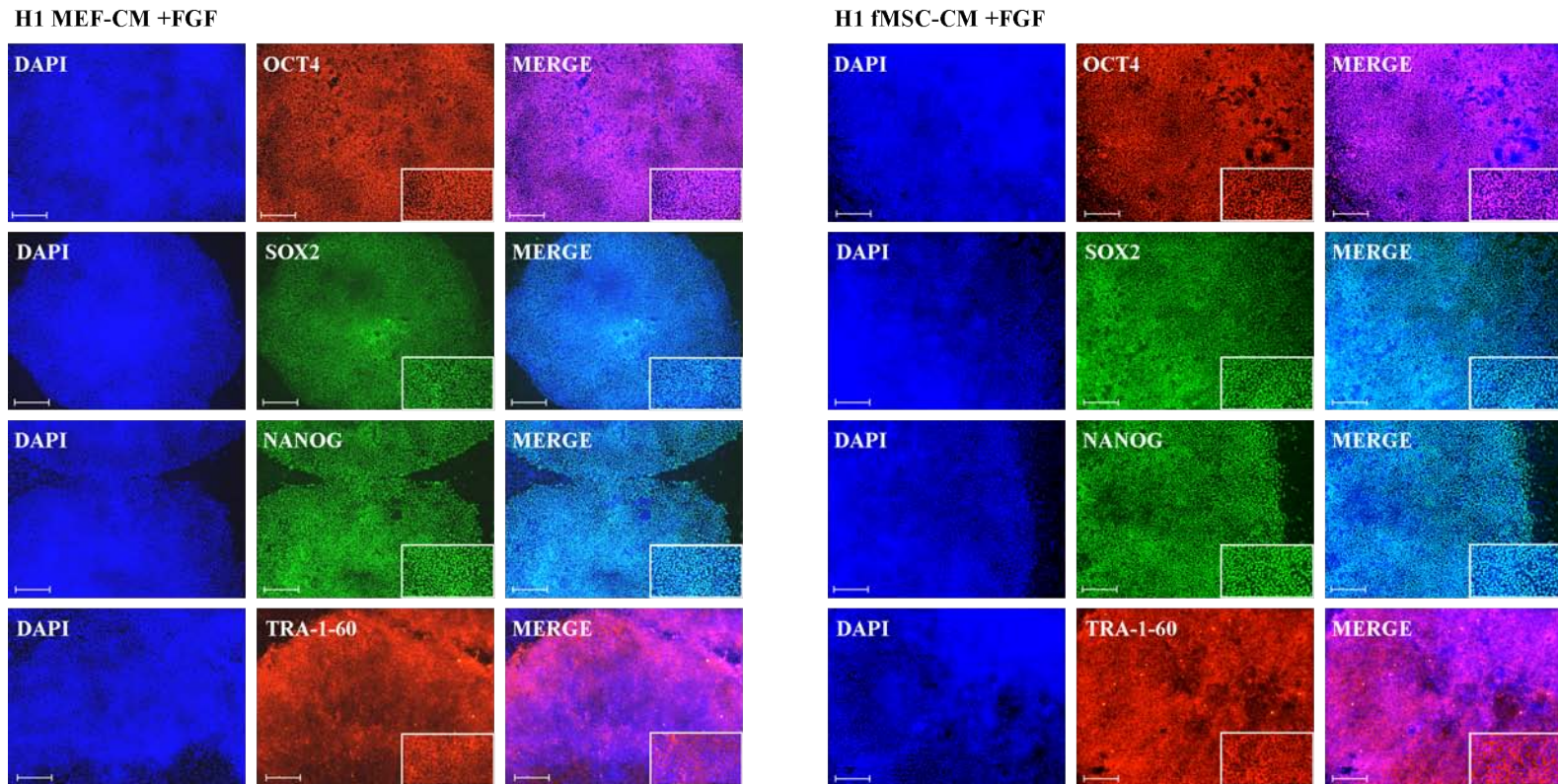
Figure S13: **Immunofluorescence-based detection of pluripotency markers in hESC-H1.**
All protein stainings for pluripotency markers OCT4, SOX2, NANOG, and the surface marker TRA-1-60 were positive. The culture of H1 on Matrigel with mouse embryonic fibroblasts (MEFs) made conditioned medium (CM) with additional FGF is depicted on the left hand side (H1 MEF-CM +FGF) and the culture of H1 on Matrigel with human fetal mesenchymal stem cells (MEFs) made CM with additional FGF is depicted on the right hand side (H1 fMSC-CM +FGF). DAPI stained the nucleus. Scale bar: 200 μm, Alexa Flour 594 (red), Alexa Fluor 488 (green).
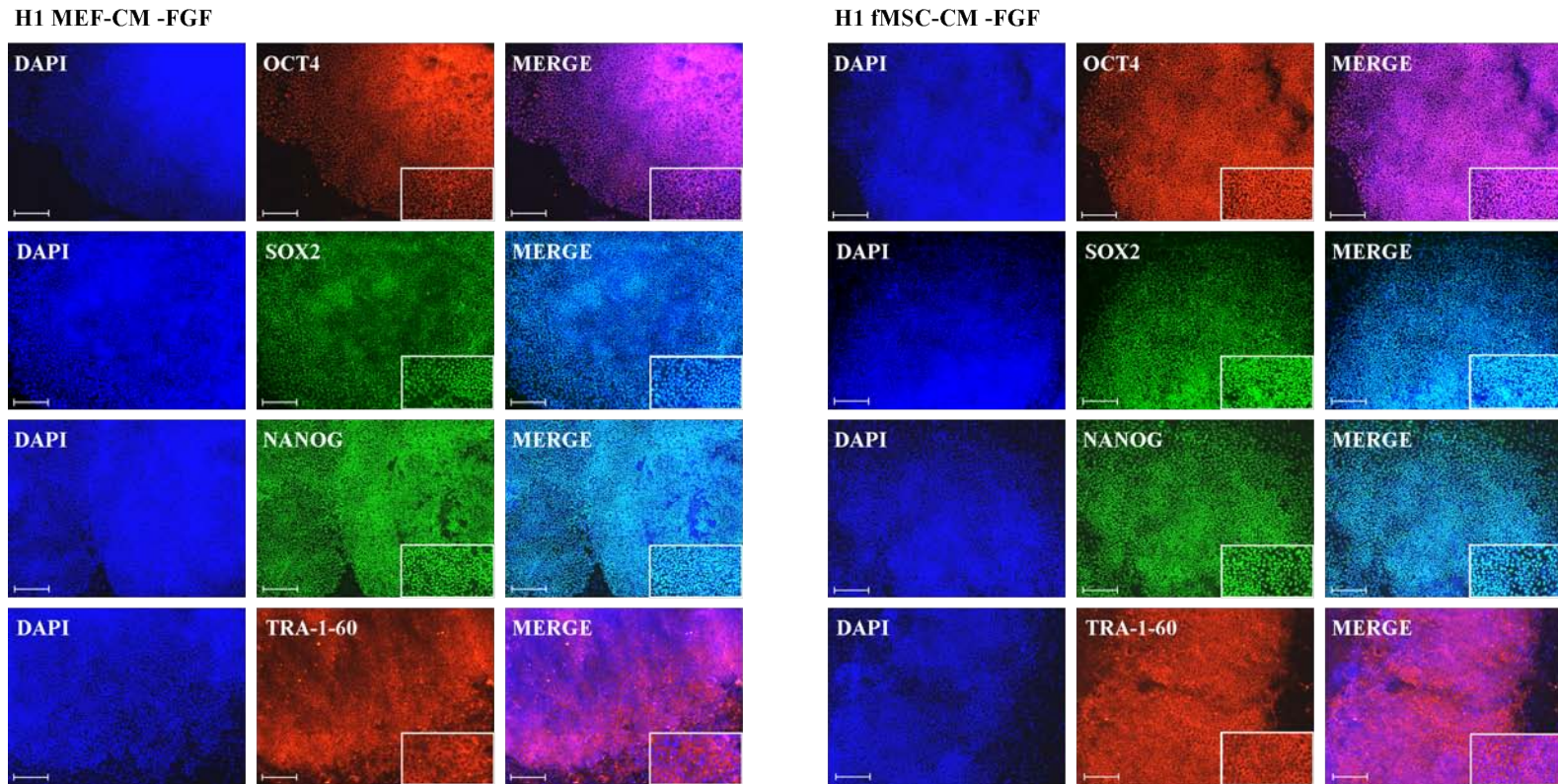
Figure S14: **Immunofluorescence-based detection of pluripotency markers in hESC-H1.**
All protein stainings for pluripotency markers OCT4, SOX2, NANOG, and the surface marker TRA-1-60 were positive. The culture of H1 on Matrigel with mouse embryonic fibroblasts (MEFs) made conditioned medium (CM) without additional FGF is depicted on the left hand side (H1 MEF-CM -FGF) and the culture of H1 on Matrigel with human fetal mesenchymal stem cells (MEFs) made CM without additional FGF is depicted on the right hand side (H1 fMSC-CM -FGF). DAPI stained the nucleus. Scale bar: 200 μm, Alexa Flour 594 (red), Alexa Fluor 488 (green).
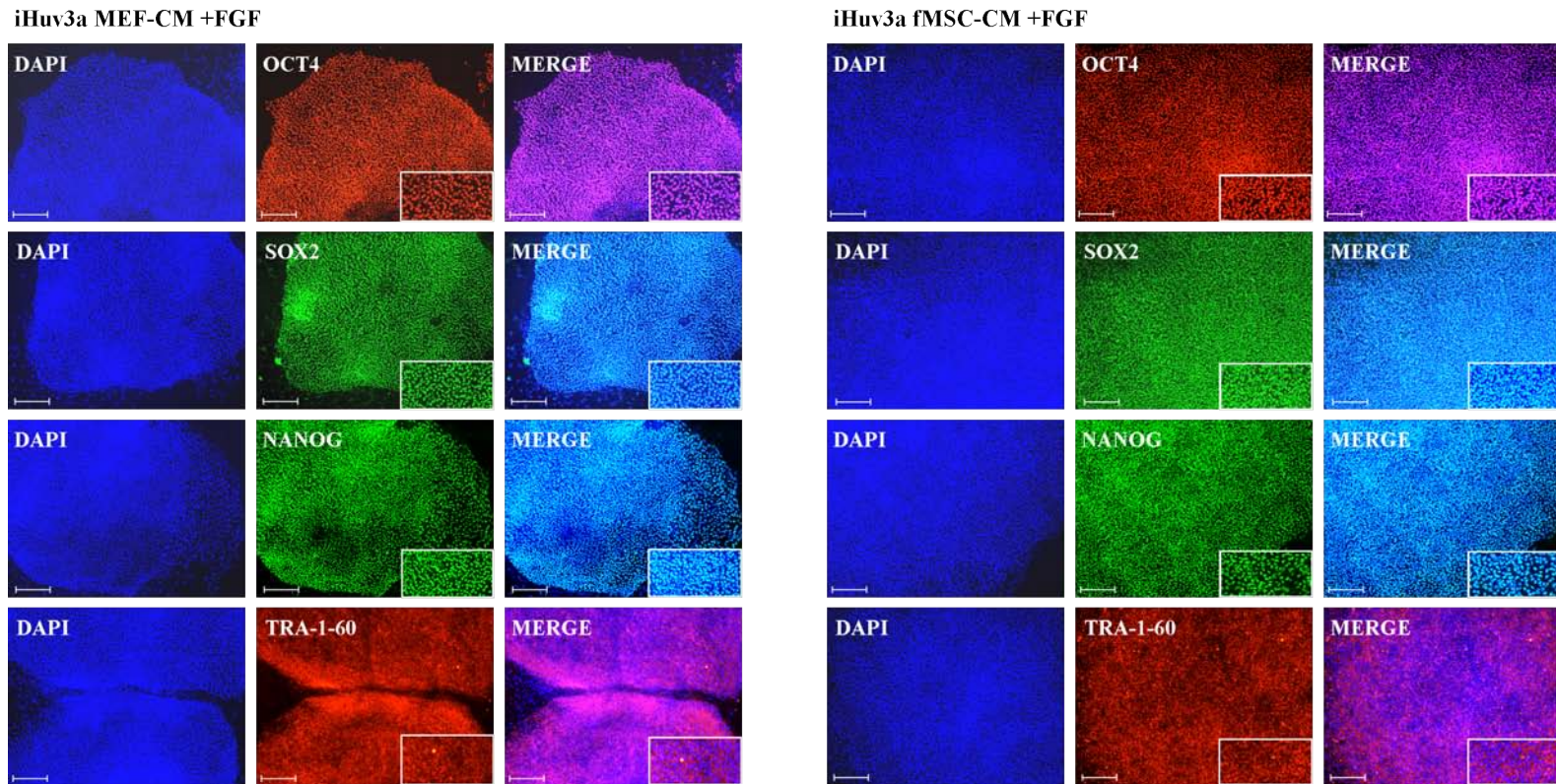
Figure S15: **Immunofluorescence-based detection of pluripotency markers in epiHUV-iPS-3a.**
All protein stainings for pluripotency markers OCT4, SOX2, NANOG, and the surface marker TRA-1-60 were positive. The culture of epiHUV-iPS-3a on Matrigel with mouse embryonic fibroblasts (MEFs) made conditioned medium (CM) with additional FGF is depicted on the left hand side (iHuv3a MEF-CM +FGF) and the culture of epiHUV-iPS-3a on Matrigel with human fetal mesenchymal stem cells (MEFs) made CM with additional FGF is depicted on the right hand side (iHuv3a fMSC-CM +FGF). DAPI stained the nucleus. Scale bar: 200 μm, Alexa Flour 594 (red), Alexa Fluor 488 (green).

iHuv3a MEF-CM -FGF

iHuv3a fMSC-CM -FGF
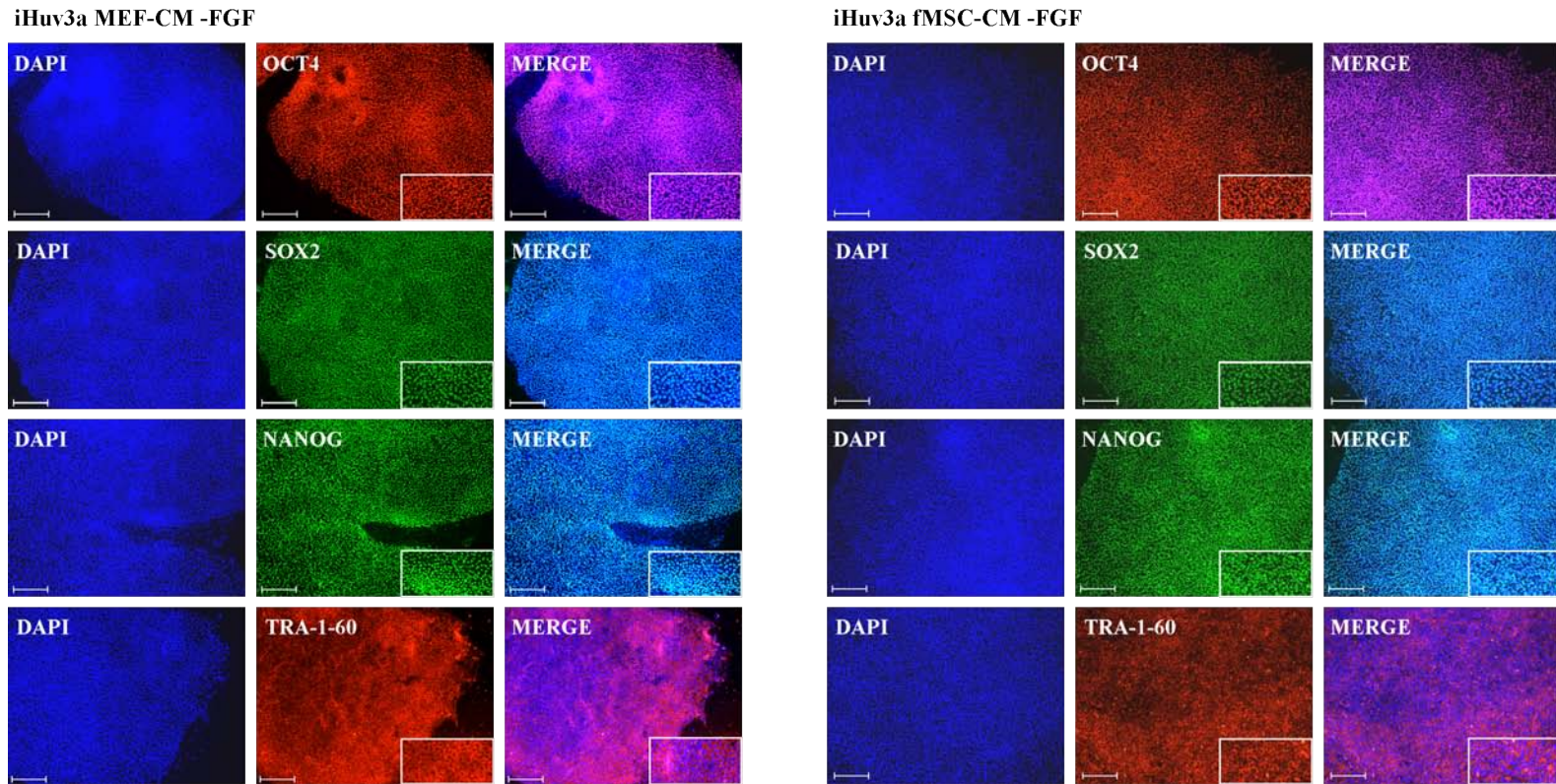
Figure S16: **Immunofluorescence-based detection of pluripotency markers in epiHUV-iPS-3a.**
All protein stainings for pluripotency markers OCT4, SOX2, NANOG, and the surface marker TRA-1-60 were positive. The culture of epiHUV-iPS-3a on Matrigel with mouse embryonic fibroblasts (MEFs) made conditioned medium (CM) without additional FGF is depicted on the left hand side (iHuv3a MEF-CM -FGF) and the culture of epiHUV-iPS-3a on Matrigel with human fetal mesenchymal stem cells (MEFs) made CM without additional FGF is depicted on the right hand side (iHuv3a fMSC-CM -FGF). DAPI stained the nucleus. Scale bar: 200 μm, Alexa Flour 594 (red), Alexa Fluor 488 (green).

Supplementary Tables are located on the second pdf.

Bibliography

T. Aasen, A. Raya, M. J. Barrero, E. Garreta, A. Consiglio, F. Gonzalez, R. Vassena, J. Bili?, V. Pekarik, G. Tiscornia, M. Edel, S. Bou, and J. C. Izpisa Belmonte. Efficient and rapid generation of induced pluripotent stem cells from human keratinocytes. *Nat Biotechnol*, 26(11):1276–1284, Nov 2008. doi: 10.1038/nbt.1503. URL http://dx.doi.org/10.1038/nbt.1503.

B. A. Afouda, A. Ciau-Uitz, and R. Patient. Gata4, 5 and 6 mediate tgfbeta maintenance of endodermal gene expression in xenopus embryos. *Development*, 132(4):763–774, Feb 2005. doi: 10.1242/dev.01647. URL http://dx.doi.org/10.1242/dev.01647.

S. Aftab, L. Semenec, J. S.-C. Chu, and N. Chen. Identification and characterization of novel human tissue-specific rfx transcription factors. *BMC Evol Biol*, 8:226, 2008. doi: 10.1186/1471-2148-8-226. URL http://dx.doi.org/10.1186/1471-2148-8-226.

S. Agarwal, K. L. Holton, and R. Lanza. Efficient differentiation of functional hepatocytes from human embryonic stem cells. *Stem Cells*, 26(5):1117–1127, May 2008. doi: 10.1634/stemcells.2007-1102. URL http://dx.doi.org/10.1634/stemcells.2007-1102.

U. Ahlgren, S. L. Pfaff, T. M. Jessell, T. Edlund, and H. Edlund. Independent requirement for isl1 in formation of pancreatic mesenchyme and islet cells. *Nature*, 385 (6613):257–260, Jan 1997. doi: 10.1038/385257a0. URL http://dx.doi.org/10.1038/385257a0.

R. M. Albano, N. Groome, and J. C. Smith. Activins are expressed in preimplantation mouse embryos and in es and ec cells and are regulated on their differentiation. *Development*, 117(2):711–723, Feb 1993.

S. H. Ali and J. A. DeCaprio. Cellular transformation by sv40 large t antigen: interaction with host proteins. *Semin Cancer Biol*, 11(1):15–23, Feb 2001. doi: 10.1006/scbi.2000.0342. URL http://dx.doi.org/10.1006/scbi.2000.0342.

A. Amador-Arjona, F. Cimadamore, C.-T. Huang, R. Wright, S. Lewis, F. H. Gage, and A. V. Terskikh. Sox2 primes the epigenetic landscape in neural precursors enabling proper gene activation during hippocampal neurogenesis. *Proc Natl Acad Sci U S A*, 112(15):E1936–E1945, Apr 2015. doi: 10.1073/pnas.1421480112. URL http://dx.doi.org/10.1073/pnas.1421480112.

L. Amicone, F. M. Spagnoli, G. Spth, S. Giordano, C. Tommasini, S. Bernardini, V. De Luca, C. Della Rocca, M. C. Weiss, P. M. Comoglio, and M. Tripodi. Transgenic expression in the liver of truncated met blocks apoptosis and permits immortalization of hepatocytes. *EMBO J*, 16(3):495–503, Feb 1997. doi: 10.1093/emboj/16.3.495. URL http://dx.doi.org/10.1093/emboj/16.3.495.

M. Amit, M. K. Carpenter, M. S. Inokuma, C. P. Chiu, C. P. Harris, M. A. Waknitz, J. Itskovitz-Eldor, and J. A. Thomson. Clonally derived human embryonic stem cell lines maintain pluripotency and proliferative potential for prolonged periods of culture. *Dev Biol*, 227(2):271–278, Nov 2000. doi: 10.1006/dbio.2000.9912. URL http://dx.doi.org/10.1006/dbio.2000.9912.

E. R. Andersson and U. Lendahl. Therapeutic modulation of notch signalling–are we there yet? *Nat Rev Drug Discov*, 13(5):357–378, May 2014. doi: 10.1038/nrd4252. URL http://dx.doi.org/10.1038/nrd4252.

E. R. Andersson, R. Sandberg, and U. Lendahl. Notch signaling: simplicity in design, versatility in function. *Development*, 138(17):3593–3612, Sep 2011. doi: 10.1242/dev. 063610. URL http://dx.doi.org/10.1242/dev.063610.

S. J. Arnold and E. J. Robertson. Making a commitment: cell lineage allocation and axis patterning in the early mouse embryo. *Nat Rev Mol Cell Biol*, 10(2):91–103, Feb 2009. doi: 10.1038/nrm2618. URL http://dx.doi.org/10.1038/nrm2618.

S. J. Arnold, U. K. Hofmann, E. K. Bikoff, and E. J. Robertson. Pivotal roles for eomesodermin during axis formation, epithelium-to-mesenchyme transition and endoderm specification in the mouse. *Development*, 135(3):501–511, Feb 2008. doi: 10.1242/dev.014357. URL http://dx.doi.org/10.1242/dev.014357.

S. Artavanis-Tsakonas, M. D. Rand, and R. J. Lake. Notch signaling: cell fate control and signal integration in development. *Science*, 284(5415):770–776, Apr 1999.

A. S. Asch, T. Kinoshita, E. A. Jaffe, and V. Nussenzweig. Decay-accelerating factor is present on cultured human umbilical vein endothelial cells. *J Exp Med*, 163(1): 221–226, Jan 1986.

S. Asgari, M. Moslem, K. Bagheri-Lankarani, B. Pournasr, M. Miryounesi, and H. Baharvand. Differentiation and transplantation of human induced pluripotent stem cell-derived hepatocyte-like cells. *Stem Cell Rev*, 9(4):493–504, Aug 2013. doi: 10.1007/ s12015-011-9330-y. URL http://dx.doi.org/10.1007/s12015-011-9330-y.

V. Baldin, A. M. Roman, I. Bosc-Bierne, F. Amalric, and G. Bouche. Translocation of bfgf to the nucleus is g1 phase cell cycle specific in bovine aortic endothelial cells. *EMBO J*, 9(5):1511–1517, May 1990.

M. Bamshad, T. Le, W. S. Watkins, M. E. Dixon, B. E. Kramer, A. D. Roeder, J. C. Carey, S. Root, A. Schinzel, L. Van Maldergem, R. J. Gardner, R. C. Lin, C. E.

Seidman, J. G. Seidman, R. Wallerstein, E. Moran, R. Sutphen, C. E. Campbell, and L. B. Jorde. The spectrum of mutations in tbx3: Genotype/phenotype relationship in ulnar-mammary syndrome. *Am J Hum Genet*, 64(6):1550–1562, Jun 1999. doi: 10.1086/302417. URL http://dx.doi.org/10.1086/302417.

H. Ban, N. Nishishita, N. Fusaki, T. Tabata, K. Saeki, M. Shikamura, N. Takada, M. Inoue, M. Hasegawa, S. Kawamata, and S.-I. Nishikawa. Efficient generation of transgene-free human induced pluripotent stem cells (ipscs) by temperature-sensitive sendai virus vectors. *Proc Natl Acad Sci U S A*, 108(34):14234–14239, Aug 2011. doi: 10.1073/pnas.1103509108. URL http://dx.doi.org/10.1073/pnas.1103509108.

N. Barker, M. B. Rookmaaker, P. Kujala, A. Ng, M. Leushacke, H. Snippert, M. van de Wetering, S. Tan, J. H. Van Es, M. Huch, R. Poulsom, M. C. Verhaar, P. J. Peters, and H. Clevers. Lgr5(+ve) stem/progenitor cells contribute to nephron formation during kidney development. *Cell Rep*, 2(3):540–552, Sep 2012. doi: 10.1016/j.celrep. 2012.08.018. URL http://dx.doi.org/10.1016/j.celrep.2012.08.018.

N. Barker, S. Tan, and H. Clevers. Lgr proteins in epithelial stem cell biology. *Development*, 140(12):2484–2494, Jun 2013. doi: 10.1242/dev.083113. URL http://dx.doi.org/10.1242/dev.083113.

S. D. Barrett, A. J. Bridges, D. T. Dudley, A. R. Saltiel, J. H. Fergus, C. M. Flamme, A. M. Delaney, M. Kaufman, S. LePage, W. R. Leopold, S. A. Przybranowski, J. Sebolt-Leopold, K. Van Becelaere, A. M. Doherty, R. M. Kennedy, D. Marston, W. A. Howard, Jr, Y. Smith, J. S. Warmus, and H. Tecle. The discovery of the benzhydroxamate mek inhibitors ci-1040 and pd 0325901. *Bioorg Med Chem Lett*, 18(24):6501–6504, Dec 2008. doi: 10.1016/j.bmcl.2008.10.054. URL http://dx.doi.org/10.1016/j.bmcl.2008.10.054.

M. Barrios-Rodiles, K. R. Brown, B. Ozdamar, R. Bose, Z. Liu, R. S. Donovan, F. Shinjo, Y. Liu, J. Dembowy, I. W. Taylor, V. Luga, N. Przulj, M. Robinson, H. Suzuki, Y. Hayashizaki, I. Jurisica, and J. L. Wrana. High-throughput mapping of a dynamic signaling network in mammalian cells. *Science*, 307(5715):1621–1625, Mar 2005. doi: 10.1126/science.1105776. URL http://dx.doi.org/10.1126/science.1105776.

J. Beers, D. R. Gulbranson, N. George, L. I. Siniscalchi, J. Jones, J. A. Thomson, and G. Chen. Passaging and colony expansion of human pluripotent stem cells by enzyme-free dissociation in chemically defined culture conditions. *Nat Protoc*, 7(11): 2029–2040, Nov 2012. doi: 10.1038/nprot.2012.130. URL http://dx.doi.org/10.1038/nprot.2012.130.

P. D. Berk and W. Stremmel. Hepatocellular uptake of organic anions. *Prog Liver Dis*, 8:125–144, 1986.

J. A. Bernal. Rna-based tools for nuclear reprogramming and lineage-conversion: towards clinical applications. *J Cardiovasc Transl Res*, 6(6):956–968, Dec 2013. doi: 10.1007/s12265-013-9494-8. URL http://dx.doi.org/10.1007/s12265-013-9494-8.

M. N. Berry and D. S. Friend. High-yield preparation of isolated rat liver parenchymal cells: a biochemical and fine structural study. *J Cell Biol*, 43(3):506–520, Dec 1969.

N. A. Bhowmick, M. Ghiassi, A. Bakin, M. Aakre, C. A. Lundquist, M. E. Engel, C. L. Arteaga, and H. L. Moses. Transforming growth factor-beta1 mediates epithelial to mesenchymal transdifferentiation through a rhoa-dependent mechanism. *Mol Biol Cell*, 12(1):27–36, Jan 2001.

F. Bladt, D. Riethmacher, S. Isenmann, A. Aguzzi, and C. Birchmeier. Essential role for the c-met receptor in the migration of myogenic precursor cells into the limb bud. *Nature*, 376(6543):768–771, Aug 1995. doi: 10.1038/376768a0. URL http://dx.doi.org/10.1038/376768a0.

L. Blanger, M. Frain, P. Baril, M. C. Gingras, J. Bartkowiak, and J. M. Sala-Trepat. Glucocorticosteroid suppression of alpha1-fetoprotein synthesis in developing rat liver. evidence for selective gene repression at the transcriptional level. *Biochemistry*, 20(23): 6665–6672, Nov 1981.

G. D. Block, J. Locker, W. C. Bowen, B. E. Petersen, S. Katyal, S. C. Strom, T. Riley, T. A. Howard, and G. K. Michalopoulos. Population expansion, clonal growth, and specific differentiation patterns in primary cultures of hepatocytes induced by hgf/sf, egf and tgf alpha in a chemically defined (hgm) medium. *J Cell Biol*, 132(6):1133–1149, Mar 1996.

D. P. Bottaro, J. S. Rubin, D. L. Faletto, A. M. Chan, T. E. Kmiecik, G. F. Vande Woude, and S. A. Aaronson. Identification of the hepatocyte growth factor receptor as the c-met proto-oncogene product. *Science*, 251(4995):802–804, Feb 1991.

R. Brandenberger, H. Wei, S. Zhang, S. Lei, J. Murage, G. J. Fisk, Y. Li, C. Xu, R. Fang, K. Guegler, M. S. Rao, R. Mandalam, J. Lebkowski, and L. W. Stanton. Transcriptome characterization elucidates signaling networks that control human es cell growth and differentiation. *Nat Biotechnol*, 22(6):707–716, Jun 2004. doi: 10.1038/nbt971. URL http://dx.doi.org/10.1038/nbt971.

R. W. Bryant, C. A. Granzow, M. I. Siegel, R. W. Egan, and M. M. Billah. Phorbol esters increase synthesis of decay-accelerating factor, a phosphatidylinositol-anchored surface protein, in human endothelial cells. *J Immunol*, 144(2):593–598, Jan 1990.

R. T. Bttcher and C. Niehrs. Fibroblast growth factor signaling during early vertebrate development. *Endocr Rev*, 26(1):63–77, Feb 2005. doi: 10.1210/er.2003-0040. URL http://dx.doi.org/10.1210/er.2003-0040.

Y. Buganim, D. A. Faddah, A. W. Cheng, E. Itskovich, S. Markoulaki, K. Ganz, S. L. Klemm, A. van Oudenaarden, and R. Jaenisch. Single-cell expression analyses during cellular reprogramming reveal an early stochastic and a late hierarchic phase. *Cell*, 150(6):1209–1222, Sep 2012. doi: 10.1016/j.cell.2012.08.023. URL http://dx.doi.org/10.1016/j.cell.2012.08.023.

Y. Buganim, D. A. Faddah, and R. Jaenisch. Mechanisms and models of somatic cell reprogramming. *Nat Rev Genet*, 14(6):427–439, Jun 2013. doi: 10.1038/nrg3473. URL http://dx.doi.org/10.1038/nrg3473.

L. N. Bull, M. J. van Eijk, L. Pawlikowska, J. A. DeYoung, J. A. Juijn, M. Liao, L. W. Klomp, N. Lomri, R. Berger, B. F. Scharschmidt, A. S. Knisely, R. H. Houwen, and N. B. Freimer. A gene encoding a p-type atpase mutated in two forms of hereditary cholestasis. *Nat Genet*, 18(3):219–224, Mar 1998. doi: 10.1038/ng0398-219. URL http://dx.doi.org/10.1038/ng0398-219.

W. H. Burgess and T. Maciag. The heparin-binding (fibroblast) growth factor family of proteins. *Annu Rev Biochem*, 58:575–606, 1989. doi: 10.1146/annurev.bi.58.070189. 003043. URL http://dx.doi.org/10.1146/annurev.bi.58.070189.003043.

F. Bussolino, M. F. Di Renzo, M. Ziche, E. Bocchietto, M. Olivero, L. Naldini, G. Gaudino, L. Tamagnone, A. Coffer, and P. M. Comoglio. Hepatocyte growth factor is a potent angiogenic factor which stimulates endothelial cell motility and growth. *J Cell Biol*, 119(3):629–641, Nov 1992.

J. Cai, Y. Zhao, Y. Liu, F. Ye, Z. Song, H. Qin, S. Meng, Y. Chen, R. Zhou, X. Song, Y. Guo, M. Ding, and H. Deng. Directed differentiation of human embryonic stem cells into functional hepatic cells. *Hepatology*, 45(5):1229–1239, May 2007. doi: 10. 1002/hep.21582. URL http://dx.doi.org/10.1002/hep.21582.

Q. Cai, T. Lin, S. Kamarajugadda, and J. Lu. Regulation of glycolysis and the warburg effect by estrogen-related receptors. *Oncogene*, 32(16):2079–2086, Apr 2013. doi: 10.1038/onc.2012.221. URL http://dx.doi.org/10.1038/onc.2012.221.

F. D. Camargo, S. Gokhale, J. B. Johnnidis, D. Fu, G. W. Bell, R. Jaenisch, and T. R. Brummelkamp. Yap1 increases organ size and expands undifferentiated progenitor cells. *Curr Biol*, 17(23):2054–2060, Dec 2007. doi: 10.1016/j.cub.2007.10.039. URL http://dx.doi.org/10.1016/j.cub.2007.10.039.

V. Cardinale, Y. Wang, G. Carpino, C.-B. Cui, M. Gatto, M. Rossi, P. B. Berloco, A. Cantafora, E. Wauthier, M. E. Furth, L. Inverardi, J. Dominguez-Bendala, C. Ricordi, D. Gerber, E. Gaudio, D. Alvaro, and L. Reid. Multipotent stem/progenitor cells in human biliary tree give rise to hepatocytes, cholangiocytes, and pancreatic islets. *Hepatology*, 54(6):2159–2172, Dec 2011. doi: 10.1002/hep.24590. URL http://dx.doi.org/10.1002/hep.24590.

G. Carpenter and Q. Ji. Phospholipase c-gamma as a signal-transducing element. *Exp Cell Res*, 253(1):15–24, Nov 1999. doi: 10.1006/excr.1999.4671. URL http://dx.doi.org/10.1006/excr.1999.4671.

G. Carpino, V. Cardinale, P. Onori, A. Franchitto, P. B. Berloco, M. Rossi, Y. Wang, R. Semeraro, M. Anceschi, R. Brunelli, D. Alvaro, L. M. Reid, and E. Gaudio. Biliary tree stem/progenitor cells in glands of extrahepatic and intraheptic bile ducts: an

anatomical in situ study yielding evidence of maturational lineages. *J Anat*, 220(2): 186–199, Feb 2012. doi: 10.1111/j.1469-7580.2011.01462.x. URL http://dx.doi.org/10.1111/j.1469-7580.2011.01462.x.

S. Cascio and K. S. Zaret. Hepatocyte differentiation initiates during endodermal-mesenchymal interactions prior to liver formation. *Development*, 113(1):217–225, Sep 1991.

C. Chang and A. Hemmati-Brivanlou. A post-mid-blastula transition requirement for tgfbeta signaling in early endodermal specification. *Mech Dev*, 90(2):227–235, Feb 2000.

H. Chavan, F. Li, R. Tessman, K. Mickey, K. Dorko, T. Schmitt, S. Kumer, S. Gunewardena, N. Gaikwad, and P. Krishnamurthy. Functional coupling of atp-binding cassette transporter abcb6 to cytochrome p450 expression and activity in liver. *J Biol Chem*, 290(12):7871–7886, Mar 2015. doi: 10.1074/jbc.M114.605386. URL http://dx.doi.org/10.1074/jbc.M114.605386.

C. Chazaud, Y. Yamanaka, T. Pawson, and J. Rossant. Early lineage segregation between epiblast and primitive endoderm in mouse blastocysts through the grb2-mapk pathway. *Dev Cell*, 10(5):615–624, May 2006. doi: 10.1016/j.devcel.2006.02.020. URL http://dx.doi.org/10.1016/j.devcel.2006.02.020.

G. Chen, K. A. Bower, C. Ma, S. Fang, C. J. Thiele, and J. Luo. Glycogen synthase kinase 3beta (gsk3beta) mediates 6-hydroxydopamine-induced neuronal death. *FASEB J*, 18(10):1162–1164, Jul 2004. doi: 10.1096/fj.04-1551fje. URL http://dx.doi.org/10.1096/fj.04-1551fje.

G. Chen, D. R. Gulbranson, Z. Hou, J. M. Bolin, V. Ruotti, M. D. Probasco, K. Smuga-Otto, S. E. Howden, N. R. Diol, N. E. Propson, R. Wagner, G. O. Lee, J. Antosiewicz-Bourget, J. M. C. Teng, and J. A. Thomson. Chemically defined conditions for human ipsc derivation and culture. *Nat Methods*, 8(5):424–429, May 2011. doi: 10.1038/nmeth.1593. URL http://dx.doi.org/10.1038/nmeth.1593.

H. Chen, C.-F. Xu, J. Ma, A. V. Eliseenkova, W. Li, P. M. Pollock, N. Pitteloud, W. T. Miller, T. A. Neubert, and M. Mohammadi. A crystallographic snapshot of tyrosine trans-phosphorylation in action. *Proc Natl Acad Sci U S A*, 105(50):19660–19665, Dec 2008. doi: 10.1073/pnas.0807752105. URL http://dx.doi.org/10.1073/pnas.0807752105.

L. Chen and G. Q. Daley. Molecular basis of pluripotency. *Hum Mol Genet*, 17(R1): R23–R27, Apr 2008. doi: 10.1093/hmg/ddn050. URL http://dx.doi.org/10.1093/hmg/ddn050.

L. Chen and L. Liu. Current progress and prospects of induced pluripotent stem cells. *Sci China C Life Sci*, 52(7):622–636, Jul 2009. doi: 10.1007/s11427-009-0092-6. URL http://dx.doi.org/10.1007/s11427-009-0092-6.

M. L. Chen, C. Pothoulakis, and J. T. LaMont. Protein kinase c signaling regulates zo-1 translocation and increased paracellular flux of t84 colonocytes exposed to clostridium difficile toxin a. *J Biol Chem*, 277(6):4247–4254, Feb 2002. doi: 10.1074/jbc.M109254200. URL http://dx.doi.org/10.1074/jbc.M109254200.

Q. Chen, C. Qiu, Y. Huang, L. Jiang, Q. Huang, L. Guo, and T. Liu. Human amniotic epithelial cell feeder layers maintain ips cell pluripotency by inhibiting endogenous dna methyltransferase 1. *Exp Ther Med*, 6(5):1145–1154, Nov 2013. doi: 10.3892/etm.2013.1279. URL http://dx.doi.org/10.3892/etm.2013.1279.

Y.-J. Chen, J.-X. Zhang, L. Shen, Q. Qi, X.-X. Cheng, Z.-R. Zhong, Z.-Q. Jiang, R. Wang, H.-Z. L, and J.-G. Hu. Schwann cells induce proliferation and migration of oligodendrocyte precursor cells through secretion of pdgf-aa and fgf-2. *J Mol Neurosci*, Jun 2015. doi: 10.1007/s12031-015-0570-1. URL http://dx.doi.org/10.1007/s12031-015-0570-1.

X. Cheng, L. Ying, L. Lu, A. M. Galvo, J. A. Mills, H. C. Lin, D. N. Kotton, S. S. Shen, M. C. Nostro, J. K. Choi, M. J. Weiss, D. L. French, and P. Gadue. Self-renewing endodermal progenitor lines generated from human pluripotent stem cells. *Cell Stem Cell*, 10(4):371–384, Apr 2012. doi: 10.1016/j.stem.2012.02.024. URL http://dx.doi.org/10.1016/j.stem.2012.02.024.

S. Chetty, F. W. Pagliuca, C. Honore, A. Kweudjeu, A. Rezania, and D. A. Melton. A simple tool to improve pluripotent stem cell differentiation. *Nat Methods*, 10(6):553–556, Jun 2013. doi: 10.1038/nmeth.2442. URL http://dx.doi.org/10.1038/nmeth.2442.

C.-H. Chiang, T.-I. Huo, C.-C. Sun, J.-H. Hsieh, Y. Chien, K.-H. Lu, and S.-D. Lee. Induced pluripotent stem cells and hepatic differentiation. *J Chin Med Assoc*, 76(11):599–605, Nov 2013. doi: 10.1016/j.jcma.2013.07.007. URL http://dx.doi.org/10.1016/j.jcma.2013.07.007.

S. Childs, R. L. Yeh, E. Georges, and V. Ling. Identification of a sister gene to p-glycoprotein. *Cancer Res*, 55(10):2029–2034, May 1995.

S. Childs, R. L. Yeh, D. Hui, and V. Ling. Taxol resistance mediated by transfection of the liver-specific sister gene of p-glycoprotein. *Cancer Res*, 58(18):4160–4167, Sep 1998.

S. M. Choi, Y. Kim, J. S. Shim, J. T. Park, R.-H. Wang, S. D. Leach, J. O. Liu, C. Deng, Z. Ye, and Y.-Y. Jang. Efficient drug screening and gene correction for treating liver disease using patient-specific stem cells. *Hepatology*, 57(6):2458–2468, Jun 2013. doi: 10.1002/hep.26237. URL http://dx.doi.org/10.1002/hep.26237.

S. S. Choi and A. M. Diehl. Epithelial-to-mesenchymal transitions in the liver. *Hepatology*, 50(6):2007–2013, Dec 2009. doi: 10.1002/hep.23196. URL http://dx.doi.org/10.1002/hep.23196.

G. C. Chu, N. R. Dunn, D. C. Anderson, L. Oxburgh, and E. J. Robertson. Differential requirements for smad4 in tgfbeta-dependent patterning of the early mouse embryo. *Development*, 131(15):3501–3512, Aug 2004. doi: 10.1242/dev.01248. URL http://dx.doi.org/10.1242/dev.01248.

D. Clements and H. R. Woodland. Vegt induces endoderm by a self-limiting mechanism and by changing the competence of cells to respond to tgf-beta signals. *Dev Biol*, 258 (2):454–463, Jun 2003.

H. Clevers and R. Nusse. Wnt/?-catenin signaling and disease. *Cell*, 149(6):1192–1205, Jun 2012. doi: 10.1016/j.cell.2012.05.012. URL http://dx.doi.org/10.1016/j.cell.2012.05.012.

F. Clotman and F. P. Lemaigre. Control of hepatic differentiation by activin/tgfbeta signaling. *Cell Cycle*, 5(2):168–171, Jan 2006.

F. Clotman, V. J. Lannoy, M. Reber, S. Cereghini, D. Cassiman, P. Jacquemin, T. Roskams, G. G. Rousseau, and F. P. Lemaigre. The onecut transcription factor hnf6 is required for normal development of the biliary tract. *Development*, 129(8): 1819–1828, Apr 2002.

F. Cobo, J. M. Navarro, M. I. Herrera, A. Vivo, D. Porcel, C. Hernndez, M. Jurado, J. Garca-Castro, and P. Menendez. Electron microscopy reveals the presence of viruses in mouse embryonic fibroblasts but neither in human embryonic fibroblasts nor in human mesenchymal cells used for hesc maintenance: toward an implementation of microbiological quality assurance program in stem cell banks. *Cloning Stem Cells*, 10(1):65–74, Mar 2008. doi: 10.1089/clo.2007.0020. URL http://dx.doi.org/10.1089/clo.2007.0020.

K. Cockburn, S. Biechele, J. Garner, and J. Rossant. The hippo pathway member nf2 is required for inner cell mass specification. *Curr Biol*, 23(13):1195–1201, Jul 2013. doi: 10.1016/j.cub.2013.05.044. URL http://dx.doi.org/10.1016/j.cub.2013.05.044.

M. R. Crompton, T. J. Bartlett, A. D. MacGregor, G. Manfioletti, E. Buratti, V. Giancotti, and G. H. Goodwin. Identification of a novel vertebrate homeobox gene expressed in haematopoietic cells. *Nucleic Acids Res*, 20(21):5661–5667, Nov 1992.

C. Crosnier, T. Atti-Bitach, F. Encha-Razavi, S. Audollent, F. Soudy, M. Hadchouel, M. Meunier-Rotival, and M. Vekemans. Jagged1 gene expression during human embryogenesis elucidates the wide phenotypic spectrum of alagille syndrome. *Hepatology*, 32(3):574–581, Sep 2000. doi: 10.1053/jhep.2000.16600. URL http://dx.doi.org/10.1053/jhep.2000.16600.

A. Cuconati, C. Mills, C. Goddard, X. Zhang, W. Yu, H. Guo, X. Xu, and T. M. Block. Suppression of akt anti-apoptotic signaling by a novel drug candidate results in growth arrest and apoptosis of hepatocellular carcinoma cells. *PLoS One*, 8(1):

e54595, 2013. doi: 10.1371/journal.pone.0054595. URL http://dx.doi.org/10.1371/journal.pone.0054595.

A. R. Cushny. The excretion of urea and sugar by the kidney. *J Physiol*, 51(1-2):36–44, Mar 1917.

K. A. D'Amour, A. D. Agulnick, S. Eliazer, O. G. Kelly, E. Kroon, and E. E. Baetge. Efficient differentiation of human embryonic stem cells to definitive endoderm. *Nat Biotechnol*, 23(12):1534–1541, Dec 2005. doi: 10.1038/nbt1163. URL http://dx.doi.org/10.1038/nbt1163.

M. de Caestecker. The transforming growth factor-beta superfamily of receptors. *Cytokine Growth Factor Rev*, 15(1):1–11, Feb 2004.

C. de Juan, M. Benito, A. Alvarez, and I. Fabregat. Differential proliferative response of cultured fetal and regenerating hepatocytes to growth factors and hormones. *Exp Cell Res*, 202(2):495–500, Oct 1992.

W. de Lau, N. Barker, T. Y. Low, B.-K. Koo, V. S. W. Li, H. Teunissen, P. Kujala, A. Haegebarth, P. J. Peters, M. van de Wetering, D. E. Stange, J. E. van Es, D. Guardavaccaro, R. B. M. Schasfoort, Y. Mohri, K. Nishimori, S. Mohammed, A. J. R. Heck, and H. Clevers. Lgr5 homologues associate with wnt receptors and mediate r-spondin signalling. *Nature*, 476(7360):293–297, Aug 2011. doi: 10.1038/nature10337. URL http://dx.doi.org/10.1038/nature10337.

G. Dennis, Jr, B. T. Sherman, D. A. Hosack, J. Yang, W. Gao, H. C. Lane, and R. A. Lempicki. David: Database for annotation, visualization, and integrated discovery. *Genome Biol*, 4(5):P3, 2003.

R. Derynck and Y. E. Zhang. Smad-dependent and smad-independent pathways in tgf-beta family signalling. *Nature*, 425(6958):577–584, Oct 2003. doi: 10.1038/nature02006. URL http://dx.doi.org/10.1038/nature02006.

G. Deutsch, J. Jung, M. Zheng, J. Lra, and K. S. Zaret. A bipotential precursor population for pancreas and liver within the embryonic endoderm. *Development*, 128(6):871–881, Mar 2001.

N. Dianat, H. Dubois-Pot-Schneider, C. Steichen, C. Desterke, P. Leclerc, A. Raveux, L. Combettes, A. Weber, A. Corlu, and A. Dubart-Kupperschmitt. Generation of functional cholangiocyte-like cells from human pluripotent stem cells and heparg cells. *Hepatology*, 60(2):700–714, Aug 2014. doi: 10.1002/hep.27165. URL http://dx.doi.org/10.1002/hep.27165.

D. S. Dimski. Ammonia metabolism and the urea cycle: function and clinical implications. *J Vet Intern Med*, 8(2):73–78, 1994.

A. Domanskyi, H. Alter, M. A. Vogt, P. Gass, and I. A. Vinnikov. Transcription factors foxa1 and foxa2 are required for adult dopamine neurons maintenance. *Front Cell Neurosci*, 8:275, 2014. doi: 10.3389/fncel.2014.00275. URL http://dx.doi.org/10.3389/fncel.2014.00275.

J. Dong, G. Feldmann, J. Huang, S. Wu, N. Zhang, S. A. Comerford, M. F. Gayyed, R. A. Anders, A. Maitra, and D. Pan. Elucidation of a universal size-control mechanism in drosophila and mammals. *Cell*, 130(6):1120–1133, Sep 2007. doi: 10.1016/j.cell.2007.07.019. URL http://dx.doi.org/10.1016/j.cell.2007.07.019.

J. Drechsler, J. Grtzinger, and H. M. Hermanns. Characterization of the rat oncostatin m receptor complex which resembles the human, but differs from the murine cytokine receptor. *PLoS One*, 7(8):e43155, 2012. doi: 10.1371/journal.pone.0043155. URL http://dx.doi.org/10.1371/journal.pone.0043155.

K. Drews, J. Jozefczuk, A. Prigione, and J. Adjaye. Human induced pluripotent stem cells–from mechanisms to clinical applications. *J Mol Med (Berl)*, 90(7):735–745, Jul 2012. doi: 10.1007/s00109-012-0913-0. URL http://dx.doi.org/10.1007/s00109-012-0913-0.

B. D'Souza, L. Meloty-Kapella, and G. Weinmaster. Canonical and non-canonical notch ligands. *Curr Top Dev Biol*, 92:73–129, 2010. doi: 10.1016/S0070-2153(10)92003-6. URL http://dx.doi.org/10.1016/S0070-2153(10)92003-6.

J. Dudas, M. Papoutsi, M. Hecht, A. Elmaouhoub, B. Saile, B. Christ, S. I. Tomarev, C. S. von Kaisenberg, L. Schweigerer, G. Ramadori, and J. Wilting. The homeobox transcription factor prox1 is highly conserved in embryonic hepatoblasts and in adult and transformed hepatocytes, but is absent from bile duct epithelium. *Anat Embryol (Berl)*, 208(5):359–366, Aug 2004. doi: 10.1007/s00429-004-0403-4. URL http://dx.doi.org/10.1007/s00429-004-0403-4.

D. Dufort, L. Schwartz, K. Harpal, and J. Rossant. The transcription factor hnf3beta is required in visceral endoderm for normal primitive streak morphogenesis. *Development*, 125(16):3015–3025, Aug 1998.

S. A. Duncan. Transcriptional regulation of liver development. *Dev Dyn*, 219(2):131–142, Oct 2000. doi: 3.0.CO;2-N. URL http://dx.doi.org/3.0.CO;2-N.

M. Ek, T. Sderdahl, B. Kppers-Munther, J. Edsbagge, T. B. Andersson, P. Bjrquist, I. Cotgreave, B. Jernstrm, M. Ingelman-Sundberg, and I. Johansson. Expression of drug metabolizing enzymes in hepatocyte-like cells derived from human embryonic stem cells. *Biochem Pharmacol*, 74(3):496–503, Aug 2007. doi: 10.1016/j.bcp.2007.05.009. URL http://dx.doi.org/10.1016/j.bcp.2007.05.009.

G. Elaut, T. Henkens, P. Papeleu, S. Snykers, M. Vinken, T. Vanhaecke, and V. Rogiers. Molecular mechanisms underlying the dedifferentiation process of isolated hepatocytes and their cultures. *Curr Drug Metab*, 7(6):629–660, Aug 2006a.

G. Elaut, P. Papeleu, M. Vinken, T. Henkens, S. Snykers, T. Vanhaecke, and V. Rogiers. Hepatocytes in suspension. *Methods Mol Biol*, 320:255–263, 2006b. doi: 10.1385/1-59259-998-2:255. URL http://dx.doi.org/10.1385/1-59259-998-2:255.

L. Emdad, S. L. D'Souza, H. P. Kothari, Z. A. Qadeer, and I. M. Germano. Efficient differentiation of human embryonic and induced pluripotent stem cells into functional astrocytes. *Stem Cells Dev*, 21(3):404–410, Feb 2012. doi: 10.1089/scd.2010.0560. URL http://dx.doi.org/10.1089/scd.2010.0560.

M. J. Engleka, E. J. Craig, and D. S. Kessler. Vegt activation of sox17 at the midblastula transition alters the response to nodal signals in the vegetal endoderm domain. *Dev Biol*, 237(1):159–172, Sep 2001. doi: 10.1006/dbio.2001.0366. URL http://dx.doi.org/10.1006/dbio.2001.0366.

A. Esteller. Physiology of bile secretion. *World J Gastroenterol*, 14(37):5641–5649, Oct 2008.

M. J. Evans and M. H. Kaufman. Establishment in culture of pluripotential cells from mouse embryos. *Nature*, 292(5819):154–156, Jul 1981.

M. Faris, B. Ensoli, N. Stahl, G. Yancopoulos, A. Nguyen, S. Wang, and A. E. Nel. Differential activation of the extracellular signal-regulated kinase, jun kinase and janus kinase-stat pathways by oncostatin m and basic fibroblast growth factor in aids-derived kaposi's sarcoma cells. *AIDS*, 10(4):369–378, Apr 1996.

Z. Farzaneh, M. Pakzad, M. Vosough, B. Pournasr, and H. Baharvand. Differentiation of human embryonic stem cells to hepatocyte-like cells on a new developed xeno-free extracellular matrix. *Histochem Cell Biol*, Jan 2014. doi: 10.1007/s00418-014-1183-4. URL http://dx.doi.org/10.1007/s00418-014-1183-4.

M. Florek, M. Haase, A.-M. Marzesco, D. Freund, G. Ehninger, W. B. Huttner, and D. Corbeil. Prominin-1/cd133, a neural and hematopoietic stem cell marker, is expressed in adult human differentiated cells and certain types of kidney cancer. *Cell Tissue Res*, 319(1):15–26, Jan 2005. doi: 10.1007/s00441-004-1018-z. URL http://dx.doi.org/10.1007/s00441-004-1018-z.

D. M. Flynn, S. Nijjar, S. G. Hubscher, J. d. V. de Goyet, D. A. Kelly, A. J. Strain, and H. A. Crosby. The role of notch receptor expression in bile duct development and disease. *J Pathol*, 204(1):55–64, Sep 2004. doi: 10.1002/path.1615. URL http://dx.doi.org/10.1002/path.1615.

C. Fougre-Deschatrette, T. Imaizumi-Scherrer, H. Strick-Marchand, S. Morosan, P. Charneau, D. Kremsdorf, D. M. Faust, and M. C. Weiss. Plasticity of hepatic cell differentiation: bipotential adult mouse liver clonal cell lines competent to differentiate in vitro and in vivo. *Stem Cells*, 24(9):2098–2109, Sep 2006. doi: 10.1634/stemcells.2006-0009. URL http://dx.doi.org/10.1634/stemcells.2006-0009.

I. J. Fox and J. R. Chowdhury. Hepatocyte transplantation. *Am J Transplant*, 4 Suppl 6:7–13, 2004.

J. Fraczek, J. Bolleyn, T. Vanhaecke, V. Rogiers, and M. Vinken. Primary hepatocyte cultures for pharmaco-toxicological studies: at the busy crossroad of various anti-dedifferentiation strategies. *Arch Toxicol*, 87(4):577–610, Apr 2013. doi: 10.1007/s00204-012-0983-3. URL http://dx.doi.org/10.1007/s00204-012-0983-3.

S. Frank, M. Zhang, H. R. Schler, and B. Greber. Small molecule-assisted, line-independent maintenance of human pluripotent stem cells in defined conditions. *PLoS One*, 7(7):e41958, 2012. doi: 10.1371/journal.pone.0041958. URL http://dx.doi.org/10.1371/journal.pone.0041958.

R. Fssler and M. Meyer. Consequences of lack of beta 1 integrin gene expression in mice. *Genes Dev*, 9(15):1896–1908, Aug 1995.

H. Fujita, H. Katoh, H. Hasegawa, H. Yasui, J. Aoki, Y. Yamaguchi, and M. Negishi. Molecular decipherment of rho effector pathways regulating tight-junction permeability. *Biochem J*, 346 Pt 3:617–622, Mar 2000.

C. M. Furdui, E. D. Lew, J. Schlessinger, and K. S. Anderson. Autophosphorylation of fgfr1 kinase is mediated by a sequential and precisely ordered reaction. *Mol Cell*, 21(5):711–717, Mar 2006. doi: 10.1016/j.molcel.2006.01.022. URL http://dx.doi.org/10.1016/j.molcel.2006.01.022.

Y. Furuta, D. W. Piston, and B. L. Hogan. Bone morphogenetic proteins (bmps) as regulators of dorsal forebrain development. *Development*, 124(11):2203–2212, Jun 1997.

L. B. R. G. W. H. A. L. T. L. M. M. A. M. S. M. M. S. G. R. Warnes, B. Bolker and B. Venables. gplots: Various r programming tools for plotting data. r package version 2.8.0. 2010. URL http://CRAN.R-project.org/package=gplots.

B. Garzel, H. Yang, L. Zhang, S.-M. Huang, J. E. Polli, and H. Wang. The role of bile salt export pump gene repression in drug-induced cholestatic liver toxicity. *Drug Metab Dispos*, 42(3):318–322, Mar 2014. doi: 10.1124/dmd.113.054189. URL http://dx.doi.org/10.1124/dmd.113.054189.

D. P. Gearing, M. R. Comeau, D. J. Friend, S. D. Gimpel, C. J. Thut, J. McGourty, K. K. Brasher, J. A. King, S. Gillis, and B. Mosley. The il-6 signal transducer, gp130: an oncostatin m receptor and affinity converter for the lif receptor. *Science*, 255(5050): 1434–1437, Mar 1992.

H. H. J. Gerets, K. Tilmant, B. Gerin, H. Chanteux, B. O. Depelchin, S. Dhalluin, and F. A. Atienzar. Characterization of primary human hepatocytes, hepg2 cells, and heparg cells at the mrna level and cyp activity in response to inducers and their

predictivity for the detection of human hepatotoxins. *Cell Biol Toxicol*, 28(2):69–87, Apr 2012. doi: 10.1007/s10565-011-9208-4. URL http://dx.doi.org/10.1007/s10565-011-9208-4.

P. Ghasemi-Dehkordi, M. Allahbakhshian-Farsani, N. Abdian, A. Mirzaeian, J. Saffari-Chaleshtori, F. Heybati, G. Mardani, A. Karimi-Taghanaki, A. Doosti, M.-S. Jami, M. Abolhasani, and M. Hashemzadeh-Chaleshtori. Comparison between the cultures of human induced pluripotent stem cells (hipscs) on feeder-and serum-free system (matrigel matrix), mef and hdf feeder cell lines. *J Cell Commun Signal*, Mar 2015. doi: 10.1007/s12079-015-0289-3. URL http://dx.doi.org/10.1007/s12079-015-0289-3.

M. Gherghiceanu, L. Barad, A. Novak, I. Reiter, J. Itskovitz-Eldor, O. Binah, and L. M. Popescu. Cardiomyocytes derived from human embryonic and induced pluripotent stem cells: comparative ultrastructure. *J Cell Mol Med*, 15(11):2539–2551, Nov 2011. doi: 10.1111/j.1582-4934.2011.01417.x. URL http://dx.doi.org/10.1111/j.1582-4934.2011.01417.x.

R. L. Gieseck, 3rd, N. R. F. Hannan, R. Bort, N. A. Hanley, R. A. L. Drake, G. W. W. Cameron, T. A. Wynn, and L. Vallier. Maturation of induced pluripotent stem cell derived hepatocytes by 3d-culture. *PLoS One*, 9(1):e86372, 2014. doi: 10.1371/journal.pone.0086372. URL http://dx.doi.org/10.1371/journal.pone.0086372.

C. Gil-Sanchis, I. Cervell, A. Mas, A. Faus, A. Pellicer, and C. Simn. Leucine-rich repeat-containing g-protein-coupled receptor 5 (lgr5) as a putative human endometrial stem cell marker. *Mol Hum Reprod*, 19(7):407–414, Jul 2013. doi: 10.1093/molehr/gat014. URL http://dx.doi.org/10.1093/molehr/gat014.

R. Girometti, G. Como, M. Bazzocchi, and C. Zuiani. Post-operative imaging in liver transplantation: State-of-the-art and future perspectives. *World J Gastroenterol*, 20 (20):6180–6200, May 2014. doi: 10.3748/wjg.v20.i20.6180. URL http://dx.doi.org/10.3748/wjg.v20.i20.6180.

P. Godoy, N. J. Hewitt, U. Albrecht, M. E. Andersen, N. Ansari, S. Bhattacharya, J. G. Bode, J. Bolleyn, C. Borner, J. Bttger, A. Braeuning, R. A. Budinsky, B. Burkhardt, N. R. Cameron, G. Camussi, C.-S. Cho, Y.-J. Choi, J. Craig Rowlands, U. Dahmen, G. Damm, O. Dirsch, M. T. Donato, J. Dong, S. Dooley, D. Drasdo, R. Eakins, K. S. Ferreira, V. Fonsato, J. Fraczek, R. Gebhardt, A. Gibson, M. Glanemann, C. E. P. Goldring, M. J. Gmez-Lechn, G. M. M. Groothuis, L. Gustavsson, C. Guyot, D. Hallifax, S. Hammad, A. Hayward, D. Hussinger, C. Hellerbrand, P. Hewitt, S. Hoehme, H.-G. Holzhtter, J. B. Houston, J. Hrach, K. Ito, H. Jaeschke, V. Keitel, J. M. Kelm, B. Kevin Park, C. Kordes, G. A. Kullak-Ublick, E. L. LeCluyse, P. Lu, J. Luebke-Wheeler, A. Lutz, D. J. Maltman, M. Matz-Soja, P. McMullen, I. Merfort, S. Messner, C. Meyer, J. Mwinyi, D. J. Naisbitt, A. K. Nussler, P. Olinga, F. Pampaloni, J. Pi, L. Pluta, S. A. Przyborski, A. Ramachandran, V. Rogiers, C. Rowe, C. Schelcher, K. Schmich, M. Schwarz, B. Singh, E. H. K. Stelzer, B. Stieger, R. Stber, Y. Sugiyama, C. Tetta, W. E. Thasler, T. Vanhaecke,

M. Vinken, T. S. Weiss, A. Widera, C. G. Woods, J. J. Xu, K. M. Yarborough, and J. G. Hengstler. Recent advances in 2d and 3d in vitro systems using primary hepatocytes, alternative hepatocyte sources and non-parenchymal liver cells and their use in investigating mechanisms of hepatotoxicity, cell signaling and adme. *Arch Toxicol*, 87(8):1315–1530, Aug 2013. doi: 10.1007/s00204-013-1078-5. URL http://dx.doi.org/10.1007/s00204-013-1078-5.

R. Goetz and M. Mohammadi. Exploring mechanisms of fgf signalling through the lens of structural biology. *Nat Rev Mol Cell Biol*, 14(3):166–180, Mar 2013. doi: 10.1038/nrm3528. URL http://dx.doi.org/10.1038/nrm3528.

O. Goldman, S. Han, M. Sourisseau, M. Sourrisseau, N. Dziedzic, W. Hamou, B. Corneo, S. D'Souza, T. Sato, D. N. Kotton, K.-D. Bissig, T. Kalir, A. Jacobs, T. Evans, M. J. Evans, and V. Gouon-Evans. Kdr identifies a conserved human and murine hepatic progenitor and instructs early liver development. *Cell Stem Cell*, 12(6):748–760, Jun 2013. doi: 10.1016/j.stem.2013.04.026. URL http://dx.doi.org/10.1016/j.stem.2013.04.026.

A. Golipour, L. David, Y. Liu, G. Jayakumaran, C. L. Hirsch, D. Trcka, and J. L. Wrana. A late transition in somatic cell reprogramming requires regulators distinct from the pluripotency network. *Cell Stem Cell*, 11(6):769–782, Dec 2012. doi: 10.1016/j.stem.2012.11.008. URL http://dx.doi.org/10.1016/j.stem.2012.11.008.

S. A. Gonzalez and E. B. Keeffe. Chronic viral hepatitis: epidemiology, molecular biology, and antiviral therapy. *Front Biosci (Landmark Ed)*, 16:225–250, 2011.

R. R. Gorman, R. D. Hamilton, and N. K. Hopkins. Stimulation of human foreskin fibroblast adenosine 3':5'-cyclic monophosphate levels by prostacyclin (prostaglandin i2). *J Biol Chem*, 254(5):1671–1676, Mar 1979.

V. Gouon-Evans, L. Boussemart, P. Gadue, D. Nierhoff, C. I. Koehler, A. Kubo, D. A. Shafritz, and G. Keller. Bmp-4 is required for hepatic specification of mouse embryonic stem cell-derived definitive endoderm. *Nat Biotechnol*, 24(11):1402–1411, Nov 2006. doi: 10.1038/nbt1258. URL http://dx.doi.org/10.1038/nbt1258.

B. Grasl-Kraupp, W. Rossmanith, B. Ruttkay-Nedecky, L. Mllauer, B. Kammerer, W. Bursch, and R. Schulte-Hermann. Levels of transforming growth factor beta and transforming growth factor beta receptors in rat liver during growth, regression by apoptosis and neoplasia. *Hepatology*, 28(3):717–726, Sep 1998. doi: 10.1002/hep.510280318. URL http://dx.doi.org/10.1002/hep.510280318.

B. Greber, H. Lehrach, and J. Adjaye. Fibroblast growth factor 2 modulates transforming growth factor beta signaling in mouse embryonic fibroblasts and human escs (hescs) to support hesc self-renewal. *Stem Cells*, 25(2):455–464, Feb 2007. doi: 10.1634/stemcells.2006-0476. URL http://dx.doi.org/10.1634/stemcells.2006-0476.

C. C. Greenberg, M. J. Jurczak, A. M. Danos, and M. J. Brady. Glycogen branches out: new perspectives on the role of glycogen metabolism in the integration of metabolic pathways. *Am J Physiol Endocrinol Metab*, 291(1):E1–E8, Jul 2006. doi: 10.1152/ajpendo.00652.2005. URL http://dx.doi.org/10.1152/ajpendo.00652.2005.

S. Greenhough, C. N. Medine, and D. C. Hay. Pluripotent stem cell derived hepatocyte like cells and their potential in toxicity screening. *Toxicology*, 278(3):250–255, Dec 2010. doi: 10.1016/j.tox.2010.07.012. URL http://dx.doi.org/10.1016/j.tox.2010.07.012.

S. J. Grille, A. Bellacosa, J. Upson, A. J. Klein-Szanto, F. van Roy, W. Lee-Kwon, M. Donowitz, P. N. Tsichlis, and L. Larue. The protein kinase akt induces epithelial mesenchymal transition and promotes enhanced motility and invasiveness of squamous cell carcinoma lines. *Cancer Res*, 63(9):2172–2178, May 2003.

R. I. Grove, C. E. Mazzucco, S. F. Radka, M. Shoyab, and P. A. Kiener. Oncostatin m up-regulates low density lipoprotein receptors in hepg2 cells by a novel mechanism. *J Biol Chem*, 266(27):18194–18199, Sep 1991.

G. Halder and R. L. Johnson. Hippo signaling: growth control and beyond. *Development*, 138(1):9–22, Jan 2011. doi: 10.1242/dev.045500. URL http://dx.doi.org/10.1242/dev.045500.

G. Halder, S. Dupont, and S. Piccolo. Transduction of mechanical and cytoskeletal cues by yap and taz. *Nat Rev Mol Cell Biol*, 13(9):591–600, Sep 2012. doi: 10.1038/nrm3416. URL http://dx.doi.org/10.1038/nrm3416.

T. Hamada, A. Sato, T. Hirano, T. Yamamoto, G. Son, M. Onodera, I. Torii, T. Nishigami, M. Tanaka, A. Miyajima, S. Nishiguchi, J. Fujimoto, and T. Tsujimura. Oncostatin m gene therapy attenuates liver damage induced by dimethylnitrosamine in rats. *Am J Pathol*, 171(3):872–881, Sep 2007. doi: 10.2353/ajpath.2007.060972. URL http://dx.doi.org/10.2353/ajpath.2007.060972.

J. Hanna, M. Wernig, S. Markoulaki, C.-W. Sun, A. Meissner, J. P. Cassady, C. Beard, T. Brambrink, L.-C. Wu, T. M. Townes, and R. Jaenisch. Treatment of sickle cell anemia mouse model with ips cells generated from autologous skin. *Science*, 318(5858): 1920–1923, Dec 2007. doi: 10.1126/science.1152092. URL http://dx.doi.org/10.1126/science.1152092.

N. R. F. Hannan, R. P. Fordham, Y. A. Syed, V. Moignard, A. Berry, R. Bautista, N. A. Hanley, K. B. Jensen, and L. Vallier. Generation of multipotent foregut stem cells from human pluripotent stem cells. *Stem Cell Reports*, 1(4):293–306, 2013. doi: 10.1016/j.stemcr.2013.09.003. URL http://dx.doi.org/10.1016/j.stemcr.2013.09.003.

N. R. F. Hannan, F. Sampaziotis, C.-P. Segeritz, N. A. Hanley, and L. Vallier. Generation of distal airway epithelium from multipotent human foregut stem cells. *Stem Cells*

Dev, Apr 2015. doi: 10.1089/scd.2014.0512. URL http://dx.doi.org/10.1089/scd.2014.0512.

B. A. Hansen, B. Krog, and H. Vilstrup. Insulin and glucose decreases the capacity of urea-n synthesis in the rat. *Scand J Clin Lab Invest*, 46(6):599–603, Oct 1986.

J. Hansson, M. R. Rafiee, S. Reiland, J. M. Polo, J. Gehring, S. Okawa, W. Huber, K. Hochedlinger, and J. Krijgsveld. Highly coordinated proteome dynamics during reprogramming of somatic cells to pluripotency. *Cell Rep*, 2(6):1579–1592, Dec 2012. doi: 10.1016/j.celrep.2012.10.014. URL http://dx.doi.org/10.1016/j.celrep.2012.10.014.

A. E. Harper. Human protein requirements. problems of maintaining nitrogen balance on a low income. *Ala J Med Sci*, 21(4):389–394, Oct 1984.

A. H. Hart, L. Hartley, K. Sourris, E. S. Stadler, R. Li, E. G. Stanley, P. P. L. Tam, A. G. Elefanty, and L. Robb. Mixl1 is required for axial mesendoderm morphogenesis and patterning in the murine embryo. *Development*, 129(15):3597–3608, Aug 2002.

A. H. Hart, T. A. Willson, M. Wong, K. Parker, and L. Robb. Transcriptional regulation of the homeobox gene mixl1 by tgf-beta and foxh1. *Biochem Biophys Res Commun*, 333(4):1361–1369, Aug 2005. doi: 10.1016/j.bbrc.2005.06.044. URL http://dx.doi.org/10.1016/j.bbrc.2005.06.044.

S. N. Hart, Y. Li, K. Nakamoto, E.-a. Subileau, D. Steen, and X.-b. Zhong. A comparison of whole genome gene expression profiles of heparg cells and hepg2 cells to primary human hepatocytes and human liver tissues. *Drug Metab Dispos*, 38(6):988–994, Jun 2010. doi: 10.1124/dmd.109.031831. URL http://dx.doi.org/10.1124/dmd.109.031831.

M. T. Hartsough and K. M. Mulder. Transforming growth factor beta activation of p44mapk in proliferating cultures of epithelial cells. *J Biol Chem*, 270(13):7117–7124, Mar 1995.

K. F. Harvey, X. Zhang, and D. M. Thomas. The hippo pathway and human cancer. *Nat Rev Cancer*, 13(4):246–257, Apr 2013. doi: 10.1038/nrc3458. URL http://dx.doi.org/10.1038/nrc3458.

D. C. Hay, D. Zhao, A. Ross, R. Mandalam, J. Lebkowski, and W. Cui. Direct differentiation of human embryonic stem cells to hepatocyte-like cells exhibiting functional activities. *Cloning Stem Cells*, 9(1):51–62, 2007. doi: 10.1089/clo.2006.0045. URL http://dx.doi.org/10.1089/clo.2006.0045.

D. C. Hay, J. Fletcher, C. Payne, J. D. Terrace, R. C. J. Gallagher, J. Snoeys, J. R. Black, D. Wojtacha, K. Samuel, Z. Hannoun, A. Pryde, C. Filippi, I. S. Currie, S. J. Forbes, J. A. Ross, P. N. Newsome, and J. P. Iredale. Highly efficient differentiation of hescs to functional hepatic endoderm requires activina and wnt3a signaling. *Proc Natl Acad*

Sci U S A, 105(34):12301–12306, Aug 2008a. doi: 10.1073/pnas.0806522105. URL http://dx.doi.org/10.1073/pnas.0806522105.

D. C. Hay, D. Zhao, J. Fletcher, Z. A. Hewitt, D. McLean, A. Urruticoechea-Uriguen, J. R. Black, C. Elcombe, J. A. Ross, R. Wolf, and W. Cui. Efficient differentiation of hepatocytes from human embryonic stem cells exhibiting markers recapitulating liver development in vivo. *Stem Cells*, 26(4):894–902, Apr 2008b. doi: 10.1634/stemcells. 2007-0718. URL http://dx.doi.org/10.1634/stemcells.2007-0718.

M. Heddad Masson, C. Poisson, A. Gurardel, A. Mamin, J. Philippe, and Y. Gosmain. Foxa1 and foxa2 regulate ?-cell differentiation, glucagon biosynthesis, and secretion. *Endocrinology*, 155(10):3781–3792, Oct 2014. doi: 10.1210/en.2013-1843. URL http://dx.doi.org/10.1210/en.2013-1843.

P. Heitzler. Biodiversity and noncanonical notch signaling. *Curr Top Dev Biol*, 92: 457–481, 2010. doi: 10.1016/S0070-2153(10)92014-0. URL http://dx.doi.org/10.1016/S0070-2153(10)92014-0.

C.-H. Heldin and A. Moustakas. Role of smads in tgf? signaling. *Cell Tissue Res*, 347 (1):21–36, Jan 2012. doi: 10.1007/s00441-011-1190-x. URL http://dx.doi.org/10.1007/s00441-011-1190-x.

B. Hentsch, I. Lyons, R. Li, L. Hartley, T. J. Lints, J. M. Adams, and R. P. Harvey. Hlx homeo box gene is essential for an inductive tissue interaction that drives expansion of embryonic liver and gut. *Genes Dev*, 10(1):70–79, Jan 1996.

F. Hess, C. Jerusalem, and M. Polak. Azathioprine hepatotoxicity, direct complication or secondary effect in rat liver transplantation. *Eur Surg Res*, 8(2):156–165, 1976.

T. Hirano, K. Nakajima, and M. Hibi. Signaling mechanisms through gp130: a model of the cytokine system. *Cytokine Growth Factor Rev*, 8(4):241–252, Dec 1997.

Y. Hirate, S. Hirahara, K.-I. Inoue, A. Suzuki, V. B. Alarcon, K. Akimoto, T. Hirai, T. Hara, M. Adachi, K. Chida, S. Ohno, Y. Marikawa, K. Nakao, A. Shimono, and H. Sasaki. Polarity-dependent distribution of angiomotin localizes hippo signaling in preimplantation embryos. *Curr Biol*, 23(13):1181–1194, Jul 2013. doi: 10.1016/j.cub. 2013.05.014. URL http://dx.doi.org/10.1016/j.cub.2013.05.014.

C.-M. Ho, A. Dhawan, R. D. Hughes, S. C. Lehec, J. Puppi, C. Philippeos, P.-H. Lee, and R. R. Mitry. Use of indocyanine green for functional assessment of human hepatocytes for transplantation. *Asian J Surg*, 35(1):9–15, Jan 2012. doi: 10.1016/j.asjsur.2012. 04.017. URL http://dx.doi.org/10.1016/j.asjsur.2012.04.017.

P.-J. Ho, M.-L. Yen, J.-D. Lin, L.-S. Chen, H.-I. Hu, C.-K. Yeh, C.-Y. Peng, C.-Y. Lin, S.-F. Yet, and B. L. Yen. Endogenous klf4 expression in human fetal endothelial cells allows for reprogramming to pluripotency with just oct3/4 and sox2–brief report. *Arterioscler Thromb Vasc Biol*, 30(10):1905–1907, Oct 2010. doi: 10.1161/ATVBAHA. 110.206540. URL http://dx.doi.org/10.1161/ATVBAHA.110.206540.

D. Hockemeyer, H. Wang, S. Kiani, C. S. Lai, Q. Gao, J. P. Cassady, G. J. Cost, L. Zhang, Y. Santiago, J. C. Miller, B. Zeitler, J. M. Cherone, X. Meng, S. J. Hinkley, E. J. Rebar, P. D. Gregory, F. D. Urnov, and R. Jaenisch. Genetic engineering of human pluripotent cells using tale nucleases. *Nat Biotechnol*, 29(8):731–734, Aug 2011. doi: 10.1038/nbt.1927. URL http://dx.doi.org/10.1038/nbt.1927.

A. F. Hofmann and L. R. Hagey. Key discoveries in bile acid chemistry and biology and their clinical applications: history of the last eight decades. *J Lipid Res*, 55(8):1553–1595, May 2014. doi: 10.1194/jlr.R049437. URL http://dx.doi.org/10.1194/jlr.R049437.

J. J. Hofmann, A. C. Zovein, H. Koh, F. Radtke, G. Weinmaster, and M. L. Iruela-Arispe. Jagged1 in the portal vein mesenchyme regulates intrahepatic bile duct development: insights into alagille syndrome. *Development*, 137(23):4061–4072, Dec 2010. doi: 10.1242/dev.052118. URL http://dx.doi.org/10.1242/dev.052118.

B. L. Hogan. Morphogenesis. *Cell*, 96(2):225–233, Jan 1999.

H. Hong, K. Takahashi, T. Ichisaka, T. Aoi, O. Kanagawa, M. Nakagawa, K. Okita, and S. Yamanaka. Suppression of induced pluripotent stem cell generation by the p53-p21 pathway. *Nature*, 460(7259):1132–1135, Aug 2009. doi: 10.1038/nature08235. URL http://dx.doi.org/10.1038/nature08235.

P. A. Hoodless, M. Pye, C. Chazaud, E. Labb, L. Attisano, J. Rossant, and J. L. Wrana. Foxh1 (fast) functions to specify the anterior primitive streak in the mouse. *Genes Dev*, 15(10):1257–1271, May 2001. doi: 10.1101/gad.881501. URL http://dx.doi.org/10.1101/gad.881501.

E. Houssaint. Differentiation of the mouse hepatic primordium. i. an analysis of tissue interactions in hepatocyte differentiation. *Cell Differ*, 9(5):269–279, Oct 1980.

O. Hovatta, M. Mikkola, K. Gertow, A.-M. Strmberg, J. Inzunza, J. Hreinsson, B. Rozell, E. Blennow, M. Andng, and L. Ahrlund-Richter. A culture system using human foreskin fibroblasts as feeder cells allows production of human embryonic stem cells. *Hum Reprod*, 18(7):1404–1409, Jul 2003.

R. B. Howard, A. K. Christensen, F. A. Gibbs, and L. A. Pesch. The enzymatic preparation of isolated intact parenchymal cells from rat liver. *J Cell Biol*, 35(3):675–684, Dec 1967.

D. P. Hoyer, C. Klein, S. Kathemann, A. Paul, and Z. Math. [left-lateral living related liver donation - the essen experience.]. *Zentralbl Chir*, May 2013. doi: 10.1055/s-0032-1328346. URL http://dx.doi.org/10.1055/s-0032-1328346.

R. Hromas, J. Radich, and S. Collins. Pcr cloning of an orphan homeobox gene (prh) preferentially expressed in myeloid and liver cells. *Biochem Biophys Res Commun*, 195(2):976–983, Sep 1993. doi: 10.1006/bbrc.1993.2140. URL http://dx.doi.org/10.1006/bbrc.1993.2140.

D. W. Huang, B. T. Sherman, and R. A. Lempicki. Systematic and integrative analysis of large gene lists using david bioinformatics resources. *Nat Protoc*, 4(1):44–57, 2009. doi: 10.1038/nprot.2008.211. URL http://dx.doi.org/10.1038/nprot.2008.211.

P. Huang, L. Zhang, Y. Gao, Z. He, D. Yao, Z. Wu, J. Cen, X. Chen, C. Liu, Y. Hu, D. Lai, Z. Hu, L. Chen, Y. Zhang, X. Cheng, X. Ma, G. Pan, X. Wang, and L. Hui. Direct reprogramming of human fibroblasts to functional and expandable hepatocytes. *Cell Stem Cell*, 14(3):370–384, Mar 2014. doi: 10.1016/j.stem.2014.01.003. URL http://dx.doi.org/10.1016/j.stem.2014.01.003.

M. Huch, C. Dorrell, S. F. Boj, J. H. van Es, V. S. W. Li, M. van de Wetering, T. Sato, K. Hamer, N. Sasaki, M. J. Finegold, A. Haft, R. G. Vries, M. Grompe, and H. Clevers. In vitro expansion of single lgr5+ liver stem cells induced by wnt-driven regeneration. *Nature*, 494(7436):247–250, Feb 2013. doi: 10.1038/nature11826. URL http://dx.doi.org/10.1038/nature11826.

C. Hudson, D. Clements, R. V. Friday, D. Stott, and H. R. Woodland. Xsox17alpha and -beta mediate endoderm formation in xenopus. *Cell*, 91(3):397–405, Oct 1997.

R. O. Hynes. Integrins: versatility, modulation, and signaling in cell adhesion. *Cell*, 69 (1):11–25, Apr 1992.

G. J. Inman, F. J. Nicols, J. F. Callahan, J. D. Harling, L. M. Gaster, A. D. Reith, N. J. Laping, and C. S. Hill. Sb-431542 is a potent and specific inhibitor of transforming growth factor-beta superfamily type i activin receptor-like kinase (alk) receptors alk4, alk5, and alk7. *Mol Pharmacol*, 62(1):65–74, Jul 2002.

R. J. Isfort, D. B. Cody, S. B. Stuard, C. J. Randall, C. Miller, G. M. Ridder, C. J. Doersen, W. G. Richards, B. K. Yoder, J. E. Wilkinson, and R. P. Woychik. The combination of epidermal growth factor and transforming growth factor-beta induces novel phenotypic changes in mouse liver stem cell lines. *J Cell Sci*, 110 (Pt 24): 3117–3129, Dec 1997.

T. Ishikawa, A. Banas, K. Hagiwara, H. Iwaguro, and T. Ochiya. Stem cells for hepatic regeneration: the role of adipose tissue derived mesenchymal stem cells. *Curr Stem Cell Res Ther*, 5(2):182–189, Jun 2010.

T. Ishizaki, M. Uehata, I. Tamechika, J. Keel, K. Nonomura, M. Maekawa, and S. Narumiya. Pharmacological properties of y-27632, a specific inhibitor of rho-associated kinases. *Mol Pharmacol*, 57(5):976–983, May 2000.

Y. Ito, T. Matsui, A. Kamiya, T. Kinoshita, and A. Miyajima. Retroviral gene transfer of signaling molecules into murine fetal hepatocytes defines distinct roles for the stat3 and ras pathways during hepatic development. *Hepatology*, 32(6):1370–1376, Dec 2000. doi: 10.1053/jhep.2000.19815. URL http://dx.doi.org/10.1053/jhep.2000.19815.

V. Jaks, N. Barker, M. Kasper, J. H. van Es, H. J. Snippert, H. Clevers, and R. Toftgrd. Lgr5 marks cycling, yet long-lived, hair follicle stem cells. *Nat Genet*, 40(11):1291–1299, Nov 2008. doi: 10.1038/ng.239. URL http://dx.doi.org/10.1038/ng.239.

D. James, A. J. Levine, D. Besser, and A. Hemmati-Brivanlou. Tgfbeta/activin/nodal signaling is necessary for the maintenance of pluripotency in human embryonic stem cells. *Development*, 132(6):1273–1282, Mar 2005. doi: 10.1242/dev.01706. URL http://dx.doi.org/10.1242/dev.01706.

D. G. J. Jennen, C. Magkoufopoulou, H. B. Ketelslegers, M. H. M. van Herwijnen, J. C. S. Kleinjans, and J. H. M. van Delft. Comparison of hepg2 and heparg by whole-genome gene expression analysis for the purpose of chemical hazard identification. *Toxicol Sci*, 115(1):66–79, May 2010. doi: 10.1093/toxsci/kfq026. URL http://dx.doi.org/10.1093/toxsci/kfq026.

J. Jensen, J. Hyllner, and P. Bjrquist. Human embryonic stem cell technologies and drug discovery. *J Cell Physiol*, 219(3):513–519, Jun 2009. doi: 10.1002/jcp.21732. URL http://dx.doi.org/10.1002/jcp.21732.

M. J. A. Jetten, J. C. S. Kleinjans, S. M. Claessen, C. Chesn, and J. H. M. van Delft. Baseline and genotoxic compound induced gene expression profiles in hepg2 and heparg compared to primary human hepatocytes. *Toxicol In Vitro*, 27(7):2031–2040, Oct 2013. doi: 10.1016/j.tiv.2013.07.010. URL http://dx.doi.org/10.1016/j.tiv.2013.07.010.

C. M. Jones, K. M. Lyons, and B. L. Hogan. Involvement of bone morphogenetic protein-4 (bmp-4) and vgr-1 in morphogenesis and neurogenesis in the mouse. *Development*, 111(2):531–542, Feb 1991.

E. A. Jones, M. Clement-Jones, and D. I. Wilson. Jagged1 expression in human embryos: correlation with the alagille syndrome phenotype. *J Med Genet*, 37(9):658–662, Sep 2000.

J. Jozefczuk, A. Prigione, L. Chavez, and J. Adjaye. Comparative analysis of human embryonic stem cell and induced pluripotent stem cell-derived hepatocyte-like cells reveals current drawbacks and possible strategies for improved differentiation. *Stem Cells Dev*, 20(7):1259–1275, Jul 2011. doi: 10.1089/scd.2010.0361. URL http://dx.doi.org/10.1089/scd.2010.0361.

J. Jozefczuk, K. Drews, and J. Adjaye. Preparation of mouse embryonic fibroblast cells suitable for culturing human embryonic and induced pluripotent stem cells. *J Vis Exp*, (64), 2012a. doi: 10.3791/3854. URL http://dx.doi.org/10.3791/3854.

J. Jozefczuk, K. Kashofer, R. Ummanni, F. Henjes, S. Rehman, S. Geenen, W. Wruck, C. Regenbrecht, A. Daskalaki, C. Wierling, P. Turano, I. Bertini, U. Korf, K. Zatloukal, H. V. Westerhoff, H. Lehrach, and J. Adjaye. A systems biology approach to deciphering the etiology of steatosis employing patient-derived dermal fibroblasts

and ips cells. *Front Physiol*, 3:339, 2012b. doi: 10.3389/fphys.2012.00339. URL http://dx.doi.org/10.3389/fphys.2012.00339.

J. Jung, M. Zheng, M. Goldfarb, and K. S. Zaret. Initiation of mammalian liver development from endoderm by fibroblast growth factors. *Science*, 284(5422):1998–2003, Jun 1999.

M. Kaloyianni and R. A. Freedland. Contribution of several amino acids and lactate to gluconeogenesis in hepatocytes isolated from rats fed various diets. *J Nutr*, 120(1):116–122, Jan 1990.

A. Kamiya, T. Kinoshita, Y. Ito, T. Matsui, Y. Morikawa, E. Senba, K. Nakashima, T. Taga, K. Yoshida, T. Kishimoto, and A. Miyajima. Fetal liver development requires a paracrine action of oncostatin m through the gp130 signal transducer. *EMBO J*, 18 (8):2127–2136, Apr 1999. doi: 10.1093/emboj/18.8.2127. URL http://dx.doi.org/10.1093/emboj/18.8.2127.

A. Kamiya, T. Kinoshita, and A. Miyajima. Oncostatin m and hepatocyte growth factor induce hepatic maturation via distinct signaling pathways. *FEBS Lett*, 492(1-2):90–94, Mar 2001.

J. S. Kang, C. Liu, and R. Derynck. New regulatory mechanisms of tgf-beta receptor function. *Trends Cell Biol*, 19(8):385–394, Aug 2009. doi: 10.1016/j.tcb.2009.05.008. URL http://dx.doi.org/10.1016/j.tcb.2009.05.008.

T. Kawamura, J. Suzuki, Y. V. Wang, S. Menendez, L. B. Morera, A. Raya, G. M. Wahl, and J. C. Izpisa Belmonte. Linking the p53 tumour suppressor pathway to somatic cell reprogramming. *Nature*, 460(7259):1140–1144, Aug 2009. doi: 10.1038/nature08311. URL http://dx.doi.org/10.1038/nature08311.

C. Khler, A. W. Bell, W. C. Bowen, S. P. Monga, W. Fleig, and G. K. Michalopoulos. Expression of notch-1 and its ligand jagged-1 in rat liver during liver regeneration. *Hepatology*, 39(4):1056–1065, Apr 2004. doi: 10.1002/hep.20156. URL http://dx.doi.org/10.1002/hep.20156.

D. Kim, C.-H. Kim, J.-I. Moon, Y.-G. Chung, M.-Y. Chang, B.-S. Han, S. Ko, E. Yang, K. Y. Cha, R. Lanza, and K.-S. Kim. Generation of human induced pluripotent stem cells by direct delivery of reprogramming proteins. *Cell Stem Cell*, 4(6):472–476, Jun 2009a. doi: 10.1016/j.stem.2009.05.005. URL http://dx.doi.org/10.1016/j.stem.2009.05.005.

D. Kim, J. Choi, K.-M. Han, B. H. Lee, J.-H. Choi, H.-W. Yoo, and Y.-M. Han. Impaired osteogenesis in menkes disease-derived induced pluripotent stem cells. *Stem Cell Res Ther*, 6(1):160, 2015. doi: 10.1186/s13287-015-0147-5. URL http://dx.doi.org/10.1186/s13287-015-0147-5.

H. J. Kim and D. Bar-Sagi. Modulation of signalling by sprouty: a developing story. *Nat Rev Mol Cell Biol*, 5(6):441–450, Jun 2004. doi: 10.1038/nrm1400. URL http://dx.doi.org/10.1038/nrm1400.

J. B. Kim, H. Zaehres, M. J. Arazo-Bravo, and H. R. Schler. Generation of induced pluripotent stem cells from neural stem cells. *Nat Protoc*, 4(10):1464–1470, 2009b. doi: 10.1038/nprot.2009.173. URL http://dx.doi.org/10.1038/nprot.2009.173.

K. Kim, Z. Lu, and E. D. Hay. Direct evidence for a role of beta-catenin/lef-1 signaling pathway in induction of emt. *Cell Biol Int*, 26(5):463–476, 2002.

S. Kim, P. Wong, and P. A. Coulombe. A keratin cytoskeletal protein regulates protein synthesis and epithelial cell growth. *Nature*, 441(7091):362–365, May 2006. doi: 10.1038/nature04659. URL http://dx.doi.org/10.1038/nature04659.

E. Kiskinis and K. Eggan. Progress toward the clinical application of patient-specific pluripotent stem cells. *J Clin Invest*, 120(1):51–59, Jan 2010. doi: 10.1172/JCI40553. URL http://dx.doi.org/10.1172/JCI40553.

M. Kiso, T. S. Hamazaki, M. Itoh, S. Kikuchi, H. Nakagawa, and H. Okochi. Synergistic effect of pdgf and fgf2 for cell proliferation and hair inductive activity in murine vibrissal dermal papilla in vitro. *J Dermatol Sci*, 79(2):110–118, Aug 2015. doi: 10.1016/j.jdermsci.2015.04.007. URL http://dx.doi.org/10.1016/j.jdermsci.2015.04.007.

Y. Kodama, M. Hijikata, R. Kageyama, K. Shimotohno, and T. Chiba. The role of notch signaling in the development of intrahepatic bile ducts. *Gastroenterology*, 127 (6):1775–1786, Dec 2004.

N. Kojima, T. Kinoshita, A. Kamiya, K. Nakamura, K. Nakashima, T. Taga, and A. Miyajima. Cell density-dependent regulation of hepatic development by a gp130-independent pathway. *Biochem Biophys Res Commun*, 277(1):152–158, Oct 2000. doi: 10.1006/bbrc.2000.3635. URL http://dx.doi.org/10.1006/bbrc.2000.3635.

Y. Kondo, T. Iwao, K. Nakamura, T. Sasaki, S. Takahashi, N. Kamada, T. Matsubara, F. J. Gonzalez, H. Akutsu, Y. Miyagawa, H. Okita, N. Kiyokawa, M. Toyoda, A. Umezawa, K. Nagata, T. Matsunaga, and S. Ohmori. An efficient method for differentiation of human induced pluripotent stem cells into hepatocyte-like cells retaining drug metabolizing activity. *Drug Metab Pharmacokinet*, 29(3):237–243, 2014a.

Y. Kondo, T. Iwao, S. Yoshihashi, K. Mimori, R. Ogihara, K. Nagata, K. Kurose, M. Saito, T. Niwa, T. Suzuki, N. Miyata, S. Ohmori, K. Nakamura, and T. Matsunaga. Histone deacetylase inhibitor valproic acid promotes the differentiation of human induced pluripotent stem cells into hepatocyte-like cells. *PLoS One*, 9(8): e104010, 2014b. doi: 10.1371/journal.pone.0104010. URL http://dx.doi.org/10.1371/journal.pone.0104010.

H. Kouhara, Y. R. Hadari, T. Spivak-Kroizman, J. Schilling, D. Bar-Sagi, I. Lax, and J. Schlessinger. A lipid-anchored grb2-binding protein that links fgf-receptor activation to the ras/mapk signaling pathway. *Cell*, 89(5):693–702, May 1997.

M. Koutsourakis, A. Langeveld, R. Patient, R. Beddington, and F. Grosveld. The transcription factor gata6 is essential for early extraembryonic development. *Development*, 126(9):723–732, May 1999.

M. Kretzschmar and J. Massagu. Smads: mediators and regulators of tgf-beta signaling. *Curr Opin Genet Dev*, 8(1):103–111, Feb 1998.

K. Kuhn, S. C. Baker, E. Chudin, M.-H. Lieu, S. Oeser, H. Bennett, P. Rigault, D. Barker, T. K. McDaniel, and M. S. Chee. A novel, high-performance random array platform for quantitative gene expression profiling. *Genome Res*, 14(11):2347–2356, Nov 2004. doi: 10.1101/gr.2739104. URL http://dx.doi.org/10.1101/gr.2739104.

G. A. Kullak-Ublick and P. J. Meier. Mechanisms of cholestasis. *Clin Liver Dis*, 4(2): 357–385, May 2000.

A. T. Kwon, D. J. Arenillas, R. Worsley Hunt, and W. W. Wasserman. opossum-3: advanced analysis of regulatory motif over-representation across genes or chip-seq datasets. *G3 (Bethesda)*, 2(9):987–1002, Sep 2012. doi: 10.1534/g3.112.003202. URL http://dx.doi.org/10.1534/g3.112.003202.

M. A. Lagarkova, M. V. Shutova, A. N. Bogomazova, E. M. Vassina, E. A. Glazov, P. Zhang, A. A. Rizvanov, I. V. Chestkov, and S. L. Kiselev. Induction of pluripotency in human endothelial cells resets epigenetic profile on genome scale. *Cell Cycle*, 9(5): 937–946, Mar 2010.

E. Lai, V. R. Prezioso, E. Smith, O. Litvin, R. H. Costa, and J. Darnell, Jr. Hnf-3a, a hepatocyte-enriched transcription factor of novel structure is regulated transcriptionally. *Genes Dev*, 4(8):1427–1436, Aug 1990.

V. Lamba, Y. Ghodke, W. Guan, and T. S. Tracy. microrna-34a is associated with expression of key hepatic transcription factors and cytochrome p450s. *Biochem Biophys Res Commun*, Feb 2014. doi: 10.1016/j.bbrc.2014.02.024. URL http://dx.doi.org/10.1016/j.bbrc.2014.02.024.

Y.-J. Lan, H. Chen, J.-Q. Chen, Q.-H. Lei, M. Zheng, and Z.-R. Shao. Immunolocalization of vimentin, keratin 17, ki-67, involucrin, ?-catenin and e-cadherin in cutaneous squamous cell carcinoma. *Pathol Oncol Res*, Sep 2013. doi: 10.1007/s12253-013-9690-5. URL http://dx.doi.org/10.1007/s12253-013-9690-5.

T. H.-W. Ldtke, V. M. Christoffels, M. Petry, and A. Kispert. Tbx3 promotes liver bud expansion during mouse development by suppression of cholangiocyte differentiation. *Hepatology*, 49(3):969–978, Mar 2009. doi: 10.1002/hep.22700. URL http://dx.doi.org/10.1002/hep.22700.

E. J. Lee, H.-N. Lee, H.-J. Kang, K.-H. Kim, J. Hur, H.-J. Cho, J. Lee, H.-M. Chung, J. Cho, M.-Y. Cho, S.-K. Oh, S.-Y. Moon, Y.-B. Park, and H.-S. Kim. Novel embryoid body-based method to derive mesenchymal stem cells from human embryonic stem cells. *Tissue Eng Part A*, 16(2):705–715, Feb 2010. doi: 10.1089/ten.tea.2008.0596. URL http://dx.doi.org/10.1089/ten.tea.2008.0596.

S.-W. Lee, X. Wang, N. R. Chowdhury, and J. Roy-Chowdhury. Hepatocyte transplantation: state of the art and strategies for overcoming existing hurdles. *Ann Hepatol*, 3(2):48–53, 2004.

F. P. Lemaigre. Development of the biliary tract. *Mech Dev*, 120(1):81–87, Jan 2003.

H. Li, M. Collado, A. Villasante, K. Strati, S. Ortega, M. Caamero, M. A. Blasco, and M. Serrano. The ink4/arf locus is a barrier for ips cell reprogramming. *Nature*, 460 (7259):1136–1139, Aug 2009. doi: 10.1038/nature08290. URL http://dx.doi.org/10.1038/nature08290.

J. Li, G. Ning, and S. A. Duncan. Mammalian hepatocyte differentiation requires the transcription factor hnf-4alpha. *Genes Dev*, 14(4):464–474, Feb 2000.

P. Li, Y. Chen, K. K. Mak, C. K. Wong, C. C. Wang, and P. Yuan. Functional role of mst1/mst2 in embryonic stem cell differentiation. *PLoS One*, 8(11):e79867, 2013. doi: 10.1371/journal.pone.0079867. URL http://dx.doi.org/10.1371/journal.pone.0079867.

V. S. W. Li, S. S. Ng, P. J. Boersema, T. Y. Low, W. R. Karthaus, J. P. Gerlach, S. Mohammed, A. J. R. Heck, M. M. Maurice, T. Mahmoudi, and H. Clevers. Wnt signaling through inhibition of ?-catenin degradation in an intact axin1 complex. *Cell*, 149(6):1245–1256, Jun 2012. doi: 10.1016/j.cell.2012.05.002. URL http://dx.doi.org/10.1016/j.cell.2012.05.002.

B. Lichtner, P. Knaus, H. Lehrach, and J. Adjaye. Bmp10 as a potent inducer of trophoblast differentiation in human embryonic and induced pluripotent stem cells. *Biomaterials*, 34(38):9789–9802, Dec 2013. doi: 10.1016/j.biomaterials.2013.08.084. URL http://dx.doi.org/10.1016/j.biomaterials.2013.08.084.

J. Lin, X. Qin, Z. Zhu, J. Mu, L. Zhu, K. Wu, H. Jiao, X. Xu, and Q. Ye. Fhl family members suppress vascular endothelial growth factor expression through blockade of dimerization of hif1? and hif1?. *IUBMB Life*, 64(11):921–930, Nov 2012. doi: 10.1002/iub.1089. URL http://dx.doi.org/10.1002/iub.1089.

J. I. Lin, C. L. C. Poon, and K. F. Harvey. The hippo size control pathway–ever expanding. *Sci Signal*, 6(259):pe4, 2013. doi: 10.1126/scisignal.2003813. URL http://dx.doi.org/10.1126/scisignal.2003813.

T. Lin, R. Ambasudhan, X. Yuan, W. Li, S. Hilcove, R. Abujarour, X. Lin, H. S. Hahm, E. Hao, A. Hayek, and S. Ding. A chemical platform for improved induction

of human ipscs. *Nat Methods*, 6(11):805–808, Nov 2009. doi: 10.1038/nmeth.1393. URL http://dx.doi.org/10.1038/nmeth.1393.

R. A. Lindberg, T. S. Juan, A. A. Welcher, Y. Sun, R. Cupples, B. Guthrie, and F. A. Fletcher. Cloning and characterization of a specific receptor for mouse oncostatin m. *Mol Cell Biol*, 18(6):3357–3367, Jun 1998.

J. Liu, R. Streiff, Y. L. Zhang, R. E. Vestal, M. J. Spence, and M. R. Briggs. Novel mechanism of transcriptional activation of hepatic ldl receptor by oncostatin m. *J Lipid Res*, 38(10):2035–2048, Oct 1997a.

J. Liu, Y. L. Zhang, M. J. Spence, R. E. Vestal, P. M. Wallace, and D. S. Grass. Liver ldl receptor mrna expression is decreased in human apob/cetp double transgenic mice and is regulated by diet as well as the cytokine oncostatin m. *Arterioscler Thromb Vasc Biol*, 17(11):2948–2954, Nov 1997b.

P. Liu, M. Wakamiya, M. J. Shea, U. Albrecht, R. R. Behringer, and A. Bradley. Requirement for wnt3 in vertebrate axis formation. *Nat Genet*, 22(4):361–365, Aug 1999. doi: 10.1038/11932. URL http://dx.doi.org/10.1038/11932.

Y. Liu, Z. Song, Y. Zhao, H. Qin, J. Cai, H. Zhang, T. Yu, S. Jiang, G. Wang, M. Ding, and H. Deng. A novel chemical-defined medium with bfgf and n2b27 supplements supports undifferentiated growth in human embryonic stem cells. *Biochem Biophys Res Commun*, 346(1):131–139, Jul 2006. doi: 10.1016/j.bbrc.2006.05.086. URL http://dx.doi.org/10.1016/j.bbrc.2006.05.086.

K. M. Loomes, D. B. Taichman, C. L. Glover, P. T. Williams, J. E. Markowitz, D. A. Piccoli, H. S. Baldwin, and R. J. Oakey. Characterization of notch receptor expression in the developing mammalian heart and liver. *Am J Med Genet*, 112(2):181–189, Oct 2002. doi: 10.1002/ajmg.10592. URL http://dx.doi.org/10.1002/ajmg.10592.

S. Lorenzini, A. Isidori, L. Catani, A. Gramenzi, S. Talarico, F. Bonifazi, V. Giudice, R. Conte, M. Baccarani, M. Bernardi, S. J. Forbes, R. M. Lemoli, and P. Andreone. Stem cell mobilization and collection in patients with liver cirrhosis. *Aliment Pharmacol Ther*, 27(10):932–939, May 2008. doi: 10.1111/j.1365-2036.2008.03670.x. URL http://dx.doi.org/10.1111/j.1365-2036.2008.03670.x.

A. A. Louis, P. Van Eyken, B. A. Haber, C. Hicks, G. Weinmaster, R. Taub, and E. B. Rand. Hepatic jagged1 expression studies. *Hepatology*, 30(5):1269–1275, Nov 1999. doi: 10.1002/hep.510300512. URL http://dx.doi.org/10.1002/hep.510300512.

J. Lu, R. Hou, C. J. Booth, S.-H. Yang, and M. Snyder. Defined culture conditions of human embryonic stem cells. *Proc Natl Acad Sci U S A*, 103(15):5688–5693, Apr 2006. doi: 10.1073/pnas.0601383103. URL http://dx.doi.org/10.1073/pnas.0601383103.

N. Ma, B. Liao, H. Zhang, L. Wang, Y. Shan, Y. Xue, K. Huang, S. Chen, X. Zhou, Y. Chen, D. Pei, and G. Pan. Transcription activator-like effector nuclease (talen)-mediated gene correction in integration-free ?-thalassemia induced pluripotent stem cells. *J Biol Chem*, 288(48):34671–34679, Nov 2013a. doi: 10.1074/jbc.M113.496174. URL http://dx.doi.org/10.1074/jbc.M113.496174.

T. Ma, M. Xie, T. Laurent, and S. Ding. Progress in the reprogramming of somatic cells. *Circ Res*, 112(3):562–574, Feb 2013b. doi: 10.1161/CIRCRESAHA.111.249235. URL http://dx.doi.org/10.1161/CIRCRESAHA.111.249235.

B. T. MacDonald, K. Tamai, and X. He. Wnt/beta-catenin signaling: components, mechanisms, and diseases. *Dev Cell*, 17(1):9–26, Jul 2009. doi: 10.1016/j.devcel.2009.06.016. URL http://dx.doi.org/10.1016/j.devcel.2009.06.016.

D. Maetzel, S. Sarkar, H. Wang, L. Abi-Mosleh, P. Xu, A. W. Cheng, Q. Gao, M. Mitalipova, and R. Jaenisch. Genetic and chemical correction of cholesterol accumulation and impaired autophagy in hepatic and neural cells derived from niemann-pick type c patient-specific ips cells. *Stem Cell Reports*, 2(6):866–880, Jun 2014. doi: 10.1016/j.stemcr.2014.03.014. URL http://dx.doi.org/10.1016/j.stemcr.2014.03.014.

N. Mah, Y. Wang, M.-C. Liao, A. Prigione, J. Jozefczuk, B. Lichtner, K. Wolfrum, M. Haltmeier, M. Flttmann, M. Schaefer, A. Hahn, R. Mrowka, E. Klipp, M. A. Andrade-Navarro, and J. Adjaye. Molecular insights into reprogramming-initiation events mediated by the oskm gene regulatory network. *PLoS One*, 6(8):e24351, 2011. doi: 10.1371/journal.pone.0024351. URL http://dx.doi.org/10.1371/journal.pone.0024351.

P. A. Maher. Nuclear translocation of fibroblast growth factor (fgf) receptors in response to fgf-2. *J Cell Biol*, 134(2):529–536, Jul 1996.

N. Maherali, T. Ahfeldt, A. Rigamonti, J. Utikal, C. Cowan, and K. Hochedlinger. A high-efficiency system for the generation and study of human induced pluripotent stem cells. *Cell Stem Cell*, 3(3):340–345, Sep 2008. doi: 10.1016/j.stem.2008.08.003. URL http://dx.doi.org/10.1016/j.stem.2008.08.003.

D. E. Malarkey, K. Johnson, L. Ryan, G. Boorman, and R. R. Maronpot. New insights into functional aspects of liver morphology. *Toxicol Pathol*, 33(1):27–34, 2005. doi: 10.1080/01926230590881826. URL http://dx.doi.org/10.1080/01926230590881826.

P. Mali, L. Yang, K. M. Esvelt, J. Aach, M. Guell, J. E. DiCarlo, J. E. Norville, and G. M. Church. Rna-guided human genome engineering via cas9. *Science*, 339(6121):823–826, Feb 2013. doi: 10.1126/science.1232033. URL http://dx.doi.org/10.1126/science.1232033.

S. K. Mallanna and S. A. Duncan. Differentiation of hepatocytes from pluripotent stem cells. *Curr Protoc Stem Cell Biol*, 26:Unit 1G.4., 2013. doi: 10.1002/9780470151808.sc01g04s26. URL http://dx.doi.org/10.1002/9780470151808.sc01g04s26.

P. K. Mandal and D. J. Rossi. Reprogramming human fibroblasts to pluripotency using modified mrna. *Nat Protoc*, 8(3):568–582, Mar 2013. doi: 10.1038/nprot.nprot.2013. 019. URL http://dx.doi.org/10.1038/nprot.nprot.2013.019.

R. M. Marin, K. Strati, H. Li, M. Murga, R. Blanco, S. Ortega, O. Fernandez-Capetillo, M. Serrano, and M. A. Blasco. A p53-mediated dna damage response limits reprogramming to ensure ips cell genomic integrity. *Nature*, 460(7259):1149–1153, Aug 2009. doi: 10.1038/nature08287. URL http://dx.doi.org/10.1038/nature08287.

J. C. Mason, E. A. Lidington, S. R. Ahmad, and D. O. Haskard. bfgf and vegf synergistically enhance endothelial cytoprotection via decay-accelerating factor induction. *Am J Physiol Cell Physiol*, 282(3):C578–C587, Mar 2002. doi: 10.1152/ajpcell.00339.2001. URL http://dx.doi.org/10.1152/ajpcell.00339.2001.

J. Massagu. Receptors for the tgf-beta family. *Cell*, 69(7):1067–1070, Jun 1992.

J. Massagu. Tgf? signalling in context. *Nat Rev Mol Cell Biol*, 13(10):616–630, Oct 2012. doi: 10.1038/nrm3434. URL http://dx.doi.org/10.1038/nrm3434.

J. Massagu, S. Cheifetz, R. A. Ignotz, and F. T. Boyd. Multiple type-beta transforming growth factors and their receptors. *J Cell Physiol Suppl*, Suppl 5:43–47, 1987.

A. Masszi, C. Di Ciano, G. Sirokmny, W. T. Arthur, O. D. Rotstein, J. Wang, C. A. G. McCulloch, L. Rosivall, I. Mucsi, and A. Kapus. Central role for rho in tgf-beta1-induced alpha-smooth muscle actin expression during epithelial-mesenchymal transition. *Am J Physiol Renal Physiol*, 284(5):F911–F924, May 2003. doi: 10.1152/ ajprenal.00183.2002. URL http://dx.doi.org/10.1152/ajprenal.00183.2002.

A. J. Matas, D. E. Sutherland, M. W. Steffes, S. M. Mauer, A. Sowe, R. L. Simmons, and J. S. Najarian. Hepatocellular transplantation for metabolic deficiencies: decrease of plasms bilirubin in gunn rats. *Science*, 192(4242):892–894, May 1976.

T. Matsui, T. Kinoshita, Y. Morikawa, K. Tohya, M. Katsuki, Y. Ito, A. Kamiya, and A. Miyajima. K-ras mediates cytokine-induced formation of e-cadherin-based adherens junctions during liver development. *EMBO J*, 21(5):1021–1030, Mar 2002. doi: 10. 1093/emboj/21.5.1021. URL http://dx.doi.org/10.1093/emboj/21.5.1021.

P. Matz and J. Adjaye. Generation of ipsc line epihuvec from human umbilical vein endothelial cells. *Stem Cell Research*, 15:581–583, 2015. doi: 10.1016/j.scr.2015.10. 004.

P. Matz and J. Adjaye. Episomal-based generation of an ips cell line from human fetal foreskin fibroblasts. *Stem Cell Research*, 16:67–69, 2016. doi: 10.1016/j.scr.2015.12. 009.

Y. Mayshar, U. Ben-David, N. Lavon, J.-C. Biancotti, B. Yakir, A. T. Clark, K. Plath, W. E. Lowry, and N. Benvenisty. Identification and classification of chromosomal

aberrations in human induced pluripotent stem cells. *Cell Stem Cell*, 7(4):521–531, Oct 2010. doi: 10.1016/j.stem.2010.07.017. URL http://dx.doi.org/10.1016/j.stem.2010.07.017.

E. M. Mazaris, C. T. Roussos, and V. E. Papalois. Hepatocyte transplantation: a review of worldwide clinical developments and experiences. *Exp Clin Transplant*, 3 (1):306–315, Jun 2005.

B. McCright, J. Lozier, and T. Gridley. A mouse model of alagille syndrome: Notch2 as a genetic modifier of jag1 haploinsufficiency. *Development*, 129(4):1075–1082, Feb 2002.

C. McKee, M. Perez-Cruet, F. Chavez, and G. R. Chaudhry. Simplified three-dimensional culture system for long-term expansion of embryonic stem cells. *World J Stem Cells*, 7(7):1064–1077, Aug 2015. doi: 10.4252/wjsc.v7.i7.1064. URL http://dx.doi.org/10.4252/wjsc.v7.i7.1064.

A. B. McLean, K. A. D'Amour, K. L. Jones, M. Krishnamoorthy, M. J. Kulik, D. M. Reynolds, A. M. Sheppard, H. Liu, Y. Xu, E. E. Baetge, and S. Dalton. Activin a efficiently specifies definitive endoderm from human embryonic stem cells only when phosphatidylinositol 3-kinase signaling is suppressed. *Stem Cells*, 25(1):29–38, Jan 2007. doi: 10.1634/stemcells.2006-0219. URL http://dx.doi.org/10.1634/stemcells.2006-0219.

V. A. McLin, S. A. Rankin, and A. M. Zorn. Repression of wnt/beta-catenin signaling in the anterior endoderm is essential for liver and pancreas development. *Development*, 134(12):2207–2217, Jun 2007. doi: 10.1242/dev.001230. URL http://dx.doi.org/10.1242/dev.001230.

E. S. Medlock and J. L. Haar. The liver hemopoietic environment: I. developing hepatocytes and their role in fetal hemopoiesis. *Anat Rec*, 207(1):31–41, Sep 1983. doi: 10.1002/ar.1092070105. URL http://dx.doi.org/10.1002/ar.1092070105.

A. J. Meijer, W. H. Lamers, and R. A. Chamuleau. Nitrogen metabolism and ornithine cycle function. *Physiol Rev*, 70(3):701–748, Jul 1990.

E. N. Meyers, M. Lewandoski, and G. R. Martin. An fgf8 mutant allelic series generated by cre- and flp-mediated recombination. *Nat Genet*, 18(2):136–141, Feb 1998. doi: 10.1038/ng0298-136. URL http://dx.doi.org/10.1038/ng0298-136.

P. J. Miettinen, R. Ebner, A. R. Lopez, and R. Derynck. Tgf-beta induced transdifferentiation of mammary epithelial cells to mesenchymal cells: involvement of type i receptors. *J Cell Biol*, 127(6 Pt 2):2021–2036, Dec 1994.

D. L. Miller, S. Ortega, O. Bashayan, R. Basch, and C. Basilico. Compensation by fibroblast growth factor 1 (fgf1) does not account for the mild phenotypic defects observed in fgf2 null mice. *Mol Cell Biol*, 20(6):2260–2268, Mar 2000.

J. M. Mir, M. Laguno, A. Moreno, A. Rimola, and H. C. O. I. H. W. G. . Management of end stage liver disease (esld): what is the current role of orthotopic liver transplantation (olt)? *J Hepatol*, 44(1 Suppl):S140–S145, 2006.

S.-H. Mirmalek-Sani, R. S. Tare, S. M. Morgan, H. I. Roach, D. I. Wilson, N. A. Hanley, and R. O. C. Oreffo. Characterization and multipotentiality of human fetal femur-derived cells: implications for skeletal tissue regeneration. *Stem Cells*, 24(4):1042–1053, Apr 2006. doi: 10.1634/stemcells.2005-0368. URL http://dx.doi.org/10.1634/stemcells.2005-0368.

T. Mitaka. The current status of primary hepatocyte culture. *Int J Exp Pathol*, 79(6):393–409, Dec 1998.

T. Mitaka, C. A. Sattler, G. L. Sattler, L. M. Sargent, and H. C. Pitot. Multiple cell cycles occur in rat hepatocytes cultured in the presence of nicotinamide and epidermal growth factor. *Hepatology*, 13(1):21–30, Jan 1991.

M. Mito, M. Kusano, and Y. Kawaura. Hepatocyte transplantation in man. *Transplant Proc*, 24(6):3052–3053, Dec 1992.

A. Mitra, A. Satelli, X. Xia, J. Cutrera, L. Mishra, and S. Li. Cell-surface vimentin: A mislocalized protein for isolating csvimentin(+) cd133(-) novel stem-like hepatocellular carcinoma cells expressing emt markers. *Int J Cancer*, Dec 2014. doi: 10.1002/ijc.29382. URL http://dx.doi.org/10.1002/ijc.29382.

K. Miyazono, S. Maeda, and T. Imamura. Bmp receptor signaling: transcriptional targets, regulation of signals, and signaling cross-talk. *Cytokine Growth Factor Rev*, 16(3):251–263, Jun 2005. doi: 10.1016/j.cytogfr.2005.01.009. URL http://dx.doi.org/10.1016/j.cytogfr.2005.01.009.

N. Miyoshi, H. Ishii, H. Nagano, N. Haraguchi, D. L. Dewi, Y. Kano, S. Nishikawa, M. Tanemura, K. Mimori, F. Tanaka, T. Saito, J. Nishimura, I. Takemasa, T. Mizushima, M. Ikeda, H. Yamamoto, M. Sekimoto, Y. Doki, and M. Mori. Reprogramming of mouse and human cells to pluripotency using mature micrornas. *Cell Stem Cell*, 8(6):633–638, Jun 2011. doi: 10.1016/j.stem.2011.05.001. URL http://dx.doi.org/10.1016/j.stem.2011.05.001.

D. Mizrak, M. Brittan, and M. Alison. Cd133: molecule of the moment. *J Pathol*, 214(1):3–9, Jan 2008. doi: 10.1002/path.2283. URL http://dx.doi.org/10.1002/path.2283.

T. Mizuguchi, T. Hui, K. Palm, N. Sugiyama, T. Mitaka, A. A. Demetriou, and J. Rozga. Enhanced proliferation and differentiation of rat hepatocytes cultured with bone marrow stromal cells. *J Cell Physiol*, 189(1):106–119, Oct 2001. doi: 10.1002/jcp.1136. URL http://dx.doi.org/10.1002/jcp.1136.

F.-J. Mller, B. M. Schuldt, R. Williams, D. Mason, G. Altun, E. P. Papapetrou, S. Danner, J. E. Goldmann, A. Herbst, N. O. Schmidt, J. B. Aldenhoff, L. C. Laurent, and J. F. Loring. A bioinformatic assay for pluripotency in human cells. *Nat Methods*, 8(4):315–317, Apr 2011. doi: 10.1038/nmeth.1580. URL http://dx.doi.org/10.1038/nmeth.1580.

M. Mller and P. L. Jansen. The secretory function of the liver: new aspects of hepatobiliary transport. *J Hepatol*, 28(2):344–354, Feb 1998.

N. Mobarra, M. Soleimani, F. Kouhkan, Z. Hesari, R. Lahmy, M. Mossahebi-Mohammadi, E. Arefian, Z. Jaafarpour, H. Nasiri, R. Pakzad, R. Tavakoli, and P. Pasalar. Efficient differentiation of human induced pluripotent stem cell (hipsc) derived hepatocyte-like cells on hmscs feeder. *Int J Hematol Oncol Stem Cell Res*, 8(4):20–29, Oct 2014.

P. Morley and J. F. Whitfield. The differentiation inducer, dimethyl sulfoxide, transiently increases the intracellular calcium ion concentration in various cell types. *J Cell Physiol*, 156(2):219–225, Aug 1993. doi: 10.1002/jcp.1041560202. URL http://dx.doi.org/10.1002/jcp.1041560202.

E. E. Morrisey, Z. Tang, K. Sigrist, M. M. Lu, F. Jiang, H. S. Ip, and M. S. Parmacek. Gata6 regulates hnf4 and is required for differentiation of visceral endoderm in the mouse embryo. *Genes Dev*, 12(22):3579–3590, Nov 1998.

B. Mosley, C. De Imus, D. Friend, N. Boiani, B. Thoma, L. S. Park, and D. Cosman. Dual oncostatin m (osm) receptors. cloning and characterization of an alternative signaling subunit conferring osm-specific receptor activation. *J Biol Chem*, 271(51):32635–32643, Dec 1996.

A. Moustakas and C.-H. Heldin. The regulation of tgfbeta signal transduction. *Development*, 136(22):3699–3714, Nov 2009. doi: 10.1242/dev.030338. URL http://dx.doi.org/10.1242/dev.030338.

L. Muglia and J. Locker. Developmental regulation of albumin and alpha-fetoprotein gene expression in the rat. *Nucleic Acids Res*, 12(17):6751–6762, Sep 1984.

C. E. Murry and G. Keller. Differentiation of embryonic stem cells to clinically relevant populations: lessons from embryonic development. *Cell*, 132(4):661–680, Feb 2008. doi: 10.1016/j.cell.2008.02.008. URL http://dx.doi.org/10.1016/j.cell.2008.02.008.

H. Nakagawa, Y. Hikiba, Y. Hirata, J. Font-Burgada, K. Sakamoto, Y. Hayakawa, K. Taniguchi, A. Umemura, H. Kinoshita, K. Sakitani, Y. Nishikawa, K. Hirano, T. Ikenoue, H. Ijichi, D. Dhar, W. Shibata, M. Akanuma, K. Koike, M. Karin, and S. Maeda. Loss of liver e-cadherin induces sclerosing cholangitis and promotes carcinogenesis. *Proc Natl Acad Sci U S A*, Jan 2014. doi: 10.1073/pnas.1322731111. URL http://dx.doi.org/10.1073/pnas.1322731111.

M. Nakagawa, M. Koyanagi, K. Tanabe, K. Takahashi, T. Ichisaka, T. Aoi, K. Okita, Y. Mochiduki, N. Takizawa, and S. Yamanaka. Generation of induced pluripotent stem cells without myc from mouse and human fibroblasts. *Nat Biotechnol*, 26(1):101–106, Jan 2008. doi: 10.1038/nbt1374. URL http://dx.doi.org/10.1038/nbt1374.

K. Nawa, T. Nakamura, A. Kumatori, C. Noda, and A. Ichihara. Glucocorticoid-dependent expression of the albumin gene in adult rat hepatocytes. *J Biol Chem*, 261(36):16883–16888, Dec 1986.

R. V. Nelakanti, N. G. Kooreman, and J. C. Wu. Teratoma formation: a tool for monitoring pluripotency in stem cell research. *Curr Protoc Stem Cell Biol*, 32:4A.8.1–4A.8.17, 2015. doi: 10.1002/9780470151808.sc04a08s32. URL http://dx.doi.org/10.1002/9780470151808.sc04a08s32.

K.-I. Nezasa, X. Tian, M. J. Zamek-Gliszczynski, N. J. Patel, T. J. Raub, and K. L. R. Brouwer. Altered hepatobiliary disposition of 5 (and 6)-carboxy-2',7'-dichlorofluorescein in abcg2 (bcrp1) and abcc2 (mrp2) knockout mice. *Drug Metab Dispos*, 34(4):718–723, Apr 2006. doi: 10.1124/dmd.105.007922. URL http://dx.doi.org/10.1124/dmd.105.007922.

P. M. Nguyen, T. L. Putoczki, and M. Ernst. Stat3-activating cytokines: A therapeutic opportunity for inflammatory bowel disease? *J Interferon Cytokine Res*, 35(5):340–350, May 2015. doi: 10.1089/jir.2014.0225. URL http://dx.doi.org/10.1089/jir.2014.0225.

S. S. Nijjar, H. A. Crosby, L. Wallace, S. G. Hubscher, and A. J. Strain. Notch receptor expression in adult human liver: a possible role in bile duct formation and hepatic neovascularization. *Hepatology*, 34(6):1184–1192, Dec 2001. doi: 10.1053/jhep.2001.29399. URL http://dx.doi.org/10.1053/jhep.2001.29399.

S. S. Nijjar, L. Wallace, H. A. Crosby, S. G. Hubscher, and A. J. Strain. Altered notch ligand expression in human liver disease: further evidence for a role of the notch signaling pathway in hepatic neovascularization and biliary ductular defects. *Am J Pathol*, 160(5):1695–1703, May 2002. doi: 10.1016/S0002-9440(10)61116-9. URL http://dx.doi.org/10.1016/S0002-9440(10)61116-9.

K. Nishimura, M. Sano, M. Ohtaka, B. Furuta, Y. Umemura, Y. Nakajima, Y. Ikehara, T. Kobayashi, H. Segawa, S. Takayasu, H. Sato, K. Motomura, E. Uchida, T. Kanayasu-Toyoda, M. Asashima, H. Nakauchi, T. Yamaguchi, and M. Nakanishi. Development of defective and persistent sendai virus vector: a unique gene delivery/expression system ideal for cell reprogramming. *J Biol Chem*, 286(6):4760–4771, Feb 2011. doi: 10.1074/jbc.M110.183780. URL http://dx.doi.org/10.1074/jbc.M110.183780.

S. Nissim, R. I. Sherwood, J. Wucherpfennig, D. Saunders, J. M. Harris, V. Esain, K. J. Carroll, G. M. Frechette, A. J. Kim, K. L. Hwang, C. C. Cutting, S. Elledge, T. E.

North, and W. Goessling. Prostaglandin e2 regulates liver versus pancreas cell-fate decisions and endodermal outgrowth. *Dev Cell*, 28(4):423–437, Feb 2014. doi: 10.1016/j.devcel.2014.01.006. URL http://dx.doi.org/10.1016/j.devcel.2014.01.006.

W. Niu, T. Zang, D. K. Smith, T. Y. Vue, Y. Zou, R. Bachoo, J. E. Johnson, and C.-L. Zhang. Sox2 reprograms resident astrocytes into neural progenitors in the adult brain. *Stem Cell Reports*, 4(5):780–794, May 2015. doi: 10.1016/j.stemcr.2015.03.006. URL http://dx.doi.org/10.1016/j.stemcr.2015.03.006.

D. T. Odom, R. D. Dowell, E. S. Jacobsen, L. Nekludova, P. A. Rolfe, T. W. Danford, D. K. Gifford, E. Fraenkel, G. I. Bell, and R. A. Young. Core transcriptional regulatory circuitry in human hepatocytes. *Mol Syst Biol*, 2:2006.0017, 2006. doi: 10.1038/msb4100059. URL http://dx.doi.org/10.1038/msb4100059.

M. Oft, K. H. Heider, and H. Beug. Tgfbeta signaling is necessary for carcinoma cell invasiveness and metastasis. *Curr Biol*, 8(23):1243–1252, Nov 1998.

S. Ogawa, J. Surapisitchat, C. Virtanen, M. Ogawa, M. Niapour, K. S. Sugamori, S. Wang, L. Tamblyn, C. Guillemette, E. Hoffmann, B. Zhao, S. Strom, R. R. Laposa, R. F. Tyndale, D. M. Grant, and G. Keller. Three-dimensional culture and camp signaling promote the maturation of human pluripotent stem cell-derived hepatocytes. *Development*, 140(15):3285–3296, Aug 2013. doi: 10.1242/dev.090266. URL http://dx.doi.org/10.1242/dev.090266.

E. Ogimura, S. Sekine, and T. Horie. Bile salt export pump inhibitors are associated with bile acid-dependent drug-induced toxicity in sandwich-cultured hepatocytes. *Biochem Biophys Res Commun*, 416(3-4):313–317, Dec 2011. doi: 10.1016/j.bbrc.2011.11.032. URL http://dx.doi.org/10.1016/j.bbrc.2011.11.032.

Y. Ohi, H. Qin, C. Hong, L. Blouin, J. M. Polo, T. Guo, Z. Qi, S. L. Downey, P. D. Manos, D. J. Rossi, J. Yu, M. Hebrok, K. Hochedlinger, J. F. Costello, J. S. Song, and M. Ramalho-Santos. Incomplete dna methylation underlies a transcriptional memory of somatic cells in human ips cells. *Nat Cell Biol*, 13(5):541–549, May 2011. doi: 10.1038/ncb2239. URL http://dx.doi.org/10.1038/ncb2239.

A. Okaya, J. Kitanaka, N. Kitanaka, M. Satake, Y. Kim, K. Terada, T. Sugiyama, M. Takemura, J. Fujimoto, N. Terada, A. Miyajima, and T. Tsujimura. Oncostatin m inhibits proliferation of rat oval cells, oc15-5, inducing differentiation into hepatocytes. *Am J Pathol*, 166(3):709–719, Mar 2005. doi: 10.1016/S0002-9440(10)62292-4. URL http://dx.doi.org/10.1016/S0002-9440(10)62292-4.

K. Okita, T. Ichisaka, and S. Yamanaka. Generation of germline-competent induced pluripotent stem cells. *Nature*, 448(7151):313–317, Jul 2007. doi: 10.1038/nature05934. URL http://dx.doi.org/10.1038/nature05934.

K. Okita, M. Nakagawa, H. Hyenjong, T. Ichisaka, and S. Yamanaka. Generation of mouse induced pluripotent stem cells without viral vectors. *Science*, 322(5903):949–953, Nov 2008. doi: 10.1126/science.1164270. URL http://dx.doi.org/10.1126/science.1164270.

G. Oliver, B. Sosa-Pineda, S. Geisendorf, E. P. Spana, C. Q. Doe, and P. Gruss. Prox 1, a prospero-related homeobox gene expressed during mouse development. *Mech Dev*, 44(1):3–16, Nov 1993.

M. J. Osborn, C. G. Starker, A. N. McElroy, B. R. Webber, M. J. Riddle, L. Xia, A. P. DeFeo, R. Gabriel, M. Schmidt, C. von Kalle, D. F. Carlson, M. L. Maeder, J. K. Joung, J. E. Wagner, D. F. Voytas, B. R. Blazar, and J. Tolar. Talen-based gene correction for epidermolysis bullosa. *Mol Ther*, 21(6):1151–1159, Jun 2013. doi: 10.1038/mt.2013.56. URL http://dx.doi.org/10.1038/mt.2013.56.

H. Osman-Ponchet, A. Boulai, M. Kouidhi, K. Sevin, M. Alriquet, A. Gaborit, B. Bertino, P. Comby, and B. Ruty. Characterization of abc transporters in human skin. *Drug Metabol Drug Interact*, 29(2):91–100, 2014. doi: 10.1515/dmdi-2013-0042. URL http://dx.doi.org/10.1515/dmdi-2013-0042.

B. Ozdamar, R. Bose, M. Barrios-Rodiles, H.-R. Wang, Y. Zhang, and J. L. Wrana. Regulation of the polarity protein par6 by tgfbeta receptors controls epithelial cell plasticity. *Science*, 307(5715):1603–1609, Mar 2005. doi: 10.1126/science.1105718. URL http://dx.doi.org/10.1126/science.1105718.

U. B. Pajvani, L. Qiang, T. Kangsamaksin, J. Kitajewski, H. N. Ginsberg, and D. Accili. Inhibition of notch uncouples akt activation from hepatic lipid accumulation by decreasing mtorc1 stability. *Nat Med*, 19(8):1054–1060, Aug 2013. doi: 10.1038/nm.3259. URL http://dx.doi.org/10.1038/nm.3259.

R. Pal, M. K. Mamidi, A. K. Das, and R. Bhonde. Diverse effects of dimethyl sulfoxide (dmso) on the differentiation potential of human embryonic stem cells. *Arch Toxicol*, 86(4):651–661, Apr 2012. doi: 10.1007/s00204-011-0782-2. URL http://dx.doi.org/10.1007/s00204-011-0782-2.

D. Pan. Hippo signaling in organ size control. *Genes Dev*, 21(8):886–897, Apr 2007. doi: 10.1101/gad.1536007. URL http://dx.doi.org/10.1101/gad.1536007.

A. D. Panopoulos, S. Ruiz, F. Yi, A. Herreras, E. M. Batchelder, and J. C. Izpisua Belmonte. Rapid and highly efficient generation of induced pluripotent stem cells from human umbilical vein endothelial cells. *PLoS One*, 6(5):e19743, 2011. doi: 10.1371/journal.pone.0019743. URL http://dx.doi.org/10.1371/journal.pone.0019743.

M. Paramasivam, A. Sarkeshik, J. R. Yates, 3rd, M. J. G. Fernandes, and D. McCollum. Angiomotin family proteins are novel activators of the lats2 kinase tumor suppressor. *Mol Biol Cell*, 22(19):3725–3733, Oct 2011. doi: 10.1091/mbc.E11-04-0300. URL http://dx.doi.org/10.1091/mbc.E11-04-0300.

H.-J. Park, Y. Zhang, S. P. Georgescu, K. L. Johnson, D. Kong, and J. B. Galper. Human umbilical vein endothelial cells and human dermal microvascular endothelial cells offer new insights into the relationship between lipid metabolism and angiogenesis. *Stem Cell Rev*, 2(2):93–102, 2006. doi: 10.1007/s12015-006-0015-x. URL http://dx.doi.org/10.1007/s12015-006-0015-x.

I.-H. Park, R. Zhao, J. A. West, A. Yabuuchi, H. Huo, T. A. Ince, P. H. Lerou, M. W. Lensch, and G. Q. Daley. Reprogramming of human somatic cells to pluripotency with defined factors. *Nature*, 451(7175):141–146, Jan 2008. doi: 10.1038/nature06534. URL http://dx.doi.org/10.1038/nature06534.

N. Pattarachotanant, V. Rakkhitawatthana, and T. Tencomnao. Effect of gloriosa superba and catharanthus roseus extracts on ifn-?-induced keratin 17 expression in hacat human keratinocytes. *Evid Based Complement Alternat Med*, 2014:249367, 2014. doi: 10.1155/2014/249367. URL http://dx.doi.org/10.1155/2014/249367.

M. F. Pera, J. Andrade, S. Houssami, B. Reubinoff, A. Trounson, E. G. Stanley, D. Ward-van Oostwaard, and C. Mummery. Regulation of human embryonic stem cell differentiation by bmp-2 and its antagonist noggin. *J Cell Sci*, 117(Pt 7):1269–1280, Mar 2004. doi: 10.1242/jcs.00970. URL http://dx.doi.org/10.1242/jcs.00970.

H. Peterson, R. Abu Dawud, A. Garg, Y. Wang, J. Vilo, I. Xenarios, and J. Adjaye. Qualitative modeling identifies il-11 as a novel regulator in maintaining self-renewal in human pluripotent stem cells. *Front Physiol*, 4:303, 2013. doi: 10.3389/fphys.2013.00303. URL http://dx.doi.org/10.3389/fphys.2013.00303.

J. Piccand, P. Strasser, D. J. Hodson, A. Meunier, T. Ye, C. Keime, M.-C. Birling, G. A. Rutter, and G. Gradwohl. Rfx6 maintains the functional identity of adult pancreatic ? cells. *Cell Rep*, 9(6):2219–2232, Dec 2014. doi: 10.1016/j.celrep.2014.11.033. URL http://dx.doi.org/10.1016/j.celrep.2014.11.033.

J. R. Plews, J. Li, M. Jones, H. D. Moore, C. Mason, P. W. Andrews, and J. Na. Activation of pluripotency genes in human fibroblast cells by a novel mrna based approach. *PLoS One*, 5(12):e14397, 2010. doi: 10.1371/journal.pone.0014397. URL http://dx.doi.org/10.1371/journal.pone.0014397.

J. M. Polo, E. Anderssen, R. M. Walsh, B. A. Schwarz, C. M. Nefzger, S. M. Lim, M. Borkent, E. Apostolou, S. Alaei, J. Cloutier, O. Bar-Nur, S. Cheloufi, M. Stadtfeld, M. E. Figueroa, D. Robinton, S. Natesan, A. Melnick, J. Zhu, S. Ramaswamy, and K. Hochedlinger. A molecular roadmap of reprogramming somatic cells into ips cells. *Cell*, 151(7):1617–1632, Dec 2012. doi: 10.1016/j.cell.2012.11.039. URL http://dx.doi.org/10.1016/j.cell.2012.11.039.

R. Prez-Carro, R. Snchez-Alcudia, B. Prez, R. Navarrete, C. Prez-Cerd, M. Ugarte, and L. Desviat. Functional analysis and in vitro correction of splicing fah mutations causing tyrosinemia type i. *Clin Genet*, Jul 2013. doi: 10.1111/cge.12243. URL http://dx.doi.org/10.1111/cge.12243.

199

A. Prigione, B. Fauler, R. Lurz, H. Lehrach, and J. Adjaye. The senescence-related mitochondrial/oxidative stress pathway is repressed in human induced pluripotent stem cells. *Stem Cells*, 28(4):721–733, Apr 2010. doi: 10.1002/stem.404. URL http://dx.doi.org/10.1002/stem.404.

X. Qi, T.-G. Li, J. Hao, J. Hu, J. Wang, H. Simmons, S. Miura, Y. Mishina, and G.-Q. Zhao. Bmp4 supports self-renewal of embryonic stem cells by inhibiting mitogen-activated protein kinase pathways. *Proc Natl Acad Sci U S A*, 101(16):6027–6032, Apr 2004. doi: 10.1073/pnas.0401367101. URL http://dx.doi.org/10.1073/pnas.0401367101.

A. Qu, C. Jiang, Y. Cai, J.-H. Kim, N. Tanaka, J. M. Ward, Y. M. Shah, and F. J. Gonzalez. Role of myc in hepatocellular proliferation and hepatocarcinogenesis. *J Hepatol*, 60(2):331–338, Feb 2014. doi: 10.1016/j.jhep.2013.09.024. URL http://dx.doi.org/10.1016/j.jhep.2013.09.024.

S. A. Rajasekaran, L. G. Palmer, S. Y. Moon, A. Peralta Soler, G. L. Apodaca, J. F. Harper, Y. Zheng, and A. K. Rajasekaran. Na,k-atpase activity is required for formation of tight junctions, desmosomes, and induction of polarity in epithelial cells. *Mol Biol Cell*, 12(12):3717–3732, Dec 2001.

S. T. Rashid, S. Corbineau, N. Hannan, S. J. Marciniak, E. Miranda, G. Alexander, I. Huang-Doran, J. Griffin, L. Ahrlund-Richter, J. Skepper, R. Semple, A. Weber, D. A. Lomas, and L. Vallier. Modeling inherited metabolic disorders of the liver using human induced pluripotent stem cells. *J Clin Invest*, 120(9):3127–3136, Sep 2010. doi: 10.1172/JCI43122. URL http://dx.doi.org/10.1172/JCI43122.

C.-A. Renard, C. Labalette, C. Armengol, D. Cougot, Y. Wei, S. Cairo, P. Pineau, C. Neuveut, A. de Reynis, A. Dejean, C. Perret, and M.-A. Buendia. Tbx3 is a downstream target of the wnt/beta-catenin pathway and a critical mediator of beta-catenin survival functions in liver cancer. *Cancer Res*, 67(3):901–910, Feb 2007. doi: 10.1158/0008-5472.CAN-06-2344. URL http://dx.doi.org/10.1158/0008-5472.CAN-06-2344.

R. A. Richman, T. H. Claus, S. J. Pilkis, and D. L. Friedman. Hormonal stimulation of dna synthesis in primary cultures of adult rat hepatocytes. *Proc Natl Acad Sci U S A*, 73(10):3589–3593, Oct 1976.

F. M. Rosa. Mix.1, a homeobox mrna inducible by mesoderm inducers, is expressed mostly in the presumptive endodermal cells of xenopus embryos. *Cell*, 57(6):965–974, Jun 1989.

S. Ross and C. S. Hill. How the smads regulate transcription. *Int J Biochem Cell Biol*, 40(3):383–408, 2008. doi: 10.1016/j.biocel.2007.09.006. URL http://dx.doi.org/10.1016/j.biocel.2007.09.006.

J. Rossant, C. Chazaud, and Y. Yamanaka. Lineage allocation and asymmetries in the early mouse embryo. *Philos Trans R Soc Lond B Biol Sci*, 358(1436):1341–8; discussion 1349, Aug 2003. doi: 10.1098/rstb.2003.1329. URL http://dx.doi.org/10.1098/rstb.2003.1329.

J. M. Rossi, N. R. Dunn, B. L. Hogan, and K. S. Zaret. Distinct mesodermal signals, including bmps from the septum transversum mesenchyme, are required in combination for hepatogenesis from the endoderm. *Genes Dev*, 15(15):1998–2009, Aug 2001. doi: 10.1101/gad.904601. URL http://dx.doi.org/10.1101/gad.904601.

L. Rui. Energy metabolism in the liver. *Compr Physiol*, 4(1):177–197, Jan 2014. doi: 10.1002/cphy.c130024. URL http://dx.doi.org/10.1002/cphy.c130024.

D. Runge, G. K. Michalopoulos, S. C. Strom, and D. M. Runge. Recent advances in human hepatocyte culture systems. *Biochem Biophys Res Commun*, 274(1):1–3, Jul 2000. doi: 10.1006/bbrc.2000.2912. URL http://dx.doi.org/10.1006/bbrc.2000.2912.

S. Saalfeld, A. Cardona, V. Hartenstein, and P. Toman?k. As-rigid-as-possible mosaicking and serial section registration of large sstem datasets. *Bioinformatics*, 26(12):i57–i63, Jun 2010. doi: 10.1093/bioinformatics/btq219. URL http://dx.doi.org/10.1093/bioinformatics/btq219.

T. Saheki, A. Ueda, M. Hosoya, T. Katsunuma, N. Ohnishi, and A. Ozawa. Comparison of the urea cycle in conventional and germ-free mice. *J Biochem*, 88(5):1563–1566, Nov 1980.

S. Sankar, J. M. Tanner, R. Bell, A. Chaturvedi, R. L. Randall, M. C. Beckerle, and S. L. Lessnick. A novel role for keratin 17 in coordinating oncogenic transformation and cellular adhesion in ewing sarcoma. *Mol Cell Biol*, 33(22):4448–4460, Nov 2013. doi: 10.1128/MCB.00241-13. URL http://dx.doi.org/10.1128/MCB.00241-13.

T. Sato, J. H. van Es, H. J. Snippert, D. E. Stange, R. G. Vries, M. van den Born, N. Barker, N. F. Shroyer, M. van de Wetering, and H. Clevers. Paneth cells constitute the niche for lgr5 stem cells in intestinal crypts. *Nature*, 469(7330):415–418, Jan 2011. doi: 10.1038/nature09637. URL http://dx.doi.org/10.1038/nature09637.

T. Sato, T. Sakuma, T. Yokonishi, K. Katagiri, S. Kamimura, N. Ogonuki, A. Ogura, T. Yamamoto, and T. Ogawa. Genome editing in mouse spermatogonial stem cell lines using talen and double-nicking crispr/cas9. *Stem Cell Reports*, 5(1):75–82, Jul 2015. doi: 10.1016/j.stemcr.2015.05.011. URL http://dx.doi.org/10.1016/j.stemcr.2015.05.011.

R. Schietke, C. Warnecke, I. Wacker, J. Schdel, D. R. Mole, V. Campean, K. Amann, M. Goppelt-Struebe, J. Behrens, K.-U. Eckardt, and M. S. Wiesener. The lysyl oxidases lox and loxl2 are necessary and sufficient to repress e-cadherin in hypoxia: insights into cellular transformation processes mediated by hif-1. *J Biol*

Chem, 285(9):6658–6669, Feb 2010. doi: 10.1074/jbc.M109.042424. URL http://dx.doi.org/10.1074/jbc.M109.042424.

J. Schindelin, I. Arganda-Carreras, E. Frise, V. Kaynig, M. Longair, T. Pietzsch, S. Preibisch, C. Rueden, S. Saalfeld, B. Schmid, J.-Y. Tinevez, D. J. White, V. Hartenstein, K. Eliceiri, P. Tomancak, and A. Cardona. Fiji: an open-source platform for biological-image analysis. *Nat Methods*, 9(7):676–682, Jul 2012. doi: 10.1038/nmeth.2019. URL http://dx.doi.org/10.1038/nmeth.2019.

T. M. Schlaeger, L. Daheron, T. R. Brickler, S. Entwisle, K. Chan, A. Cianci, A. DeVine, A. Ettenger, K. Fitzgerald, M. Godfrey, D. Gupta, J. McPherson, P. Malwadkar, M. Gupta, B. Bell, A. Doi, N. Jung, X. Li, M. S. Lynes, E. Brookes, A. B. C. Cherry, D. Demirbas, A. M. Tsankov, L. I. Zon, L. L. Rubin, A. P. Feinberg, A. Meissner, C. A. Cowan, and G. Q. Daley. A comparison of non-integrating reprogramming methods. *Nat Biotechnol*, 33(1):58–63, Jan 2015. doi: 10.1038/nbt.3070. URL http://dx.doi.org/10.1038/nbt.3070.

C. Schmidt, F. Bladt, S. Goedecke, V. Brinkmann, W. Zschiesche, M. Sharpe, E. Gherardi, and C. Birchmeier. Scatter factor/hepatocyte growth factor is essential for liver development. *Nature*, 373(6516):699–702, Feb 1995. doi: 10.1038/373699a0. URL http://dx.doi.org/10.1038/373699a0.

S. K. Schmidt, A. Mller, K. Heseler, C. Woite, K. Spekker, C. R. MacKenzie, and W. Dubener. Antimicrobial and immunoregulatory properties of human tryptophan 2,3-dioxygenase. *Eur J Immunol*, 39(10):2755–2764, Oct 2009. doi: 10.1002/eji.200939535. URL http://dx.doi.org/10.1002/eji.200939535.

B. Schmierer and C. S. Hill. Tgfbeta-smad signal transduction: molecular specificity and functional flexibility. *Nat Rev Mol Cell Biol*, 8(12):970–982, Dec 2007. doi: 10.1038/nrm2297. URL http://dx.doi.org/10.1038/nrm2297.

R. E. Schwartz, J. L. Linehan, M. S. Painschab, W.-S. Hu, C. M. Verfaillie, and D. S. Kaufman. Defined conditions for development of functional hepatic cells from human embryonic stem cells. *Stem Cells Dev*, 14(6):643–655, Dec 2005. doi: 10.1089/scd.2005.14.643. URL http://dx.doi.org/10.1089/scd.2005.14.643.

R. F. Searle and B. Flaks. A technique for liver transplantation in the inbred mouse. *Transplantation*, 22(3):256–264, Sep 1976.

P. O. Seglen. Preparation of isolated rat liver cells. *Methods Cell Biol*, 13:29–83, 1976.

K. Sekine, T. Takebe, Y. Suzuki, A. Kamiya, H. Nakauchi, and H. Taniguchi. Highly efficient generation of definitive endoderm lineage from human induced pluripotent stem cells. *Transplant Proc*, 44(4):1127–1129, May 2012. doi: 10.1016/j.transproceed.2012.03.001. URL http://dx.doi.org/10.1016/j.transproceed.2012.03.001.

A. Seth, J. Ye, N. Yu, F. Guez, D. C. Bedford, G. A. Neale, S. Cordi, P. K. Brindle, F. P. Lemaigre, K. H. Kaestner, and B. Sosa-Pineda. Prox1 ablation in hepatic progenitors causes defective hepatocyte specification and increases biliary cell commitment. *Development*, 141(3):538–547, Feb 2014. doi: 10.1242/dev.099481. URL http://dx.doi.org/10.1242/dev.099481.

U. Settmacher, A. Bauschke, C. Malessa, H. Scheuerlein, J. Zanow, and F. Rauchfu. [liver transplantation with living donor : current aspects, perspectives and significance in germany]. *Chirurg*, 84(5):398–408, May 2013. doi: 10.1007/s00104-012-2414-7. URL http://dx.doi.org/10.1007/s00104-012-2414-7.

J. Shan, R. E. Schwartz, N. T. Ross, D. J. Logan, D. Thomas, S. A. Duncan, T. E. North, W. Goessling, A. E. Carpenter, and S. N. Bhatia. Identification of small molecules for human hepatocyte expansion and ips differentiation. *Nat Chem Biol*, 9 (8):514–520, Aug 2013. doi: 10.1038/nchembio.1270. URL http://dx.doi.org/10.1038/nchembio.1270.

M. M. Shen. Nodal signaling: developmental roles and regulation. *Development*, 134(6): 1023–1034, Mar 2007. doi: 10.1242/dev.000166. URL http://dx.doi.org/10.1242/dev.000166.

S. Shimaoka, T. Nakamura, and A. Ichihara. Stimulation of growth of primary cultured adult rat hepatocytes without growth factors by coculture with nonparenchymal liver cells. *Exp Cell Res*, 172(1):228–242, Sep 1987.

N. Shiojiri. The origin of intrahepatic bile duct cells in the mouse. *J Embryol Exp Morphol*, 79:25–39, Feb 1984.

N. Shiojiri, J. M. Lemire, and N. Fausto. Cell lineages and oval cell progenitors in rat liver development. *Cancer Res*, 51(10):2611–2620, May 1991.

W. Shu, H. Yang, L. Zhang, M. M. Lu, and E. E. Morrisey. Characterization of a new subfamily of winged-helix/forkhead (fox) genes that are expressed in the lung and act as transcriptional repressors. *J Biol Chem*, 276(29):27488–27497, Jul 2001. doi: 10.1074/jbc.M100636200. URL http://dx.doi.org/10.1074/jbc.M100636200.

K. Shuai and B. Liu. Regulation of jak-stat signalling in the immune system. *Nat Rev Immunol*, 3(11):900–911, Nov 2003. doi: 10.1038/nri1226. URL http://dx.doi.org/10.1038/nri1226.

K. Si-Tayeb, F. K. Noto, M. Nagaoka, J. Li, M. A. Battle, C. Duris, P. E. North, S. Dalton, and S. A. Duncan. Highly efficient generation of human hepatocyte-like cells from induced pluripotent stem cells. *Hepatology*, 51(1):297–305, Jan 2010. doi: 10.1002/hep.23354. URL http://dx.doi.org/10.1002/hep.23354.

R. Siller, S. Greenhough, E. Naumovska, and G. J. Sullivan. Small-molecule-driven hepatocyte differentiation of human pluripotent stem cells. *Stem Cell Reports*, 4(5):

939–952, May 2015. doi: 10.1016/j.stemcr.2015.04.001. URL http://dx.doi.org/10.1016/j.stemcr.2015.04.001.

K. P. Simeonov and H. Uppal. Direct reprogramming of human fibroblasts to hepatocyte-like cells by synthetic modified mrnas. *PLoS One*, 9(6):e100134, 2014. doi: 10.1371/journal.pone.0100134. URL http://dx.doi.org/10.1371/journal.pone.0100134.

J. E. Smith, O. Afonja, H. T. Yee, G. Inghirami, and K. Takeshita. Chromosomal mapping to 15q14 and expression analysis of the human meis2 homeobox gene. *Mamm Genome*, 8(12):951–952, Dec 1997.

A. Somers, J.-C. Jean, C. A. Sommer, A. Omari, C. C. Ford, J. A. Mills, L. Ying, A. G. Sommer, J. M. Jean, B. W. Smith, R. Lafyatis, M.-F. Demierre, D. J. Weiss, D. L. French, P. Gadue, G. J. Murphy, G. Mostoslavsky, and D. N. Kotton. Generation of transgene-free lung disease-specific human induced pluripotent stem cells using a single excisable lentiviral stem cell cassette. *Stem Cells*, 28(10):1728–1740, Oct 2010. doi: 10.1002/stem.495. URL http://dx.doi.org/10.1002/stem.495.

C. A. Sommer, A. G. Sommer, T. A. Longmire, C. Christodoulou, D. D. Thomas, M. Gostissa, F. W. Alt, G. J. Murphy, D. N. Kotton, and G. Mostoslavsky. Excision of reprogramming transgenes improves the differentiation potential of ips cells generated with a single excisable vector. *Stem Cells*, 28(1):64–74, Jan 2010. doi: 10.1002/stem.255. URL http://dx.doi.org/10.1002/stem.255.

B. Sosa-Pineda, J. T. Wigle, and G. Oliver. Hepatocyte migration during liver development requires prox1. *Nat Genet*, 25(3):254–255, Jul 2000. doi: 10.1038/76996. URL http://dx.doi.org/10.1038/76996.

A. Soto-Gutierrez, N. Navarro-Alvarez, J. D. Rivas-Carrillo, Y. Chen, T. Yamatsuji, N. Tanaka, and N. Kobayashi. Differentiation of human embryonic stem cells to hepatocytes using deleted variant of hgf and poly-amino-urethane-coated nonwoven polytetrafluoroethylene fabric. *Cell Transplant*, 15(4):335–341, 2006.

R. Sridharan, J. Tchieu, M. J. Mason, R. Yachechko, E. Kuoy, S. Horvath, Q. Zhou, and K. Plath. Role of the murine reprogramming factors in the induction of pluripotency. *Cell*, 136(2):364–377, Jan 2009. doi: 10.1016/j.cell.2009.01.001. URL http://dx.doi.org/10.1016/j.cell.2009.01.001.

M. Stadtfeld, M. Nagaya, J. Utikal, G. Weir, and K. Hochedlinger. Induced pluripotent stem cells generated without viral integration. *Science*, 322(5903):945–949, Nov 2008. doi: 10.1126/science.1162494. URL http://dx.doi.org/10.1126/science.1162494.

L. F. Stancato, M. Sakatsume, M. David, P. Dent, F. Dong, E. F. Petricoin, J. J. Krolewski, O. Silvennoinen, P. Saharinen, J. Pierce, C. J. Marshall, T. Sturgill, D. S. Finbloom, and A. C. Larner. Beta interferon and oncostatin m activate raf-1 and

mitogen-activated protein kinase through a jak1-dependent pathway. *Mol Cell Biol*, 17(7):3833–3840, Jul 1997.

M. Subba Rao, M. Sasikala, and D. Nageshwar Reddy. Thinking outside the liver: induced pluripotent stem cells for hepatic applications. *World J Gastroenterol*, 19 (22):3385–3396, Jun 2013. doi: 10.3748/wjg.v19.i22.3385. URL http://dx.doi.org/10.3748/wjg.v19.i22.3385.

G. J. Sullivan, D. C. Hay, I.-H. Park, J. Fletcher, Z. Hannoun, C. M. Payne, D. Dalgetty, J. R. Black, J. A. Ross, K. Samuel, G. Wang, G. Q. Daley, J.-H. Lee, G. M. Church, S. J. Forbes, J. P. Iredale, and I. Wilmut. Generation of functional human hepatic endoderm from human induced pluripotent stem cells. *Hepatology*, 51(1):329–335, Jan 2010. doi: 10.1002/hep.23335. URL http://dx.doi.org/10.1002/hep.23335.

C. Suloway, J. Pulokas, D. Fellmann, A. Cheng, F. Guerra, J. Quispe, S. Stagg, C. S. Potter, and B. Carragher. Automated molecular microscopy: the new leginon system. *J Struct Biol*, 151(1):41–60, Jul 2005. doi: 10.1016/j.jsb.2005.03.010. URL http://dx.doi.org/10.1016/j.jsb.2005.03.010.

S. Sulzbacher, I. S. Schroeder, T. T. Truong, and A. M. Wobus. Activin a-induced differentiation of embryonic stem cells into endoderm and pancreatic progenitors-the influence of differentiation factors and culture conditions. *Stem Cell Rev*, 5(2):159–173, Jun 2009. doi: 10.1007/s12015-009-9061-5. URL http://dx.doi.org/10.1007/s12015-009-9061-5.

R. Sumazaki, N. Shiojiri, S. Isoyama, M. Masu, K. Keino-Masu, M. Osawa, H. Nakauchi, R. Kageyama, and A. Matsui. Conversion of biliary system to pancreatic tissue in hes1-deficient mice. *Nat Genet*, 36(1):83–87, Jan 2004. doi: 10.1038/ng1273. URL http://dx.doi.org/10.1038/ng1273.

G. H. Swift, Y. Liu, S. D. Rose, L. J. Bischof, S. Steelman, A. M. Buchberg, C. V. Wright, and R. J. MacDonald. An endocrine-exocrine switch in the activity of the pancreatic homeodomain protein pdx1 through formation of a trimeric complex with pbx1b and mrg1 (meis2). *Mol Cell Biol*, 18(9):5109–5120, Sep 1998.

S. Tada, T. Era, C. Furusawa, H. Sakurai, S. Nishikawa, M. Kinoshita, K. Nakao, T. Chiba, and S.-I. Nishikawa. Characterization of mesendoderm: a diverging point of the definitive endoderm and mesoderm in embryonic stem cell differentiation culture. *Development*, 132(19):4363–4374, Oct 2005. doi: 10.1242/dev.02005. URL http://dx.doi.org/10.1242/dev.02005.

K. Takahashi and S. Yamanaka. Induction of pluripotent stem cells from mouse embryonic and adult fibroblast cultures by defined factors. *Cell*, 126(4):663–676, Aug 2006. doi: 10.1016/j.cell.2006.07.024. URL http://dx.doi.org/10.1016/j.cell.2006.07.024.

K. Takahashi, K. Okita, M. Nakagawa, and S. Yamanaka. Induction of pluripotent stem cells from fibroblast cultures. *Nat Protoc*, 2(12):3081–3089, 2007a. doi: 10.1038/nprot.2007.418. URL http://dx.doi.org/10.1038/nprot.2007.418.

K. Takahashi, K. Tanabe, M. Ohnuki, M. Narita, T. Ichisaka, K. Tomoda, and S. Yamanaka. Induction of pluripotent stem cells from adult human fibroblasts by defined factors. *Cell*, 131(5):861–872, Nov 2007b. doi: 10.1016/j.cell.2007.11.019. URL http://dx.doi.org/10.1016/j.cell.2007.11.019.

K. Takayama, M. Inamura, K. Kawabata, K. Tashiro, K. Katayama, F. Sakurai, T. Hayakawa, M. K. Furue, and H. Mizuguchi. Efficient and directive generation of two distinct endoderm lineages from human escs and ipscs by differentiation stage-specific sox17 transduction. *PLoS One*, 6(7):e21780, 2011. doi: 10.1371/journal.pone.0021780. URL http://dx.doi.org/10.1371/journal.pone.0021780.

K. Takayama, M. Inamura, K. Kawabata, M. Sugawara, K. Kikuchi, M. Higuchi, Y. Nagamoto, H. Watanabe, K. Tashiro, F. Sakurai, T. Hayakawa, M. K. Furue, and H. Mizuguchi. Generation of metabolically functioning hepatocytes from human pluripotent stem cells by foxa2 and hnf1? transduction. *J Hepatol*, 57(3):628–636, Sep 2012. doi: 10.1016/j.jhep.2012.04.038. URL http://dx.doi.org/10.1016/j.jhep.2012.04.038.

K. Takayama, Y. Morisaki, S. Kuno, Y. Nagamoto, K. Harada, N. Furukawa, M. Ohtaka, K. Nishimura, K. Imagawa, F. Sakurai, M. Tachibana, R. Sumazaki, E. Noguchi, M. Nakanishi, K. Hirata, K. Kawabata, and H. Mizuguchi. Prediction of interindividual differences in hepatic functions and drug sensitivity by using human ips-derived hepatocytes. *Proc Natl Acad Sci U S A*, 111(47):16772–16777, Nov 2014. doi: 10.1073/pnas.1413481111. URL http://dx.doi.org/10.1073/pnas.1413481111.

T. Takebe, R.-R. Zhang, H. Koike, M. Kimura, E. Yoshizawa, M. Enomura, N. Koike, K. Sekine, and H. Taniguchi. Generation of a vascularized and functional human liver from an ipsc-derived organ bud transplant. *Nat Protoc*, 9(2):396–409, Feb 2014. doi: 10.1038/nprot.2014.020. URL http://dx.doi.org/10.1038/nprot.2014.020.

M. Tanaka, T. Hara, N. G. Copeland, D. J. Gilbert, N. A. Jenkins, and A. Miyajima. Reconstitution of the functional mouse oncostatin m (osm) receptor: molecular cloning of the mouse osm receptor beta subunit. *Blood*, 93(3):804–815, Feb 1999.

N. Tanimizu and A. Miyajima. Notch signaling controls hepatoblast differentiation by altering the expression of liver-enriched transcription factors. *J Cell Sci*, 117(Pt 15): 3165–3174, Jul 2004. doi: 10.1242/jcs.01169. URL http://dx.doi.org/10.1242/jcs.01169.

N. Tanimizu, M. Nishikawa, H. Saito, T. Tsujimura, and A. Miyajima. Isolation of hepatoblasts based on the expression of dlk/pref-1. *J Cell Sci*, 116(Pt 9):1775–1786, May 2003.

B. D. Tarlow, C. Pelz, W. E. Naugler, L. Wakefield, E. M. Wilson, M. J. Finegold, and M. Grompe. Bipotential adult liver progenitors are derived from chronically injured mature hepatocytes. *Cell Stem Cell*, 15(5):605–618, Nov 2014. doi: 10.1016/j.stem.2014.09.008. URL http://dx.doi.org/10.1016/j.stem.2014.09.008.

G. Tavernier, K. Wolfrum, J. Demeester, S. C. De Smedt, J. Adjaye, and J. Rejman. Activation of pluripotency-associated genes in mouse embryonic fibroblasts by non-viral transfection with in vitro-derived mrnas encoding oct4, sox2, klf4 and cmyc. *Biomaterials*, 33(2):412–417, Jan 2012. doi: 10.1016/j.biomaterials.2011.09.062. URL http://dx.doi.org/10.1016/j.biomaterials.2011.09.062.

R. D. C. Team. R: A language and environment for statistical computing. 2010. URL http://www.R-project.org.

J. H. Teckman and A. Jain. Advances in alpha-1-antitrypsin deficiency liver disease. *Curr Gastroenterol Rep*, 16(1):367, Jan 2014. doi: 10.1007/s11894-013-0367-8. URL http://dx.doi.org/10.1007/s11894-013-0367-8.

D. ten Berge, D. Kurek, T. Blauwkamp, W. Koole, A. Maas, E. Eroglu, R. K. Siu, and R. Nusse. Embryonic stem cells require wnt proteins to prevent differentiation to epiblast stem cells. *Nat Cell Biol*, 13(9):1070–1075, Sep 2011. doi: 10.1038/ncb2314. URL http://dx.doi.org/10.1038/ncb2314.

A. K. K. Teo, S. J. Arnold, M. W. B. Trotter, S. Brown, L. T. Ang, Z. Chng, E. J. Robertson, N. R. Dunn, and L. Vallier. Pluripotency factors regulate definitive endoderm specification through eomesodermin. *Genes Dev*, 25(3):238–250, Feb 2011. doi: 10.1101/gad.607311. URL http://dx.doi.org/10.1101/gad.607311.

A. K. K. Teo, Y. Ali, K. Y. Wong, H. Chipperfield, A. Sadasivam, Y. Poobalan, E. K. Tan, S. T. Wang, S. Abraham, N. Tsuneyoshi, L. W. Stanton, and N. R. Dunn. Activin and bmp4 synergistically promote formation of definitive endoderm in human embryonic stem cells. *Stem Cells*, 30(4):631–642, Apr 2012. doi: 10.1002/stem.1022. URL http://dx.doi.org/10.1002/stem.1022.

B. Thisse and C. Thisse. Functions and regulations of fibroblast growth factor signaling during embryonic development. *Dev Biol*, 287(2):390–402, Nov 2005. doi: 10.1016/j.ydbio.2005.09.011. URL http://dx.doi.org/10.1016/j.ydbio.2005.09.011.

P. Q. Thomas, A. Brown, and R. S. Beddington. Hex: a homeobox gene revealing peri-implantation asymmetry in the mouse embryo and an early transient marker of endothelial cell precursors. *Development*, 125(1):85–94, Jan 1998.

J. A. Thomson, J. Itskovitz-Eldor, S. S. Shapiro, M. A. Waknitz, J. J. Swiergiel, V. S. Marshall, and J. M. Jones. Embryonic stem cell lines derived from human blastocysts. *Science*, 282(5391):1145–1147, Nov 1998.

207

M. Tomizawa, F. Shinozaki, T. Sugiyama, S. Yamamoto, M. Sueishi, and T. Yoshida. Single-step protocol for the differentiation of human-induced pluripotent stem cells into hepatic progenitor-like cells. *Biomed Rep*, 1(1):18–22, 1 2013. doi: 10.3892/br. 2012.2. URL http://dx.doi.org/10.3892/br.2012.2.

M. Totonchi, A. Taei, A. Seifinejad, M. Tabebordbar, H. Rassouli, A. Farrokhi, H. Gourabi, N. Aghdami, G. Hosseini-Salekdeh, and H. Baharvand. Feeder- and serum-free establishment and expansion of human induced pluripotent stem cells. *Int J Dev Biol*, 54(5):877–886, 2010. doi: 10.1387/ijdb.092903mt. URL http://dx.doi.org/10.1387/ijdb.092903mt.

A. M. Tremblay and F. D. Camargo. Hippo signaling in mammalian stem cells. *Semin Cell Dev Biol*, 23(7):818–826, Sep 2012. doi: 10.1016/j.semcdb.2012.08.001. URL http://dx.doi.org/10.1016/j.semcdb.2012.08.001.

K. D. Tremblay and K. S. Zaret. Distinct populations of endoderm cells converge to generate the embryonic liver bud and ventral foregut tissues. *Dev Biol*, 280(1):87–99, Apr 2005. doi: 10.1016/j.ydbio.2005.01.003. URL http://dx.doi.org/10.1016/j.ydbio.2005.01.003.

K. D. Tremblay, P. A. Hoodless, E. K. Bikoff, and E. J. Robertson. Formation of the definitive endoderm in mouse is a smad2-dependent process. *Development*, 127(14): 3079–3090, Jul 2000.

A. Tsuchiya, J.-H. Kang, D. Asai, T. Mori, T. Niidome, and Y. Katayama. Transgene regulation system responding to rho associated coiled-coil kinase (rock) activation. *J Control Release*, 155(1):40–46, Oct 2011. doi: 10.1016/j.jconrel.2011.05.002. URL http://dx.doi.org/10.1016/j.jconrel.2011.05.002.

S. Tsuji, K. Kaji, and S. Nagasawa. Decay-accelerating factor on human umbilical vein endothelial cells. its histamine-induced expression and spontaneous rapid shedding from the cell surface. *J Immunol*, 152(3):1404–1410, Feb 1994.

N. Turner and R. Grose. Fibroblast growth factor signalling: from development to cancer. *Nat Rev Cancer*, 10(2):116–129, Feb 2010. doi: 10.1038/nrc2780. URL http://dx.doi.org/10.1038/nrc2780.

D. Umulis, M. B. O'Connor, and S. S. Blair. The extracellular regulation of bone morphogenetic protein signaling. *Development*, 136(22):3715–3728, Nov 2009. doi: 10.1242/dev.031534. URL http://dx.doi.org/10.1242/dev.031534.

J. Utikal, J. M. Polo, M. Stadtfeld, N. Maherali, W. Kulalert, R. M. Walsh, A. Khalil, J. G. Rheinwald, and K. Hochedlinger. Immortalization eliminates a roadblock during cellular reprogramming into ips cells. *Nature*, 460(7259):1145–1148, Aug 2009. doi: 10.1038/nature08285. URL http://dx.doi.org/10.1038/nature08285.

M. Utsumi, A. Takaki, Y. Umeda, K. Koike, S. C. Napier, N. Watanabe, H. Sadamori, S. Shinoura, R. Yoshida, D. Nobuoka, T. Yasunaka, E. Nakayama, K. Yamamoto, T. Fujiwara, and T. Yagi. Frequency of regulatory t-cell and hepatitis c viral antigen-specific immune response in recurrent hepatitis c after liver transplantation. *Transpl Immunol*, Jun 2014. doi: 10.1016/j.trim.2014.05.006. URL http://dx.doi.org/10.1016/j.trim.2014.05.006.

N. Uyama, Y. Shimahara, N. Kawada, S. Seki, H. Okuyama, Y. Iimuro, and Y. Yamaoka. Regulation of cultured rat hepatocyte proliferation by stellate cells. *J Hepatol*, 36(5): 590–599, May 2002.

C. Vanderpool, E. E. Sparks, K. A. Huppert, M. Gannon, A. L. Means, and S. S. Huppert. Genetic interactions between hepatocyte nuclear factor-6 and notch signaling regulate mouse intrahepatic bile duct development in vivo. *Hepatology*, 55(1):233–243, Jan 2012. doi: 10.1002/hep.24631. URL http://dx.doi.org/10.1002/hep.24631.

X. Varelas, R. Sakuma, P. Samavarchi-Tehrani, R. Peerani, B. M. Rao, J. Dembowy, M. B. Yaffe, P. W. Zandstra, and J. L. Wrana. Taz controls smad nucleocytoplasmic shuttling and regulates human embryonic stem-cell self-renewal. *Nat Cell Biol*, 10 (7):837–848, Jul 2008. doi: 10.1038/ncb1748. URL http://dx.doi.org/10.1038/ncb1748.

X. Varelas, P. Samavarchi-Tehrani, M. Narimatsu, A. Weiss, K. Cockburn, B. G. Larsen, J. Rossant, and J. L. Wrana. The crumbs complex couples cell density sensing to hippo-dependent control of the tgf-?-smad pathway. *Dev Cell*, 19(6):831–844, Dec 2010. doi: 10.1016/j.devcel.2010.11.012. URL http://dx.doi.org/10.1016/j.devcel.2010.11.012.

A. Villanueva, C. Alsinet, K. Yanger, Y. Hoshida, Y. Zong, S. Toffanin, L. Rodriguez-Carunchio, M. Sol, S. Thung, B. Z. Stanger, and J. M. Llovet. Notch signaling is activated in human hepatocellular carcinoma and induces tumor formation in mice. *Gastroenterology*, 143(6):1660–1669.e7, Dec 2012. doi: 10.1053/j.gastro.2012.09.002. URL http://dx.doi.org/10.1053/j.gastro.2012.09.002.

S. D. Vincent, N. R. Dunn, S. Hayashi, D. P. Norris, and E. J. Robertson. Cell fate decisions within the mouse organizer are governed by graded nodal signals. *Genes Dev*, 17(13):1646–1662, Jul 2003. doi: 10.1101/gad.1100503. URL http://dx.doi.org/10.1101/gad.1100503.

J. Vogt, R. Traynor, and G. P. Sapkota. The specificities of small molecule inhibitors of the tgf and bmp pathways. *Cell Signal*, 23(11):1831–1842, Nov 2011. doi: 10.1016/j.cellsig.2011.06.019. URL http://dx.doi.org/10.1016/j.cellsig.2011.06.019.

W. R. Waldrip, E. K. Bikoff, P. A. Hoodless, J. L. Wrana, and E. J. Robertson. Smad2 signaling in extraembryonic tissues determines anterior-posterior polarity of the early mouse embryo. *Cell*, 92(6):797–808, Mar 1998.

Y. Wang and J. Adjaye. A cyclic amp analog, 8-br-camp, enhances the induction of pluripotency in human fibroblast cells. *Stem Cell Rev*, 7(2):331–341, Jun 2011. doi: 10.1007/s12015-010-9209-3. URL http://dx.doi.org/10.1007/s12015-010-9209-3.

Y. Wang, N. Mah, A. Prigione, K. Wolfrum, M. A. Andrade-Navarro, and J. Adjaye. A transcriptional roadmap to the induction of pluripotency in somatic cells. *Stem Cell Rev*, 6(2):282–296, Jun 2010. doi: 10.1007/s12015-010-9137-2. URL http://dx.doi.org/10.1007/s12015-010-9137-2.

Y. Wang, B.-K. Chou, S. Dowey, C. He, S. Gerecht, and L. Cheng. Scalable expansion of human induced pluripotent stem cells in the defined xeno-free e8 medium under adherent and suspension culture conditions. *Stem Cell Res*, 11(3):1103–1116, Nov 2013a. doi: 10.1016/j.scr.2013.07.011. URL http://dx.doi.org/10.1016/j.scr.2013.07.011.

Y. Wang, G. Lanzoni, G. Carpino, C.-B. Cui, J. Dominguez-Bendala, E. Wauthier, V. Cardinale, T. Oikawa, A. Pileggi, D. Gerber, M. E. Furth, D. Alvaro, E. Gaudio, L. Inverardi, and L. M. Reid. Biliary tree stem cells, precursors to pancreatic committed progenitors: evidence for possible life-long pancreatic organogenesis. *Stem Cells*, 31(9):1966–1979, Sep 2013b. doi: 10.1002/stem.1460. URL http://dx.doi.org/10.1002/stem.1460.

L. Warren, P. D. Manos, T. Ahfeldt, Y.-H. Loh, H. Li, F. Lau, W. Ebina, P. K. Mandal, Z. D. Smith, A. Meissner, G. Q. Daley, A. S. Brack, J. J. Collins, C. Cowan, T. M. Schlaeger, and D. J. Rossi. Highly efficient reprogramming to pluripotency and directed differentiation of human cells with synthetic modified mrna. *Cell Stem Cell*, 7(5):618–630, Nov 2010. doi: 10.1016/j.stem.2010.08.012. URL http://dx.doi.org/10.1016/j.stem.2010.08.012.

T. Watabe and K. Miyazono. Roles of tgf-beta family signaling in stem cell renewal and differentiation. *Cell Res*, 19(1):103–115, Jan 2009. doi: 10.1038/cr.2008.323. URL http://dx.doi.org/10.1038/cr.2008.323.

K. Watanabe, M. Ueno, D. Kamiya, A. Nishiyama, M. Matsumura, T. Wataya, J. B. Takahashi, S. Nishikawa, S.-i. Nishikawa, K. Muguruma, and Y. Sasai. A rock inhibitor permits survival of dissociated human embryonic stem cells. *Nat Biotechnol*, 25(6):681–686, Jun 2007. doi: 10.1038/nbt1310. URL http://dx.doi.org/10.1038/nbt1310.

A. J. Watt, E. A. Jones, J. M. Ure, D. Peddie, D. I. Wilson, and L. M. Forrester. A gene trap integration provides an early in situ marker for hepatic specification of the foregut endoderm. *Mech Dev*, 100(2):205–215, Feb 2001.

A. J. Watt, W. D. Garrison, and S. A. Duncan. Hnf4: a central regulator of hepatocyte differentiation and function. *Hepatology*, 37(6):1249–1253, Jun 2003. doi: 10.1053/jhep.2003.50273. URL http://dx.doi.org/10.1053/jhep.2003.50273.

A. J. Watt, R. Zhao, J. Li, and S. A. Duncan. Development of the mammalian liver and ventral pancreas is dependent on gata4. *BMC Dev Biol*, 7:37, 2007. doi: 10.1186/ 1471-213X-7-37. URL http://dx.doi.org/10.1186/1471-213X-7-37.

M. Wehrli, S. T. Dougan, K. Caldwell, L. O'Keefe, S. Schwartz, D. Vaizel-Ohayon, E. Schejter, A. Tomlinson, and S. DiNardo. arrow encodes an ldl-receptor-related protein essential for wingless signalling. *Nature*, 407(6803):527–530, Sep 2000. doi: 10.1038/35035110. URL http://dx.doi.org/10.1038/35035110.

M. Weinstein, X. Xu, K. Ohyama, and C. X. Deng. Fgfr-3 and fgfr-4 function cooperatively to direct alveogenesis in the murine lung. *Development*, 125(18):3615–3623, Sep 1998.

M. Weinstein, S. P. Monga, Y. Liu, S. G. Brodie, Y. Tang, C. Li, L. Mishra, and C. X. Deng. Smad proteins and hepatocyte growth factor control parallel regulatory pathways that converge on beta1-integrin to promote normal liver development. *Mol Cell Biol*, 21(15):5122–5131, Aug 2001. doi: 10.1128/MCB.21.15.5122-5131.2001. URL http://dx.doi.org/10.1128/MCB.21.15.5122-5131.2001.

B. C. Willis and Z. Borok. Tgf-beta-induced emt: mechanisms and implications for fibrotic lung disease. *Am J Physiol Lung Cell Mol Physiol*, 293(3):L525–L534, Sep 2007. doi: 10.1152/ajplung.00163.2007. URL http://dx.doi.org/10.1152/ ajplung.00163.2007.

P. A. Wilson and A. Hemmati-Brivanlou. Induction of epidermis and inhibition of neural fate by bmp-4. *Nature*, 376(6538):331–333, Jul 1995. doi: 10.1038/376331a0. URL http://dx.doi.org/10.1038/376331a0.

K. Wolfrum, Y. Wang, A. Prigione, K. Sperling, H. Lehrach, and J. Adjaye. The large principle of cellular reprogramming: lost, acquired and retained gene expression in foreskin and amniotic fluid-derived human ips cells. *PLoS One*, 5(10):e13703, 2010. doi: 10.1371/journal.pone.0013703. URL http://dx.doi.org/10.1371/journal. pone.0013703.

K. Woltjen, I. P. Michael, P. Mohseni, R. Desai, M. Mileikovsky, R. Hmlinen, R. Cowling, W. Wang, P. Liu, M. Gertsenstein, K. Kaji, H.-K. Sung, and A. Nagy. piggybac transposition reprograms fibroblasts to induced pluripotent stem cells. *Nature*, 458 (7239):766–770, Apr 2009. doi: 10.1038/nature07863. URL http://dx.doi.org/10. 1038/nature07863.

K. H. Wrighton and X.-H. Feng. To (tgf)beta or not to (tgf)beta: fine-tuning of smad signaling via post-translational modifications. *Cell Signal*, 20(9):1579–1591, Sep 2008. doi: 10.1016/j.cellsig.2008.02.003. URL http://dx.doi.org/10.1016/j.cellsig. 2008.02.003.

M. Y. Wu and C. S. Hill. Tgf-beta superfamily signaling in embryonic development and homeostasis. *Dev Cell*, 16(3):329–343, Mar 2009. doi: 10.1016/j.devcel.2009.02.012. URL http://dx.doi.org/10.1016/j.devcel.2009.02.012.

X. Wu, H. Ge, B. Lemon, S. Vonderfecht, H. Baribault, J. Weiszmann, J. Gupte, J. Gardner, R. Lindberg, Z. Wang, and Y. Li. Separating mitogenic and metabolic activities of fibroblast growth factor 19 (fgf19). *Proc Natl Acad Sci U S A*, 107(32):14158–14163, Aug 2010. doi: 10.1073/pnas.1009427107. URL http://dx.doi.org/10.1073/pnas.1009427107.

C. Xu, M. S. Inokuma, J. Denham, K. Golds, P. Kundu, J. D. Gold, and M. K. Carpenter. Feeder-free growth of undifferentiated human embryonic stem cells. *Nat Biotechnol*, 19(10):971–974, Oct 2001. doi: 10.1038/nbt1001-971. URL http://dx.doi.org/10.1038/nbt1001-971.

R.-H. Xu, X. Chen, D. S. Li, R. Li, G. C. Addicks, C. Glennon, T. P. Zwaka, and J. A. Thomson. Bmp4 initiates human embryonic stem cell differentiation to trophoblast. *Nat Biotechnol*, 20(12):1261–1264, Dec 2002. doi: 10.1038/nbt761. URL http://dx.doi.org/10.1038/nbt761.

R.-H. Xu, T. L. Sampsell-Barron, F. Gu, S. Root, R. M. Peck, G. Pan, J. Yu, J. Antosiewicz-Bourget, S. Tian, R. Stewart, and J. A. Thomson. Nanog is a direct target of tgfbeta/activin-mediated smad signaling in human escs. *Cell Stem Cell*, 3(2):196–206, Aug 2008. doi: 10.1016/j.stem.2008.07.001. URL http://dx.doi.org/10.1016/j.stem.2008.07.001.

T. Yamada, M. Yoshikawa, S. Kanda, Y. Kato, Y. Nakajima, S. Ishizaka, and Y. Tsunoda. In vitro differentiation of embryonic stem cells into hepatocyte-like cells identified by cellular uptake of indocyanine green. *Stem Cells*, 20(2):146–154, 2002. doi: 10.1634/stemcells.20-2-146. URL http://dx.doi.org/10.1634/stemcells.20-2-146.

T. P. Yamaguchi, R. A. Conlon, and J. Rossant. Expression of the fibroblast growth factor receptor fgfr-1/flg during gastrulation and segmentation in the mouse embryo. *Dev Biol*, 152(1):75–88, Jul 1992.

T. P. Yamaguchi, A. Bradley, A. P. McMahon, and S. Jones. A wnt5a pathway underlies outgrowth of multiple structures in the vertebrate embryo. *Development*, 126(6):1211–1223, Mar 1999.

M. Yamamoto, C. Meno, Y. Sakai, H. Shiratori, K. Mochida, Y. Ikawa, Y. Saijoh, and H. Hamada. The transcription factor foxh1 (fast) mediates nodal signaling during anterior-posterior patterning and node formation in the mouse. *Genes Dev*, 15(10):1242–1256, May 2001. doi: 10.1101/gad.883901. URL http://dx.doi.org/10.1101/gad.883901.

J. Yang and R. A. Weinberg. Epithelial-mesenchymal transition: at the crossroads of development and tumor metastasis. *Dev Cell*, 14(6):818–829, Jun 2008. doi: 10.1016/j.devcel.2008.05.009. URL http://dx.doi.org/10.1016/j.devcel.2008.05.009.

K. Yanger, Y. Zong, L. R. Maggs, S. N. Shapira, R. Maddipati, N. M. Aiello, S. N. Thung, R. G. Wells, L. E. Greenbaum, and B. Z. Stanger. Robust cellular reprogramming occurs spontaneously during liver regeneration. *Genes Dev*, 27(7):719–724, Apr 2013. doi: 10.1101/gad.207803.112. URL http://dx.doi.org/10.1101/gad.207803.112.

S. Yao, S. Chen, J. Clark, E. Hao, G. M. Beattie, A. Hayek, and S. Ding. Long-term self-renewal and directed differentiation of human embryonic stem cells in chemically defined conditions. *Proc Natl Acad Sci U S A*, 103(18):6907–6912, May 2006. doi: 10.1073/pnas.0602280103. URL http://dx.doi.org/10.1073/pnas.0602280103.

H. Yasuo and P. Lemaire. A two-step model for the fate determination of presumptive endodermal blastomeres in xenopus embryos. *Curr Biol*, 9(16):869–879, Aug 1999.

J. Yates, N. Warren, D. Reisman, and B. Sugden. A cis-acting element from the epstein-barr viral genome that permits stable replication of recombinant plasmids in latently infected cells. *Proc Natl Acad Sci U S A*, 81(12):3806–3810, Jun 1984.

L. Ye, J. Wang, A. I. Beyer, F. Teque, T. J. Cradick, Z. Qi, J. C. Chang, G. Bao, M. O. Muench, J. Yu, J. A. Levy, and Y. W. Kan. Seamless modification of wild-type induced pluripotent stem cells to the natural ccr5?32 mutation confers resistance to hiv infection. *Proc Natl Acad Sci U S A*, 111(26):9591–9596, Jul 2014. doi: 10.1073/pnas.1407473111. URL http://dx.doi.org/10.1073/pnas.1407473111.

C. H. Yi, J. A. Terrett, Q. Y. Li, K. Ellington, E. A. Packham, L. Armstrong-Buisseret, P. McClure, T. Slingsby, and J. D. Brook. Identification, mapping, and phylogenomic analysis of four new human members of the t-box gene family: Eomes, tbx6, tbx18, and tbx19. *Genomics*, 55(1):10–20, Jan 1999. doi: 10.1006/geno.1998.5632. URL http://dx.doi.org/10.1006/geno.1998.5632.

D. Yimlamai, C. Christodoulou, G. G. Galli, K. Yanger, B. Pepe-Mooney, B. Gurung, K. Shrestha, P. Cahan, B. Z. Stanger, and F. D. Camargo. Hippo pathway activity influences liver cell fate. *Cell*, 157(6):1324–1338, Jun 2014. doi: 10.1016/j.cell.2014.03.060. URL http://dx.doi.org/10.1016/j.cell.2014.03.060.

A. H. Yin, S. Miraglia, E. D. Zanjani, G. Almeida-Porada, M. Ogawa, A. G. Leary, J. Olweus, J. Kearney, and D. W. Buck. Ac133, a novel marker for human hematopoietic stem and progenitor cells. *Blood*, 90(12):5002–5012, Dec 1997.

Q. L. Ying, J. Nichols, I. Chambers, and A. Smith. Bmp induction of id proteins suppresses differentiation and sustains embryonic stem cell self-renewal in collaboration with stat3. *Cell*, 115(3):281–292, Oct 2003.

N. Yoshioka, E. Gros, H.-R. Li, S. Kumar, D. C. Deacon, C. Maron, A. R. Muotri, N. C. Chi, X.-D. Fu, B. D. Yu, and S. F. Dowdy. Efficient generation of human ipscs by a synthetic self-replicative rna. *Cell Stem Cell*, 13(2):246–254, Aug 2013. doi: 10.1016/j.stem.2013.06.001. URL http://dx.doi.org/10.1016/j.stem.2013.06.001.

V. R. Young and J. S. Marchini. Mechanisms and nutritional significance of metabolic responses to altered intakes of protein and amino acids, with reference to nutritional adaptation in humans. *Am J Clin Nutr*, 51(2):270–289, Feb 1990.

V. R. Young, A. E. El-Khoury, C. A. Raguso, A. H. Forslund, and L. Hambraeus. Rates of urea production and hydrolysis and leucine oxidation change linearly over widely varying protein intakes in healthy adults. *J Nutr*, 130(4):761–766, Apr 2000.

J. Yu, M. A. Vodyanik, K. Smuga-Otto, J. Antosiewicz-Bourget, J. L. Frane, S. Tian, J. Nie, G. A. Jonsdottir, V. Ruotti, R. Stewart, I. I. Slukvin, and J. A. Thomson. Induced pluripotent stem cell lines derived from human somatic cells. *Science*, 318 (5858):1917–1920, Dec 2007. doi: 10.1126/science.1151526. URL http://dx.doi.org/10.1126/science.1151526.

J. Yu, K. Hu, K. Smuga-Otto, S. Tian, R. Stewart, I. I. Slukvin, and J. A. Thomson. Human induced pluripotent stem cells free of vector and transgene sequences. *Science*, 324(5928):797–801, May 2009. doi: 10.1126/science.1172482. URL http://dx.doi.org/10.1126/science.1172482.

J. Yu, K. F. Chau, M. A. Vodyanik, J. Jiang, and Y. Jiang. Efficient feeder-free episomal reprogramming with small molecules. *PLoS One*, 6(3):e17557, 2011. doi: 10.1371/journal.pone.0017557. URL http://dx.doi.org/10.1371/journal.pone.0017557.

Z.-Y. Yu, Y.-N. Bai, L.-X. Luo, H. Wu, and Y. Zeng. Expression of microrna-150 targeting vascular endothelial growth factor-a is downregulated under hypoxia during liver regeneration. *Mol Med Rep*, 8(1):287–293, Jul 2013. doi: 10.3892/mmr.2013.1493. URL http://dx.doi.org/10.3892/mmr.2013.1493.

K. Yusa, S. T. Rashid, H. Strick-Marchand, I. Varela, P.-Q. Liu, D. E. Paschon, E. Miranda, A. Ordez, N. R. F. Hannan, F. J. Rouhani, S. Darche, G. Alexander, S. J. Marciniak, N. Fusaki, M. Hasegawa, M. C. Holmes, J. P. Di Santo, D. A. Lomas, A. Bradley, and L. Vallier. Targeted gene correction of ?1-antitrypsin deficiency in induced pluripotent stem cells. *Nature*, 478(7369):391–394, Oct 2011. doi: 10.1038/nature10424. URL http://dx.doi.org/10.1038/nature10424.

M. J. Zamek-Gliszczynski, H. Xiong, N. J. Patel, R. Z. Turncliff, G. M. Pollack, and K. L. R. Brouwer. Pharmacokinetics of 5 (and 6)-carboxy-2',7'-dichlorofluorescein and its diacetate promoiety in the liver. *J Pharmacol Exp Ther*, 304(2):801–809, Feb 2003. doi: 10.1124/jpet.102.044107. URL http://dx.doi.org/10.1124/jpet.102.044107.

K. S. Zaret. Regulatory phases of early liver development: paradigms of organogenesis. *Nat Rev Genet*, 3(7):499–512, Jul 2002. doi: 10.1038/nrg837. URL http://dx.doi.org/10.1038/nrg837.

S. Zender, I. Nickeleit, T. Wuestefeld, I. Srensen, D. Dauch, P. Bozko, M. El-Khatib, R. Geffers, H. Bektas, M. P. Manns, A. Gossler, L. Wilkens, R. Plentz, L. Zender, and N. P. Malek. A critical role for notch signaling in the formation of cholangiocellular carcinomas. *Cancer Cell*, 23(6):784–795, Jun 2013. doi: 10.1016/j.ccr.2013.04.019. URL http://dx.doi.org/10.1016/j.ccr.2013.04.019.

B. Zhao, X. Wei, W. Li, R. S. Udan, Q. Yang, J. Kim, J. Xie, T. Ikenoue, J. Yu, L. Li, P. Zheng, K. Ye, A. Chinnaiyan, G. Halder, Z.-C. Lai, and K.-L. Guan. Inactivation of yap oncoprotein by the hippo pathway is involved in cell contact inhibition and tissue growth control. *Genes Dev*, 21(21):2747–2761, Nov 2007. doi: 10.1101/gad.1602907. URL http://dx.doi.org/10.1101/gad.1602907.

B. Zhao, K. Tumaneng, and K.-L. Guan. The hippo pathway in organ size control, tissue regeneration and stem cell self-renewal. *Nat Cell Biol*, 13(8):877–883, Aug 2011a. doi: 10.1038/ncb2303. URL http://dx.doi.org/10.1038/ncb2303.

R. Zhao and S. A. Duncan. Embryonic development of the liver. *Hepatology*, 41(5): 956–967, May 2005. doi: 10.1002/hep.20691. URL http://dx.doi.org/10.1002/hep.20691.

T. Zhao, Z.-N. Zhang, Z. Rong, and Y. Xu. Immunogenicity of induced pluripotent stem cells. *Nature*, 474(7350):212–215, Jun 2011b. doi: 10.1038/nature10135. URL http://dx.doi.org/10.1038/nature10135.

Y. Zhao, X. Yin, H. Qin, F. Zhu, H. Liu, W. Yang, Q. Zhang, C. Xiang, P. Hou, Z. Song, Y. Liu, J. Yong, P. Zhang, J. Cai, M. Liu, H. Li, Y. Li, X. Qu, K. Cui, W. Zhang, T. Xiang, Y. Wu, Y. Zhao, C. Liu, C. Yu, K. Yuan, J. Lou, M. Ding, and H. Deng. Two supporting factors greatly improve the efficiency of human ipsc generation. *Cell Stem Cell*, 3(5):475–479, Nov 2008. doi: 10.1016/j.stem.2008.10.002. URL http://dx.doi.org/10.1016/j.stem.2008.10.002.

H. Zhou, S. Wu, J. Y. Joo, S. Zhu, D. W. Han, T. Lin, S. Trauger, G. Bien, S. Yao, Y. Zhu, G. Siuzdak, H. R. Schler, L. Duan, and S. Ding. Generation of induced pluripotent stem cells using recombinant proteins. *Cell Stem Cell*, 4(5):381–384, May 2009. doi: 10.1016/j.stem.2009.04.005. URL http://dx.doi.org/10.1016/j.stem.2009.04.005.

J. Zhou, P. Su, D. Li, S. Tsang, E. Duan, and F. Wang. High-efficiency induction of neural conversion in human escs and human induced pluripotent stem cells with a single chemical inhibitor of transforming growth factor beta superfamily receptors. *Stem Cells*, 28(10):1741–1750, Oct 2010. doi: 10.1002/stem.504. URL http://dx.doi.org/10.1002/stem.504.

W. Zhou, L. Wang, S.-M. Gou, T.-L. Wang, M. Zhang, T. Liu, and C.-Y. Wang. Shrna silencing glycogen synthase kinase-3 beta inhibits tumor growth and angiogenesis in pancreatic cancer. *Cancer Lett*, 316(2):178–186, Mar 2012. doi: 10.1016/j.canlet.2011. 10.033. URL http://dx.doi.org/10.1016/j.canlet.2011.10.033.

Y. Zong, A. Panikkar, J. Xu, A. Antoniou, P. Raynaud, F. Lemaigre, and B. Z. Stanger. Notch signaling controls liver development by regulating biliary differentiation. *Development*, 136(10):1727–1739, May 2009. doi: 10.1242/dev.029140. URL http://dx.doi.org/10.1242/dev.029140.

Publications

<u>P. Matz</u>, R. Oreffo, and J. Adjaye. Culturing human pluripotent stem cells using human fetal femur derived MSCs and mouse embryonic fibroblasts: A comparative study. Enliven: J Stem Cells Regen Med 3(1):001, 2016.

    <u>P. Matz</u>, and J. Adjaye. Episomal-based generation of an iPS cell line from human fetal foreskin fibroblasts. *Stem Cell Research*, 16:6769, 2016. doi: 10.1016/j.scr.2015.12.009.

    <u>P. Matz</u>, W. Wruck, and J. Adjaye. Comparative induction of pluripotency in human umbilical vein endothelial cells and dermal fibroblasts and further differentiation into Hepatocytes. *Z Gastroenterol*, 53:A$2_1$3$, 2015. doi : 10.1055/s - 0035 - 1567985$.

    Katharina Drews, <u>P. Matz</u>, and J. Adjaye. Generation of iPSC lines from primary human amniotic fluid cells. *Stem Cell Research*, 15:712714, 2015. doi: 10.1016/j.scr.2015.11.003.

    Björn Lichtner, <u>P. Matz</u>, and J. Adjaye. Generation of iPSC line epiHUVEC from primary human chorionic villi cells. *Stem Cell Research*, 15:697699, 2015. doi: 10.1016/j.scr.2015.10.011.

    <u>P. Matz</u>, and J. Adjaye. Generation of iPSC line epiHUVEC from human umbilical vein endothelial cells. *Stem Cell Research*, 15:581583, 2015. doi: 10.1016/j.scr.2015.10.004.

    N. Graffmann, <u>P. Matz</u>, W. Wruck, and J. Adjaye. The promise of induced pluripotent stem cells for liver disease, toxicology and drug discovery. *Drug target Review*, 1, 2015.

    <u>P. Matz</u>, and J.Adjaye. Characterisation of human induced pluripotent stem cell-derived hepatocyte-like cells and endodermal progenitors. *European Journal of Medical Research*, 19(1):S8, 2014. doi: 10.1186/2047-783X-19-S1-S8.

    F. Diedrichs, B. Mlody, <u>P. Matz</u>, H. Fuchs, L. Chavez, K. Drews, and J. Adjaye. Comparative molecular portraits of human unfertilized oocytes and primordial germ cells at 10 weeks of gestation. *Int J Dev Biol*, 56(10-12):789-797, 2012. doi: 10.1387/ijdb.120230ja.

P. Matz, W. Wruck, B. Fauler, D. Herebian, T. Mielke, and J. Adjaye. Footprint-free human fetal foreskin derived iPSCs: a tool for modeling hepatogenesis associated gene regulatory networks. *Scientific Reports*, manuscript under review.

P. Matz, L. Spitzhorn, H. Yigit, J. Otte, and J. Adjaye. Use of Stem Cells in Toxicology. *Elsevier*, manuscript under review.

P. Matz, W. Wruck, and J. Adjaye. Comparative hepatocyte differentiation of human umbilical vein endothelial cell- and dermal fibroblast-derived iPSC line to study hepatogenesis *in vitro*. Manuscript in preparation.

P. Matz, W. Wruck, and J. Adjaye. Using endodermal progenitors to study the early time span of hepatogenesis. Manuscript in preparation

A. Prigione, M. Megges, M. Bohndorf, P. Matz, and J. Adjaye. Generation and characterization of aged donor-derived iPSC lines. Stem Cell Research, manuscript in preparation.

Selbständigkeitserklärung

Hiermit erkläre ich, die Dissertation selbstständig und nur unter Verwendung der angegebenen Hilfen und Hilfsmittel angefertigt zu haben. Ich habe mich anderwärts nicht um einen Doktorgrad beworben und besitze keinen entsprechenden Doktorgrad.
Ich erkläre, dass ich die Dissertation oder Teile davon nicht bereits bei einer anderen wissenschaftlichen Einrichtung eingereicht habe und dass sie dort weder angenommen noch abgelehnt wurde.

Peggy Matz, Berlin den 05. März 2016